MODIFICATION AND ENHANCEMENT OF EPOXIDE COATINGS VIA ELASTOMERIC POLYSULFIDES, SELF-ASSEMBLED NANOPHASE PARTICLES, FUNCTIONAL SOL-GELS, AND ANTI-CORROSION ADDITIVES

A Dissertation

Presented to

The Graduate Faculty of the University of Akron

In Partial Fulfillment

of the Requirements for the

Degree Doctor of Philosophy

Eric McClanahan

April, 2017

MODIFICATION AND ENHANCEMENT OF EPOXIDE COATINGS VIA ELASTOMERIC POLYSULFIDES, SELF-ASSEMBLED NANOPHASE PARTICLES, FUNCTIONAL SOL-GELS, AND ANTI-CORROSION ADDITIVES

Eric McClanahan

Dissertation

Approved:

_____
Advisor
Dr. Mark D. Soucek

_____
Committee Member
Dr. Alamgir Karim

_____
Committee Member
Dr. Kevin Cavicchi

_____
Committee Member
Dr. Toshi Miyoshi

_____
Committee Member
Dr. Edward Evans

Accepted:

_____
Department Chair
Dr. Sadhan C. Jana

_____
Dean of the College
Dr. Eric J. Amis

_____
Dean of the Graduate School
Dr. Chand Midha

_____
Date

ABSTRACT

Epoxides are widely used in the coatings industry as coating binders. Epoxide binders have several useful characteristics, which include the ability to react with polysulfide resin modifiers and thermosetting amide curatives. In order to improve the characteristics of epoxide coatings, various additives and resins can be grafted or added to the epoxide binder.

The first study involved the use of reacting polysulfides with epoxides and crosslinking with a polyamide to form films and coatings. While epoxide-polysulfides have heavily investigated in the literature for physical and fracture properties, a study investigating the fracture properties of epoxide-polysulfides at cold, ambient, and hot temperatures has not been attempted. The results indicated a toughening phenomenon at 5-10 wt. % polysulfides that led to enhancements in the fracture properties. Also, the addition of polysulfide content led to improvements in the flexibility and the impact resistance of the formulations.

Self-assembled NAnoPhase (SNAP) particles are nano-scale functional sol-gels that were pioneered as corrosion-resistant surface preparations on aluminum substrates. No studies have investigated the use of SNAP particles as functional additives within epoxide-polyamide coating systems. SNAP sol-gel particles were

formulated and added into epoxide-polyamide films and coatings. It was found that SNAP sol-gel particles were able to enhance the mechanical properties and corrosion resistance of the coatings. These studies are a novel discovery because the SNAP functional sol-gels are also able to act as a primer additive.

In the last study, carbon nanotubes and magnesium were both added into epoxide-polyamide films and coatings systems, which were tested for mechanical and corrosion resistance properties, respectively. While existing studies have investigated the use of magnesium or carbon nanotubes as anti-corrosion additives in epoxide coatings, the tandem use of nanotubes and magnesium has not yet been investigated in the literature in terms of corrosion and mechanical properties. In the absence of magnesium, the addition of carbon nanotubes enhanced the mechanical properties (fracture and tensile properties) of the epoxide-polyamide films, although the enhancement was marginalized when magnesium was added. The carbon nanotubes also aided in the enhancement of the coating's corrosion resistance as measured via electrochemical impedance spectroscopy (EIS).

DEDICATION

I would like to dedicate this dissertation to my lovely wife Erin, my parents Robert and Denise, and my brother Kyle, who passed away last year.

ACKNOWLEDGEMENTS

I would like to express my gratitude to Dr. Mark Soucek, who provided assistance, encouragement, and advice during my time working in his research group. In addition, he provided me several opportunities that were invaluable to my professional development. In addition, I would like to thank Drs. Elizabeth Berman and Walter Juzukonis, who advised me during my time at the Wright-Patterson Air Force Base. The time I spent working for Wright-Patterson Air Force Base was one of the highlights of my graduate career and was very helpful in my professional development. Furthermore, I would like to thank Todd Hawkins, Charlie Simpson, and Dr. Jorma Virtanen for advising me during my time at Tesla NanoCoatings and for providing some of the materials used in the studies.

Second, I would like to thank my committee members, Drs. Alamgir Karim, Dr. Kevin Cavicchi, and Nicole Zacharia of Polymer Engineering, Dr. Toshi Miyoshi of Polymer Science, and Dr. Edward Evans of Chemical and Biomolecular Engineering.

Last, I would like to thank the individuals in Dr. Mark Soucek's research group, especially Abed Hasheminesab, who provided invaluable assistance with molecular characterization of the SNAP sol-gel particles.

TABLE OF CONTENTS

Page

LIST OF TABLES

Table Page

LIST OF FIGURES

Figure Page

LIST OF ABBREVIATIONS

°C	Degrees Celsius
°F	Degrees Fahrenheit
η	Viscosity
v_e	Crosslink Density
a	Notch length (fracture toughness sample)
AEW	Amine Equivalent Weight
APTES	3-Aminopropyltriethoxysilane
APTMS	3-Aminopropyltrimethoxysilane
ASTM	American Society for Testing and Materials
ATR-IR	Attenuated Total Reflection Infrared Spectroscopy
b	Thickness (fracture toughness sample)
BuOH	n-butanol
CNT	Carbon nanotubes
COOH	Carboxylic Acid

CPVC	Critical Pigment Volume Concentration
CVP	Chemical Vapor Deposition
D	Diffusion Coefficient
DABCO	1,4-Diazabicyclo[2,2,2]octane
DBTL	Dibutyltin Dilaurate
DDS	4,4'-Diaminodiphenylsulfone
DETA	Diethylene Triamine
DGEBA	Diglycidyl Ether of Bisphenol A
DGEBF	Diglycidyl Ether of Bisphenol F
DICY	Dicyandiamide
DLS	Dynamic Light Scattering
DSC	Differential Scanning Calorimetry
DMA, DMTA	Dynamical Mechanical (Thermal) Analysis
E	Elastic Modulus
E’	Storage Modulus
E”	Loss Modulus
EEW	Epoxide Equivalent Weight

EIS	Electrochemical Impedance Spectroscopy
ESI MS	Electrospray Ionization Mass Spectroscopy
Et	Ethyl
F	Force
FEG-SEM	Field Emission Gun Scanning Electron Microscopy
FT	Fourier Transform
FTIR	Fourier Transform Infrared Spectroscopy
G4	Akzo-Nobel G4 Polysulfide
G112	Akzo-Nobel G112 Polysulfide
G_C	Elastic Energy Release Rate (fracture property)
G_{IC}	Planar Elastic Energy Rate (fracture property)
GD OES	Glow-Discharge Optical Emission Spectroscopy
GPTMS	3-glycidyloxypropyltrimethoxysilane
H_2O	Water
HBr	Hydrobromic acid
Hz	Hertz
IPN	Interpenetrating Network

IPTES	3-isocyanatopropyltriethoxysilane
J	Joule
K	Kelvin
K_C	Fracture toughness
K_{IC}	Planar fracture toughness
LED	Light Emitting Diode
LM	Loss Modulus
m	Meter
MN	Mega-Newton
MPa	Mega-Pascal
MALDI-MS	Matrix-Assisted Laser Desorption/Ionization Mass Spectroscopy
MEK	Methyl Ethyl Ketone
Mg	Magnesium
Mg-Rich	Magnesium-Rich
MIBK	Methyl Isobutyl Ketone
MTMS	Methyltrimethoxysilane

mV	Millivolt
MWCNT	Multi-walled Carbon Nanotube
N	Newton
NaCl	Sodium Chloride
NMR (^{13}C)	Carbon-13 Nuclear Magnetic Resonance
NMR (^{1}H)	Hydrogen-1 Nuclear Magnetic Resonance
NMR (^{29}Si)	Silicon-29 Nuclear Magnetic Resonance
OTMOS	Octyltrimethoxysilane
PDS	Potentiodynamic Scanning
PEO	Poly(ethylene oxide)
PET	Polyethylene Terephthalate
Pht	Phthalate
POPDA	Poly(oxypropylene) Diamine
psi	Pounds per Square Inch
PTEOS	Phenyltriethoxysilane
PVC	Pigment Volume Concentration
R	Ideal Gas Constant

R_H	Hydrodynamic Radius
RMS	Root Mean Square
SAXS	Small Angle X-Ray Scattering
STEM	Scanning Transmission Electron Microscopy
SM	Storage Modulus
SNAP	Self-Assembled Nanophase
SVET	Scanning Vibration Electrode Technique
SWCNT	Single-Walled Carbon Nanotubes
T	Temperature
TEM	Transmission Electron Microscopy
TEOS	Tetraethyl Orthosilicate
T_G	Glass Transition Temperature
TGA	Thermal Gravimetric Analysis
THF	Tetrahydrofuran
TiO_2	Titanium Dioxide
TMOS	Tetramethyl orthosilicate
USAXS	Ultra Small X-Ray Scattering

UV	Ultraviolet
V	Volt
VOC	Volatile Organic Content
w	Width (fracture toughness sample)
XPS	X-Ray Photoelectron Spectroscopy
Z’	Real Part of the Impedance
Z”	Imaginary Part of the Impedance
|Z|	Impedance Modulus
Zn	Zinc
Zn-Rich	Zinc-Rich

CHAPTER 1

INTRODUCTION

Coatings are continuous, solid films that are applied to protect a substrate. There are four main components that constitute a coating: binders, volatiles, pigments, and additives.[1] A binder is the component that hardens to form a film on a substrate and encompasses the other coatings components (additives and pigments). In the case of thermosets, binders will react with curing agents to form a solid, hardened film. Epoxide binders (binders with oxirane end groups) are common thermosetting coating binders and are often used on metal (steel and aluminum) substrates.[1] The benefits of epoxide binders include low material costs, minimal dimensional shrinkage during curing, and the ability to oligomerize with different types of modifiers.[2-3]

One type of modifier is the polysulfide. Polysulfides are added as oligomers to epoxides in order to provide flexibility and toughening. Therefore, crosslinked epoxide-polysulfides are often utilized as "bridge coatings" for metal surfaces with unusual geometries.[4] The term bridge coating is attributed to air pockets forming under the coating from difficulty applying the coating during the application process.[4] Crosslinked epoxide-polysulfides are used as coatings on the exterior surfaces of flying aircraft,

particularly around screws and rivets. In these applications, weatherability, flexibility and resistance to fracture are necessarily. Epoxide-polysulfide coatings with low polysulfide content are generally excellent in this regard and provide enhanced flexibility and toughness over neat epoxides.[5] Epoxide-polysulfides have been thoroughly investigated in literature for thermal and mechanical properties, which includes tensile[5], adhesion[5], and fracture characteristics[6]. Topics that have not been investigated are the fracture characteristics as a function of both the temperature and the polysulfide content. This is an imperative topic that will determine the damage tolerance of the epoxide-polysulfides at the wide variety of temperatures that the coating is exposed to during flight. Also, Chapter 3 investigated various mechanical properties of epoxide-polysulfides which included the adhesion strength, dynamical mechanical thermal properties, and the fracture properties and related the various properties together. The dynamic moduli as measured via DMTA was useful in terms of relating to some of the mechanical properties, particularly the fracture properties at different temperatures. The polysulfide content was varied along with the molecular weight of the polysulfide to observe the effects on the fracture, mechanical, and coatings properties.

Besides functional oligomers, epoxide coatings and composites are enhanced by silica-based additives. Silica-based additives are dispersed into the epoxide binder/matrix and can enhance the mechanical properties (adhesion strength, weatherability, resistance to fracture, etc.) and corrosion resistance of the coating. Also, silica-based materials are more environmentally benign than existing coating

additives such as chromates and chromate conversion coatings. Therefore, silica-based materials are useful additives for replacing chromates. There are two types of silica content in epoxide coatings systems: class I and II silica content. Class I silica content does not bond with the epoxide binder and/or curing agent, while class II silica content will crosslink with the epoxide resin, curing agents, or substrate.[7]

Specific to Class II silica materials are self-assembled nanophase (SNAP) particles. In previous literature, SNAP particles were utilized as a surface preparation on aluminum substrates.[8] Surface preparations act as thin passivating layers and coupling agents between the metal substrates and primers. As a surface preparation, SNAP particles have provided corrosion resistance for aluminum substrates. SNAP particles have not been utilized as an additive for epoxide coatings. Using SNAP particles as an additive for epoxide coatings instead of as a surface preparation would be an improvement over earlier use because it could potentially improve both the mechanical properties and the corrosion resistance of an epoxide coating. In Chapters 4 and 5, SNAP particles with oxirane and amine end groups, respectively, were added in various ratios to epoxide films and coatings. The particles reacted with the epoxide matrix or amide curing agent to form a continuous system. The films and coatings were tested for mechanical properties and corrosion resistance. SNAP particles contributed to enhancements to both the mechanical properties and corrosion resistance.

Besides silica content, sacrificial metals can enhance the corrosion resistance of epoxide primer coatings cast on metal substrates.[9] Sacrificial metals are more active

than the metal substrates and thus corrode first in presence of a corrosive agent such as salt water or oxygen. The resulting oxides created act as a passivating layer that prevents corrosive agents from penetrating the substrate. Zinc-rich epoxide coatings are the industry standard for exterior steel substrates such as bridges, pipes, and offshore oil platforms, since zinc is more active than iron. Chromate-loaded coatings have been the industry standard for exterior aluminum substrates, but chromates are being eliminated because of toxicity and environmental health concerns. A useful replacement for chromate-loaded coatings is the magnesium-rich coating, since magnesium is more active than aluminum.[10]

To provide sufficient corrosion protection, it is necessary for the metal weight content to be very high (70 wt. % and above).[9] This ensures that there is contact between the sacrificial metal particles and the substrate. This weakens the primer coating and augments the porosity. To provide a proper barrier against physical and corrosive bombardment, multiple coats must be added on top of the primer.

To reduce coating costs while maintaining corrosion resistance, carbon nanotubes can be added to metal-rich primers.[11] Carbon nanotubes are electrically conductive and can act as linkages between sacrificial metal particles. Therefore, by substituting some of the sacrificial metal content with carbon nanotubes, the corrosion resistance of the coating is maintained. The porosity is thereby reduced and the coating is strengthened by the removal of some of the metal content. One of the top coats can be removed, which reduces the cost. Also, carbon nanotubes are mechanically robust

and can enhance the mechanical properties of epoxide coatings and films.[12] Past literature has investigated the corrosion resistance of epoxide coatings with carbon nanotubes only[13] and carbon nanotubes with zinc.[11] The corrosion resistance of epoxide contents loaded with both carbon nanotubes and magnesium has not been explored yet by researchers. Chapter 6 will focus on the corrosion resistance and mechanical properties of epoxide coatings loaded with both carbon nanotubes and magnesium. Since carbon nanotubes can enhance the mechanical properties and metal content will diminish the properties of epoxide coatings, it is useful to ascertain how the two additive pigments in tandem will affect the epoxide coating. This has also not yet been explored by previous researchers.

CHAPTER II

BACKGROUND

2.1 Epoxide Resins

Epoxide resins and materials are frequently utilized in the coating and materials world as coating matrix materials, binders, and modifiers. The materials are noted by the epoxide or oxirane functional group, which can react with various curatives to form a crosslinked or cured film material. The name “epoxide” can stand for the base prepolymer material or the crosslinked film material.[14] The base epoxide ring structure is shown in Figure 1.

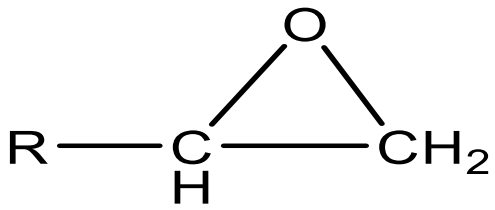

Figure 2.1: Epoxide Basic Structure[15]

2.1.1 History and Current Uses of Epoxide Resins

Epoxide resins were first made available to the public in the 1940s and were synthesized from the reaction of epichlorohydrin and bisphenol A.[16] The first available patent is attributed to P. Caston and deTrey Frers of the Ciba Company in Germany. The earliest usage of epoxide resins occurred in the 1940s where the resins were utilized as surface coatings.[16] Some examples included floor finishes, automotive coatings, and coatings for metal surfaces. The earliest commercial applications of epoxide coatings utilized the bisphenol A epoxides undergoing esterification with C18 fatty acids.

Pioneering achievements by the Shell Companies resulted in the introduction of epoxide-amine two-part coating systems.[16] 1955 saw the introduction of an amine adduct utilized as a curative for epoxides, which led to enhancements in the properties of the coating. This was an improvement over the traditional aliphatic polyamine curatives.

Concurrently, General Mills pioneered a series of polyamide resins with free amino functional groups.[16] The curatives provided enhancements to the substance resistance and the ability to be dried under ambient conditions. Other pioneering achievements in the 1950s included epoxide materials added with phenolic and amino based materials, high MW epoxide materials with solvent invulnerability and added physical capabilities, high solids epoxide resin powder coatings, and thermoplastic epoxide resins by Union Carbide and Shell (1960). The latter resins were utilized in the industry for automotive coatings and as a resin matrix material for zinc-rich coatings.

Currently, epoxide resins are used as binder materials in coatings and composites. Some examples include molds and castings (such as Kevlar-based materials), wind turbines, water-based epoxide paints, aerospace materials, marine caulkers, adhesives and glues, art paints, floor coatings, and coatings for metal surfaces (can coatings, aerospace coatings, etc.).[17]

2.1.2 Types, Curing Mechanisms, and Properties of Epoxide Resins

Epoxides can be formed from a wide variety of monomeric materials, which includes Bisphenol A epoxides, bisphenol F epoxides, novolac epoxide resins, and aliphatic epoxide resins. The bisphenol A epoxide is one of the most common epoxide, and it is commonly used in architectural and aerospace coatings. A bisphenol A base catalyzed epoxide reaction is shown in Figure 2.2.[18] The reactants are bisphenol A and epichlorohydrin, and the end product is diglycidyl ether of bisphenol A.

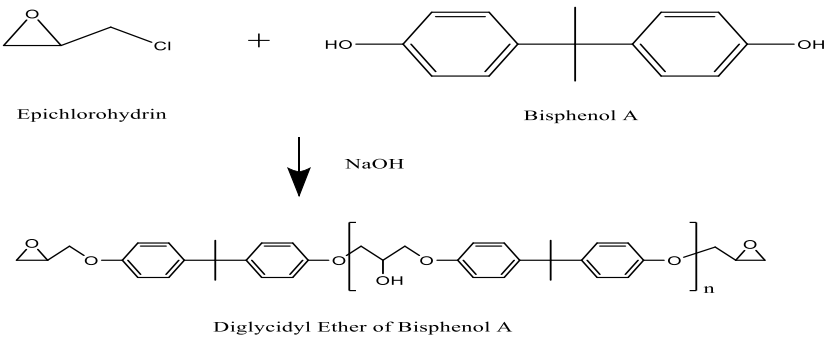

Figure 2.2: Bisphenol-A Epoxide (DGEBA) Reaction[18]

Epoxides can cure with a wide variety of materials, which includes amines, anhydrides, thiols, and phenols. Curing mechanisms of epoxide materials utilizes the creation of firm crosslinked domains utilizing reactions with curatives with

functionalities greater than 2 and base epoxides with functionalities greater than or equal to 2.[14] The epoxide curing mechanism leads to crosslinked moieties that steadily become bigger and more intricately branched. This reaction occurs within a solvent medium. The juncture at which noticeable physical differences are observed is the point of gelation. This occurs when the crosslinked molecule permeates through the entire medium and the structures changes from being dissolved in the solvent to becoming a solid structure. For the coating to turn into a film material, however, the solvent amount must disappear or become negligible through continued curing and solvent evaporation. An example of an epoxide amine reactions is shown in Figure 2.3, and an epoxide-amide reaction is shown in Figure 2.4.

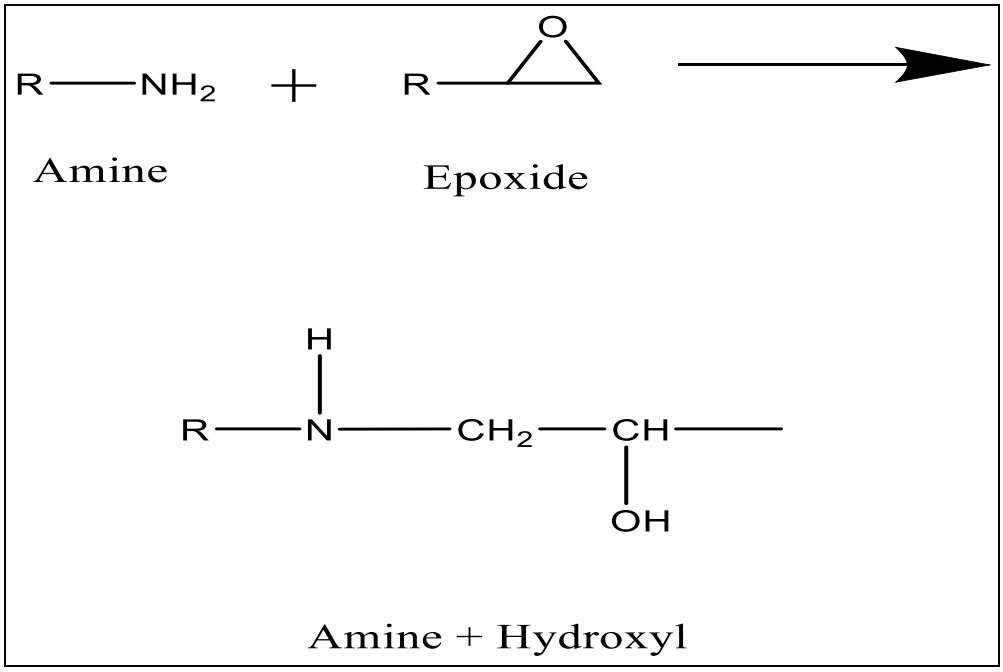

Figure 2.3: Epoxide-Amine Reactions[3]

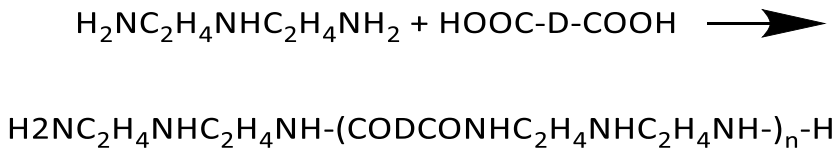

Figure 2.4: Epoxide-Amide Reaction[19]

Epoxide materials have many beneficial properties that are ideal for use in coatings, composites, adhesives, and other materials. Some of them include enhanced adhesion strength, which arises from the polarity of the materials, minimal shrinkage during curing, the ability to copolymerize, zero VOC (volatile organic content) from the epoxide reactions, toughness of the final materials, chemical and solvent resistance, and the ability to bond with different modifiers.[20] Such examples include thermoplastics and elastomers (which include polysulfides), both of which can enhance the toughness of the epoxide materials.

2.2 Polysulfides and Polysulfide-Based Materials

One type of modifier for epoxide materials is the polysulfide, which is elastomeric and is used as a toughening/flexibilizing agent when bonded with epoxides and other materials. Polysulfide materials can take the form of a resin or solid material. Polysulfide molecules have the following rudimentary structure, as depicted by the *Encyclopedia of Polymer Science and Technology*:

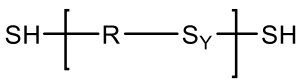

Figure 2.5: Polysulfide Structure[21]

The variable y is known as the rank and stands for the average amount of sulfur atoms in the repeat unit. The variable R stands for an aliphatic group. Polysulfides were first developed in 1838 by scientists in Switzerland. The Thiokol Corporation was the first entity to develop it for commercial applications. The first polysulfide commercial product was Thiokol A, which came out in 1928 and was utilized as a chemical-resistant sealant. Early commercial uses of polysulfides included sealants for tanks, hoses, hulls, and decks. Currently, polysulfides are commonly used as outdoor sealants for aircraft, windows, construction, and other areas. The benefits of polysulfides include flexibility, weathering and chemical resistance, and ability to withstand low temperatures. Generally, the polysulfide-based formulations have two parts. Part A consists of liquid polysulfides, filler, plasticizers, thixotropes, and adhesion promoters. Part B includes the curing agent, plasticizer, filler, and a chemical accelerator or retarder. Reviews on polysulfides include Fettes et al.[22], who discussed various synthesis methods of polysulfides, the types of crosslinkers, and the physical properties of the final formulations. Lowe et al.[23] discussed the curing phenomena of polysulfides as well as available curing agents, which include metal peroxides, manganese dioxide, metal chlorates, dichromates, and permanganates, and organic peroxides and hydroperoxides. Primary and secondary amines are also used for certain types of polysulfide copolymers and oligomers.

2.2.1 Epoxide-Polysulfides

A special type of copolymer or co-oligomer that that can be developed from polysulfides is the epoxide-polysulfide, which involves the synthesis of epoxides and polysulfides. The generic reaction is shown below:

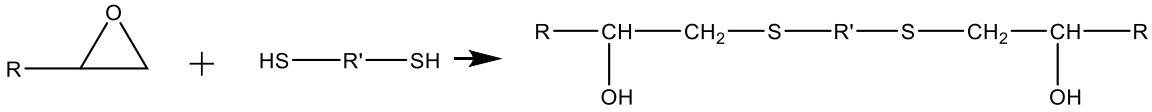

Figure 2.6: Epoxide-Polysulfide Reaction[21]

Polysulfides with molecular weights of 1,000 generally are used for addition to epoxides.[24] Primary or secondary amines are used as curing agents for epoxide-polysulfide materials. The addition of polysulfide structures to epoxides in smaller amounts will generally improve the ductility, impact strength, chemical resistance, and adhesion properties of the material.

2.2.1.1 Properties of Epoxide-Polysulfides with Low Levels of Polysulfide

There have been many researchers that have characterized the properties of epoxide-polysulfide resins and materials. Generally, low levels of polysulfides are best suited to epoxide toughening. Arundati et. al.[5] explored the reaction of polysulfides to epoxides in levels of 10 to 50 parts per hundred and determined that smaller amounts of polysulfide contributed to enhancements in the tensile strength, flexural strength, hardness, and impact strength. These parameters decreased after a peak at 20 parts per hundred. The physical specimens were analyzed via scanning electron microscopy (SEM). The researchers observed a “rigid continuous epoxide matrix with a dispersed

rubbery phase as isolated particles." The researchers attributed the toughening mechanisms associated with polysulfide content to crack deflection, crazing, and elastic deformation that prevented the fracture of the rigid neat epoxides. To fracture, the epoxide phases must twist around the rubbery phases, which delays fracture. Also, the polysulfide particle phases dissipate the tensile forces throughout the sample, resulting in crazing instead of complete rupture. Last, the presence of the rubbery particle phases resulted in higher elastic deformations, which in turn delayed fracture. At higher levels of polysulfide, there was a transition to more malleable materials, which culminated in the reduction of tensile strength, flexural strength, hardness, and impact strength.

Like Arundati et al., Farajpour et al.[6] tested low polysulfide (5-20% wt.) epoxide-polysulfide copolymers based upon G4 or G112 resins. G112 resins have larger molecular weights than G4. The coatings were crosslinked with an amine hardener and tested for impact strength and adhesion strength. Both parameters were maximized at 10% G4 and 15% G112. Further increases in the polysulfide content resulted in a reduction of the adhesion and impact strengths. The researchers attributed the enhancements to the reduction of the epoxide matrix crosslink density. During the copolymerization reaction of the polysulfide and the epoxide, the two oligomers form bond together to form a copolymer. This culminates in increased chain toughness, but without increasing the likelihood of fracture. This results in an increase in parameters such as the impact strength and fracture toughness. The impact strength and adhesion strength were slightly higher for G112 epoxide-polysulfides. Cranker et al. also reported

an increase in the impact strength with polysulfide content, which they attributed to the polysulfide content lessening the residual strains within the epoxide content.[25]

2.2.1.2 Properties of Epoxide-Polysulfide Materials with Elevated Levels of Polysulfide

To determine the effect of elevated amounts (20 wt. % and above) of polysulfide content in crosslinked epoxide-polysulfide copolymer films, Abdouss et al.[26] tested the hardness and tensile properties at polysulfide levels of 20 wt. % and above. G4 polysulfide resin was utilized as a polysulfide chain extruder with diglycidyl ether of bisphenol A (Epon 828). An amine hardener was utilized as a crosslinker. The resulting formulations were tested for tensile properties. The researchers noted that the addition of polysulfide to epoxide groups led to enhanced elongational properties of the final specimens. In a second study, Abdouss et al.[27] studied the effect of the same epoxide-polysulfide materials at polysulfide: epoxide weight ratios of 100:70, 100:80, 100:90, and 100:100. The addition of **epoxide** to the formulations led to improvements in the hardness, tensile strength, and a reduction in the elongation %. This and the previous studies indicate that higher levels of polysulfide (above 10-15 wt. %) in epoxide-polysulfides will diminish the hardness, rigidity, and tensile strength of the crosslinked films. Since polysulfide content contributes to the flexibility of the crosslinked films, the elongation % of the films increases with polysulfide content. Comparable results were found by Zhang et al.[28], who determined that polysulfide content copolymers composed of bisphenol-A diacrylate epoxide-polysulfides resulted in higher flexibilities and lower hardness values.

Increasing the polysulfide content in epoxide-polysulfide copolymers leads to a lower glass transition temperature. This is attributed to the flexibility of the polysulfide content at low temperatures. This phenomenon has been noted by various researchers.[29,30]

2.3 Additives in Epoxide Composite Films and Coatings

Besides acting as a resin material that can react with elastomeric and thermoplastic modifiers, epoxides can also act as binder/matrix materials for composites and coatings. Additives and filler materials are commonly added to composites and coating materials to enhance various properties of the system, which include the mechanical properties and the ability to prevent corrosion. Common additive materials for epoxides (particularly in the field of coatings) include silica-based materials. Silica-based materials enhance mechanical properties of the epoxide composite/coating and act as a passivating barrier against corrosion if the epoxide is a coating binder cast on a metal surface. Passivation is one of several types of methods to prevent corrosion to a metal substrate.

Another type of corrosion prevention is the use of sacrificial metal additives in epoxide coatings. In the case of epoxide coatings on metal substrates, sacrificial metals can act as a corrosion prevention mechanism by corroding in lieu of the substrate and by creating a passivating layer that acts as a barrier against further corrosion. New advancements in epoxide additives include carbon content such as carbon fibers and

nanotubes, which can aid both the mechanical properties and corrosion resistance of an epoxide composite/coating.

2.3.1 Silica Content in Epoxide Materials

Epoxide-silica hybrid nanocomposites have been thoroughly researched in past literature for their synergy in terms of mechanical and corrosion related properties. Epoxide materials are commonly used as coating materials because the materials are inexpensive and simple to develop. In addition, epoxides have enhanced mechanical properties, undergo minimal shrinkage during curing, and adhere well to various substrates.[31,32] The limiting factor of epoxide materials is temperature stability and hardness.[31] The inorganic content of silica-based materials can improve these attributes and further enhance these properties if they are nano-sized and well-dispersed in the epoxide matrix.[33] There are two types of epoxide-silica hybrid materials: Class I and Class II materials. Class I materials have non-functional silica content in which the two phases (epoxide and silica) have weak interactions, while Class II materials are covalently bonded with one another.[7]

2.3.1.1 Class I Silica Materials in Epoxide Materials

Class I silica materials are non-functional but aid in various properties of the composite by forming weak interactions with the epoxide binder. These properties include the fracture toughness, modulus, and tensile strength. Some of these properties have been researched at length by various researchers, which will be

elucidated in the following section. The section will focus on the enhancement of the fracture properties (toughness, energy) of epoxide composite via silica loading.

Wetzel et al.[34] described how the inclusion of nanoparticles (silica or otherwise) in epoxide thermosets can lead to the enhancement of fracture properties. Silica nanoparticles often prevent fracture through zone shielding. Zone shielding means that the crack propagation is prevented by downgrading the stress around the crack zone. There are a few several possible ways this can happened. The first is crack deflection or pinning, which means that the presence of a particle can impede the propagation of a crack. The crack must propagate around the silica, typically by torsion in a planar or three-dimensional fashion. Plastic deformation is another type of mechanism. Generally, thermosets have more difficulty undergoing plastic deformation than traditional thermoplastics due to the crosslinked nature of thermosets. The presence and mechanical nature of the particles can lead to shear yielding. This means that the sample undergoes a plane strain-stress transition. This culminates in the presence of "voids, cavities, and debonding" of the particle from the matrix. Last, the addition of particles can impart residual stress to the matrix during thermoset curing, which ultimately strengthens the composite and enhances the fracture properties. Last, the epoxide binder and silica can form weak interactions that enhance the toughness of the composite. Generally, aggregation of silica particles will ultimately weaken an epoxide-silica composite. Silica that is properly dispersed within an epoxide binder will lead to a composite with better fracture properties.

In the study by Chen et al.[35], nanocomposites were processed with Epon 862 resins (DGEBF) and SiO_2 nanoparticles. The SiO_2 nanoparticles were dispersed in MEK (30 wt. %). The SiO_2 nanoparticles (12-nm diameter) were added into the epoxide formulations at weight percentages up to 25 wt. %. Later, the particles were analyzed via TEM and DLS. The composites were analyzed via ultra-small angle X-ray scattering (USAXS), DSC, DMA, tensile mechanical tests, and fracture toughness tests. The microscopy results indicated that the SiO_2 nanoparticles showed proper dispersion at all levels observed. The fracture toughness increased by 30% with the addition of silica particles. There was an increase in the modulus as well. The enhancement of the fracture toughness was attributed to shear banding phenomena, while the enhancement in the modulus was attributed to the presence of a strain zone surrounding the dispersed particles.

Zhang et al.[36] measured the fracture mechanics of in situ nanoparticle epoxide composites. The fracture mechanics were measured under ambient conditions and at 80 degrees Celsius. The impact resistance, elastic modulus, and hardness were also measured. The nanosized silica particles positively affected the fracture behaviors of the material. The enhancement of the fracture properties was attributed to a zone of "plastic deformability" created by the presence of the silica nanoparticles. The force imposed upon the samples during fracture testing results in the creation of dispersed micro-voids, which in turn results in plastic deformation at the crack site. This results in delayed crack propagation of the sample. This phenomenon is present at ambient conditions and at elevated temperatures (80°C).

Johnsen et al.[37] used of 20 nm silica nanoparticles in epoxide-anhydride films. Microscopy results indicated a good degree of dispersion within the epoxide resin. Neat epoxide materials have a K_{IC} of 0.59 MN/$m^{1.5}$, while materials with 13.4 vol. % nanoparticles have a K_{IC} of 1.42 MN/$m^{1.5}$. The G_{IC} for neat epoxides was 103 J/m^2, while the maximum G_{IC} value observed with nanoparticle filled epoxides was 460 J/m^2. The researchers concluded that the nanoparticles provided toughening for the epoxide material. The researchers ruled out crack deflection as a possible toughening phenomenon due to the crack propagation occurring in dimensions much larger than the size of the nanoparticles. The researchers concluded from the microscopy results that nanoparticle debonding and propagation of voids were the reasons behind the toughening mechanism.

In the work by Bray et al.[38], three varied sizes of silica particles (23, 74, and 170 nm) were deposited into epoxide thermosets cured with piperidine. The fracture mechanics study indicated that shear band yielding begun in the silica nanoparticles and extended to the epoxide. It was followed by silica debonding from the epoxide matrix. The relationship between particle loading and the fracture energy (G_C) was linear. The researchers did not find any relationship between particle diameter and fracture toughness.

In the work by Rosso et al.[39], silica nanoparticles were added to epoxide formulations. The loading was 5 vol. %. The elastic modulus (tensile testing) was measured as well as the K_C and G_C values from fracture toughness testing. The elastic

modulus increased by 20% with the addition of the silica nanoparticles, while K_C increased by 70% and G_C by 140%. The glass transition temperature decreased from 95 to 89°C. The researchers also noted enhancements in the stiffness of the materials from cryogenic levels up to the glass transition temperature. The enhancements in the fracture toughness were attributed to crack deflection.

In the study by Ma et al.[40], silica nanoparticles were added into epoxide-amine networks based upon two distinct types of epoxide, Jeffamine D230, and 4,4'-daminodiphenyl sulfone (DDS). The silica nanoparticles were added into the system in weight percentages of 10% and 20%. The researchers noted that one of the systems showed a K_C increase from 0.73 (neat epoxide) to 1.68 MPa*$m^{0.5}$ at a silica loading of 20%. The other system showed an increase from 0.51 to 0.82 MPa*$m^{0.5}$. The researchers also observed the fracture mechanics of the system. They attributed the fracture toughness expansion to the suppression of void propagation by the presence of the silica particles.

In the study by Zhang et al.[41], silica nanoparticles with an average diameter of 25 nm were put into epoxide materials with contents up to 14 vol. % or 23 wt. %. The silica nanoparticles increased the toughness and moduli of the epoxide materials. Crack pinning was one of the mechanisms behind the enhancement in the fracture toughness. The researchers also observed that the most significant improvements to the macroscopic mechanical properties came when the interparticle spacing was smaller than the diameters of the particles themselves.

In the research work by Preghenella et al.[42], silica nanoparticles were put into DGEBA epoxide materials in volume ratios of 3.3%, 6.4%, or 9.2%. A solvent based approach was utilized to disperse the silica in the epoxide material. The researchers observed a reduction in the tensile strength of the materials with the addition of silica particles. Enhancements in the K_{IQ} and G_{IQ} (fracture parameters) were observed at 3.3% silica, but the K_{IQ} and G_{IQ} decreased at higher levels of silica loading. The enhancements were attributed to robust binder-particle interactions.

In the work by Cantwell et al.[43], this study investigated the fracture mechanics of silica-filled epoxide materials at various temperatures ranging from ambient conditions up to 100 degrees Celsius. The researchers investigated the fracture phenomena at the different temperatures and found that the phenomena were dependent upon the temperature. At room temperature, the crack propagated after one debonding event. At 50 and 85°C, the crack size grew through debonding in a miniscule area in the front of the crack. At 105°C, the elevated temperatures led to higher strain, which in turn led to crack growth.

In the study by Spanoudakis et al.[44], epoxide-amine thermosets were filled with glass particles with sizes of 4.5, 16, 32, 47, or 62 microns. The fracture phenomena of the composites were studied. The researchers found that fracture toughening can occur via crack front pinning.

2.3.1.2 Class II Silica Materials in Epoxide Materials and Coatings Systems

Class II silica materials are differentiated from Class I silica materials by the ability of said materials to form covalent bonds with either the binder or the substrate material (metal). Functional sol-gel materials are incorporated within this classification of silica materials. Class II silica materials can act as functional additives within composites, films, and coatings, or as a surface preparation. Due to the bonding of the silica content to the epoxide matrix, class II silica materials can enhance the physical properties of the composite (modulus, tensile strength, fracture properties, abrasion resistance, etc.). In addition, class II silica materials can enhance the performance window of epoxides. Last, class II silica materials can form a passivating layer and thus can act as a barrier coating against corrosion. This section will discuss the available literature of class II silica materials in epoxide composites and coatings as well as the use of Class II silica materials as surface preparations for metal substrates.

2.3.1.2.1 Thermal Properties of Class II Silica Materials

Due to the thermal stability siloxane bonds, class II silica materials are thermally stable can enhance the performance window of epoxides. In a study by Wu et. al.[31], a hybrimer made from an epoxide resin and sol-gel precursors was made in to act as a hybrid encapsulant for LED lights. The researchers were looking to create a material with good durability/mechanical properties (a hallmark of epoxide resins, which are typically used as encapsulants for LED lights) and UV/heat stability (a shortcoming of epoxide resins). In this study, the epoxide resins were bisphenol-A based epoxides. The process of synthesizing epoxide sol-gel hybrids was an acid catalyzed reaction utilizing 3-

isocyanatopropyltriethoxysilane (IPTES) and phenyltriethoxysilane (PTEOS). The final amounts of the phenyl-siloxane sol-gels (IPTEOS + PTEOS) were in amounts of 5%, 10%, or 15% weight of the epoxide. The final samples showcased improved thermal stability and UV resistance when compared to the neat epoxides. The thermal stability was attributed to the bond dissociation energy of the siloxane networks.

Kang et al.[45] also studied the thermal performance of epoxide/nanosilica hybrid composites. Nano-sized silica particles were functionalized with oxiranes, amines, or isocyanates and then underwent reactions with an epoxide. The contents were later solidified with a curing agent. Epoxides loaded with non-functionalized nano-sized silica particles were processed as a control sample. The dynamical mechanical thermal properties of the composites were tested. The researchers reported that the additional of functionalized particles into the epoxide matrix increased the glass transition temperature, which they attributed to the fillers inhibiting the movement of the polymer backbones in the epoxide matrix.

Wang et al.[46] also studied the thermal properties of DGEBA epoxide-silica hybrids. Functional silica content was created by hydrolyzing TEOS with a glycidoxypropylmethyldiethoxysilane coupling agent. Unmodified silica was utilized as a reference. Later, the contents were added to the epoxide material along with a dicyandiamide (DICY) curing agent. Later, the cured materials were tested via TGA and DSC. The effect of the sol gels and coupling agents increased the decomposition and glass transition temperatures (80 to 113°C) by a significant degree. The authors

attributed the increases to the covalent bonding of the coupling agent between the epoxide binder and silica content.

In the work by Macan et al.[47], GPTMS was added into epoxide-amine coatings with DGEBA acting as the epoxide and Jeffamine D230 acting as the curing agent. DSC and TGA were performed on the cured materials. The inorganic sol-gel content increased the TGA degradation temperatures of the epoxide composites due to the temperature stability of the siloxanes.

2.3.1.2.2 Mechanical Properties of Epoxides/Class II Silica Hybrid Materials/Coatings

Class II silica content can also enhance the mechanical properties of epoxide composites. This includes wear resistance, modulus, tensile strength, and fracture toughness. The wear resistance arises from the ability of the silica content to absorb energy from impacts and wear, while the silica epoxide covalent bonding and crack deflection are responsible for enhancements to the tensile strength, modulus, and fracture toughness/energy. If the silica content takes the form of particles, the fracture toughness is enhanced by crack deflection. Also, the silica content can form covalent siloxane bonds with metal substrates, which can enhance the adhesion strength of coatings cast onto metal.

Perchacz et al.[48] loaded GPTMS-based sol-gels into epoxide-amine coating networks to enhance the mechanical properties of the coatings. The epoxide was DGEBA and the amine was Jeffamine D-230. The hybrid matrices were characterized via SAXS, AFM, DMTA, TEM, tensile tests, TGA, and XRF. DABCO or DBTL were utilized as

catalysts. DABCO is a basic catalyst, and DBTL is a neutral catalyst. The researchers found that DABCO-catalyzed silica hybrids created spherical systems with "cage" formations. The researchers also found that DABCO catalyzed systems led to an increase in the energy to break, elongation %, and tensile strength, although the increase of the latter was marginal. The DBTL showed a higher prevalence of IPNs and affinity with the epoxide-amine matrix when compared to the DABCO catalyzed systems. There was a threshold to the loading, however. The highest amounts (22 wt. %) contributed to a decrease in the mechanical properties of the material. The increase in the tensile properties at low silica loading levels was attributed to covalent bonding of the silica to the epoxide as well as concentration of the stresses around the particles and through the epoxide binder. Higher levels of silica loading (greater than 5%) resulted in the formation of larger silica structures, which in turn made the samples more brittle.

In the work by Oh et al.[49], epoxide-silica hybrid resins were processed and tested to improve the efficiency and life of coatings for floor finishing applications. The coupling agent was GPTMS, and micron-sized silica particles were utilized for silica content. Adhesion strength, impact resistance, abrasion resistance, and a few other mechanical tests were employed to measure the mechanical properties of the coating system. The best performance was obtained with a silica/GPTMS mass ratio of 1 to 1.75. Microscopy was utilized to observe the coatings after abrasion, impact, and other tests. Improvements in the impact resistance were due to the energy absorption of the coupling agents. The improvements in the abrasion resistance were due to the

enhancement of silica-epoxide bonding from the presence of GPTMS. The improvements in the adhesion strength were due to the siloxane bonds (from the coupling agent) between the epoxide and concrete surface.

In the study by Olsson et al.[7], ferrite nanoparticles (50 nm diameter) were grafted with GPTMS, aminopropyltrimethoxysilane (APTMS), or methylsilsesquioxane (MTMS) and later added into epoxide formulations to form epoxide nanocomposites. The researchers concluded that the grafting of functional silanes onto the particles improved their compatibility with the epoxide and mitigated phase separation and agglomeration. In addition, the area between the particles and the epoxide was toughened, which thereby improved the fracture toughness.

In the study by Saliba et al.[50], the purpose was to utilize 3-GPTMS and 3-APTES as coupling agents to improve the adhesion strength of fusion bonded epoxides to steel substrates. The adhesion strength and mode of rupture changed as coupling agents were added to the formulations, indicating that the presence of coupling agents bonded to the metal surface improved the adhesion strength.

In the study by Cakir et al.[51], alkoxysilane solutions were synthesized and placed into epoxide-amine thermosets. The alkoxysilane solution was 55% TEOS, 6% GOTMS (glycidoxypropyltrimethoxysilane), 14% H_2O, 0.5% catalyst, and 24.5% C_2H_5OH by weight. The epoxide resin material was Epikote 828, and the curing agent was Epikure 205. BDMA (amine material) was utilized as a catalyst/accelerator for the crosslinking reactions. The tensile modulus, tensile strength, elongation at break, Izod hardness,

wear resistance, and water absorption of the materials were measured as a function of TEOS weight content. The tensile modulus and hardness of the materials increased with the silica content.

In the study by Nikje et al.[52], APTES was grafted onto nano-sized silica and added into epoxide nanocomposites based on DGEBA (Araldite GY 6010) and a cycloaliphatic polyamine (Aradur 43). The silica content was varied between 0% and 3% in increments of 0.5%.

The tensile strength and elongation % increased with the silica content, the shore A hardness increased with silica content, and the thickness loss from abrasion decreased with silica content. The glass transition temperature increased with the silica content.

2.3.1.2.3 Corrosion Resistance of Class II Silica Materials and Epoxides Incorporating Class II Silica Materials

Besides enhancing the mechanical properties of an epoxide composite or coating, class II silica materials can act as a barrier against corrosion, either as a functional additive within a coating or a surface preparation. Surface preparations are thin coating layers cast onto a substrate that generally act as a connective layer between the primer and substrate. The surface preparations contribute as a protective barrier against corrosion and as an adhesion promoter.

In this study by Bakhshandeh et al.[53], epoxide-silica hybrids were investigated for their ability to prevent corrosion. To create the hybrids, 1 mol of TEOS was put into 3.84 mol of ethanol and 0.5 mol of distilled water. Later, this material was added into water (3:1 molar ratio of water to TEOS). At this point in this process, APTES (3-aminopropyltriethoxysilane) were combined in various amounts (molar ratios of epoxide group to N-H of APTES – 2:1, 4:1, 8:1, and 16:1 ratios). Later, a solution of this modified epoxide in THF was created (25 wt. % silica-modified epoxide). Later, the water/TEOS mixture was added. The final sample sets were tested for FTIR spectra. Also, the TEOS precursors were tested for ^{29}Si NMR. Final sample sets were tested for mechanical properties as well as EIS. The hydrolyzed TEOS precursor showed chemical shifts at -89.98, -95.68, and -96.45 which the researchers attributed to Si-O-Si$(OEt)_3$, cyclic rings (Si-O-Si$(OEt)_2$-O-Si, and linear Si-O-Si $(OEt)_2$-O-Si groups, respectively. The adhesion strength of the coatings showed a positive correlation with TEOS content, but a negative correlation with APTES content. EIS studies were employed with Bode and

Nyquist plots of coated steel panels in 3.5% NaCl for periods up to 45 days. The microhardness values of the coatings went up with increasing APTES and TEOS content in the coatings. The silica domains had the greatest frequency in terms of the 20-40 nm range. The researchers noticed an increase in the corrosion resistance of the coatings with silica content, which they attributed to a silica stratum between the coating and the steel surface.

In the study by Lamaka et al.[54], corrosion-resistant coatings were developed in order to protect AZ31B magnesium alloys from corrosion. The coatings were sol-gel based. The sol-gels were developed from the polymerization of epoxide-siloxane and titanium/zirconium alkoxides. The final coating was 5 microns thick. The coatings were characterized via TEM, SEM, EIS, and XPS. The EIS results indicated that the coatings prevented corrosion in 5 mM NaCl in water for at least 14 days. The corrosion resistance was attributed to the barrier properties provided by the sol-gel content.

In the publication by Zandi-Zand et al.[55], GPTMS underwent a sol-gel reaction (hydrolysis and condensation) in H_2O and HCl (acidic catalyst) and later was crosslinked with Bisphenol A and dip coated on an aluminum surface. Characterization with ATR-IR and SEM showed the development of sol-gel networks on the aluminum surface. Corrosion tests were performed on the coatings, which indicated that the sol-gel coating formed a barrier network with enhanced corrosion resistance.

In the work by Tavandashti et al.[56], GPTMS, TMOS, and aluminum isopropoxide were synthesized together onto boehmite nanoparticles to make sol-gel coatings for

AA2024 aluminum substrates. AFM and SEM were utilized to observe the coatings. The corrosion resistance of the coating systems was measured via EIS and potentiodynamic scanning (PDS). The results indicated an enhancement to the corrosion resistance of the aluminum substrates through passivation (barrier network).

In a second work by Tavandashti et al.[57], GPTMS and TMOS were synthesized together in an acidic aqueous environment to produce sol-gels, which were later dip-coated onto AA2024 aluminum substrates. The water content and stoichiometric amounts of GPTMS and TEOS were varied to determine their effect on the final film and corrosion properties. The coatings were observed via SEM and EDS, and the corrosion protection characteristics were observed via PDS and salt spray tests. The superior corrosion resistance of the film coatings was attributed to the sol-gel passivating layers.

In the publication by Chen et al.[58], nanorods made of boemite (AlOOH) materials were put into a sol-gel coating based from a GPTMS precursor material. The nanorods were added in weight percentages up to 40%. The nanorods were aligned with the coating surface. Enhancements were observed in the indentation crack toughness. The researchers attributed the increase in fracture toughness to the presence of the nanorods, which impeded the growth of the cracks. The GPTMS precursor material also ensured proper dispersion of the nanorods. The GPTMS content also improved the "stress transfer" of the composite, which enhanced the crack toughness.

2.3.1.3 SNAP Coatings

Specific to Class II silica materials are SNAP coatings, which are amine-crosslinked inorganic-organic sol-gel particles utilized as surface preparations on aluminum substrates. The use of SNAP coatings was pioneered by Vreugdenhil et. al.[8] and first reported in 2001. The need for SNAP coatings arose as a non-toxic replacement for existing aircraft coating systems utilizing hexavalent chromium. There are many benefits of using a SNAP sol-gel system. The first is the hydrolytic stability offered by the SNAP sol-gel system coatings. Another benefit is the adhesion strength arising from the bonds between the metal oxide substrate and the SNAP sol-gel surface preparation. A third benefit is the inorganic-organic functionalities of the sol-gel coatings.

SNAP coating systems are depicted in Figure 2.7:

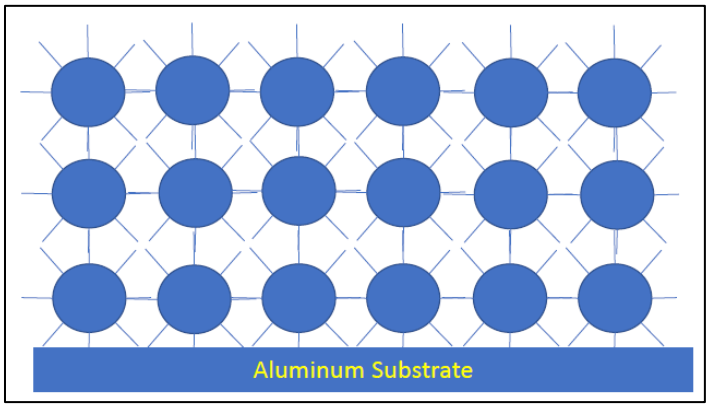

Figure 2.7: Schematic of SNAP Surface Preparation[8]

SNAP particles were formulated by adding a 3:1 molar ratio of 3-glycidyltrimethoxysilane (GPTMS) and tetramethyl orthosilicate into deionized water. The sol-gel reaction was acid-catalyzed with acetic acid. Later, the particles were

crosslinked with diethylenetriamine (DETA), applied to Al 2024-T3 aluminum substrates via immersion, and were set aside to cure for 24 hours. The researchers then tested the coated panels for corrosion resistance via potentiodynamic scanning (PDS) and electrochemical impedance spectroscopy (EIS). The SNAP-coated panels provided enhanced corrosion resistance, which the researchers attributed to higher amounts of epoxide providing enhanced hydrolytic stability as well as proficient barrier and anti-corrosion properties.

Other studies with SNAP coatings consisted of corrosion and weathering testing of SNAP coatings added with organic corrosion inhibitors[59-61], epoxide primers, and polyurethane topcoats[59], formulation of SNAP particles based upon the reaction of tetraethoxysilane (TEOS) and GPTMS[62], crosslinking of SNAP particles with other amine[63-64] and amino-silane crosslinking agents[65], formulation of SNAP particles utilizing TMOS, GPTMS, and methyltrimethoxysilane (MTMOS)[66], insertion of cerium nitrate and zirconia nanoparticle into SNAP particles[67], formulation of SNAP coatings with organosilane materials such as methyltrimethoxysilane (MTMS) and octyltrimethoxysilane (OTMOS)[68], formulation of SNAP coatings with hollow silica nanoparticles[69], testing of oxygen barrier properties when applied upon thermoplastic substrates[70,71], and application of SNAP coatings onto magnesium alloy substrates[72]. In the literature that involved corrosion testing, the researchers noted an enhancement to the corrosion resistance of the SNAP-coated aluminum substrates via passivation.

2.3.1.4 Anti-Corrosion Additives: Sacrificial Metals and Carbon Nanostructures in Epoxide Materials

Besides being loaded with silica based materials, epoxide materials can also be loaded with metals and carbon based structures. In the case of epoxide coatings, the addition of metals can provide sacrificial corrosion protection by corroding before the metal substrate that the coating is placed upon. Carbon based structures such as nanotubes can enhance the mechanical properties of an epoxide composite or coating and can also aid in the corrosion protection of metal substrates. In the next section, the addition of metals to epoxide materials will be discussed. This includes zinc-rich epoxide primers for steel substrates and magnesium-rich epoxide primers for aluminum substrates. Last, the addition of carbon nanotubes will be discussed for epoxide materials and coatings. This will include without and with the presence of sacrificial metals.

2.3.1.4.1 Zinc Based Primers

Zinc based primers are utilized frequently for paints on steel substrates, which includes the exterior surfaces of pipelines, offshore platforms, and bridges.[9] The primers have a solid reputation for longevity and generally last up to a few decades. Zinc based primers generally work by two mechanisms: cathodic protection and passivation. Zinc is a more active metal than iron (main component of steel), so when in contact with a corrosive agent such as water or oxygen the zinc content will corrode first (cathodic protection) by forming an oxide layer. The resulting hydroxide and/or hydroxycarbonate layers act as a protective layer against further infiltration by corrosive

agents. This process is known as passivation. The non-corroded zinc particles can also act as a passivating layer. To provide cathodic protection of the steel substrate, the zinc particles must be physically in contact with other zinc particles as well the substrate. This means that the loading of zinc must be very high (generally at 80% weight loading or greater). Other term for this phenomenon is known as the critical pigment volume concentration (CPVC). To provide cathodic protection of a steel substrate, the zinc loading within paint must have a PVC that is greater than the CPVC. Figure 2.8 shows a cross section of a zinc-based primer.

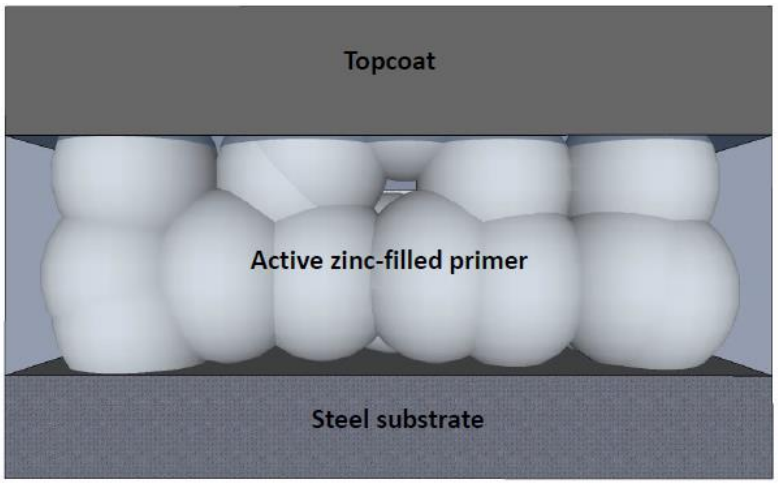

Figure 2.8: Zinc-Based Primer Cross-Section[9]

Two types of powder manufacturing techniques are utilized to produce the zinc powders in zinc-rich primers: distillation or atomization. Atomization based zinc powders generally have sphere-like geometries, while distillation based powders are generally spherical in nature. Zinc based paints can also be classified into two paint classes: zinc primers and zinc-rich primers. Zinc primers generally have lower amounts of loading of zinc (25-70% by weight) and are used for steel substrates located in milder

conditions. In addition, zinc primers are generally intended for shorter amounts of substrate protection (generally 6-12 months). These paints are generally applied at thicknesses of 10-15 microns. Zinc-rich primers have weight loadings that exceed 80%.

Zinc primers can be added to a variety of inorganic and organic binders, which includes solvent-borne and waterborne epoxides. Solvent-borne epoxides are generally cured with polyamides and amine adducts.

To add zinc primers to a steel substrate, the steel must first be blasted to create sufficient adhesion to the substrate. This is generally achieved via blasting to a roughness of 25-45 microns. Afterwards, zinc primers are added to the steel substrates via conventional or airless spraying procedures. After the primer has been added, at least one topcoat is added.

2.3.1.4.2 Magnesium-Rich Coatings

Magnesium-rich primers, like zinc-rich primers, provide cathodic protection of metal substrates. The main difference is that magnesium-rich primers protect aluminum substrates instead of steel substrates. Magnesium is a more active metal than aluminum and hence will act as a sacrificial metal. Due to the need the need to find a suitable, non-toxic replacement for chromate based coating systems that are utilized on airplane aluminum exterior surfaces, a large potential market for magnesium-rich coatings is the military and commercial aerospace industry.

Magnesium-rich coatings were pioneered by Bierwagen et al.[10] as part of an ongoing collaboration between North Dakota State University and the Department of

Defense. The promise as an anti-corrosion coating for aluminum substrates was elucidated in several military reports[74-80] that were later published as academic literature. In addition, Bierwagen et al. and Rawlins et al. have written reviews on the subject.[81-82]

The idea for magnesium-rich coatings arose from magnesium rich primers for aluminum substrates function in the same manner as zinc-rich primers for steel substrates.[10] Primer coatings are loaded with metals that are more active than the substrate they are placed upon. To protect the substrate from corrosion, the metals in the coating, when confronted with an oxidizing/corrosive substance such as oxygen or water, will react to form an oxide instead of the substrate. The resulting oxide that is formed can provide a passivating layer that creates a barrier against permeating corrosive agents.

Drawing upon the work of others, Bierwagen stated that there are several requirements for the provision of cathodic protection of coatings systems.[10,83-84] First, the metal pigment volume concentration (PVC) must exceed the critical pigment volume concentration (CPVC) in order to provide adequate corrosion protection of the substrate. When the PVC is greater than or equal to the CPVC, the pigments are all physically connected and in contact with the steel substrate. Also, the metal pigments must be in physical contact with the substrate, and the pigment must have an anodic potential which exceed that of the anodic potential of the substrate. The coating binder or matrix must be physically and chemically robust enough to hold the pigments, and it

must be able to adhere well to the substrate. Last, the primer coating should have a topcoat to enhance the lifetime of the coating system. The topcoat provides a physical barrier against electrolyte corrosion and physical bombardment.

The researchers utilized a magnesium pigment with an oxide cover to prevent it from premature corrosion.[10] The pigment had a weight content of 96% pure magnesium and 4% magnesium oxide. This mitigated the possibly of magnesium as a fire hazard within the coating systems. The researchers tested the magnesium-rich coatings with electrochemical impedance spectroscopy (EIS) in 3% NaCl and noted three distinct periods of behavior. The first period is noted by an activation of the magnesium metal when in contact sodium chloride. This occurs during the first day of immersion. The second period occurs at Days 5-7 of immersion, and the period is noted by cathodic protection. The third period, which occurs roughly at Day 21 of immersion, is noted by a transition from cathodic protection to oxygen reduction of the magnesium. The oxidation of magnesium will result in a porous layer of magnesium within the magnesium rich primer that provides corrosion protection through passivation.[85] The best protection against corrosion was achieved with a PVC of 46%, which was assumed to be in the range of the CPVC. Comparable results were confirmed by Rawlins et al. in two studies[86-87]; magnesium PVCs of 45% provided the most superior corrosion protection in epoxide coatings.

Besides pure magnesium, magnesium-aluminum alloys can also provide cathodic protection of primer coatings. Work with three different magnesium-aluminum alloys

at various loading levels was completed by Bierwagen et al.[88] An epoxide-polyamide polymeric binder formulation was utilized. Electrochemical impedance spectroscopy (EIS) was utilized as a measure of corrosion during exposure of the various primers to cyclic Prohesion testing. The researchers found that, like magnesium, magnesium-aluminum alloys will also provide cathodic protection to aluminum substrates. In addition, the results also showed that the particle alloy size played a role in the cathodic protection. Smaller particle sizes are superior to larger ones due to their larger surface area.

2.3.1.4.3 Carbon Nanotubes in Epoxide Materials and Coatings

Novel developments in epoxide composites and coatings have resulted in the inclusion of carbon nanotubes. The inclusion of carbon nanotubes has resulted in improvements to the physical properties (i.e. tensile and fracture properties) of the coating system as well as improvements to the corrosion resistance of the epoxide coating. These concepts will be elucidated upon in this section. Attention will be paid strictly to the presence of carbon nanotubes without any metal materials. The first section will be devoted to the mechanical properties of carbon nanotube and epoxide composites, while the second section will be devoted towards the corrosion resistance of epoxide-CNT coatings.

2.3.1.4.3.1 Carbon Nanotubes in Epoxide Materials: Effect on Mechanical Properties

Carbon nanotubes can enhance the mechanical properties of coatings and composites. The mechanical properties include the tensile and fracture properties.[89-100] Carbon nanotubes are mechanically robust and provide molecular interactions that strengthen the film or coating. Also, carbon nanotubes can allay fracture and contribute to the tensile strength/modulus by forming entanglements with the binder. Proper dispersion of carbon nanotubes is imperative for the improvement of the physical properties.[94] In addition, functionalization of carbon nanotubes to the epoxide binder is helpful in improving the mechanical properties of the coating/composite.

In the work by Ganesan et al.[101], the interfacial shear strength and interfacial fracture energy (G_C) were measured for a multi-walled carbon nanotube-DGEBA interface. The carbon nanotubes were functionalized via fluorination. Both values were higher than non-functionalized MWCNT-DGEBA composites. The researchers attributed the enhancement to interlocking of the interfaces as well as electrostatic interactions between the functionalized nanotubes and epoxide.

In the study by Yoonessi et al.[102], carbon nanotubes were functionalized with aromatic, aliphatic, and aliphatic ether diamines. TGA and XPS were utilized to verify that the carbon nanotubes were functionalized. The functionalized CNTs were added into epoxide formulations in 0.1 wt. % ratios and were tested for mechanical and thermal properties. The storage modulus (DMA) increased by 190% when measured below the glass transition temperature and a 400% increase in the storage modulus

above the glass transition temperature. The aromatic diamine system created the greatest enhancement to the shear modulus at all levels and greatest enhancement to the glass transition temperature. The researchers also reported an increase in the interfacial adhesion strength between the epoxide matrix and CNT. They attributed this increase to covalent bonding.

In the work by Brancato et al.[103], the researchers functionalized multi-walled carbon nanotubes with either carboxylic groups or amino groups and loaded them into epoxide resins. Non-functionalized carbon nanotubes were utilized as a comparison. Low amounts of carbon nanotubes (0.2%-0.4%) results in increases to the mechanical properties for both functionalized and non-functionalized carbon nanotubes, which includes the flexural stress and fracture strain. The researchers determined that the improvement in mechanical properties was due to the thorough dispersion of the nanotubes in the epoxide. Higher amounts of carbon nanotube loading, particularly non-functionalized carbon nanotube loading of 0.8 wt. %, result in a decrease in the mechanical properties because of fragility. The amino-functionalized carbon nanotubes increased the glass transition temperature, which non-functionalized carbon nanotubes had a slightly negative effect.

In the work by Ya et al.[104], single-walled carbon nanotubes (SWCNTs) were loaded into epoxide resins via sonication and tested for mechanical properties. The researchers found that 0.5% wt. carbon nanotube loading achieved the best properties, which diminished before and after this loading threshold. The composites were tested

for tensile properties. Electron microscope imaging of the fractured tensile specimens indicated a debonding effect took place between interfacial epoxide surrounding the carbon nanotubes and the matrix epoxide prior to fracture.

In the publication by Tsuda et al.[105], composite sheets made of aligned carbon nanotubes and epoxides were processed. Distinct types of composites were made by varying the carbon nanotube content. The researchers utilized scanning electron microscopy to determine the alignment of carbon nanotubes within the epoxide matrix. They noted a substantial increase in the tensile strength and Young's modulus with carbon nanotube loading, indicating that the most enhanced mechanical properties were observed at carbon nanotube volume fractions of 32.8 volume %. The researchers also noted that orientation/alignment of the carbon nanotubes was necessary for the improvement of the mechanical properties of the composites.

In the work by Li et al.[106], composite films created from epoxides and carbon nanotubes were created from chemical vapor deposition (CVD). The researchers measured tensile strengths and toughness values for the films of 405 MPa and 122 J/g, respectively. This is a 74% increase of the toughness when compared to conventional CNT loading methods. The researchers noted that the carbon nanotubes formed a lamellar network in the epoxide matrix, which improved the mechanical properties of the system.

In the study by Opelt et al.[107], fillers such as carbon nanotubes or alumina were added into epoxide resins and tested for tensile and fracture properties. The fillers

were added in using weight percentages of 0.15%, 0.5%, or 1.5%. The researchers observed increases in all mechanical properties, with the most enhanced properties observed at 0.5% CNT loading (17% increase in the elastic modulus and 22% increase in tensile strength). The researchers also observed the fracture phenomena that led to fracture (crack bridging – pull out for epoxide/CNT composite materials).

In the work by Ma et al.[108], carbon nanotubes were aligned in epoxide with the help of Ni catalyst particles. The glass transition temperature, fracture toughness, and electrical properties of the composites were measured. The fracture toughness increased for composites aligned and unaligned with the composite. The greatest enhancements to the composite in terms of fracture toughness were achieved with 3 wt. % loading of carbon nanotubes transversely aligned to the propagation of the crack.

In the study by Sul et al.[109], MWCNTs were added into epoxide systems and measured for thermal properties via DSC, TGA, and DMA. 0.1 and 1 wt. % MWCNTs were added into the epoxide systems. The storage modulus of the systems increased while the glass transition temperature decreased. The DSC results indicated that the amount of unreacted epoxide increases with the weight percentage of carbon nanotubes in the system. The researchers concluded that the carbon nanotubes contributed to a reduction in the crosslink density of the epoxide system.

In the work by Hsieh et al.[110], epoxides cured with anhydrides were loaded with MWCNTs. The dispersion was measured via FEG-SEM. The fracture parameters of the systems increased from 133 to 223 J/m^2 (fracture energy) when going from neat

epoxide to 0.5 wt. % carbon nanotubes. In addition, the strain energy release rate went from 24 J/m^2 for neat epoxide to 73 J/m^2 for the same carbon nanotube loaded system. The researchers noticed that debonding, nanotube pull-out, and void propagation contributed to the fracture propagation. The first two phenomena gave the greatest contribution to the fracture toughness.

In the work by Park et al.[111], MWCNTs were functionalized via oxidation and amidation and were added to DGEBF epoxide resin formulations. The formulations were later tested for dispersion, rheology, and fracture toughness. Dispersion was easier with functionalized carbon nanotubes. The aminated MWCNT formulation had the longest gel time. The best fracture toughness values were observed with the aminated CNT formulations, which the researchers attributed to a proper degree of dispersion of CNTs in the epoxide matrix.

2.3.1.4.3.2 The Use of Carbon Nanotubes in Epoxide Coatings to Enhance the Corrosion Resistance

Several researchers have explored the idea of using carbon nanotubes in epoxide coatings order to prevent salt water corrosion of metal substrates. There are several reasons why. Carbon nanotubes reduce the porosity of epoxide coatings and hence reduce the water uptake into epoxide coatings. In addition, researchers have observed that carbon nanotubes contribute to hydrophobicity. The next section will discuss the use of carbon nanotubes in epoxide coatings. Sacrificial metal content is not included.

In the publication by Khun et al.[112], EIS tests were completed on epoxide coatings with MWCNT content. The coatings were placed on AA 2024-T3 metal surfaces. EIS tests indicated that MWCNT content increased the impedance by shrinking the porosity of the coating. In the work by Baltzis et al.[168], carbon nanotubes were added to epoxide coating systems and then applied onto SS304 stainless steel or carbon-reinforced SS304 stainless steel. When tested for corrosion properties, the researchers discovered that the presence of carbon nanotubes enhanced the galvanic effect but also were effective in mitigating corrosion.

In the study by Jeon et al.[113], epoxide coatings were loaded with MWCNTs and their effect on the hydrophobicity and water transport properties were observed. The coatings were tested via hygrothermal cyclic tests and EIS. The addition of carbon nanotubes result in a transition from hydrophiblic to hydrophobic surfaces. In addition, the water uptake of the epoxide coatings was lower when carbon nanotubes were added to the coatings. This contributed to an increase in the corrosion resistance in the coating systems, as confirmed via EIS.

In a study by Shen et al.[114], MWCNTs were added into epoxide resins and then added onto carbon steel via electrostatic spraying. The coatings were quantified via FTIR, SEM, electrochemical impedance spectroscopy, and potentiodynamic polarization curves. The corrosion resistance of the coatings was improved when compared to bare steel. The best corrosion resistance was observed with 2 wt. % carbon nanotubes.

In a work by Gkikas et al.[115], the researchers added MWCNTs into epoxide-based aerospace adhesives. The questions they set out to answer were how the MWCNTS affected the electrochemical characteristics of the adhesive, if MWCNTs contributed or mitigated galvanic corrosion of the aluminum substrate, and the macroscopic effects of MWCNTS on coating degradation. The researchers found that adding 0.1 wt. % MWCNTs into epoxides can mitigate the galvanic corrosion phenomenon between the aluminum substrate and the epoxide matrix. 0.5 wt. % MWCNTs will increase it. The researchers attributed this to a "percolation threshold" somewhere between 0.1 and 0.5 wt. % MWCNTs. They found that the ability of MWCNTs to prevent corrosion is an effect of the binder matrix, curing agent, and method in which the coating was placed on the substrate.

2.3.1.4.3.3 The Use of Carbon Nanotubes and Metal Content in Epoxide Coatings to Aid in Corrosion Resistance

The use of carbon nanotubes and sacrificial metal content is a novel way to prevent corrosion resistance in epoxide coatings. As explained earlier, cathodic corrosion protection requires the connectivity between sacrificial metal particles. The disadvantage is that the sacrificial metal particles must be loaded into a primer at very high levels to provide proper corrosion protection, which weakens the primer mechanically and augments the porosity. Multiple topcoats are required to create an effective barrier. The use of carbon nanotubes can enhance the corrosion resistance by providing linkages between the sacrificial metals. Due to the geometries of carbon nanotubes (high aspect ratio), the presence of carbon nanotubes can enhance the

barrier properties of the coating system, which in turn hinders corrosion protection. Furthermore, the carbon nanotubes can maintain the corrosion resistance of the coating system if some of the sacrificial metal content is removed. Last, the coating is strengthened by the addition of carbon nanotubes.

In a publication by Castaneda et al.[116], less than 1 wt. % carbon nanotubes were added into Zn-rich epoxide systems with zinc content ranging from 60 to 90 wt. % in 10 wt. % increments. The coatings were placed on carbon steel and tested for corrosion resistance in the presence of chloride ions. The carbon nanotubes provided corrosion protection because of the barrier properties (60 wt. % zinc), cathodic protection, and Faradaic phenomena at 70 wt. % zinc, and cathodic protection only at 80 and 90 wt. % zinc. A control formulation consisting of 70 wt. % zinc only (no CNTs). No cathodic protection was observed. The researchers concluded that carbon nanotubes are instrumental in providing cathodic protection by acting as linkages between zinc particles and the substrate. At 80 and 90 wt. % zinc, cathodic protection of the substrate was the main source of corrosion protection.

Park et al.[117] also found evidence of cathodic protection of steel substrates by zinc-CNT epoxide-polyamide coatings. Carbon nanotubes and zinc were added into epoxide-polyamide coatings in ratios of 20%, 40%, and 60% for zinc and 0%, 0.1%, and 0.25 wt. % for MWCNTs. The coating systems were tested for corrosion and coating properties. The researchers found that higher amounts of CNTs resulted in augmented conductivity, which they attributed to cathodic protection of the substrate by the zinc

sacrificial metal. The presence of MWCNTs contributed to higher adhesion strengths, and corrosion was mitigated with the presence of zinc and MWCNTs.

In the study of Gergely et al.[118], epoxide coatings were tested via EIS, GD OES, XPS, and FT-Raman spectroscopy. The corrosion results indicated better galvanic corrosion protection and barrier properties than the zinc-rich epoxide paints by themselves. The researchers theorized that the corrosion protection provided by the MWCNTs was due to galvanic corrosion protection and electrical percolation. A second publication by Gergely et al.[119] confirmed the same corrosion protection mechanisms when tested with Zn-rich epoxide paint coatings doped with PPy/alumina/MWCNTs composite particles.

In the study by Yi et al.[120], MWCTs were functionalized to form MWCNT-COOH. Later, the aluminum oxide particles were grafted to the surface of the nanotubes. A composite film was created by varying the amount of pristine MWCNTs and aluminum oxide coated MWCNTs and placing them in epoxide coatings. Later, the flexibility and corrosion resistance of the coatings systems were tested. The results indicated that aluminum oxide coated MWCNTs in epoxide coatings are enhanced in terms of their corrosion resistance but limited in their flexibility.

CHAPTER III

FORMULATION AND EVALUATION OF CROSSLINKED EPOXIDE-POLYSULFIDE FILMS AND COATINGS

3.1 Introduction

As noted in Chapter 2, epoxide materials are widely used in the coatings industry. Epoxide materials are noted for having superior adhesion characteristics, thermal properties, and for being able to crosslink with a variety of curatives. The downside of epoxide materials is limited flexibility and fracture toughness.[121] In order to improve the flexibility and fracture properties of the materials, low molecular weight polysulfides are often blended with epoxides. During the blending process, the epoxides and polysulfides undergo co-polymerization. After curing with a crosslinker, the result is an epoxide-polysulfide, a phase-separated material consisting of a continuous epoxide phase and dispersed polysulfide elastomer phase. The material is more flexible and resistant to fracture.

Because of the flexibility and fracture toughness of the materials, epoxide-polysulfide are currently used in a variety of applications, such as sealants for aircraft,

windows, construction, and other areas. The enhanced damage tolerance and flexibility of the materials is which makes such formulations useful as sealants for metal substrates with unusual geometries.[4] Many researchers have also focused on the mechanical properties of polysulfides, polysulfide formulations, and polysulfide based polymers.[5,24-29,122-126] In these publications, the researchers noted improvements in tensile properties (specifically the elongation behavior), coating adhesion strength, fracture properties, and corrosion resistance.

Damage tolerance and flexibility are important attributes for epoxide-polysulfide materials, especially since epoxide-polysulfides are used as sealant materials for unusual geometries on airplanes. Airplane exteriors are exposed to a wide range of temperatures and weather events, and therefore the coating materials must remain resilient over time to these types of conditions. While mechanical properties such as tensile strength and elongation are useful for measuring weatherability, tensile fracture properties are a better method of measuring the long-term damage tolerance of coating materials because the tensile fracture properties are synergistic in nature and therefore relatable to other coating properties (adhesion strength, impact resistance, hardness, and modulus). Since epoxide-polysulfide coatings are exposed to a wide variety of exterior temperatures (exterior aircraft temperatures can range from -55°C in the air to 60°C on the ground)[127-129], it would be useful to determine the performance of epoxide-polysulfides at the extremes of this temperature range. The tensile fracture properties of epoxide-polysulfides have only been discussed by a few researchers, and fracture property testing of epoxide-polysulfides at different temperatures has not yet been

attempted. Also, the exact relationship between the tensile fracture properties and other coating properties has not been ascertained for epoxide-polysulfides. To give an example, would the addition of polysulfide content to an epoxide affect the fracture properties of the material at various temperatures, and would an increase in the fracture toughness translate to an increase in the adhesion strength?

To answer these questions, the adhesion strength, reverse impact strength, fracture toughness (K_{IC}) and the elastic energy release rate (G_{IC}) at temperatures of -55, 20, and 60°C, tensile properties such as the tensile strength, elastic modulus, and the elongation-at-break percentage (%), pendulum hardness, and corrosion coating barrier properties via electrochemical impedance spectroscopy (EIS) were measured for epoxide-polysulfide coatings. Each epoxide-polysulfide was also tested for thermal properties (glass transition, storage modulus) via DMA. The listed properties were measured as functions of the polysulfide content, which was varied between 5 and 20 weight % in increments of 5 weight %. Two distinct types of polysulfide were used, which varied in terms of the molecular weight and the length of the backbone and side chains. The aim of this study is to determine:

1. To determine the performance characteristics of epoxide-polysulfides on aircraft, how does polysulfide content affect the fracture properties of epoxide-polysulfides at low, ambient, and elevated temperatures?

2. What are the dynamic mechanical thermal performance characteristics of epoxide-polysulfides at the same temperatures, and how do they relate to the epoxide-polysulfides?
3. What are the conventional coating properties of the epoxide-polysulfides (adhesion strength, tensile properties, corrosion resistance), are these properties a function of the polysulfide content, and how are these properties relatable to the tensile fracture properties?
4. Does the molecular weight of the polysulfide play a role in the fracture properties?

3.2 Experimental Section

3.2.1 Materials

Epon 828 (DGEBA) was utilized as the epoxide for the experiment and was purchased from Hexion. Ancamide 702B75 (polyamide curative) was purchased from Air Products. G4 and G112, the two polysulfides utilized for the experiments, were donated by Akzo-Nobel. Hydrobromic acid (HBr), acetic acid, potassium acid phthalate (Pht), methyl violet indicator, and methyl isobutylketone (MIBK), the materials utilized to measure the epoxide equivalent weight, were purchased from Sigma Aldrich. All materials were used as received.

The G4 and G112 polysulfide molecular structures are shown in Figure 3.1.

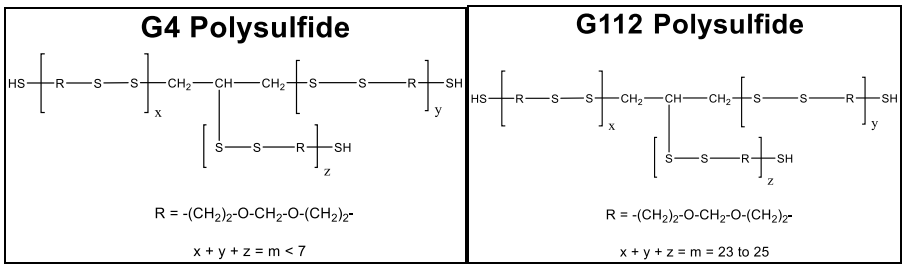

Figure 3.1: G4 and G112 Polysulfide Molecular Structures[130-131]

The molecular structure of Epon 828 is shown in Figure 3.2.

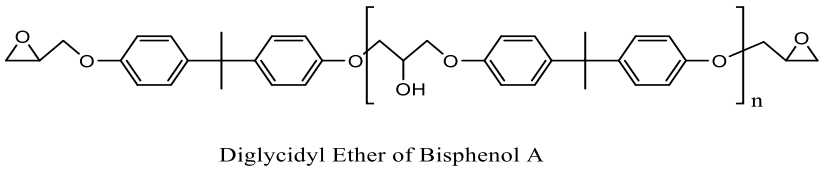

Figure 3.2: Diglycidyl Ether of Bisphenol A Molecular Structure[6,132]

3.2.2 Formulation of G4 Epoxide-Polysulfides

G4 epoxide-polysulfides were synthesized by adding varying amounts of Epon 828 and G4 liquid polysulfide. Four distinct types of G4 epoxide-polysulfides were created by varying the weight percentage of G4 from 5 to 20 weight percent in increments of 5%. The weights of each component are listed in grams in Table 3.1. Neat epoxide was used as a control.

Table 3.1: G4 Epoxide-Polysulfide Resin Formulations

Formulation	Name	Epon 828 (g)	G4 Polysulfide (g)
1	Epoxide Only	50.0	0.0
2	5% G4	47.5	2.5
3	10% G4	45.0	5.0
4	15% G4	42.5	7.5
5	20% G4	40.0	10.0

Epon 828 and G4 polysulfide were put into 250-mL round bottomed flasks and stirred for 3 hours at 200 rpm and with a temperature of 50°C. The contents were stirred via a magnetic stir bar and Corning magnetic hot plate. Afterwards, the epoxide-polysulfides were placed into sealed polypropylene containers and stored under ambient conditions for 2 weeks to allow for the epoxide-polysulfides to react to completion.

3.2.3 Formulation of G112 Epoxide-Polysulfides

G112 epoxide-polysulfides were synthesized by adding varying amounts of Epon 828 to G112 liquid polysulfides. Four distinct types of G112 epoxide-polysulfides were created by varying the weight percentage of G112 from 5 to 20 weight percent in increments of 5%. The weights of each component are listed in grams in Table 3.2. Neat epoxide was used as a control.

Table 3.2: G112 Epoxide-Polysulfide Resin Formulations

Formulation	Name	Epon 828 (g)	G112 Polysulfide (g)
1	Epoxide Only	50.0	0.0
2	5% G112	47.5	2.5
3	10% G112	45.0	5.0
4	15% G112	42.5	7.5
5	20% G112	40.0	10.0

Epon 828 and G112 polysulfide were put into 250-mL round bottomed flasks and stirred for 3 hours at 200 rpm and with a temperature of 50°C. The contents were stirred via a magnetic stir bar and Corning magnetic hot plate. Afterwards, the epoxide-polysulfides were placed into sealed polypropylene containers and stored under

ambient conditions for 2 weeks to allow for the epoxide-polysulfides to completely react.

3.2.4 Determination of Epoxide Equivalent Weight of Epoxies and Epoxide-Polysulfides

The epoxide equivalent weights of the epoxides, epoxide-polysulfides, and Ancamide 702B75 were measured according to Tex-815-B, which is a modification of ASTM D1652 and D2074.[133-135] Potassium acid phthalate was used as a standard, and hydrobromic acid was used as the analyte. The epoxide equivalent weights (EEW) or amine equivalent weight (AEW) of the neat epoxide, epoxide-polysulfides, and Ancamide 702B75 are listed in Table 3.3.

Table 3.3: Epoxide Equivalent Weights of Resins

Name	EEW/AEW
Epoxide Only	212.8
5% G4	214.4
10% G4	240.5
15% G4	255.5
20% G4	280.6
5% G112	213.6
10% G112	222.5
15% G112	254.2
20% G112	253.6
Ancamide 702B75	170.0

3.2.5 Formulation of Polyamide Crosslinked Epoxides and Epoxide-Polysulfides

Neat epoxide and G4 and G112 epoxide-polysulfides, based upon the epoxide equivalent weight, were mixed with varying amounts of Ancamide 702B75 via a Thinky mixer for 5 minutes at 2,000 revolutions per minute. Afterwards, the formulations were cast onto either PET plastic substrates or 2024 12” x 3” aluminum substrates at wet film

thicknesses of 5 mils. They were set aside to cure for one week before use. The amounts of epoxide or epoxide-polysulfide and the Ancamide 702B75 used for each formulation is indicated in Table 3.4

Table 3.4: Crosslinked Epoxide and Epoxide-Polysulfide Formulations

Name	Base Amount (g)	Ancamide 702B75 (g)
Epoxide Only	40.0	32.0
5% G4	40.0	31.7
10% G4	40.0	28.3
15% G4	40.0	26.6
20% G4	40.0	24.2
5% G112	40.0	31.8
10% G112	40.0	30.6
15% G112	40.0	26.8
20% G112	40.0	26.8

Once cured, the films were removed from the PET film substrate via a metal blade and later tested for DMA, tensile, and fracture properties. The films that were cast onto aluminum substrates were tested for pendulum hardness, pull-off adhesion strength, and electrochemical impedance spectroscopy tests.

3.2.6 SEM Studies of Epoxide-Polysulfide Coatings

SEM studies were completed for crosslinked neat epoxide, G4 epoxide-polysulfide coatings, and G112 epoxide-polysulfide coatings. The coatings were initially cast onto PET substrates and removed manually via a blade. The coating tops were sputter coated and later investigated for epoxide and polysulfide domains via a FEI-Philips Model Tecnai T12T Scanning Transmission Electron Microscope (STEM) using 10,000X magnification.

3.2.7 Thermal-Viscoelastic Measurements via Dynamic Mechanical Analysis

Dynamic mechanical thermal analysis of the crosslinked epoxide-polysulfide films was conducted via dynamic mechanical thermal analysis (DMTA) (TA Instruments Q800 Model). The dynamic mechanical thermal analyzer exposed a 30 mm x 6 mm x 0.2 mm sample to temperatures of -60 degrees Celsius to 150 degrees Celsius at a heating rate of 3 degrees Celsius per minute. The DMTA tests exposed the sample to a cyclic strain of 0.1%. The DSC measured the heat flux versus the temperature, while the DMTA measured the storage modulus (E'), loss modulus (E"), and tangent δ as functions of the temperature. The storage moduli and glass transition temperatures measured via E', E", and tangent δ were later plotted as a function of the polysulfide wt. %.

The DMTA tests exposed the sample to a cyclic strain of 0.1%. The DSC measured the heat flux versus the temperature, while the DMTA measured the storage modulus (E'). In addition, the DMTA determined the crosslink density of the samples, which was determined by the following equation[84]:

$$\nu_e = \frac{E'}{3RT} \qquad 4.2$$

The crosslink density ν_e is the number of moles of elasticity effective network chains per mL of material. The term E' describes the storage modulus in the rubbery region (measured at a temperature of 130 degrees Celsius or 403 Kelvin), the term T is the temperature (in Kelvin) at which the storage modulus was measured, and R is the gas constant. 3 samples were tested per sample set for both DSC and DMTA. Generally,

heating a sample at rates of 2-3 degrees Celsius per minute are acceptable for most polymeric materials.

3.2.8 Tensile Testing of Crosslinked Epoxide and Epoxide-Polysulfide Films

Tensile tests were conducted were conducted via a Linkam tensile testing machine utilizing a 200 N load cell. The tensile samples were rectangular and had dimensions of 30 mm x 10 mm x 0.1 mm. The Linkam device employed an extension speed of 1 mm/min. The tensile strength and elongation % were measured directly by the Linkam tensile tester, while the elastic modulus was measured by analyzing the linear portions of the stress vs. strain curves. The tensile strength and elastic modulus were measured in units of MPa, and the elongation at break was measured in %. 10 samples were tested per sample set.

3.2.9 Pull-Off Adhesion Testing of Crosslinked Epoxide-Polysulfide Materials

The pull-off adhesion tests were completed according to ASTM D7234.[136] A DeFelsko PosiTest AT-A automatic pull-off adhesion tester was used with 20 mm wide adhesive buttons with epoxide glue. Five samples were utilized for the experiment.

3.2.10 Reverse Impact Tests

A TGSC impact tester was utilized to test G4 based epoxide-polysulfides and neat epoxide-polyamide coatings on 2024 aluminum substrates for reverse impact tests. The units were reported in kg/cm. The results were reported as the highest values that did not result in a visible rupture of the coating from the substrate.

3.2.11 Fracture Toughness Testing of Crosslinked Epoxide and Epoxide-Polysulfide Films

Fracture toughness tests were conducted via a Linkam tensile testing machine utilizing a 200 N load cell. The Instron and fracture toughness testing machine both employed extension rates of 1 mm per minute. The fracture toughness samples were rectangular in nature and had dimensions of 30 mm x 10 mm x 0.1 mm. A notch was cut into each fracture toughness sample via a blade. The notches were approximately 1 mm long and 1 mm wide.

The fracture toughness (K_{IC}) of the sample was calculated via the following equation[136,137]:

$$K_{IC} = \sqrt{3.94\left(\frac{2w}{\pi a}\right)\tan\left(\frac{\pi a}{2w}\right)}\sqrt{a}\left(\frac{F}{[w-a]b}\right) \qquad 3.1$$

The variable "w" signifies the width of the sample, the variable "a" signifies the notch length, the variable "b" signifies the thickness, and the variable "F" signifies the force required to propagate the size of the notch.

The planar energy release rate per unit crack area (G_{IC}) at fracture was indicated by the equation below[136,137]:

$$G_{IC} = \frac{K_{IC}^2}{E} \qquad 3.2$$

The term K_{IC} indicates the planar fracture toughness, and the term E indicates the elastic modulus during sample testing.

The variable K_{IC} was measured in units of MPa*$m^{0.5}$, and the variable G_{IC} was measured in units of J/m^2. Fracture toughness tests were employed at -55°C, 20°C and at 60°C.

3.2.12 Contact Angle Tests

Contact angle tests on crosslinked neat epoxide and G4 epoxide-polysulfides were performed with a VGA Optima (AST Industries). DI water was utilized as the test solvent. Five samples were taken per test. The angle measurements were measured manually via the computer software. The tops of the films were tested for the contact angle via a drop volume of 2 microliters.

3.2.13 Electrochemical Impedance Spectroscopy (EIS) Tests

Electrochemical impedance spectroscopy (EIS) tests were carried out by immersing coated areas of the panel in sea water (3.5% NaCl). The EIS tests incorporated three electrodes. A saturated calomel electrode was incorporated as a reference electrode, a platinum mesh was incorporated as a counter electrode, and the coating surface was incorporated as the working electrode. A Zive SP1 apparatus utilized frequencies ranging from 100 kHz to 10 MHz, and it utilized an alternating current (AC) and an open current potential. The voltage utilized was 10 mV (RMS). The immersed coating area (working electrode) was 1.76 cm^2, and a clamp and glass cylindrical tube was utilized to hold in the sea water.[139] The software was utilized to create Nyquist and Bode plots at Day 30 of immersion as well as the impedance modulus at 1 Hz versus the day of immersion (0, 2, 5, 10, 20, and 30 days).

The EIS measurements were also used to measure the water uptake versus the day of immersion. The water uptake percentage is measured by the Brasher-Kingsbury Equation[140]:

$$\phi = \frac{\log(C_t/C_0)}{\log 80} \qquad 3.3$$

The variable C_t is the coating capacitance at time t, and the variable C_0 is the capacitance at time 0.

Figure 3.3 shows the setup for the electrochemical impedance spectroscopy apparatus.

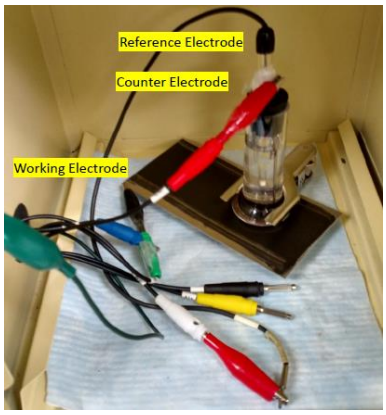

Figure 3.3: Electrochemical Impedance Spectroscopy Setup[139]

3.3 Results

3.3.1 Reaction of Epoxide-Polysulfides

The reaction of the epoxide-polysulfides proceeded as follows. Under mixing and heat, diglycidal ether of bisphenol A (Epon 828) underwent copolymerization with G4 or G112 polysulfides via an oxirane ring opening reaction and bonding with the thiol end and side groups on the polysulfides. Later, the unopened oxirane end groups underwent a crosslinking reaction

with the polyamide. Figure 3.4 shows the proposed copolymerization scheme of the epoxide and polysulfide, while Figure 3.5 shows the proposed crosslinking reaction of the oxirane end group to the polyamide (for simplicity, a generic polyamide is shown).

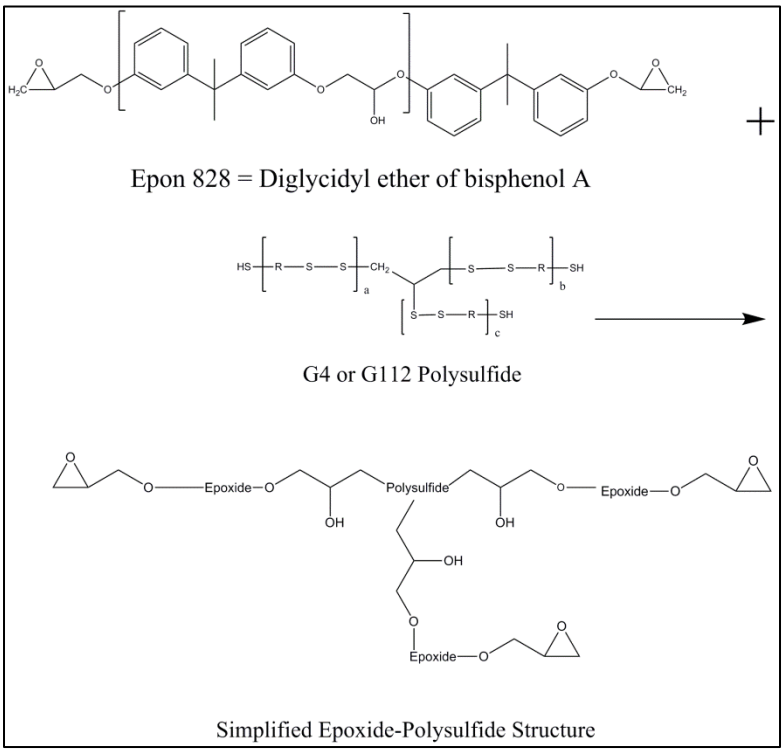

Figure 3.4: Copolymerization of DGEBA Epoxide and G4/G112 Elastomeric Polysulfide

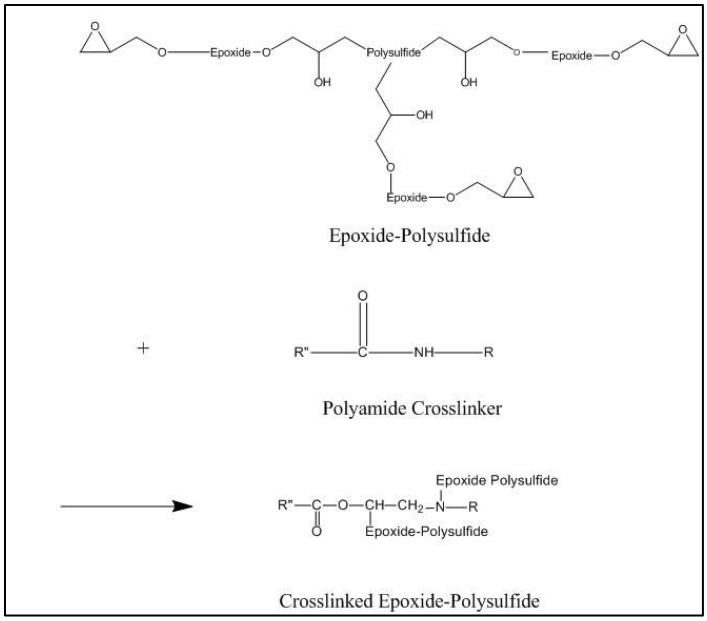

Figure 3.5: Epoxide-Polysulfide Crosslinking Reaction with a Polyamide

3.3.2 SEM Studies of G4 and G112 Epoxide-Polysulfides

SEM pictures of neat epoxide and G4 epoxide-polysulfides are shown in Figure 3.6. Neat epoxide shows minimal roughness, while epoxide-polysulfides show increasing amounts of polysulfide "globule" phases present on the surface and isolated from the continuous epoxide phase compromising the rest of the surface.[141] Unlike past literature, the globules do not increase in size with polysulfide content (remaining on average from 1 to a few microns in size), but rather comprise an increasing amount of the surface of the sample. The increasing size of the collective polysulfide phases would later contribute to more flexible, malleable samples with higher elongation and lower moduli and toughness.

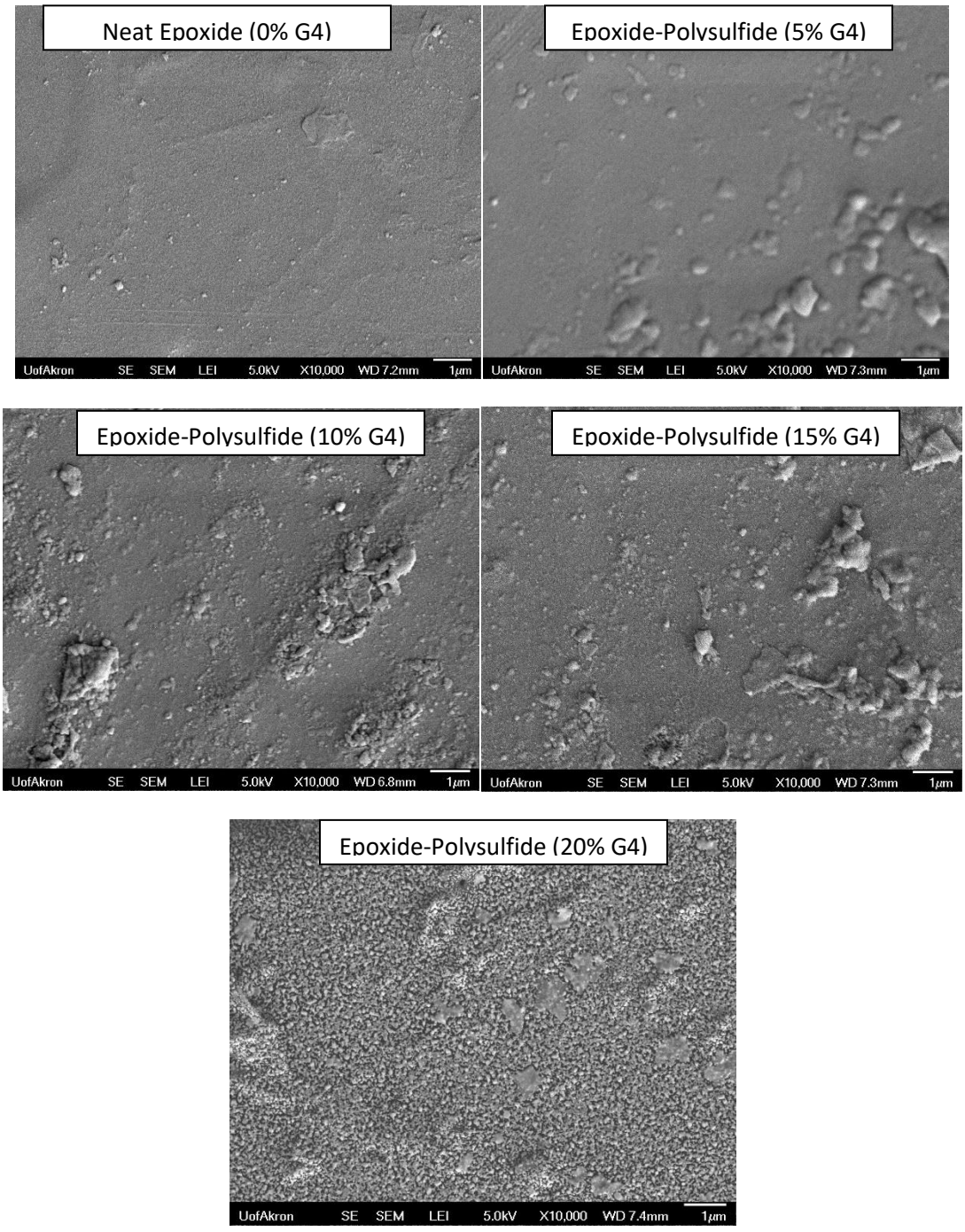

Figure 3.6: SEM Pictures of Neat Epoxide and G4 Epoxide-Polysulfides

SEM pictures of the G112 epoxide-polysulfides are shown in Figure 3.7.

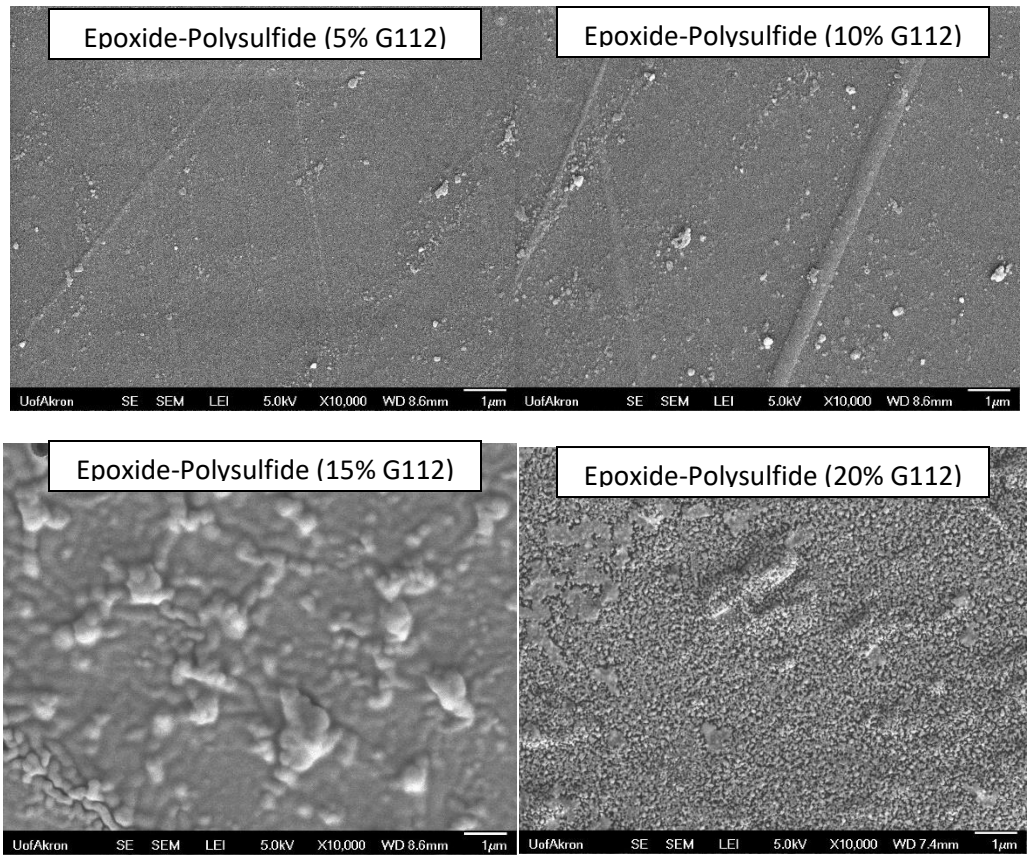

Figure 3.7: SEM Pictures of G112 Epoxide-Polysulfides

Like the G4 epoxide-polysulfides, the presence of the G112 polysulfide results in isolated polysulfide phases that become larger with greater polysulfide content. The size of the individual globules is unrelated to the amount of polysulfide content.

The presence of a two-phase system marked by isolated phases of polysulfide encompassed by the epoxide matrix matches results observed in literature (Figure 3.8).

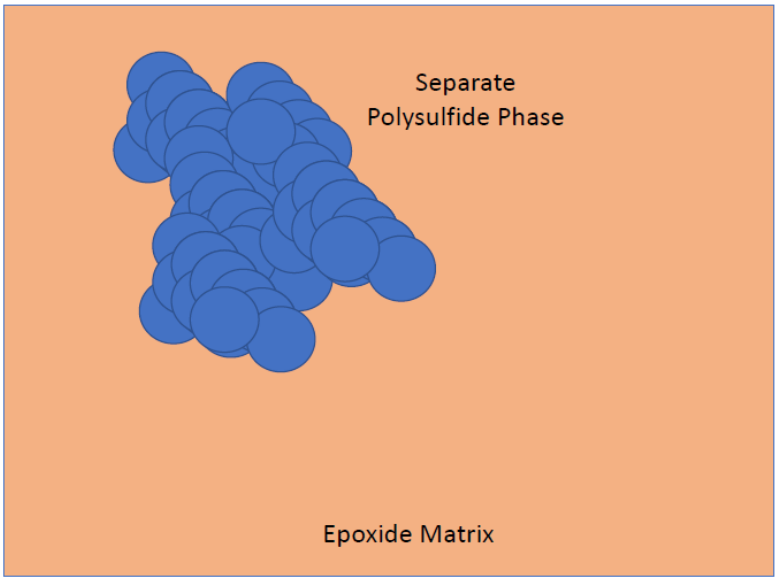

Figure 3.8: Epoxy-Polysulfide Two-Phase Structure[141]

3.3.3 DMA Thermal-Mechanical Properties of Crosslinked Epoxide and Epoxide-Polysulfide Films

Several parameters were tested via DMTA testing. The storage modulus of each type of G4 epoxide-polysulfide is shown in Figure 3.9. The average storage modulus is measured at -55°C, 20°C, and 60°C as a function of the G4 polysulfide wt. %. At each temperature, there is an increase in the storage modulus to a maximum at 5-10% G4 polysulfide before decreasing to below the average storage modulus of the neat epoxide. This indicates epoxide-polysulfide toughening at low levels of polysulfide content.

The storage modulus is a measure of the stiffness of the material that is tested via dynamic mechanical analysis. At low tensile forces and within the realm of elastic deformation, it is equivalent/relatable to the elastic modulus (also a measure of the

stiffness of a viscoelastic material). The loss modulus is related to the release of energy of a material undergoing a cyclic stress. This energy is removed as heat and is unrecoverable. Tangent delta indicates the ratio of the loss modulus to the storage modulus. A large tangent delta means that the material is stiffer, while a smaller tangent delta means that the material is more malleable and ductile.

The storage modulus is on the same level as reported with epoxide-polysulfides in past literature[6,142], although the increase in the storage modulus at low polysulfide levels deviates from past literature (which indicated a reduction in the storage modulus with the addition of polysulfide).[6] The toughening effect is due to the addition of polysulfide aliphatic chains, which at low levels form a larger molecule without a subsequent reduction in crosslink density. Other researchers attributed the increase in stiffness to the bonding of the thiol groups in the polysulfide oligomers to the polar groups in the epoxide oligomers.[143] At higher levels, the larger amount of polysulfide content contributes to larger rubber phases in the continuous epoxide matrix, reducing the internal stresses of the system and therefore the storage modulus.[29] As expected, there is a reduction in the storage modulus at higher temperatures, since it has been well-established that the stiffness of a polymeric film decreases at higher temperatures.

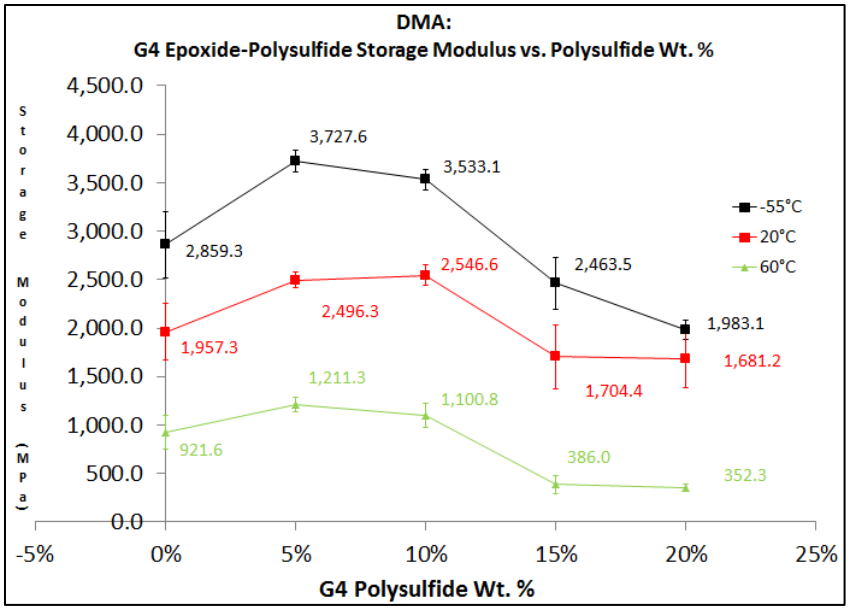

Figure 3.9: Average Storage Moduli vs. G4 Polysulfide Wt. %

The average storage modulus of the G112 epoxide-polysulfide films is shown in Figure 3.10. The average storage modulus is plotted as a function of the G112 polysulfide wt. %. Like the G4 epoxide-polysulfides, the G112 epoxide-polysulfides show toughening at low levels of polysulfide content. The G112 epoxide-polysulfides are at levels comparable to the G4 epoxide-polysulfide, which is in agreement with past literature.[6]

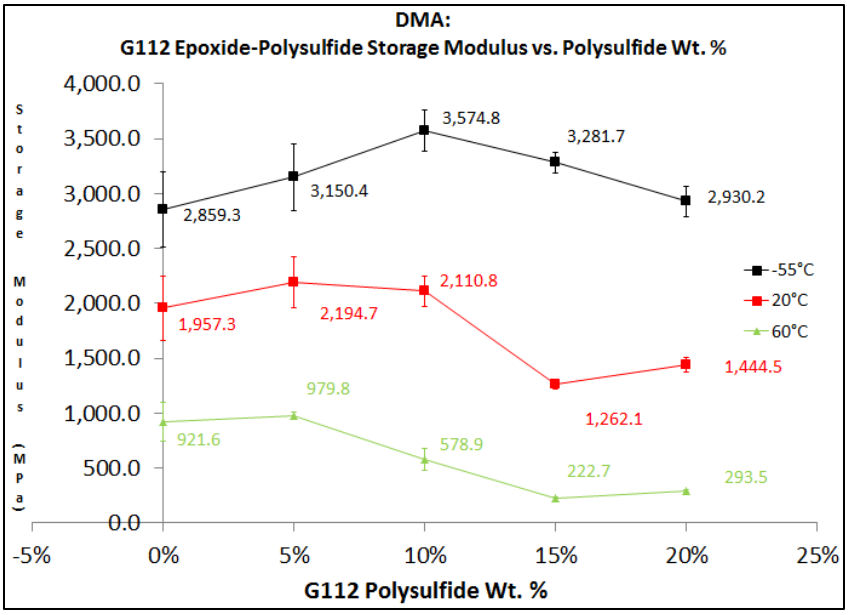

Figure 3.10: Average Storage Moduli vs. G112 Polysulfide Wt. %

The average storage moduli of the G4 epoxide-polysulfides as a function of the temperature are shown in Figure 3.11. The average storage moduli decrease as a function of the temperature. The same phenomenon is exhibited for G112 epoxide-polysulfides (Figure 3.12).

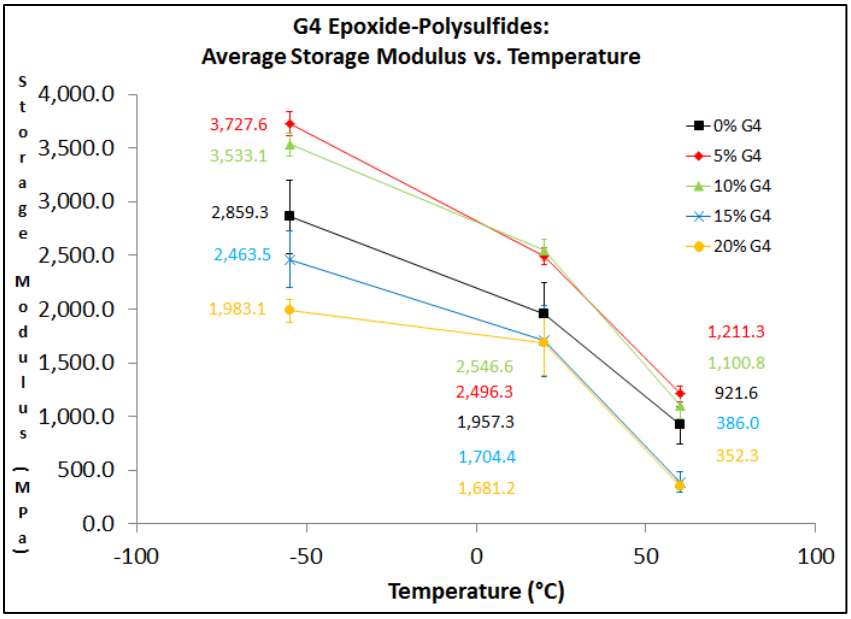

Figure 3.11: Average Storage Modulus vs. Temperature (G4 Epoxide-Polysulfides)

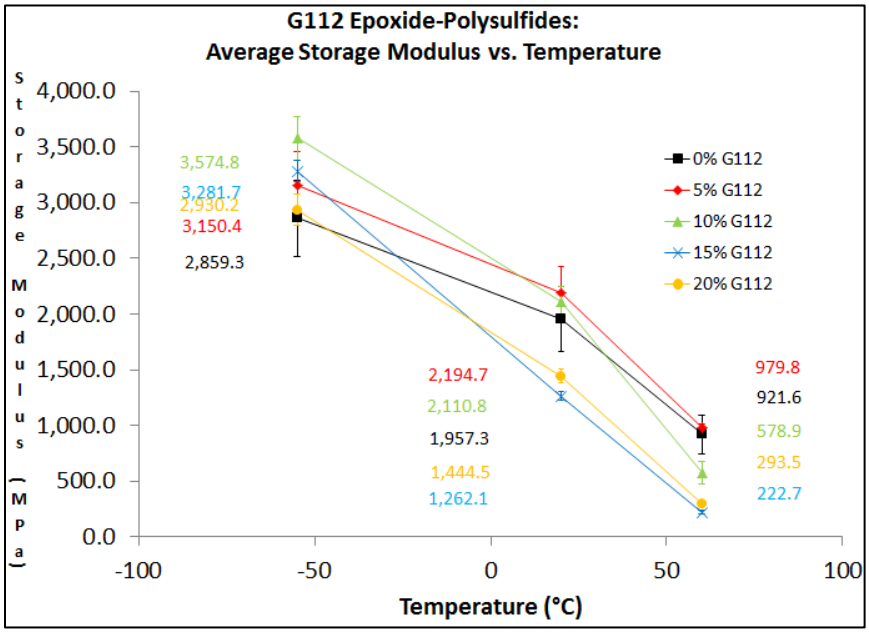

Figure 3.12: Average Storage Modulus vs. Temperature (G112 Epoxide-Polysulfides)

The glass transition temperature of viscoelastic materials can be measured via dynamic mechanical analysis. This is done by measuring changes in the storage modulus (a measure of the film's stored energy or elasticity), the loss modulus (a measure of the

film's released energy or viscosity), and tangent δ (δ is the ratio between the loss and storage moduli). The average glass transition temperature of the G4 and G112 epoxide-polysulfides is shown in Figure 3.13. The average glass transition temperature is plotted as a function of the polysulfide wt. %.

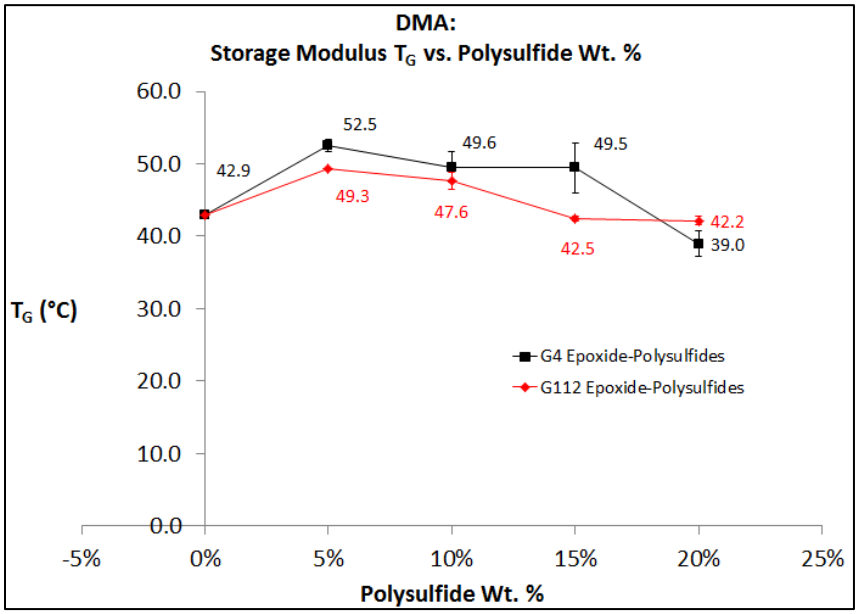

Figure 3.13: Storage Modulus T_G vs. Polysulfide Wt. %

The average glass transition temperature of neat epoxide is 42.9°C. Both types of epoxide-polysulfides show an increase in the glass transition temperature to a maximum at 5% polysulfide wt. There are marginal decreases in the glass transition temperature thereafter. At 15-20% polysulfide, the glass transition temperature decreases to below the glass transition temperature of neat epoxide. The decrease in the glass transition temperature at 15-20% polysulfide is due to the lower glass transition temperature of the polysulfide domain and the lower levels of epoxide. It is notable that at lower levels of polysulfide (5-10%), there is an increase in the glass

transition temperature concurrent with higher storage moduli. In addition, the toughening phenomenon (longer aliphatic chain without a reduction in the crosslink density) at 5-10% wt. polysulfide leads to increases in the glass transition temperature.

The average glass transition temperature as measured by the loss modulus is plotted in Figure 3.14. The average glass transition temperature is plotted as a function of the polysulfide wt. %.

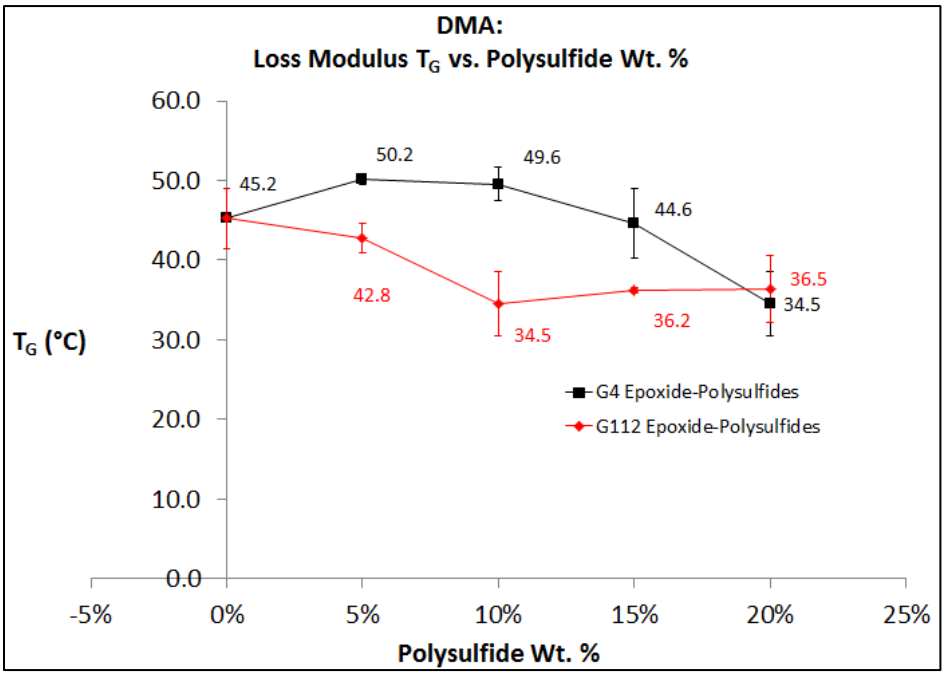

Figure 3.14: Loss Modulus T_G vs. Polysulfide Wt. %

Like the storage moduli, there is an increase in the G4 epoxide-polysulfide glass transition temperature until a maximum at 5-10 polysulfide wt. %. The G112 epoxide-polysulfide glass transition temperature decreases to a minimum at 10% wt. polysulfide at stays level at larger polysulfide wt. %s. The decrease in the G112 epoxide-polysulfide might be related to the larger side chains existent in the G112 polysulfide domain.

The glass transition temperatures measured by the tangent δ are shown in Figure 3.15. The average glass temperatures are plotted as a function of the polysulfide wt. %.

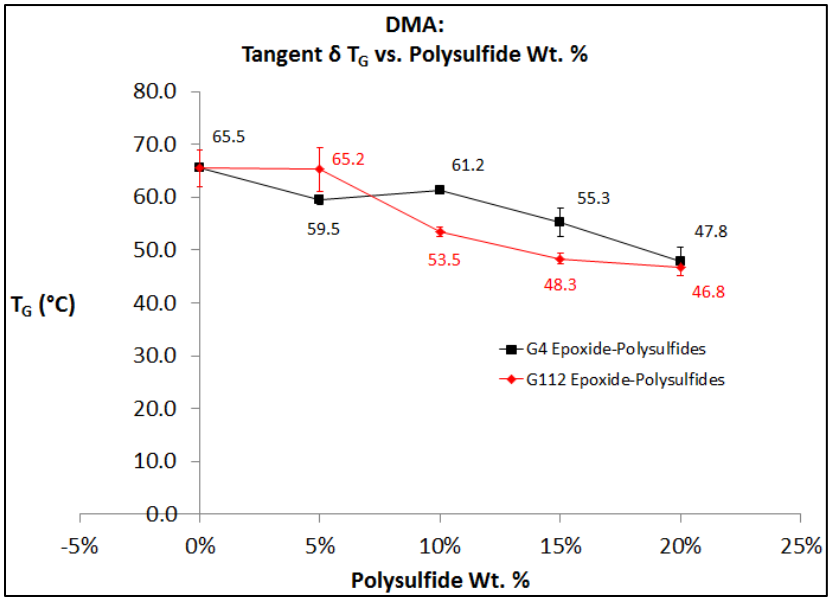

Figure 3.15: Tangent δ T_G vs. Polysulfide Wt. %

The glass transition temperature decreases as the polysulfide wt. % increases. This is concurrent with past literature that indicates a decrease in the glass transition temperature with increasing polysulfide content.[143] The polysulfide domain generally has a lower glass transition temperature due to the elastomeric, more flexible nature of the domain as compared to the rigid epoxide.[26] It is notable that past literature with the same base materials (G4 and Epon 828) indicated glass transition temperatures that were significantly higher (100°C), although an amine hardener with a significantly higher amine equivalent weight (4 times higher than the epoxide) was used instead of a polyamide.[6] As noted from the literature, the glass transition temperature reported by

tangent δ is always higher than the glass transition temperature measured by the loss modulus.[144]

It should also be noted that additional peaks corresponding to the polysulfide glass transition temperature were found for films with higher levels of polysulfide content. The temperatures are indicated in Table 3.5. This is in agreement with past literature and is indicative of the two-phase system inherent in epoxide-polysulfides.[27]

Table 3.5: List of Polysulfide T_G Values

Name	Type of Polysulfide	Polysulfide %	SM T_G 1 Onset Avg (°C)	LM T_G 1 Onset Avg (°C)	Tan δ T_G 1 Onset Avg (°C)
EP1	None	0%	NA	NA	NA
EP2	G4	5%	NA	NA	NA
EP3	G4	10%	NA	NA	NA
EP4	G4	15%	-39.5	NA	NA
EP5	G4	20%	-42.9	NA	NA
EP6	G112	5%	NA	NA	NA
EP7	G112	10%	-53.5	NA	NA
EP8	G112	15%	-49.5	-52.0	-51.1
EP9	G112	20%	-50.0	-52.5	-51.8

The crosslink densities of the neat epoxide and epoxide-polysulfides measured via DMA are shown in Figure 3.16.

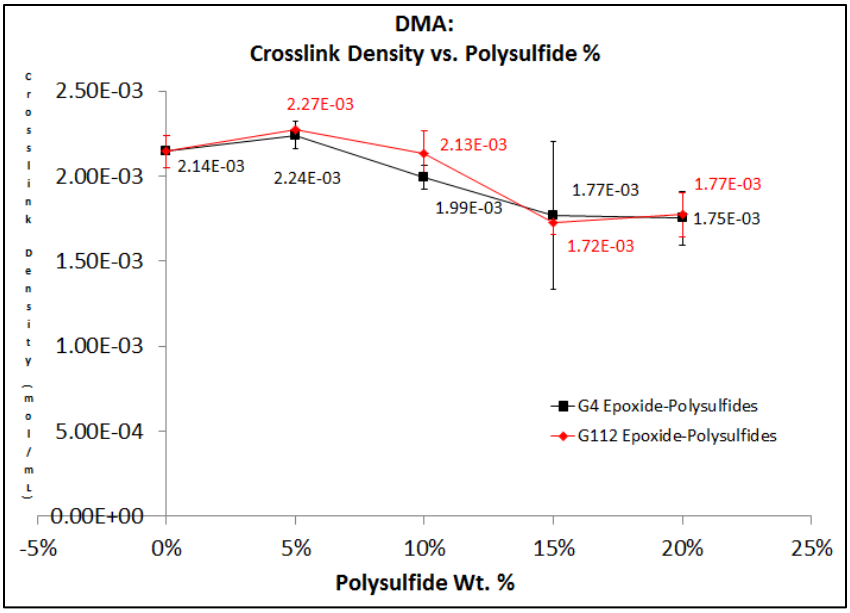

Figure 3.16: Crosslink Densities of Neat Epoxide and Epoxide Polysulfides

There is little change in the crosslink density from 0% polysulfide to 10% polysulfide, after which there is a decrease. The decrease is attributed to the presence of unreacted thiol groups and the steric hindrance of the polysulfide content preventing the reaction of epoxides. The effect is minimal at lower amounts of polysulfide content. The larger copolymer that results from the effect of polysulfide content as well as the elastomeric properties of the polysulfides contribute to a concomitant increase in the dynamic modulus, elastic modulus, and elongation of the sample, allowing for a tougher and more flexible film.

3.3.4 Tensile Properties of Crosslinked Epoxide and Epoxide-Polysulfide Films

The crosslinked epoxide and epoxide-polysulfide films were tested for tensile properties, specifically the tensile strength, elongation %, and elastic modulus. The tensile strengths of the G4 epoxide-polysulfides versus the polysulfide % are shown in

Figure 3.17. The tensile strength is plotted as a function of the G4 polysulfide wt. %. Neat epoxide-polyamide films have an average tensile strength of 18.9 MPa, and there is a 34% increase in the tensile strength to 24.4 MPa at 5 wt. % G4. The tensile strength decreases to 16.3 MPa at a polysulfide % of 20%. The increase in the tensile strength is due to the toughening of the epoxide with the addition of small levels of polysulfide %. As elucidated in past literature[29], the epoxide-polysulfides show interesting phenomena when compared to neat epoxide. It is uncommon for a material to show a concomitant increase in the tensile strength and the elongation at break. The polysulfide rubber content in the epoxide-polysulfide material decrease the "internal stresses"[5] normally present within rigid crosslinked neat epoxide. The subsequent decrease in the tensile strength beyond 5% G4 was due to the larger polysulfide rubber content as well as the decrease in the crosslink density due to the polysulfide content.[5]

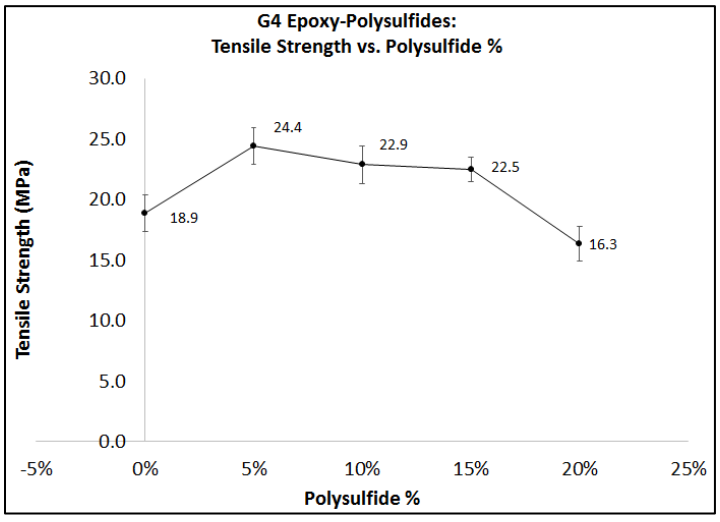

Figure 3.17: Tensile Strength of G4 Epoxide-Polysulfides vs. Polysulfide Wt. %

The G4 epoxide-polysulfide tensile strength 2-sample T p-value are listed in Table 3.6. The 5% and 15% sample sets are significantly different from the neat epoxide sample set.

Table 3.6: G4 Tensile Strength 2-Sample T P-Value Results

Name	Polysulfide Weight %	2-Sample T P-Value from Control	Significant?
5% G4	5%	0.044	Yes
10% G4	10%	0.284	No
15% G4	15%	0.005	Yes
20% G4	20%	0.253	No

The elongations at break percentages of the G4 epoxide-polysulfides are shown in Figure 3.18. The elongation % is plotted as function of the polysulfide weight %. Neat epoxide-polyamide films have an elongation at break % of 2.8%, and with the addition of 5% G4 there is a 3-fold increase to 8.1% elongation. This is due to the flexibility of the G4 polysulfide content, which is greater than the epoxide domain. The slight reduction of the elongation at break may be due to unreacted thiol groups.[143]

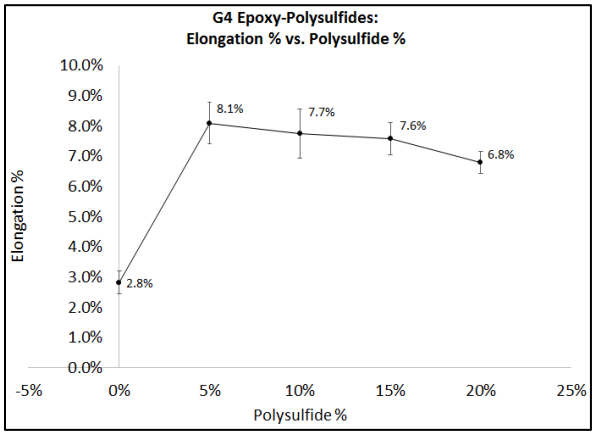

Figure 3.18: Elongation-at-Break % vs. Polysulfide Wt. % (G4 Epoxide-Polysulfides)

The G4 epoxide-polysulfide elongation at break 2-sample T results are listed in Table 3.7. The 5%, 15%, and 20% G4 sample sets are significantly different from the neat epoxide sample set.

Table 3.7: G4 Elongation at Break 2-Sample T P-Value Results

Name	Polysulfide Weight %	2-Sample T P-Value from Control	Significant?
5% G4	5%	0.000	Yes
10% G4	10%	0.115	No
15% G4	15%	0.000	Yes
20% G4	20%	0.000	Yes

The elastic moduli of the G4 epoxide-polysulfides are plotted versus the polysulfide weight % are shown in Figure 3.19. The elastic modulus at 0% polysulfide is 1,843 MPa. There is a modest increase to 2,163.1 MPa at a polysulfide % of 10%. There is a steep decrease to 1,175.4 MPa at 20% polysulfide. The increase in the elastic modulus is due to the bonding of the thiol end groups of the polysulfide group and the polar end groups of the epoxide.[143] A further increase in the polysulfide content reduces the crosslink density, which reduces the modulus.

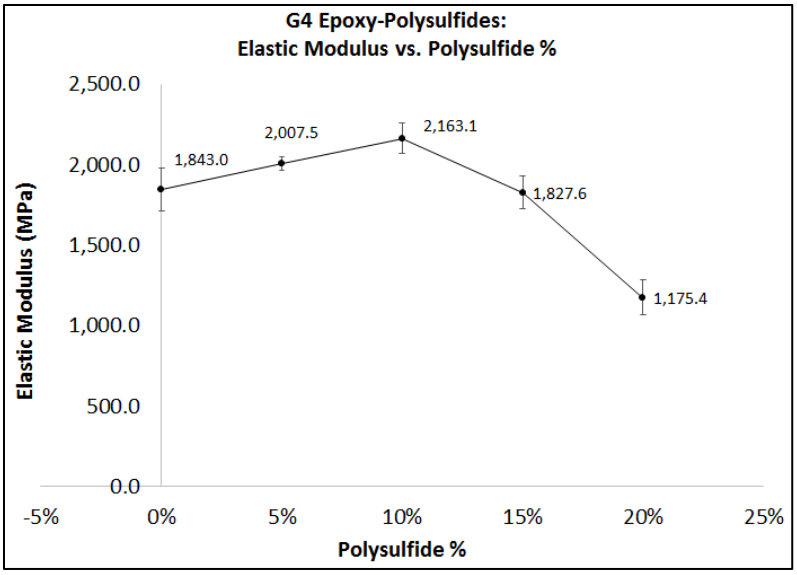

Figure 3.19: Elastic Modulus vs. Polysulfide Wt. % (G4 Epoxide-Polysulfides)

The G4 epoxide-polysulfide elastic modulus 2-sample T results are listed in Table 3.8. The only significantly different sample set is the 20% G4 sample set.

Table 3.8: G4 Elastic Modulus 2-Sample T P-Value Results

Name	Polysulfide Weight %	2-Sample T P-Value from Control	Significant?
5% G4	5%	0.517	No
10% G4	10%	0.127	No
15% G4	15%	0.655	No
20% G4	20%	0.001	Yes

The tensile strengths of the G112 based epoxide-polysulfides are plotted in Figure 3.20. The tensile strength is plotted as a function of the G112 polysulfide %. There is a 35% increase in the tensile strength from neat epoxide-polyamide films to 10% G112 polysulfide. There is a steep decrease in the tensile strength at 15% and 20% polysulfide. The same phenomenon occurs with G112 epoxide-polysulfides. The tensile strength values are roughly in line with the values of the G4 epoxide-polysulfides.

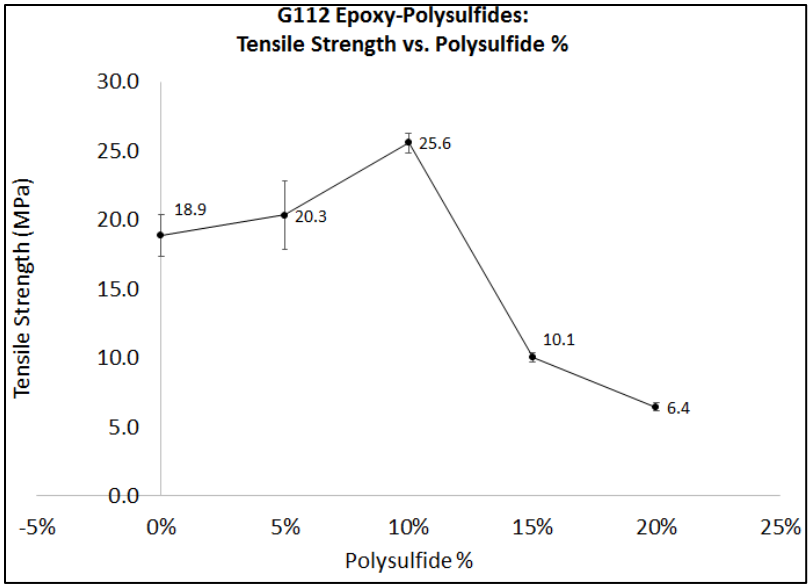

Figure 3.20: Tensile Strengths vs. Polysulfide Wt. % (G112 Epoxide-Polysulfides)

The G112 epoxide-polysulfide tensile strength 2-sample T results are listed in Table 3.9. All sample sets show a significant difference.

Table 3.9: G112 Tensile Strength 2-Sample T P-Value Results

Name	Polysulfide Weight %	2-Sample T P-Value from Control	Significant?
5% G112	5%	0.815	Yes
10% G112	10%	0.003	Yes
15% G112	15%	0.001	Yes
20% G112	20%	0.000	Yes

The epoxide-polysulfide elongation at break % is plotted in Figure 3.21 as a function of the G112 polysulfide content. There is a minimal increase in the elongation %, but the increase is minimal considering the range of error. At 15% and 20% polysulfide content, there is a steep reduction in the elongation at break %. The smaller elongation percentages are at odds with the conventional wisdom that longer side chains lead to greater amounts of physical polymeric entanglements and higher elongation percentages. As mentioned in past literature[145], the reduction in the

elongation at break may be due to unreacted thiol groups. The larger molecular content and steric hindrance of the G112 polysulfide domain may hinder the copolymerization reactions, resulting in a greater reduction in the elongation at break than the G4 epoxide-polysulfides.

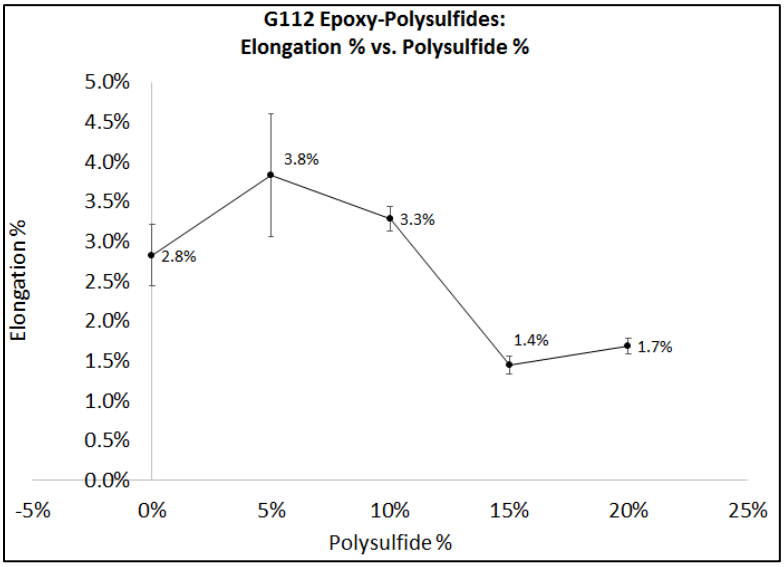

Figure 3.21: Elongation-at-Break % vs. Polysulfide Wt. % (G112 Epoxide-Polysulfides)

The G112 epoxide-polysulfide elongation at break 2-sample T results are listed in Table 3.10. The 15% and 20% G112 sample sets show a significant difference.

Table 3.10: G112 Elongation at Break 2-Sample T P-Value Results

Name	Polysulfide Weight %	2-Sample T P-Value from Control	Significant?
5% G112	5%	0.295	No
10% G112	10%	0.309	No
15% G112	15%	0.018	Yes
20% G112	20%	0.035	Yes

The epoxide polysulfide elastic modulus as a function of the G112 polysulfide content is plotted in Figure 3.22. There is a modest, statistically insignificant increase in the elastic modulus from neat epoxide-polyamide films up to 10% polysulfide content.

There is a steep decrease of the elastic modulus from 10% polysulfide content to 15% and 20%. The behavior of the elastic moduli correlates with previous experiments with the G4 epoxide-polysulfides.

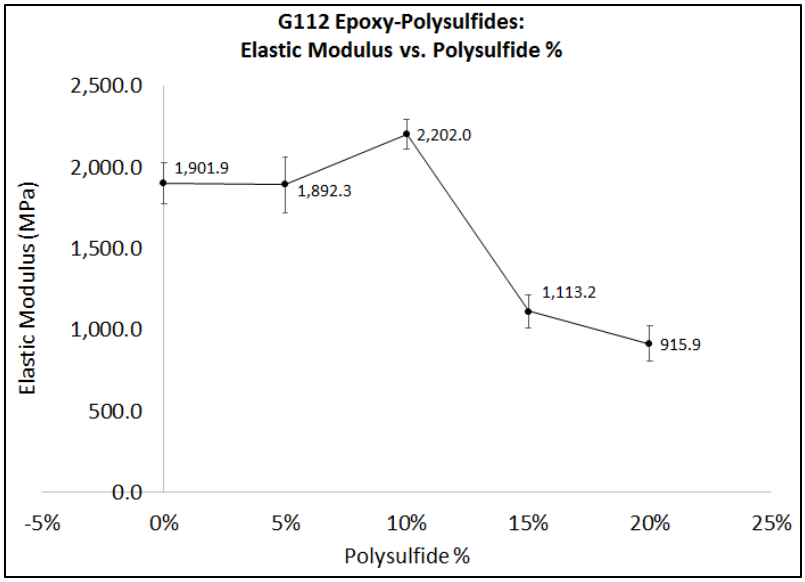

Figure 3.22: Elastic Modulus vs. Polysulfide Wt. % (G112 Epoxide-Polysulfides)

The G112 epoxide-polysulfide elastic modulus 2-sample T results are listed in Table 3.11. The 15% and 20% G112 sample sets show a significant difference.

Table 3.11: G112 Elastic Modulus 2-Sample T P-Value Results

Name	Polysulfide Weight %	2-Sample T P-Value from Control	Significant?
5% G112	5%	0.964	No
10% G112	10%	0.094	No
15% G112	15%	0.001	Yes
20% G112	20%	0.000	Yes

3.3.5 Adhesion Strength of Crosslinked Epoxide and Epoxide-Polysulfide Coatings

The adhesion strengths of the G4 epoxide-polysulfides are plotted in Figure 3.23 as a function of the G4 polysulfide content. There is a gradual increase in the adhesion

strength from 0% G4 (neat epoxide-polyamide coating) to 20% G4. The adhesion strength at 20% G4 is 435 psi, which is 40% greater than neat epoxide-polyamides (311.4 psi). This is confirmed by past researchers[145], who noted a continuous increase in adhesion strength until 30 wt. % polysulfide. The researchers attributed the increase in adhesion strength to augmented "wetting" and "polarity" of the material because of the presence of the polysulfide material.

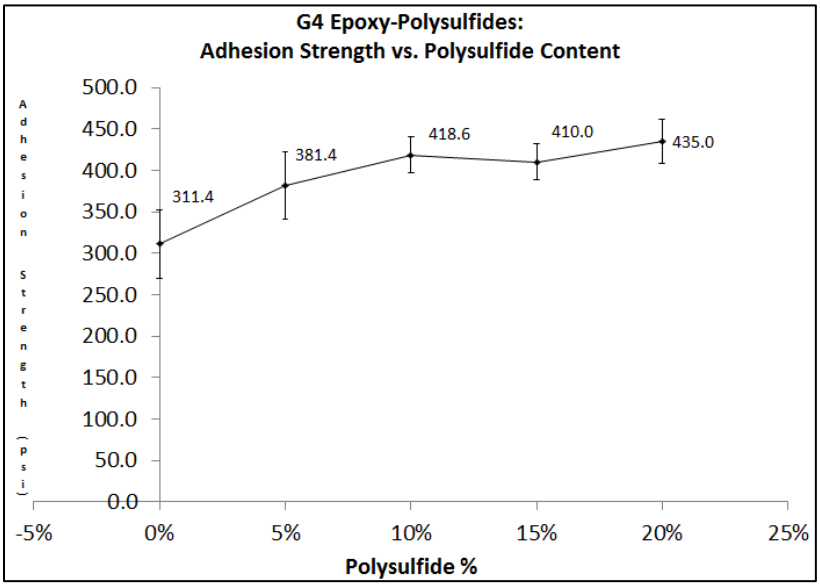

Figure 3.23: Adhesion Strength vs. Polysulfide Wt. % (G4 Epoxide-Polysulfides)

The pull-off adhesion strength 2-sample T results of the G4 epoxide-polysulfide films are listed in Table 3.12. Only the 20% G4 sample set is significantly different from the neat epoxide film set.

Table 3.12: G4 Pull-Off Adhesion 2-Sample T P-Value Results

Name	Polysulfide Weight %	2-Sample T P-Value from Control	Significant?
5% G4	5%	0.261	No
10% G4	10%	0.062	No
15% G4	15%	0.083	No
20% G4	20%	0.041	Yes

3.3.6 Reverse Impact Strengths of G4 Epoxide Polysulfides

The reverse impact strengths of the G4 epoxide polysulfides are shown in Figure 3.24, which indicate that there is an increase with the addition of G4 polysulfide content. At 15% polysulfide content, there a four-fold increase in the average reverse impact resistance. This is due to the increased flexibility of the polysulfide polymeric units and the enhanced adhesion strength of the epoxide-polysulfides. According to past researchers, the augmentation of impact strength is also due to the increased flexibility from the presence of polysulfide content.[6] As noted from the SEM results, the polysulfide phases delay the fracture and rupture of the epoxide-polysulfide from the metal substrate.

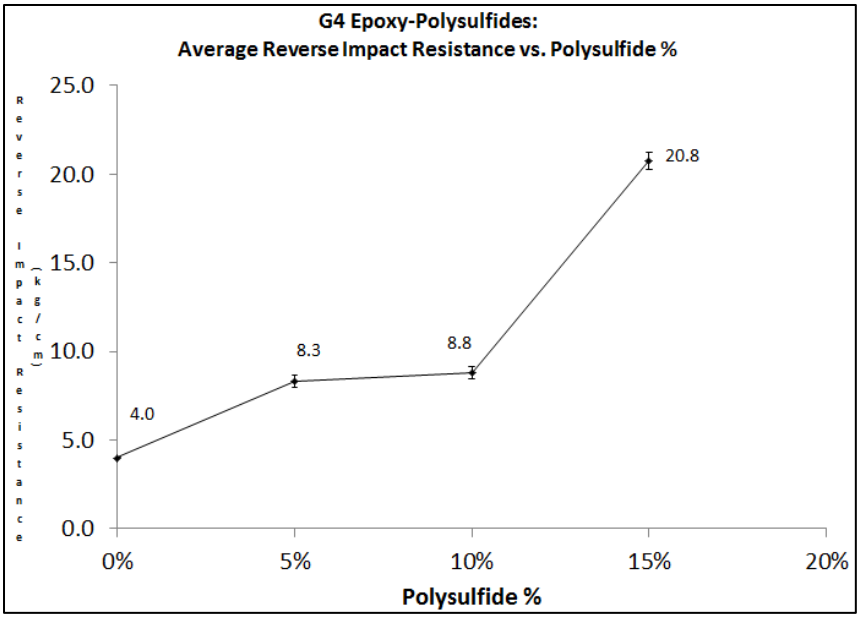

Figure 3.24: Reverse Impact Strengths vs. Polysulfide Wt. % (G4 Epoxide-Polysulfides)

The reverse impact 2-sample T results of the G4 epoxide-polysulfide films are listed in Table 3.13. All three sample sets are significantly different than the neat epoxide film set.

Table 3.13: G4 Reverse Impact 2-Sample T P-Value Results

Name	Polysulfide Weight %	2-Sample T P-Value from Control	Significant?
5% G4	5%	0.006	Yes
10% G4	10%	0.004	Yes
15% G4	15%	0.000	Yes

3.3.7 Fracture Properties of the Crosslinked Epoxide and Epoxide-Polysulfide Films

The K_{IC} at -55°C as a function of the G4 polysulfide content is plotted in Figure 3.25. There is an almost two-fold increase in the average K_{IC} to a maximum of 1.218 MPa*$m^{0.5}$ at a G4 polysulfide content of 10%. Afterwards, the fracture toughness decreases to 0.932 MPa*$m^{0.5}$ at a G4 polysulfide content of 20%. This is attributed to

the higher dynamic/elastic moduli and elongation %s of G4 epoxide-polysulfides. It is notable that the fracture toughness behavior at -55°C is like the behavior at 20°C, indicating that the epoxide-polysulfides will have the same damage tolerance at lower temperatures. Also, the fracture behavior agrees with the tensile strength behavior, indicating that the two parameters are closely related in terms of damage tolerance. Other researchers indicated that the increase in toughness is due to "crazing, shear bonding, and elastic deformation."[5] This arises from the presence of polysulfide rubber content in the continuous epoxide binder material. The polysulfide phases delay complete fracture of the material that would otherwise occur for the rigid epoxide matrix.

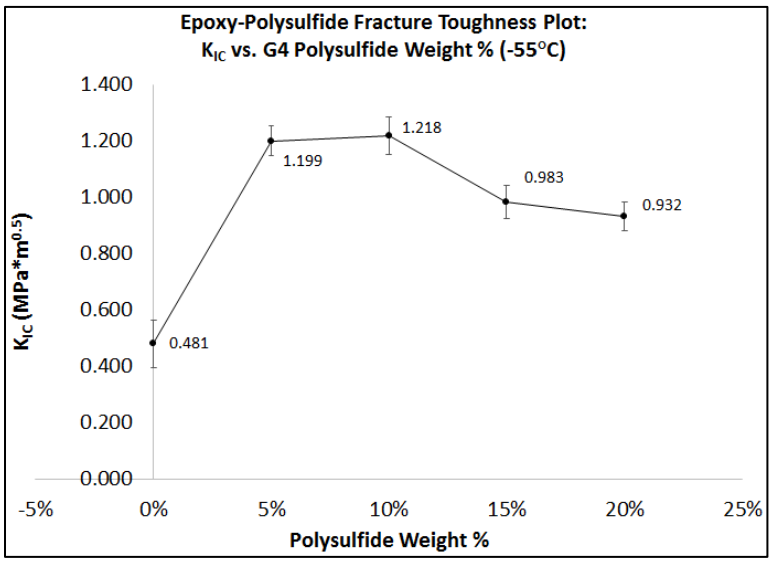

Figure 3.25: Average K_{IC} at -55°C vs. Polysulfide Wt. % (G4 Epoxide-Polysulfides)

The K_C 2-sample T results for the G4 epoxide-polysulfide films at -55°C are listed in Table 3.14. All sample sets are significantly different from the neat epoxide film set.

Table 3.14: G4 K_C at 55°C 2-Sample T P-Value Results

Name	Temperature (°C)	Polysulfide Weight %	2-Sample T P-Value from Control	Significant?
5% G4	-55	5%	0.006	Yes
10% G4	-55	10%	0.002	Yes
15% G4	-55	15%	0.008	Yes
20% G4	-55	20%	0.020	Yes

The G_{IC} at -55°C as a function of the G4 polysulfide content is plotted in Figure 3.26. The increase in the G_{IC} at lower temperatures is credited to the ability of the G4 polysulfide polymeric component to enhance the flexibility and moduli at lower temperatures. It is also in line with the assertions of past researchers that the fracture energy is "directly related" to the polysulfide content in the system.[29]

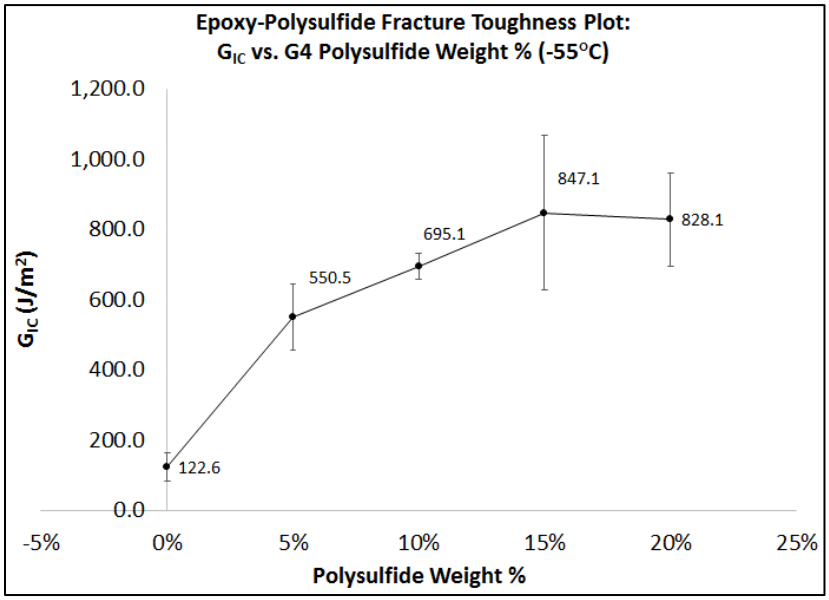

Figure 3.26: Average G_{IC} at -55°C vs. Polysulfide Wt. % (G4 Epoxide-Polysulfides)

The G_C 2-sample T results for the G4 epoxide-polysulfide films at -55°C are listed in Table 3.15. Except for 10% G4, all sample sets are significantly different from the neat epoxide film set.

Table 3.15: G4 G_C at-55°C 2-Sample T P-Value Results

Name	Temperature (°C)	Polysulfide Weight %	2-Sample T P-Value from Control	Significant?
5% G4	-55	5%	0.033	Yes
10% G4	-55	10%	0.108	No
15% G4	-55	15%	0.006	Yes
20% G4	-55	20%	0.047	Yes

The average fracture toughness (K_{IC}) at room temperature (20°C) is plotted in Figure 3.27 as a function of the G4 polysulfide content. There is a 1-fold increase in the fracture toughness from neat epoxide-polyamide film to 5% G4 polysulfide. The presence of G4 correlates with an enhancement to the fracture toughness, although larger amounts of G4 polysulfide do not correlate with larger increases to the fracture toughness.

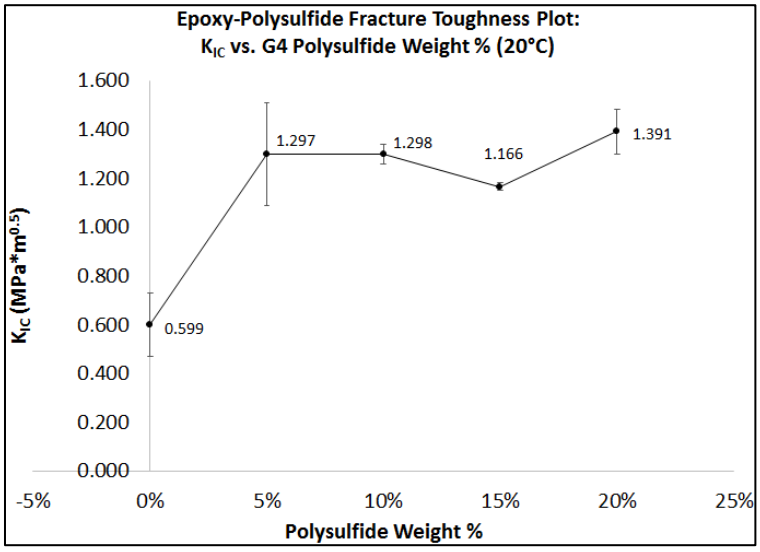

Figure 3.27: Average K_{IC} at 20°C vs. Polysulfide Wt. % (G4 Epoxide-Polysulfides)

The K_C 2-sample T results for the G4 epoxide-polysulfide films at 20°C are listed in Table 3.16. Only the 20% G4 set shows a significant difference.

Table 3.16: G4 K_C at 20°C 2-Sample T P-Value Results

Name	Temperature (°C)	Polysulfide Weight %	2-Sample T P-Value from Control	Significant?
5% G4	20	5%	0.091	No
10% G4	20	10%	0.097	No
15% G4	20	15%	0.268	No
20% G4	20	20%	0.039	Yes

The planar strain energy release rate (G_{IC}) is plotted in Figure 3.28 as a function of the G4 polysulfide weight percentage. There is a gradual increase from 0% G4 polysulfide up to 20% G4 polysulfide. The G_{IC} for 20% polysulfide is three times greater than the G_{IC} for neat epoxide films. The increase in the strain energy release rate is due to the flexibility of the G4 polysulfide component, which indicates that epoxide-polysulfides with elevated polysulfide content will absorb more energy than neat epoxides or epoxide-polysulfides with limited polysulfide content.

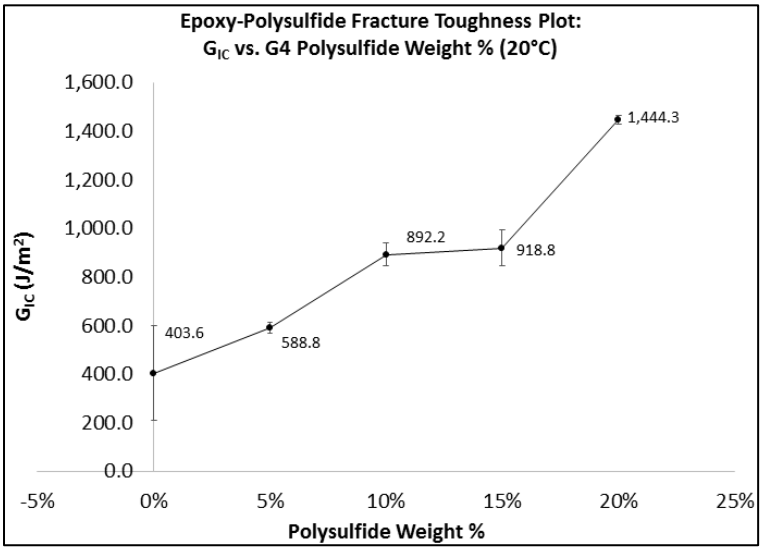

Figure 3.28: Average G_{IC} at 20°C vs. Polysulfide Wt. % (G4 Epoxide-Polysulfides)

The G_C 2-sample T results for the G4 epoxide-polysulfide films at 20°C are listed in Table 3.17. There is no sample set that is significantly different from the neat epoxide film set.

Table 3.17: G4 G_C at 20°C 2-Sample T P-Value Results

Name	Temperature (°C)	Polysulfide Weight %	2-Sample T P-Value from Control	Significant?
5% G4	20	5%	0.920	No
10% G4	20	10%	0.375	No
15% G4	20	15%	0.402	No
20% G4	20	20%	0.138	No

The K_{IC} at 60°C is plotted in Figure 3.29 as a function of the G4 polysulfide weight %. There is a linear decrease from neat epoxide to 10% G4. After reaching a minimum of 0.168 MPa*$m^{0.5}$, the K_{IC} remains constant for higher levels of G4 polysulfide. The decrease in K_{IC} is attributed to decreased temperature stability of the polysulfide domain (when compared to the epoxide domain) at elevated temperatures and the fact that there is a large temperature differential between 60°C and the glass transition temperature of the epoxide-polysulfide resins with large polysulfide content. The temperature differential is smaller for neat epoxide. It's also worth noting that the storage modulus measured at 60°C is higher for neat epoxide than most of the epoxide-polysulfide formulations, indicating that the ability to store energy is more diminished for epoxide-polysulfides than neat epoxides. Therefore, the elastic energy release rate is lower at 60°C for epoxide-polysulfides than for neat epoxides.

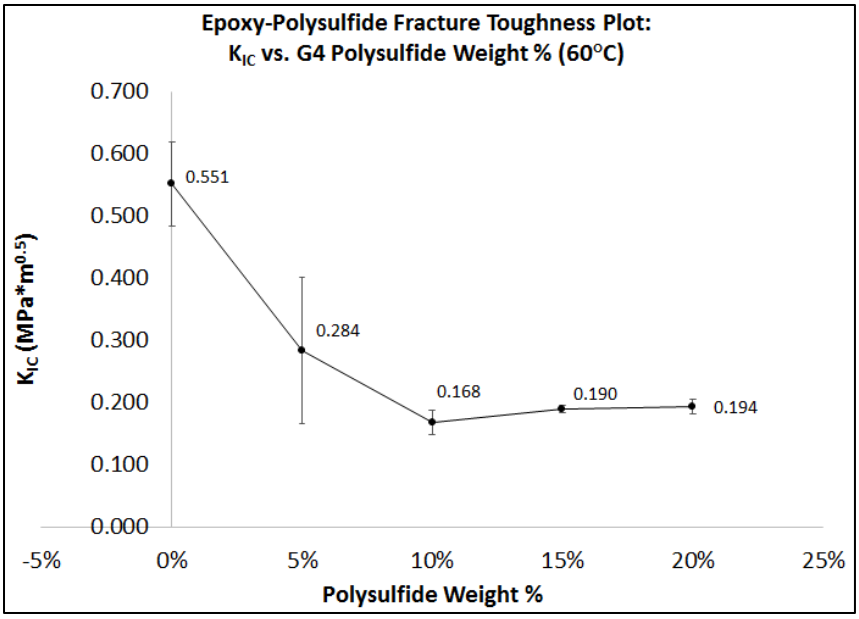

Figure 3.29: Average K_{IC} at 60°C vs. Polysulfide Wt. % (G4 Epoxide-Polysulfides)

The K_C 2-sample T results for the G4 epoxide-polysulfide films at 60 C are listed in Table 3.18. The 10% and 20% sets are significantly different from the neat epoxide film set.

Table 3.18: G4 K_C at 60°C 2-Sample T P-Value Results

Name	Temperature (°C)	Polysulfide Weight %	2-Sample T P-Value from Control	Significant?
5% G4	60	5%	0.079	No
10% G4	60	10%	0.005	Yes
15% G4	60	15%	0.058	No
20% G4	60	20%	0.007	Yes

The G_{IC} at 60°C is plotted in Figure 3.30 as a function of the G4 polysulfide weight %. There is a steep decrease in the G_{IC} from neat epoxide to 5% G4. All epoxide-polysulfide films have G_{IC} values between 80 and 105 J/m^2.

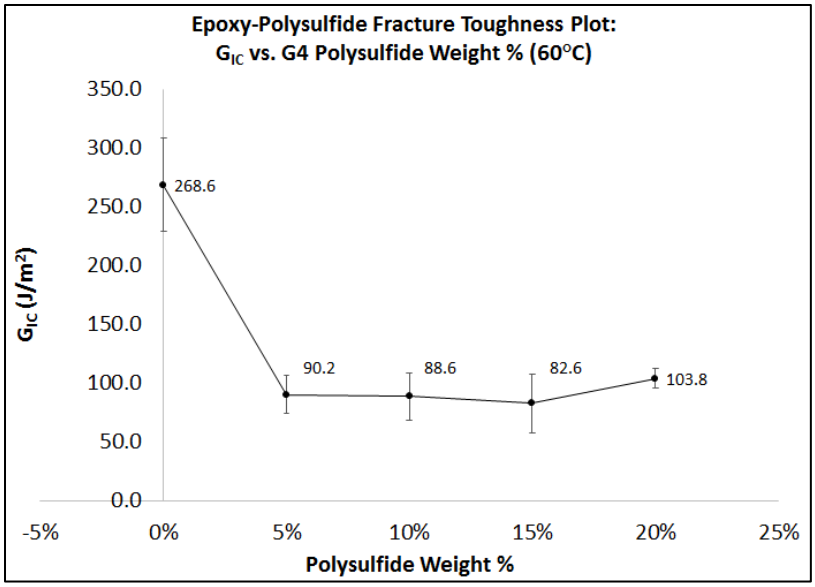

Figure 3.30: Average G_{IC} at 60°C vs. Polysulfide Wt. % (G4 Epoxide-Polysulfides)

The G_C 2-sample T results for the G4 epoxide-polysulfide films at 60°C are listed in Table 3.19. There is no sample set that is significantly different from the neat epoxide film set.

Table 3.19: G4 G_C at 60°C 2-Sample T P-Value Results

Name	Temperature (°C)	Polysulfide Weight %	2-Sample T P-Value from Control	Significant?
5% G4	60	5%	0.053	No
10% G4	60	10%	0.083	No
15% G4	60	15%	0.560	No
20% G4	60	20%	0.827	No

The fracture toughness values of G4 epoxide-polysulfides are plotted in Figure 3.31 as a function of the test temperature (-55, 20, or 60°C). The fracture toughness values of the neat epoxide films remain constant from low (-55°C) to elevated temperatures (60°C). At -55°C and 20°C, the fracture toughness values of the epoxide-polysulfides are larger than the neat epoxide films. They undergo a substantial decrease to below the fracture toughness values of the neat epoxide films at 60°C. Judging by the

intersection points of the fracture toughness plots of the neat epoxide and epoxide-polysulfides, the fracture toughness values of the epoxide-polysulfides would exceed the neat epoxide values up until a temperature between 40 and 50°C (104-122°F).

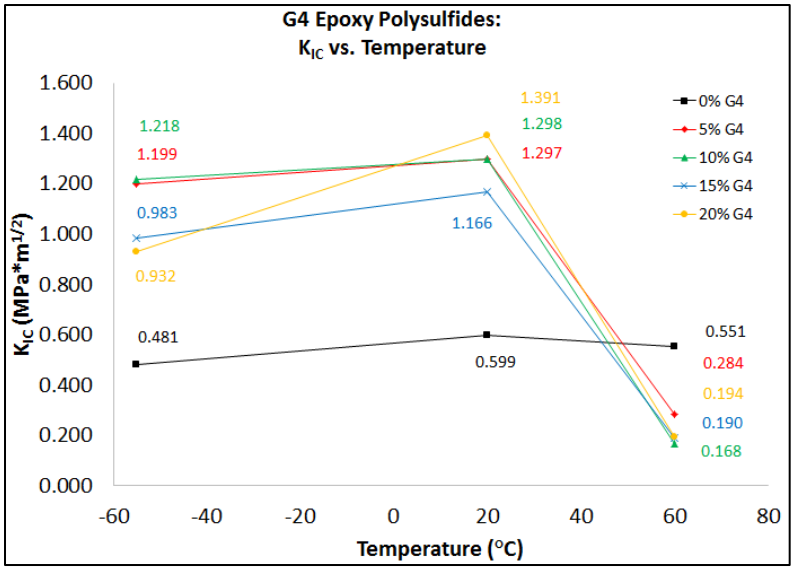

Figure 3.31: Average K_{IC} vs. Temperature (G4 Epoxide-Polysulfides)

The G_{IC} values of G4 epoxide-polysulfides are plotted in Figure 3.32 as a function of the test temperature (-55, 20, or 60°C). All formulations undergo an increase in the G_{IC} from -55°C to 20°C and a decrease from 20°C to 60°C, although the phenomenon is more augmented with the presence of the polysulfide polymeric units. At -55°C and 20°C, the values of the epoxide-polysulfides are larger than the neat epoxide films. They undergo a substantial decrease to below the G_{IC} values of the neat epoxide films at 60°C. Judging by the intersection points of the fracture toughness plots of the neat epoxide and epoxide-polysulfides, the fracture toughness values of the epoxide-polysulfides would exceed the neat epoxide values up until a temperature between 40 and 55°C (104-131°F).

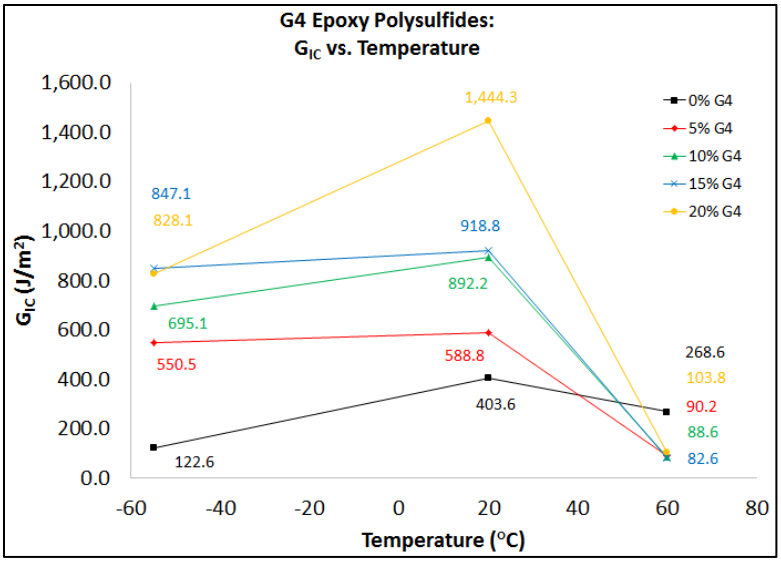

Figure 3.32: Average G_{IC} vs. Temperature (G4 Epoxide-Polysulfides)

The K_{IC} at -55°C is plotted as a function of the G112 polysulfide weight % in Figure 3.33. There was a linear increase in the K_{IC} from neat epoxide up to 10% G112 polysulfide. Afterwards, the fracture toughness decreased at higher levels of polysulfide. The fracture toughness values are slightly lower for G112 epoxide-polysulfides than for G4 epoxide-polysulfides, which may be due to greater amounts of unreacted thiol groups.[145]

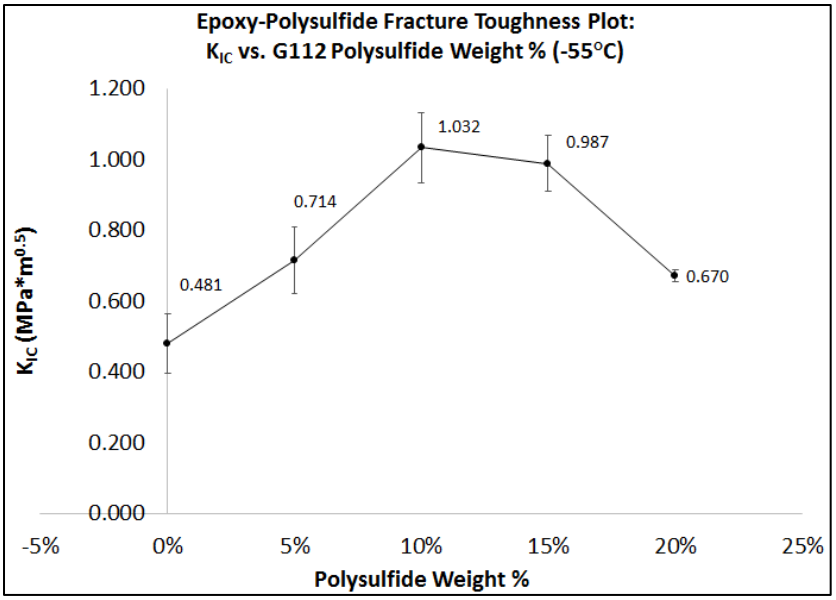

Figure 3.33: Average K_{IC} at -55°C vs. Polysulfide Wt. % (G112 Epoxide-Polysulfides)

The K_C 2-sample T results for the G112 epoxide-polysulfide films at -55°C are listed in Table 3.20. The only significant different sample set is the 10% G112 sample set.

Table 3.20: G112 K_C at -55°C 2-Sample T P-Value Results

Name	Temperature (°C)	Polysulfide Weight %	2-Sample T P-Value from Control	Significant?
5% G112	-55	5%	0.731	No
10% G112	-55	10%	0.024	Yes
15% G112	-55	15%	0.074	No
20% G112	-55	20%	0.655	No

The G_{IC} at -55°C is plotted in Figure 3.34 as a function of the G112 polysulfide weight %. There is a linear increase from neat epoxide to a maximum of 461.1 J/m^2 at 10% G112 polysulfide weight %. There is a linear decrease thereafter to 20% G112 polysulfide %. The elastic energy strain rates are lower for G112 epoxide-polysulfides than for G4 epoxide-polysulfides, which may be due to greater amounts of unreacted thiol groups.[145]

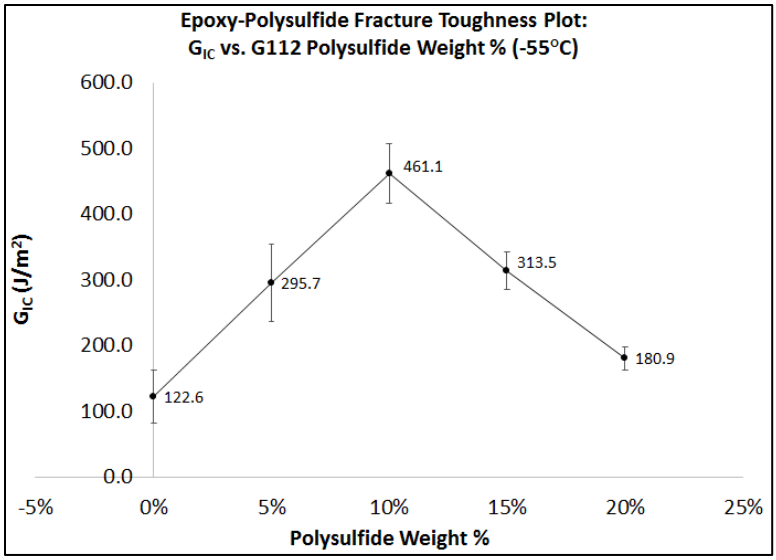

Figure 3.34: Average G_{IC} at -55°C vs. Polysulfide Wt. % (G112 Epoxide-Polysulfides)

The G_C 2-sample T results for the G112 epoxide-polysulfide films at -55°C are listed in Table 3.21. The 10% and 15% G112 sample sets are significantly different from the neat epoxide film set.

Table 3.21: G112 G_C at -55°C 2-Sample T P-Value Results

Name	Temperature (°C)	Polysulfide Weight %	2-Sample T P-Value from Control	Significant?
5% G112	-55	5%	0.092	No
10% G112	-55	10%	0.011	Yes
15% G112	-55	15%	0.031	Yes
20% G112	-55	20%	0.313	No

The average K_{IC} at 20°C as a function of the G112 polysulfide content is shown in Figure 3.35. There is an increase in the K_{IC} from neat epoxide polyamide film to a maximum of 1.173 MPa*$m^{0.5}$ at a G112 polysulfide content of 10%. There is a gradual decrease to 0.918 MPa*$m^{0.5}$ at a G112 polysulfide content of 20%. The presence of polysulfides toughens the epoxide at low polysulfide levels, but weakens at higher polysulfide levels. The fracture toughness is still higher than neat epoxide even at 20%

polysulfide. The elevated fracture toughness values are due to the toughening of the epoxides with the addition of polysulfide content.

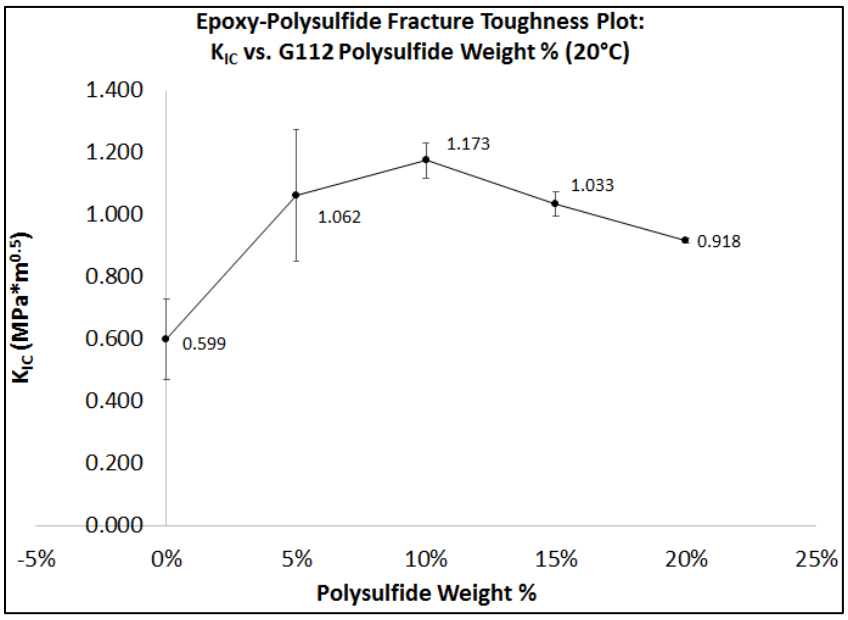

Figure 3.35: Average K_{IC} at 20°C vs. Polysulfide Wt. % (G112 Epoxide-Polysulfides)

The K_C 2-sample T results for the G112 epoxide-polysulfide films at 20°C are listed in Table 3.22. There are no sample sets that are significantly different from the neat epoxide film set.

Table 3.22: G112 K_C at 20°C 2-Sample T P-Value Results

Name	Temperature (°C)	Polysulfide Weight %	2-Sample T P-Value from Control	Significant?
5% G112	20	5%	0.069	No
10% G112	20	10%	0.126	No
15% G112	20	15%	0.682	No
20% G112	20	20%	0.792	No

The G_{IC} as a function of the G112 polysulfide content is plotted in Figure 3.36. There is a one-fold increase in the G_{IC} to a maximum of 868.3 J/m^2 at a G112 polysulfide content of 10%. Afterward, the G_{IC} decreased to 614.8 J/m^2 at a G112 polysulfide

content of 20%, but is still greater than the G_{IC} of the neat epoxide. The reduction in the G_{IC} was attributed to the reduction of the elongation % at higher levels of G112 polysulfide.

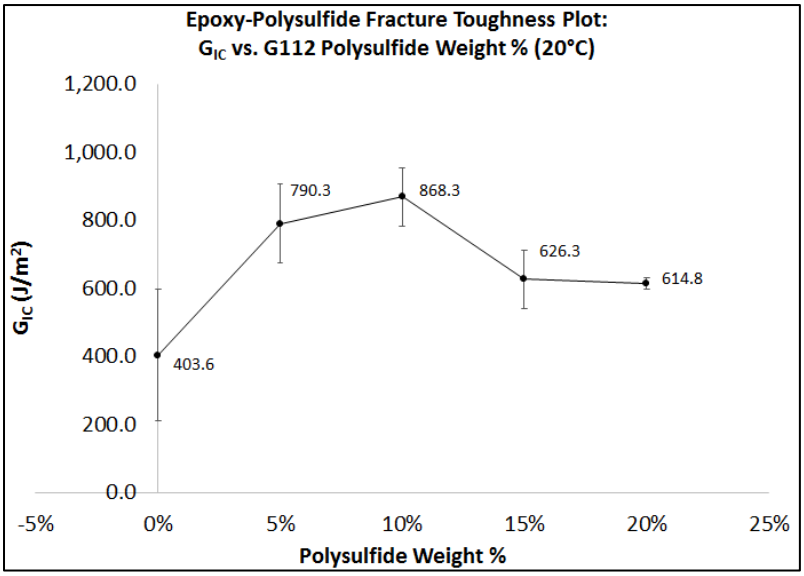

Figure 3.36: Average G_{IC} at 20°C vs. Polysulfide Wt. % (G112 Epoxide-Polysulfides)

The G_C 2-sample T results for the G112 epoxide-polysulfide films at 20°C are listed in Table 3.23. There are no sample sets that are significantly different from the neat epoxide film set.

Table 3.23: G112 G_C at 20°C 2-Sample T P-Value Results

Name	Temperature (°C)	Polysulfide Weight %	2-Sample T P-Value from Control	Significant?
5% G112	20	5%	0.555	No
10% G112	20	10%	0.867	No
15% G112	20	15%	0.096	No
20% G112	20	20%	0.341	No

The K_{IC} at 60°C is plotted in Figure 3.37 as a function of the G112 polysulfide weight %. There is a linear decrease from neat epoxide to 10% G112. After decreasing

to 0.110 MPa*$m^{0.5}$ at 10% G4, the K_{IC} remains constant for higher levels of G112 polysulfide. The K_{IC} behavior of the G112 epoxide-polysulfides is like the behavior observed for the G4 epoxide-polysulfides.

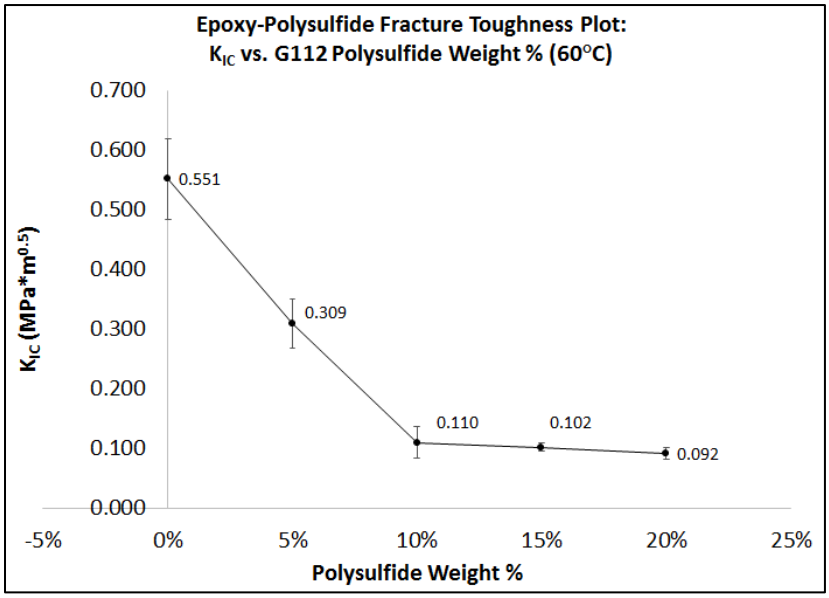

Figure 3.37: Average K_{IC} at 60°C vs. Polysulfide Wt. % (G112 Epoxide-Polysulfides)

The K_C 2-sample T results for the G112 epoxide-polysulfide films at 60°C are listed in Table 3.24. The 5%, 10%, and 20% sample sets are significantly different from the neat epoxide sample set.

Table 3.24: G112 K_C at 60°C 2-Sample T P-Value Results

Name	Temperature (°C)	Polysulfide Weight %	2-Sample T P-Value from Control	Significant?
5% G112	60	5%	0.022	Yes
10% G112	60	10%	0.002	Yes
15% G112	60	15%	0.390	No
20% G112	60	20%	0.002	Yes

The G_{IC} at 60°C is plotted in Figure 3.38 as a function of the G112 polysulfide weight %. There is a gradual decrease from neat epoxide to a minimum of 125.9 J/m^2 at 20% G112.

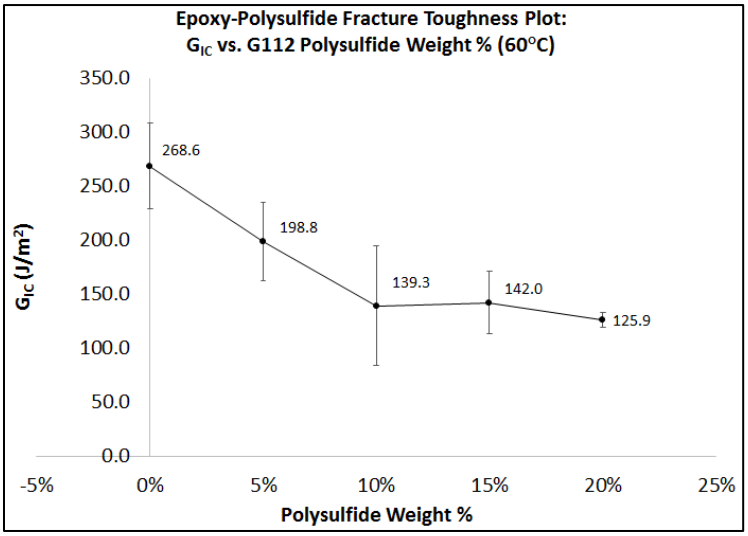

Figure 3.38: Average G_{IC} at 60°C vs. Polysulfide Wt. % (G112 Epoxide-Polysulfides)

The G_C 2-sample T results for the G112 epoxide-polysulfide films at 60°C are listed in Table 3.25. The 10% and 20% sample sets are significantly different from the neat epoxide sample set.

Table 3.25: G112 G_C at 60°C 2-Sample T P-Value Results

Name	Temperature (°C)	Polysulfide Weight %	2-Sample T P-Value from Control	Significant?
5% G112	60	5%	0.285	No
10% G112	60	10%	0.035	Yes
15% G112	60	15%	0.895	No
20% G112	60	20%	0.018	Yes

The fracture toughness values of G112 epoxide-polysulfides are plotted in Figure 3.39 as a function of the test temperature (-55, 20, or 60°C). The fracture toughness values of the epoxide-polyamide films are similar from low (-55°C) to elevated

temperatures (60°C). At -55°C and 20°C, the fracture toughness values of the epoxide-polysulfides are larger than the neat epoxide films. They undergo a substantial decrease to below the fracture toughness values of the neat epoxide films at 60°C. As observed from the graph, the fracture toughness values of the epoxide-polysulfides would exceed the neat epoxide values until a temperature between 40 and 50°C (104-122°F).

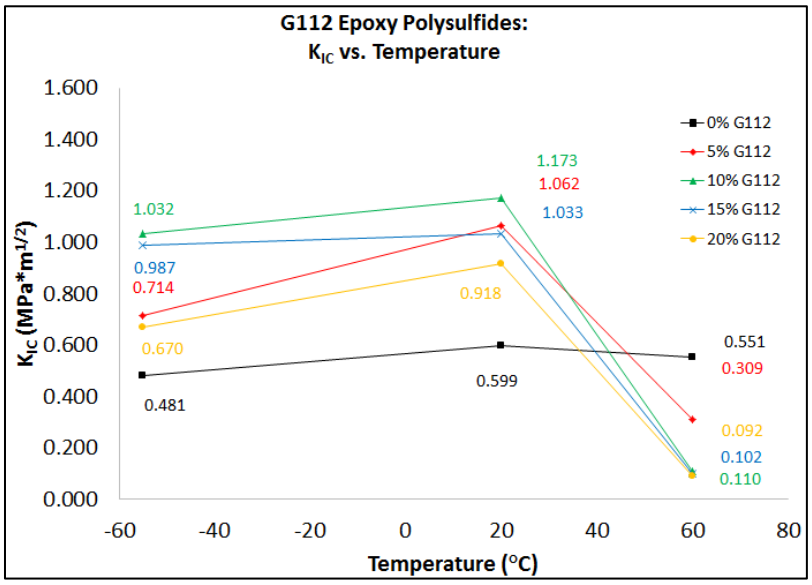

Figure 3.39: Average K_{IC} vs. Temperature (G112 Epoxide-Polysulfides)

The G_{IC} values of the G112 epoxide-polysulfides are plotted in Figure 3.40 as a function of the test temperature (-55, 20, or 60°C). All formulations undergo an increase in the G_{IC} from -55°C to 20°C and a decrease from 20°C to 60°C. At -55°C and 20°C, the values of the epoxide-polysulfides are larger than the neat epoxide films. They undergo a substantial decrease to below the G_{IC} values of the neat epoxide films at 60°C. As observed from the graph, the fracture toughness values of the epoxide-polysulfides would exceed the neat epoxide values up until a temperature between 40 and 55°C (104-131°F).

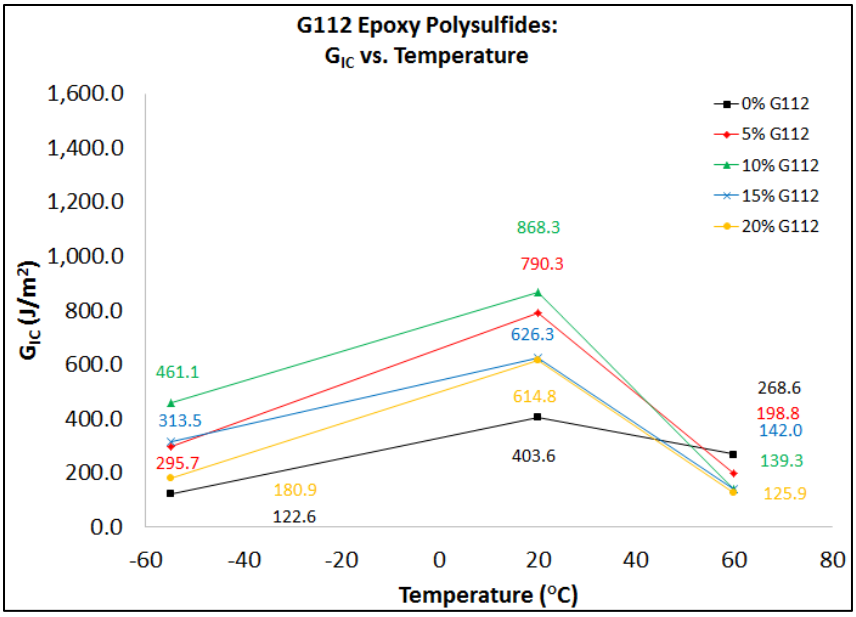

Figure 3.40: Average G_{IC} vs. Temperature (G112 Epoxide-Polysulfides)

3.3.8 Contact Angle Measurements of Crosslinked Epoxide and Epoxide-Polysulfide Coatings

In conjunction with EIS measurements, contact angle measurements were conducted on G4 epoxide-polysulfide coatings. In Figure 3.41, the contact angle is plotted versus the polysulfide content. Neat epoxide is included (0% polysulfide).

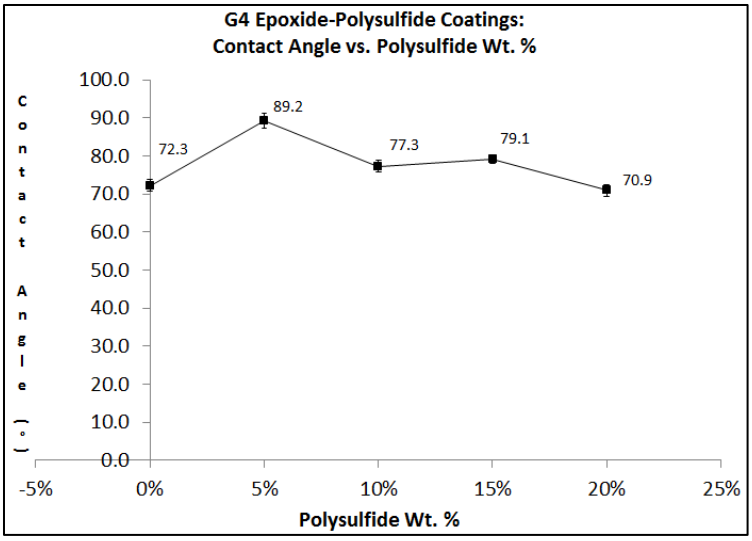

Figure 3.41: Contact Angle vs. G4 Polysulfide Wt. %

The contact angle increases from 72.3° for neat epoxide to 89.2° for 5% G4. The contact angle decreases to 77.3°, 79.1°, and 70.9° for 10%, 15%, and 20% G4, respectively. According to past researchers[144], the contact angle (hydrophobicity) increases from the reduced porosity (related to the presence of aliphatic polysulfide chains. The enhanced toughness may also contribute to the surface tension, which increases the contact angle. This is turn contributes to the hydrophobicity of the material and therefore the reduced water uptake later observed via EIS measurements. The reduction in the contact angle at higher levels of polysulfide, as indicated by past researchers, is due to a reduction in the "resistance" of the material from water.[143] This also contributes to the elevated water uptake (indicated by EIS measurements).

The contact angle 2-sample T results of the G4 epoxide-polysulfide films are listed in Table 3.26. Except for 20% G4, all sample sets are significantly different from the neat epoxide film set.

Table 3.26: G4 Contact Angle 2-Sample T P-Value Results

Name	Polysulfide Weight %	2-Sample T P-Value from Control	Significant?
5% G4	5%	0.000	Yes
10% G4	10%	0.058	No
15% G4	15%	0.010	Yes
20% G4	20%	0.569	No

3.3.9 EIS Measurements of Crosslinked Epoxide and Epoxide-Polysulfide Coatings

The EIS Nyquist plots for neat epoxide and G4 epoxide-polysulfides are shown in Figure 3.42. Neat epoxide coatings, 10% G4, and 15% G4 show coating failure. 5% G4 shows a proper coating barrier against corrosion by the immersion of sea water. The results show that the presence of polysulfide can toughen crosslinked epoxide-polysulfide copolymers (leading to films with elevated barrier properties), but increasing amounts of G4 polysulfide can result in a copolymer that is too flimsy to act as a proper barrier. In addition, the coating barrier properties (as measured via EIS) are also a measure of the water uptake and contact angle. Elevated contact angles and reduced water uptake indicate a better barrier against corrosion.

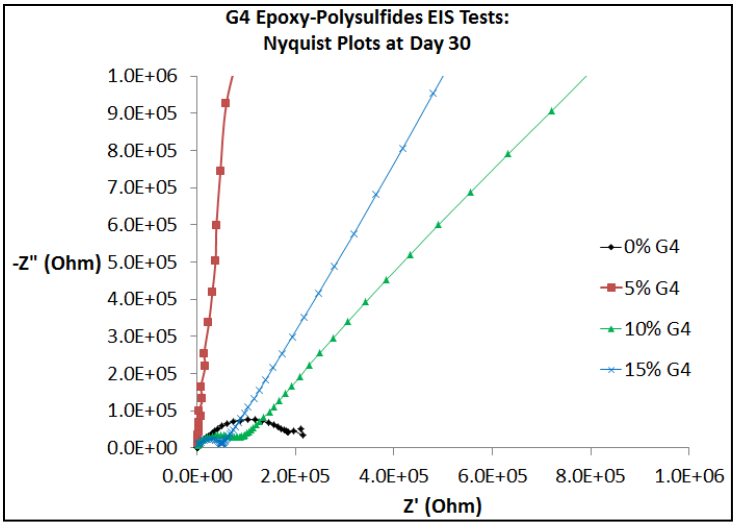

Figure 3.42: EIS Nyquist Plots of G4 Epoxide-Polysulfides at Day 30 of Immersion

The EIS Bode plots of the 0%, 5%, 10%, and 15% G4 polysulfides are plotted in Figure 3.43. The impedance moduli are plotted as a function of the frequency. 0%, 10%, and 15% G4 polysulfide show coating failure, while 5% G4 polysulfide shows a low level of coating resistance.

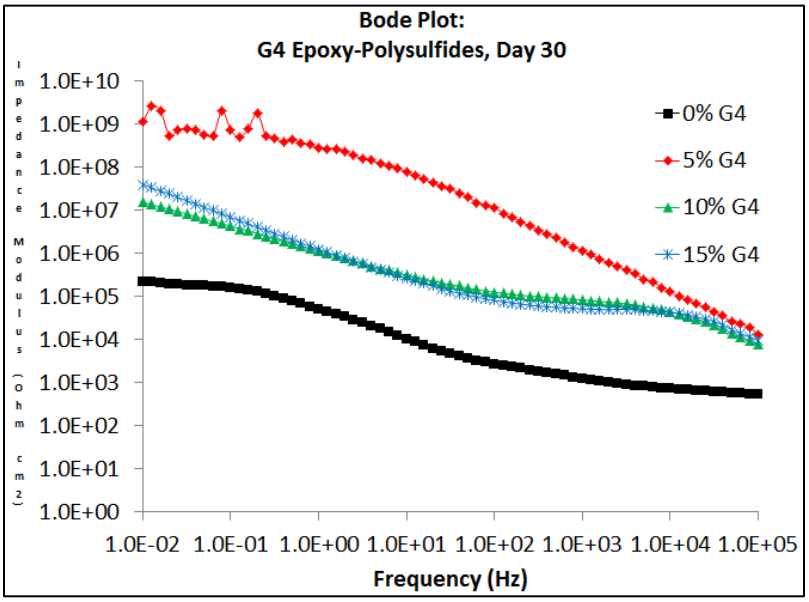

Figure 3.43: EIS Bode Plots of G4 Epoxide-Polysulfides at Day 30 of Immersion

The Bode impedance moduli for 0%, 5%, 10%, and 15% G4 epoxide-polysulfides is plotted in Figure 3.43 as a function of the sea water immersion days. All coating formulations show a reduction in the impedance modulus from Days 0 to 2. 5%, 10%, and 15% G4 epoxide-polysulfides show an additional reduction from Days 2 to 20, while neat epoxide show constant impedance moduli until Day 20 and then a reduction afterward. All epoxide-polysulfides show larger impedance moduli than neat epoxide formulations, which is an indication of the more enhanced barrier properties of the epoxide-polysulfides. 5% G4 shows the greatest resistance to corrosion.

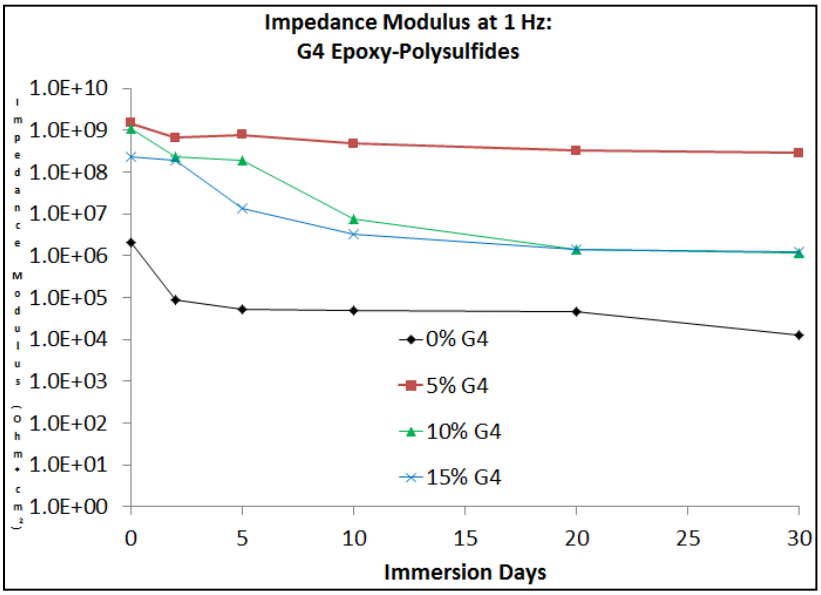

Figure 3.44: Impedance Moduli of G4 Epoxide-Polysulfides vs. Days of Immersion

The EIS water uptake versus the polysulfide content is graphed in Figure 3.45.

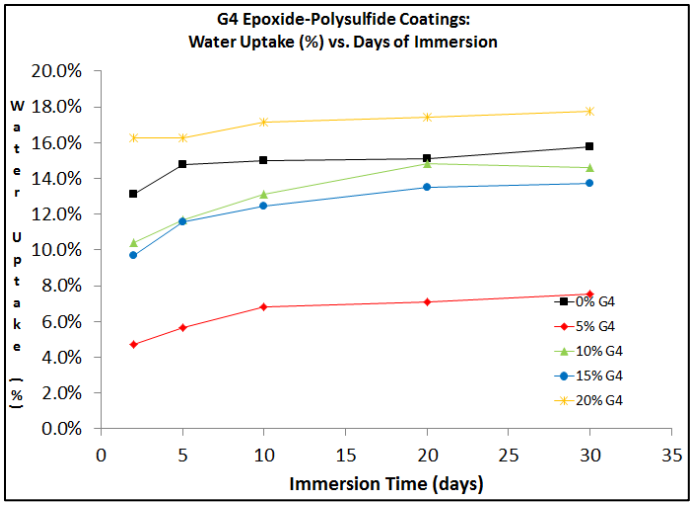

Figure 3.45: Water Uptake of G4 Epoxide-Polysulfide Coatings vs. Day of Immersion

20% G4 polysulfide has the highest water uptake, while 5% G4 has the lowest water uptake. The water uptake for the epoxide-polysulfides agrees with the water uptake and EIS Bode/Nyquist results, indicating that elevated levels of polysulfide content correlate with low water barrier properties.

3.4 Discussion

The epoxide-polysulfides were measured for dynamic mechanical properties, coating corrosion resistance, water uptake and contact angle, tensile properties, adhesion strength, and the fracture properties at -55°C, 20°C, and 60°C. Measurement of the dynamic mechanical moduli and fracture properties at low, ambient, and elevated temperatures was particularly important in terms of mimicking the behavior observed on aircraft substrates in the air and on the ground. This is important in measuring how polysulfide-based coatings might perform on aircraft substrates and the effect that temperature may have on the damage tolerance of the coating systems. Polysulfide materials are bonded to epoxides to provide coatings with weatherability

and longevity, which are necessary considering the expenses involved to fly and repaint planes.

The most interesting aspect is that the toughening phenomenon that occurs at 5-10% polysulfide contributes to increases in the fracture toughness, elastic energy strain rate, tensile properties, corrosion resistance, adhesion strength, and flexibility. This indicates that the best balance of coating properties is achieved with low (5-10%) levels of polysulfide by reducing the porosity, augmenting the barrier properties, and increasing the flexibility without reductions in the strength of the material. This is achieved by augmenting the size of the epoxide polymer via extension with an elastomeric polysulfide. At low levels, the polysulfide does not impede the crosslink density, leading to a longer, tougher polymeric backbone. The presence of the elastomeric polysulfide also contributes to an augmentation of the elongation from a rigid epoxide.

The dynamic mechanical analysis results indicated higher storage moduli and glass transition temperatures at 5-10% polysulfide content. Decreases in both properties were observed at 15% polysulfide content and above. As indicated by past literature, lesser amounts of polysulfide can toughen epoxides by increasing the chain rigidity. This phenomenon was observed in the form of higher storage moduli and glass transition temperatures. At higher polysulfide levels, the larger polysulfide phases contributed to reductions in the storage moduli. The flexibility of the polysulfide phases led to lower glass transition temperatures. This is in concordance with past literature.

Last, the storage moduli were dependent on temperature, decreasing at higher temperatures.

The epoxides and epoxide-polysulfides were also tested for tensile properties. The presence of G4 polysulfide content resulted in steep increases to the elongation at break %. This was attributed to the flexibility of the polysulfide domain units. The elastic moduli underwent increases until 10% G4 polysulfide and then decreased. This mirrored the behavior of the storage moduli. The elastic moduli increased due to the film toughening at low polysulfide levels. The tensile strength increased from neat epoxide to 15% G4 polysulfide and decreased to a level below the tensile strength for neat epoxide. The increase in the tensile strength was attributed to the polysulfide toughening, while the decrease in the tensile strength at higher levels of polysulfide was attributed to the decreased rigidity from the polysulfide content. The tensile strength and elastic moduli behavior of the G112 epoxide-polysulfides was the same as the G4 epoxide-polysulfides, but the elongation behavior was different. The G112 epoxide-polysulfides display decreased elongation percentages with increased polysulfide content and are roughly half the elongation percentages of the G4 epoxide-polysulfides. This may be an effect of unreacted thiol groups from the presence of greater steric hindrance from the larger polysulfide oligomers (G112).

The fracture toughness values of the neat epoxides and epoxide-polysulfides were dependent on temperature. The fracture toughness values of the epoxide-polysulfides were greater than the neat epoxide films at low (-55°C) and ambient (20°C)

temperatures, but were less than the fracture toughness values measured at 60°C. On the other hand, epoxides maintain their toughness at elevated temperatures while polysulfide based materials undergo a sharp decrease. This is attributed to neat epoxide materials maintaining the modulus more sufficiently than polysulfide-based materials while at elevated temperatures. It is assumed that the fracture toughness is a synergistic property that is a function of both the modulus and elongation properties of the material, indicating that materials with both flexibility and elevated moduli will have elevated fracture toughness values. The enhanced fracture toughness values of the epoxide-polysulfides at low and ambient conditions is notable because it signifies that the materials have a greater damage tolerance under these temperatures conditions, which coincidently occur while a hypothetical plane is in flight at high altitudes or near the ground. This means that polysulfide content will generally lead to a coating with greater damage tolerance under most flying conditions.

The moderate increase in the adhesion strength of the G4 based epoxide-polysulfides is attributed to the added flexibility of the materials as well as the rupture strength of the materials (proven by the increase in the fracture toughness). The reduction in the hardness values of the G4 based epoxide-polysulfides is attributed to the added content of the polysulfides, although it is notable that the G4 epoxide-polysulfides are roughly equivalent to neat epoxide until 20% G4 polysulfide content. The sharp increase in the reverse impact strength of the G4 epoxide polysulfide materials is due in part to the enhanced adhesion strength of the materials as well as the flexibility of the epoxide-polysulfide polymeric units.

The use of G4 epoxide-polysulfides led to an increase in the barrier properties versus neat epoxide, which was attributed to epoxide-polysulfide toughening. The same phenomenon also contributed to higher contact angles (hydrophobicity) and lower water uptake. The toughening produced by the polysulfide content also contributed to the barrier properties against corrosion. The barrier properties were maximized at 5% G4, the same formulation with one of the highest fracture toughness values, storage and elastic moduli, and glass transition temperatures.

G4 based epoxide-polysulfides display superior fracture properties to G112 based epoxide-polysulfides. This might be due to less thiol groups G112 epoxide-polysulfides are less flexible, which lead to a lower damage tolerance in the form of less energy required to propagate fracture. It was deemed that the larger molecular weight of the G112 polysulfide did not contribute positively to the coating mechanical and fracture properties.

The most interesting aspect of the epoxide-polysulfide study was the balance of epoxide and polysulfide necessary for the maximization of various coating properties. Much of this was contingent upon the size of the polysulfide phases within the matrix. The balance is obtained by having polysulfide phases large enough to aid in damage resistance of the matrix but not large enough to make the material flimsy. Generally, this was achieved at polysulfide weight percentages of 5-10%. Another interesting aspect of the material enhancements to the coatings was the concurrent increase in both the tensile strength and elongation % of the material. As noted by other

researchers, generally one property is enhanced at the expense of the other. For example, an additive that increases the tensile strength may make the material more brittle (decreasing the elongation %), but an additive that increases the flexibility of the matrix material may also lead to the material becoming flimsier. The explanation lies in the two-phase morphology of the material. The addition of the polysulfide increases the flexibility of the epoxide material due to the elastomeric nature of the polysulfide (which is much more flexible than the stiff epoxide). The isolated phases formed by the presence of the polysulfide material delay macroscopic fracture, which culminates in enhancements to the fracture properties and tensile strength and modulus of the material. At low levels of polysulfide, there is an insignificant change in the crosslink density of the material, which prevents a decrease in the tensile strength and modulus of the material.

What's notable is the fact that the tensile properties, fracture properties, corrosion resistance, and hydrophobicity all were maximized at low levels of polysulfide, indicating a possible relationship between the properties. The toughness imparted by the polysulfides minimized the possibility of pores, which in turn created a more hydrophobic material with an enhanced ability to prevent corrosion.

Unexpected results from the epoxide-polysulfide study are the fact that the polysulfide with the higher molecular weight (G112) led to less mechanically robust epoxide-polysulfide coating systems. This is a departure from past studies.[6,146]

Another interesting aspect of the polysulfide project include the fact that reverse impact, adhesion strength, and the tensile elongation % of the G4 epoxide-polysulfide were all maximized at the highest levels of polysulfide (20 wt. %), indicating a relationship between the three parameters. Reverse impact strength and adhesion strength are closely related due to both tests measuring a coating's ability to adhere to a substrate. While adhesion strength is more closely related to the polarity of a coating than the flexibility of the material, flexibility will aid in adhesion strength due to a flexible coating strongly adhering to a substrate without fracturing.

3.5 Conclusion

Epoxide-polysulfides based upon the reaction of DGEBA and either G4 or G112 polysulfides were cured with polyamides and tested for various mechanical and coating properties. While adhesion strength and reverse impact strength correlated with the polysulfide content, the fracture and tensile properties and the corrosion resistance largely peaked at smaller levels of polysulfide. In lesser amounts, polysulfides will toughen epoxides. Also, epoxide-polysulfides show enhanced fracture properties when tested under ambient and colder conditions. These properties indicated that epoxide-polysulfide materials are suited well for irregular geometries on aircraft, especially at lower temperatures.

CHAPTER IV

CHARACTERIZATION, MECHANICAL PROPERTIES, AND CORROSION RESISTANCE OF EPOXIDE-SNAP SOL-GEL COMPOSITE FILMS AND COATINGS

4.1 Introduction

Epoxide-silica hybrid composites and coatings have been thoroughly researched in past literature for their synergy in terms of mechanical and corrosion related properties. Epoxide materials are commonly used as coating materials because they are inexpensive and simple to develop. In addition, epoxide materials undergo minimal shrinkage during curing, and adhere well to metal substrates.[23,32] Consequently, epoxides are frequently utilized as primers on metal surfaces, particularly on aluminum and steel. Aluminum surfaces include aircraft, and steel surfaces include exteriors of pipelines, bridges, and offshore platforms. There are a few disadvantages to using epoxide materials as coatings. Epoxide materials are limited by temperature stability, mechanical properties, and hardness.[23] In addition, epoxide coatings require various additives and surface preparations to improve the corrosion resistance, such as chromates (as chromate conversion coating surface preparations or primer additives) and sacrificial metals like magnesium or zinc (mainly utilized as pigment additives in

primers). Zinc and magnesium are useful as sacrificial metal corrosion inhibitors, but the use of zinc and magnesium in epoxide coatings physically weakens the coating and adds to the porosity. Multiple topcoats are needed to protect the primer from physical bombardment and corrosion, adding to the cost of coating systems utilizing sacrificial metal additives. Chromates are excellent as corrosion inhibitors and passivating layers for aluminum substrates, but are toxic and carcinogenic and have been eliminated for most commercial applications. Chromates are still utilized for military applications but are being phased out in favor of more environmentally benign and non-toxic additives. There is a need for benign additives that enhance both the corrosion resistance and mechanical properties of the coating, thereby ensuring coating longevity while eliminating costs and health concerns.

Silica-based materials can improve these attributes and enhance other properties such as corrosion resistance and adhesion strength if the silica-based materials are nano-sized and well-dispersed in the epoxide matrix.[147] There are two types of epoxide-silica hybrid materials: Class I and Class II materials. Class I materials have non-functional silica content in which the two phases (epoxide and silica) have weak interactions, while Class II materials are covalently bonded with one another.[148] Furthermore, Class II materials can be classified via *in situ and ex situ* processes. *In situ* processes are silica sol-gels which undergo hydrolysis and condensation reactions in a polymeric matrix, which *ex situ* processes are silica sol-gels which undergo hydrolysis and condensation reactions separate from a polymeric matrix and later are added into the matrix.[149]

Class I and Class II epoxide-silica hybrids have been thoroughly studied in the literature and have been noted for enhancing fracture properties, mechanical properties, and corrosion resistance of epoxide materials.[34-38, 40-44, 47, 150-154] Class I materials, notably in the use of nano-sized silica particles, have been instrumental in improving the fracture and mechanical properties (toughness, modulus) of epoxide-silica composites, provided that the materials are compatible with the epoxide matrix.[34-44, 47,150, 152-154] Class II materials, which includes organic silane content grafted to silica particles, have also been instrumental in improving the mechanical properties of the system. The silanes can crosslink with the organic epoxide matrix and provide barrier protection against corrosion.[7,31,45-58] The fracture properties are useful as synergistic tests relatable to several types of coating mechanical tests (tensile, impact resistance, flexibility, damage tolerance), and the tensile properties are useful in terms of measuring the flexibility, weatherability and aging strength of coating systems.

One specific type of organo-silane is the inorganic-organic hybrid sol-gel material, which is an inorganic silane component bonded to an organic alkoxysilane material. The inorganic component is responsible for improving the hardness and toughness of the films, while the organic component contributes to greater flexibility.[60,71,155,156] One specific type of inorganic-organic hybrid sol-gel material is the Self-Assembled NAnoPhase (SNAP) sol-gel material. Self-assembled NAnoPhase (SNAP) particles are environmentally benign nanoparticles created from the synthesis of inorganic and organic silanes.[59] The particles are created from the reaction of an inorganic precursor material (tetramethyl orthosilicate) with an organic alkoxysilane

material (3-glycidyloxytrimethoxysilane or GPTMS). The reaction takes place in a polar solvent such as water. The resulting hydrolysis and condensation reactions culminate in the creation of nano-sized particles. The SNAP particles have oxirane end groups because of the organic silane precursor (GPTMS). This means that they can react with amide and amine-based materials to form a crosslinked matrix. The SNAP particles also can bond with the substrate via siloxane bonding. This makes them ideal as surface pre-treatments because of their ability to bond with metal substrates and the primers that are cast upon them. The crosslinked matrix created from the reaction with a curing agent creates a passivating barrier useful for preventing corrosion, as shown in several publications.

SNAP particles, due to the inorganic and organic silane components present in the colloids constituting the particles, should have the capacity to contribute to the mechanical properties of an epoxide system, such as flexibility and adhesion strength. In addition, SNAP particles have oxirane end groups, which can bond to amines and amides (which common curatives for epoxide coatings). SNAP particles should be able to form covalent bonds with metal substrates and form continuous one-phase matrices by bonding with the curatives along with the base epoxides (diglycidyl ether of bisphenol A). Therefore, SNAP particles should be useful additives to enhance both the corrosion resistance and mechanical properties of epoxide coating systems.

Two different solvent ratios (10 and 20) were employed to create SNAP particles, which were later added into epoxide-polyamide films and coating systems using four

different weight ratios. As past literature has elucidated, solvent ratios of 15 or later (when related to the silane content) can produce larger, more intricate sol-gel networks.[156] Would this apply to a non-aqueous solvent, and how might the solvent ratio play a role in the molecular content of the silica colloids constituting the SNAP particles, the size of the SNAP particles, and ultimately the coating system or film? The SNAP particles were characterized via ^{1}H, ^{13}C, and ^{29}Si nuclear magnetic resonance (NMR). Later, the SNAP particles are added into epoxide-polyamide films and tested for thermal properties using DSC, crosslink density via dynamic mechanical thermal analysis (DTMA), fracture mechanics (fracture toughness and elastic energy release rate), and tensile testing (modulus and tensile strength). Last, the SNAP particles were added into military specification epoxide-polyamide coating systems and tested for pull-off adhesion strength, abrasion resistance, and barrier properties against corrosion via electrochemical impedance spectroscopy (EIS).

4.2 Experimental Section

4.2.1 Materials

3-glycidyloxypropyltrimethoxysilane (GPTMS, 98%), tetramethyl orthosilicate (TMOS, 98%), n-butanol (ACS reagent, 99.4%), and acetic acid (ACS reagent, 99.7%) were all purchased from Sigma-Aldrich. Epon 828 (diglycidyl ether of bisphenol A epoxide) was purchased from Hexion, Ancamide 507 and Ancamide 700B75 were both purchased from Air Products, Disparlon 6500 and Disparlon NS-30 were purchased from King Industries, Nicron 503 was purchased from Imerys Talc, Tipure TiO_2 was purchased

from DuPont/Chemours, and Naphtha was purchased from VM&P. Hydrobromic acid (HBr), acetic acid, potassium acid phthalate (Pht), methyl violet indicator, and methyl isobutylketone (MIBK), the materials utilized to measure the epoxide equivalent weight, were purchased from Sigma Aldrich. All materials were used as received. All materials were used as supplied.

4.2.2 Synthesis of SNAP Particles in H_2O

Except for the solvent type and amount, SNAP particles were synthesized similarly to previous literature.[59] GPTMS and TMOS were combined in a 3:1 molar ratio and manually shook in a glass vial. Later, the contents were added dropwise into a 250-mL round-bottomed flask containing 0.05 M acetic acid in H_2O. The amount of solvent was calculated by multiplying the cumulative molar amount of silanes (GPTMS and TMOS) by 10. The contents were continuously stirred via a magnetic stir bar during and silane addition. To complete the synthesis of SNAP particles via hydrolysis and condensation, the stirring continued for another 72 hours. The solution was then stored until further use. This sample was used as a control for NMR characterization experiments.

4.2.3 Synthesis of SNAP Particles in n-Butanol

Except for the solvent type and amount, SNAP particles were synthesized according to previous literature.[59] GPTMS and TMOS were combined in a 3:1 molar ratio and manually shook in a glass vial. Later, the contents were added dropwise into a 250-mL round-bottomed flask containing 0.05 M acetic acid in 1-butanol. 1-butanol was

utilized as a solvent instead of water due to its polarity and ability to dissolve the epoxide, polyamide curing agents, and SNAP particles. The contents were continuously stirred via a magnetic stir bar during and silane addition. To complete the synthesis of SNAP particles via hydrolysis and condensation, the stirring continued for another 72 hours. The solution was then stored until further use.

Two different sets of SNAP particles were synthesized by utilizing different amounts of solvent. The amount of solvent was calculated by multiplying the cumulative molar amount of silanes (GPTMS and TMOS) by 10 or 20. A SNAP particle synthesized from a 1-butanol amount that is 10 times greater than the cumulative amount of GPTMS and TMOS is termed a 10:1 GPTMS-TMOS SNAP particle, and so on. The intent was to see if the amount of solvent would play a difference in the size, morphology, and ultimately the physical and corrosion properties of the coating systems into which they were inserted.

4.2.4 Electrospray Ionization Mass Spectroscopy (ESI-MS) of SNAP Particles

The molecular weight distributions of the silica colloid components compromising the SNAP particles were determined via ESI-MS. The ESI-MS measurements were determined with a Bruker HCTultra QIT Mass Spectrometer.

4.2.5 Solution NMR

The functionalities and molecular bonds of the 10:1 SNAP particles dissolved in either H_2O or n-butanol were tested for ^{29}Si, ^{13}C, and ^{1}H NMR via a Varian NMRS 500-01. The tests were conducted at ambient temperatures. To prepare the NMR samples, the

samples were dissolved in equal parts H_2O and chloroform. The characterization of GPTMS via ^{29}Si, ^{13}C, and ^{1}H NMR was utilized as a control.

4.2.6 Solid-State NMR

The functionalities and molecular bonds of the 20:1 SNAP particles were tested with ^{29}Si and ^{13}C solid state NMR. 20:1 SNAP particles in butanol-solution were mixed with an equal weight of diethylene triamine (DETA) and were left to cure over the span of seven days. The ^{29}Si and ^{13}C NMR tests were tested with a Varian INOVA 750 solid state NMR apparatus available within the Chemistry Department at the University of Akron. The tests were conducted at ambient temperatures using spectral widths of 50.0 kHz and gains of 56 dB. The solid-state NMR utilized 1H decoupling and a spinner rate of 15 kHz.

4.2.7 Transmission Electron Microscopy (TEM)

Microscopic pictures of the SNAP particles were taken via transmission electron microscopy (TEM). The SNAP particles in solution were added dropwise to TEM sample holders and set to dry. Pictures of the SNAP particles were taken after the butanol solvent encapsulating the particles completely evaporated. The TEM pictures were taken with a JEOL Model JSM-1230 TEM apparatus. The intent of the TEM tests was to get a visualization of the SNAP particles and to determine their shape and dimensions (i.e. radius).

4.2.8 Dynamic Light Scattering (DLS)

Dynamic light scattering (DLS) acted as a supplement to TEM in determining the dimensions of the SNAP particles. DLS tests are measure the sizes of the SNAP particles while they are still suspended in solvent, which removes the possibility of SNAP particle shrinkage post-evaporation. DLS measurements were carried out using an apparatus within Dr. Tianbo Liu's research group at the University of Akron. The algorithm to determine the characteristic linewidth, which is utilized to calculate the diffusion coefficient D and later the hydrodynamic radius via the Stokes-Einstein equation[158]:

$$R_h = \frac{k_B T}{6\pi\eta D} \qquad 4.1$$

The variable k_B is the Boltzmann constant, T is the temperature, D is the diffusion constant, and η is the viscosity of the solvent.

4.2.9 Determination of Epoxide Equivalent Weight of GPTMS and SNAP Particles

The epoxide equivalent weights of neat GPTMS, SNAP particles in H_2O, and SNAP particles in n-butanol were measured to the description in Section 3.2.4.[128-130] Potassium acid phthalate was used as a standard, and hydrobromic acid was used as the analyte.

4.2.10 Epoxide-Polyamide Film Preparation and Application

Films were created by mixing the epoxide, polyamide crosslinkers, and the SNAP functional sol-gel particles dissolved in 1-butanol. The epoxide was Epon 828, and the polyamide crosslinkers were Ancamide 700B75 and Ancamide 507. The components

and amounts are taken from military specification 24441 epoxide-polyamide coating systems. For purposes of simplicity, all non-functional content (pigments, thixotropes, etc.) weren't included in the formulation.

Each set of SNAP particles (10 and 20 solvent molar ratios) were added to the mixtures in weight percentages of 1%, 2.5%, 5%, or 7.5% of the total weight of the base epoxide. In order to keep the epoxide weight content (Epon 828 + SNAP) the same for each formulation, Epon 828 was deducted by the same weight that the SNAP was added. Crosslinked epoxide-polyamide films with no SNAP added were prepared as controls. The component and component weights for the sample sets are shown in Table 4.1.

Table 4.1: Epoxide-Polyamide Film Formations with SNAP Addition

SNAP Wt. %	Solvent Molar Ratio	Ancamide 507 (g)	Ancamide 700B75 (g)	Epon 828 (g)	SNAP (g)	SNAP + n-Butanol (g)
0.0%	NA	0.68	9.64	17.21	0.00	0.00
1.0%	10	0.68	9.64	17.04	0.17	0.75
2.5%	10	0.68	9.64	16.79	0.42	1.86
5.0%	10	0.68	9.64	16.39	0.82	3.62
7.5%	10	0.68	9.64	16.01	1.20	5.31
1.0%	20	0.68	9.64	17.04	0.17	1.34
2.5%	20	0.68	9.64	16.79	0.42	3.29
5.0%	20	0.68	9.64	16.39	0.82	6.43
7.5%	20	0.68	9.64	16.01	1.20	9.42

After mixing, each formulation was cast onto PET film via a drawdown bar. PET film was used to provide a non-stick surface to ensure easy removal of crosslinked epoxide matrix films. The wet film thickness was 8 mils. After application onto PET, the cast film was left to dry and cure under ambient conditions.

4.2.11 SEM Pictures of 10:1 and 20:1 SNAP-Loaded Epoxide Films

SEM pictures were taken of the films loaded with either the 10:1 and 20:1 SNAP-loaded epoxide films in weight percentages of 1%, 2.5%, 5%, or 7.5% wt. The tests were conducted as described in Section 3.2.6.

4.2.12 Thermal and Thermal-Viscoelastic Measurements of Epoxide-Polyamide Films

Thermal characterization of the epoxide-polyamide films was conducted via differential scanning calorimetry (DSC) (TA Instruments Q2000 Model), and viscoelastic testing was conducted via dynamic mechanical thermal analysis (DMTA) (TA Instruments Q800 Model). The differential scanning calorimeter exposed a 1-10 mg sample from -50 °C to 150°C at a heating rate of 10°C/minute, and the dynamic mechanical thermal analyzer exposed a 30 mm x 6 mm x 0.1 mm sample to temperatures of -50°C to 150°C at a heating rate of 3°C/minute.

4.2.13 Tensile Testing of Epoxide-Polyamide Films

Tensile tests were conducted (ASTM D2370[159]) via an Instron 5567 Tensile Tester utilizing a 1 kN load cell. The tensile samples were rectangular and had dimensions of 100 mm x 20 mm x 0.1 mm. The Instron employed an extension speed of 1 mm/min. The tensile strength was measured directly by the Instron. 10-15 samples were tested per sample set.

4.2.14 Fracture Toughness Testing of Epoxide-Polyamide Films

The fracture toughness was conducted as described in Section 3.2.11.[137,138] Fracture toughness tests were employed at 20°C and at 60°C. 10-15 samples were tested per sample set.

4.2.15 Coating Preparation and Application

The SNAP particles were included with MIL-DTL-24441 Epoxide-Polyamide White[161] coating samples at percentages of 1.0%, 2.5%, 5.0%, and 7.5% weight. The weight percentage is indicated as a weight percentage of the epoxide material (Epon 828) in the coating system. The amount of Epon 828 was adjusted to keep the total weight of functional material (epoxide and SNAP) constant for each sample set. Table 4.1 indicates the components added to the formulations listed in Table 4.2.

Table 4.2: MIL-DTL 24441 Paint Formulations

Formulation	SNAP Wt. %	Solvent to Silane Ratio	Disparlon 6500 (g)	Nicron 503 (g)	Naphtha (g)	Disparlon NS-30 (g)	TiO2 (g)	N-Butanol to Add (g)
No SNAP	0.0%	NA	0.49	8.6	7.18	0.49	20.42	8.77
GPTMS-TMOS SNAP	1.0%	10	0.49	8.6	7.18	0.49	20.42	8.18
GPTMS-TMOS SNAP	2.5%	10	0.49	8.6	7.18	0.49	20.42	7.33
GPTMS-TMOS SNAP	5.0%	10	0.49	8.6	7.18	0.49	20.42	5.96
GPTMS-TMOS SNAP	7.5%	10	0.49	8.6	7.18	0.49	20.42	4.66
GPTMS-TMOS SNAP	1.0%	20	0.49	8.6	7.18	0.49	20.42	7.6
GPTMS-TMOS SNAP	2.5%	20	0.49	8.6	7.18	0.49	20.42	5.89
GPTMS-TMOS SNAP	5.0%	20	0.49	8.6	7.18	0.49	20.42	3.16
GPTMS-TMOS SNAP	7.5%	20	0.49	8.6	7.18	0.49	20.42	0.55

The coating formulations were mixed together in a Thinky mixer for 5 minutes at 2,000 revolutions per minute. Afterwards, they were cast onto Al-2024 aluminum

samples at wet film thicknesses of 5 mils and steel Taber Abrasion 4” x 4” panels at thicknesses of 10 mils. Figure 4.1 shows the drawdown casting processes.

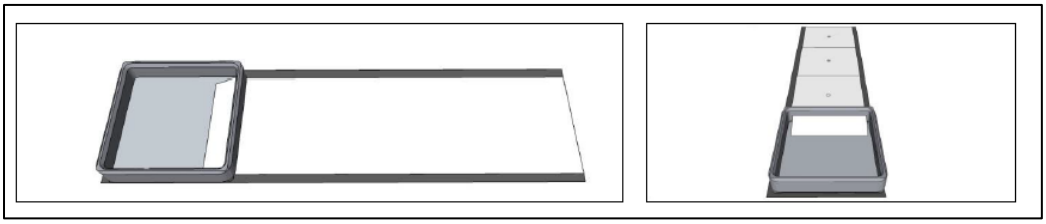

Figure 4.1: Draw-Down Coating Application onto Al-2024 Panels (Left) and Steel Taber Abrasion Panels (Right)

The aluminum samples were utilized for pull-off adhesion and EIS tests. The Taber Abrasion panels were utilized for Taber Abrasion tests.

4.2.16 Taber Abrasion Tests on MIL-DTL-24441 Coatings

The Taber Abrasion tests were completed according to ASTM D4060.[162] A Taber Abrader was used with CS-17 wheels. 1,000 g weights were used, and the panels were subjected to 1,000 cycles of abrasion. Three samples were utilized for each test. The weight loss was measured after 500 and 1,000 cycles of abrasion. A schematic of the Taber Abrader is shown below:

Figure 4.2: Taber Abrasion Apparatus

4.2.17 Pull-Off Adhesion Tests of MIL-DTL-24441 Coatings

The pull-off adhesion tests were completed according to the same conditions and instrumentation as Section 3.2.8. Neat MIL-DTL 24441 epoxide-polyamide and MIL-DTL-24441 coating systems loaded with 1%, 2.5%, 5%, or 7.5% of either 10:1 or 20:1 SNAP particles were tested for pull-off adhesion tests.

4.2.18 Electrochemical Impedance Spectroscopy (EIS) Tests of MIL-DTL-24441 Coatings

Electrochemical impedance spectroscopy (EIS) tests were carried out according to the same conditions as Section 3.2.13. Neat MIL-DTL 24441 epoxide-polyamide and MIL-DTL-24441 coating systems loaded with 1%, 2.5%, 5%, or 7.5% of either 10:1 or 20:1 SNAP particles were tested for EIS tests over a 30-day period. The coatings were tested at Days 0, 2, 5, 10, 20, and 30.

4.2.19 EIS Water Uptake Measurements of SNAP-Loaded Epoxide Coatings

EIS water uptake was measured as described in Section 3.2.13. The coatings were tested at Days 0, 2, 5, 10, 20, and 30.

4.2.20 Contact Angle Measurements of SNAP-Loaded Epoxide Films

Contact angle measurements of the SNAP-loaded epoxide films were conducted as described in Section 3.2.12. Neat epoxide and SNAP-loaded epoxide formulations were cast onto a PET substrate and removed later (after fully curing) via a blade. The tops of the films were tested for the contact angle via a drop volume of 2 microliters.

4.3 Results

The intent of the testing was to investigate several types of properties pertaining to the formation of the particles, the properties of the epoxide films, and the properties of the epoxide coatings. In order to determine if SNAP coatings are functional additives that can enhance the properties of epoxide coatings, information must be gathered that determines the molecular properties and functionalities of the structures constituting the SNAP particles, the size and aggregation of the SNAP particles that are formed, if the SNAP particles form a continuous one-phase system with the epoxide coating, and if the SNAP particles can enhance the thermal and mechanical properties and the corrosion resistance if added as an additive into the coatings. Also, does the loading of the SNAP particles into the epoxide coatings and solvent amount used in the preparation of the SNAP particles play a role in the final coating properties? Epoxides are used in a variety of applications (metal substrates, floor coatings, etc.), and the goal is to indicate that SNAP particles can enhance the properties of epoxide coatings in the various applications in which epoxides are used.

In order to determine the molecular structures and functionalities of the SNAP particles and to determine the effect of the solvent amount on the molecular structure and functionalities of the colloids constituting the particles, the particles in solution were investigated via ^{1}H, ^{13}C, and ^{29}Si NMR. This was to ensure that oxirane groups were present within the structures and to determine that hydrolysis and condensation reactions were occurring between the inorganic and organic silanes in non-aqueous mediums (n-butanol). This would ensure ultimately the formation of sol-gel networks.

GPTMS was utilized as a control. The molecular weights of the structures constituting the particles were investigated via mass spectroscopy. This was to determine how solvent amount might affect the formation and molecular weights of the structures forming the SNAP particles and to determine ultimately how the structures affected the film and coating properties. The SNAP particles were characterized for particle size via dynamic light scattering (DLS) and transmission electron microscopy (TEM) in order to ensure the nano-sized dimensions of the particles, to determine the aggregation behaviors of the particles (which is relatable to the aggregation behavior of the particles in epoxide matrices), and to determine if the particle size is dependent upon the solvent amount.

There were two sets of formulations incorporating SNAP particles: MIL-DTL 24441 epoxide-polyamide formulations with just the base epoxide (DGEBA) and curing agents, and the entire coating formulation. The composite formulations with just the base and curing agents were tested for thermal, dynamic, fracture, and tensile properties, while the coating formulations were tested for adhesion strength, abrasion resistance, and corrosion resistance via electrochemical impedance spectroscopy (EIS). The former were properties primarily pertaining to coatings unattached to a metal substrate. Therefore, only the essential reactive components were included. The epoxide films were tested with differential scanning calorimetry to determine the effect of the SNAP particles on the glass transition temperature on the composite coating film. Silica content can affect the glass transition temperature, and generally composites/coatings with higher glass transition temperatures have a wider thermal

performance window and indicate greater consistency in terms of performance. This is especially useful if SNAP particles are utilized in epoxide coatings for applications that involve a wide variety of temperatures (coatings on aircraft are exposed to temperatures ranging from -55°C to 60°C). Crosslink density can play a role in the performance of other coating parameters (tensile and fracture properties, elastic modulus, barrier properties against corrosion and corrosive substances, etc.). In addition, the crosslink density can be affected by the presence of sol-gel networks in the coating. The fracture properties are useful in determining the damage tolerance of a coating, composite, or film and are relatable to several other types of coating properties, notably the tensile properties, modulus, abrasion resistance, impact and reverse impact resistance. Also, the fracture properties are useful for gleaning information on how resistant a coating is to the aging process and weatherability, especially at various temperatures (ambient and hot conditions). The tensile properties are also useful in gleaning information on the weatherability of coating systems.[160]

In terms of the properties of coatings on metal substrates, the pull-off adhesion strength, abrasion resistance, and corrosion resistance were measured. The pull-off adhesion strength is a useful parameter measuring how tightly fastened the binder is to the substrate. While epoxides have good adhesion strength, the presence of siloxane groups covalently bonded to the metal substrate can enhance the adhesion strength of epoxide coatings. Silica content is resistant to abrasion and therefore enhances the abrasion resistance of epoxide coatings. Epoxides are often utilized as floor coatings, and the presence of sol-gel in epoxides can add to the longevity of these coatings. Last,

aluminum often is exposed to corrosive salt water environments (aluminum boats, aircraft stationed in marine environments, etc.), so it is useful to determine the barrier properties of SNAP loaded epoxide coatings immersed in sea water.

4.3.1 Characterization of SNAP Particles and GPTMS: NMR and ESI-MS

The 10:1 SNAP particles in butanol are shown in Figure 4.3 along with the most prevalent structures. GPTMS is one of the structures.

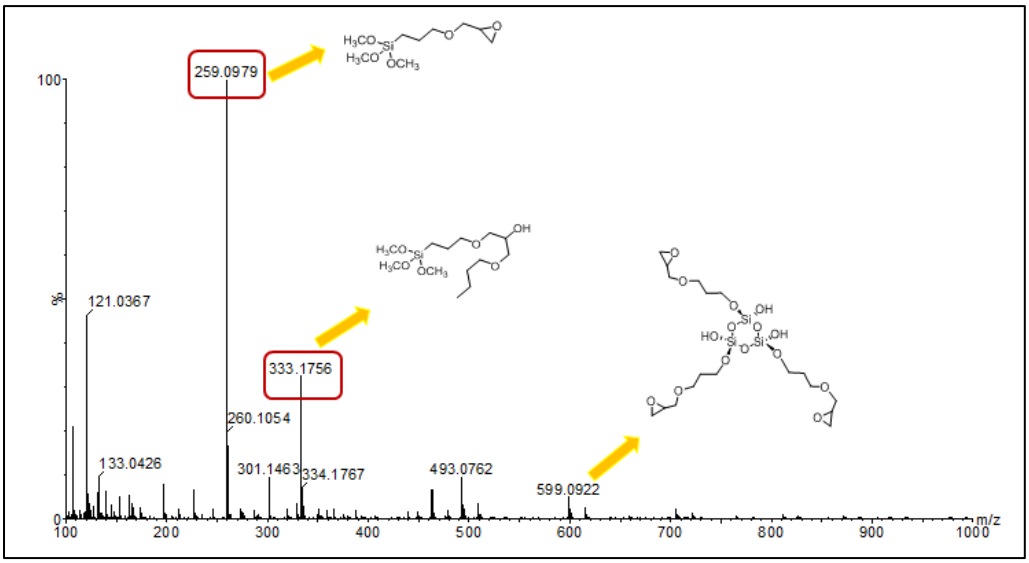

Figure 4.3: ESI-MS of 10:1 n-Butanol SNAP Structures

The most common structures observed for the 10:1 SNAP structures are shown in Figures 4.4 and 4.5. GPTMS is the most common structure, indicating that the much of the organo silane did not react in the non-aqueous solution. Other common structures include TMOS, TMOS and GPTMS-based organic silane structures that have undergone hydrolysis, siloxane, and polyether bonding.[163-171]

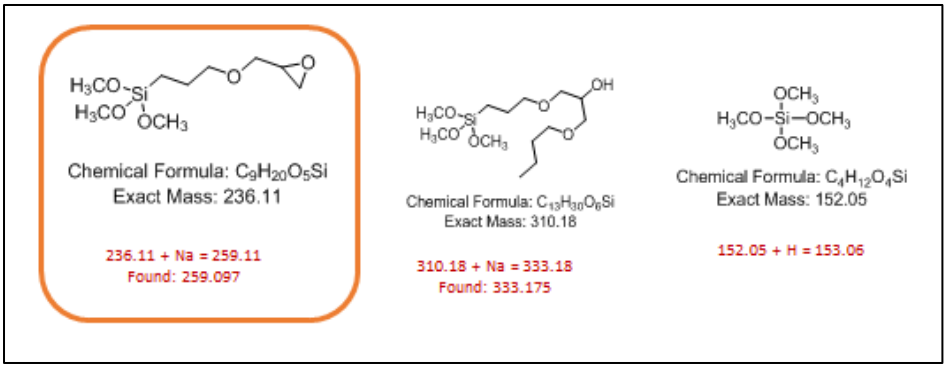

Figure 4.4: Proposed Structures of 10:1 SNAP in n-Butanol

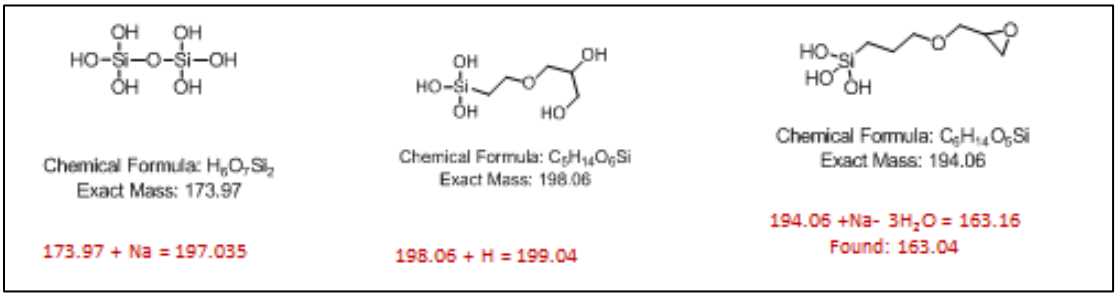

Figure 4.5: Proposed Structures of 10:1 SNAP in n-Butanol (2)

The spectrum in Figure 4.6 is the mass spectroscopy graph for the SNAP particles dissolved in H_2O. Most of the most common structures are polyether chains based upon the reaction of GPTMS.[163-171] It was difficult to predict the structures at molecular weights higher than 700.

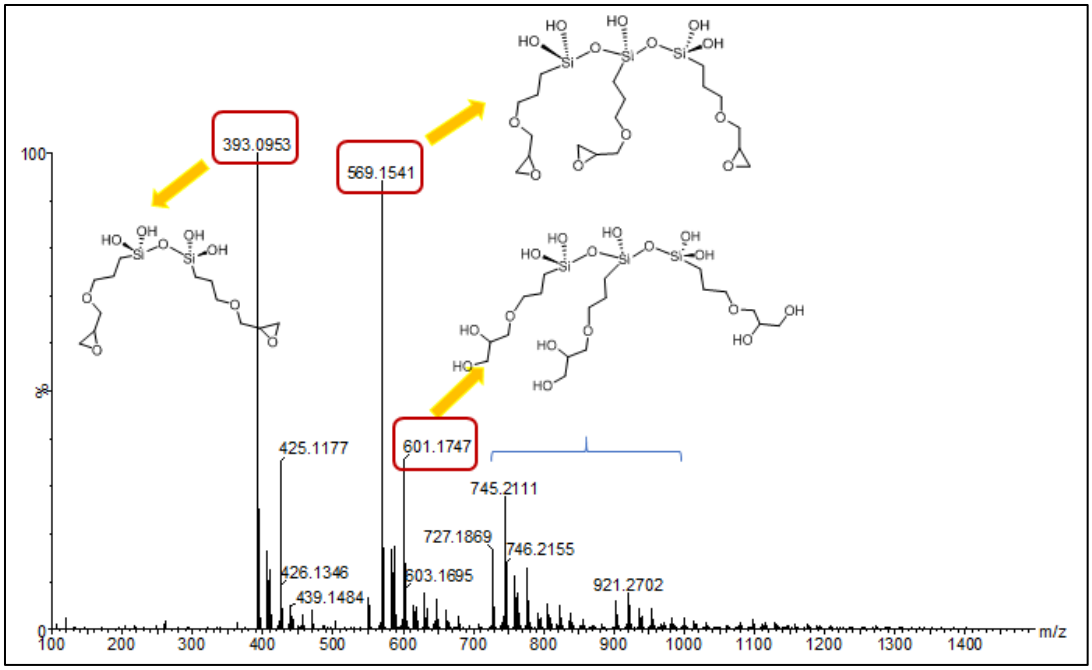

Figure 4.6: ESI-MS of 10:1 H_2O SNAP Structures

The most common structures are listed in Figure 4.7. Most of the most common structures are polyether chains based upon GPTMS. Some of the molecules have oxirane end groups that have undergone ring-opening reactions.

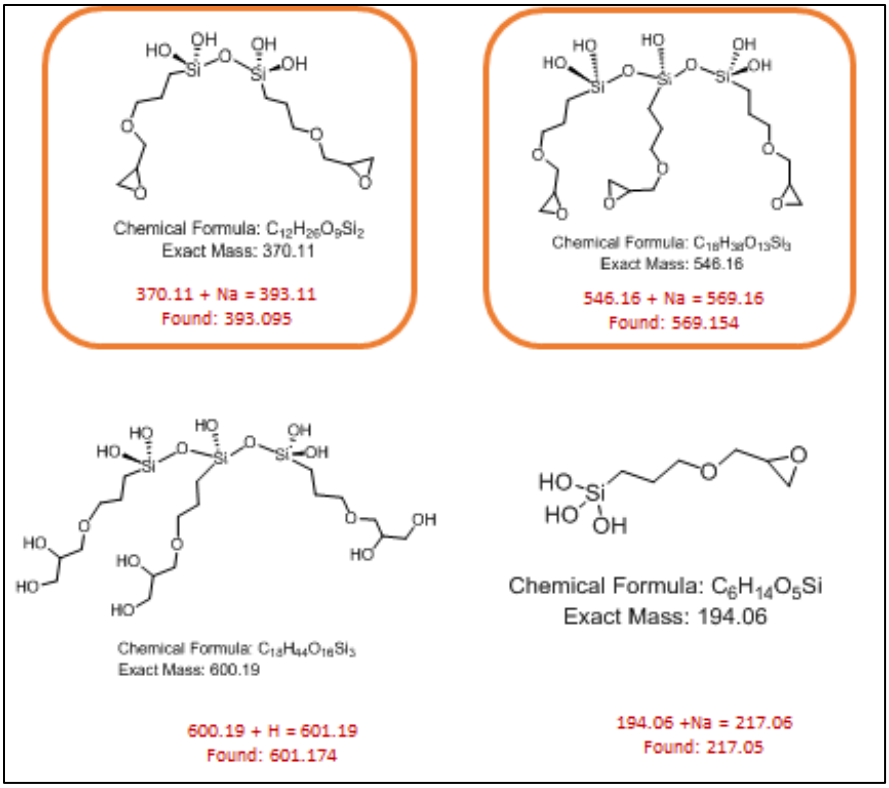

Figure 4.7: Proposed Structures of 10:1 SNAP in H_2O

The ^{29}Si NMR results for the SNAP particles in H_2O are shown in Figure 4.8. There are chemical shift peaks at -39.04, -48.55, -56.77, -58.22, -82.55, -90.83, and -92.02 ppm. The peak at -39.04 is associated with the T0 siloxane functionality (free hydrolyzed GPTMS), the peak at -48.55 is associated with the T1 siloxane functionality, the peaks at -56.77 and -58.22 are associated with the T2 functionality, the peak at -82.55 is associated with free non-hydrolyzed TMOS, and the peaks at the -90.83 and -92.02 are associated with the Q2 functionalities of TMOS.[163-171] Assuming a 3:1 molar ratio of GPTMS to TMOS, it should be assumed that the majority of the silicate molecules will be singly (T1) or doubly (T2) condensed.[163-171] The peaks from -64 to -67 would indicate triple condensation of GPTMS (T3).[163-171]

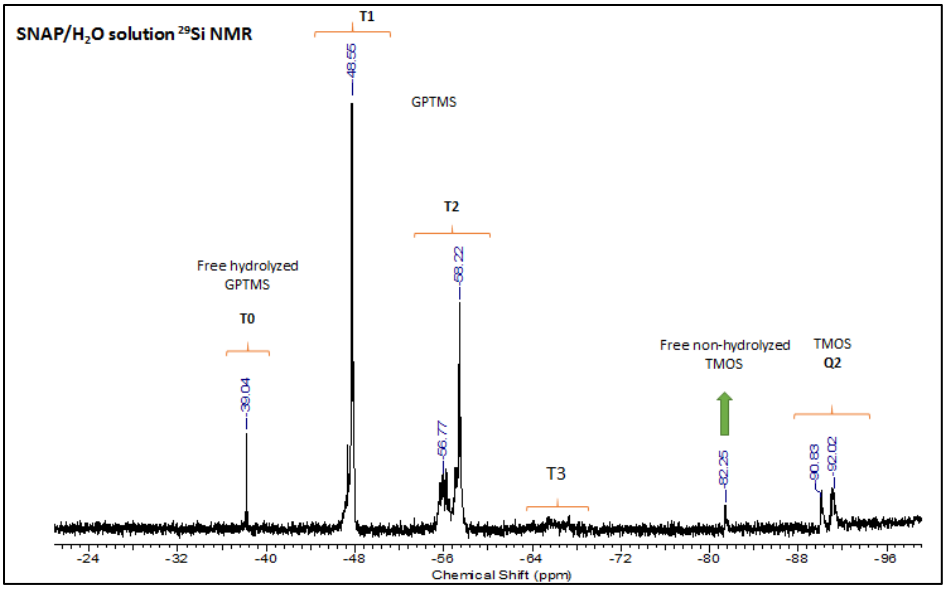

Figure 4.8: SNAP/H_2O Solution ^{29}Si NMR

The ^{29}Si NMR spectrum for the SNAP particles in butanol is shown in Figure 4.9. There are peaks at -39.12, -40.93, -48.17, -48.62, -81.95, and -91.40 ppm. The peak at -39.12 ppm is associated with the TO siloxane functionality, the peak at -40.03 ppm is associated with free hydrolyzed GPTMS, the peaks at -48.17 and -48.62 are associated with the T1 functionalities in GPTMS, the peak at -81.95 ppm is associated with free non-hydrolyzed TMOS, and the peak at -91.40 ppm is associated with the Q2 functionality in TMOS.[163-171] Comparing the NMR spectra for the SNAP particles in H_2O and butanol, the butanol SNAP particles are missing the T2 and T3 siloxane functionalities existent for the SNAP particles in H_2O. There are two peaks for the Q2 TMOS functionality for the SNAP particles in H_2O, while there is only one peak for the SNAP particles in butanol. The peak at -40.93 ppm (free non-hydrolyzed GPTMS) is only existent for the SNAP particles in butanol.

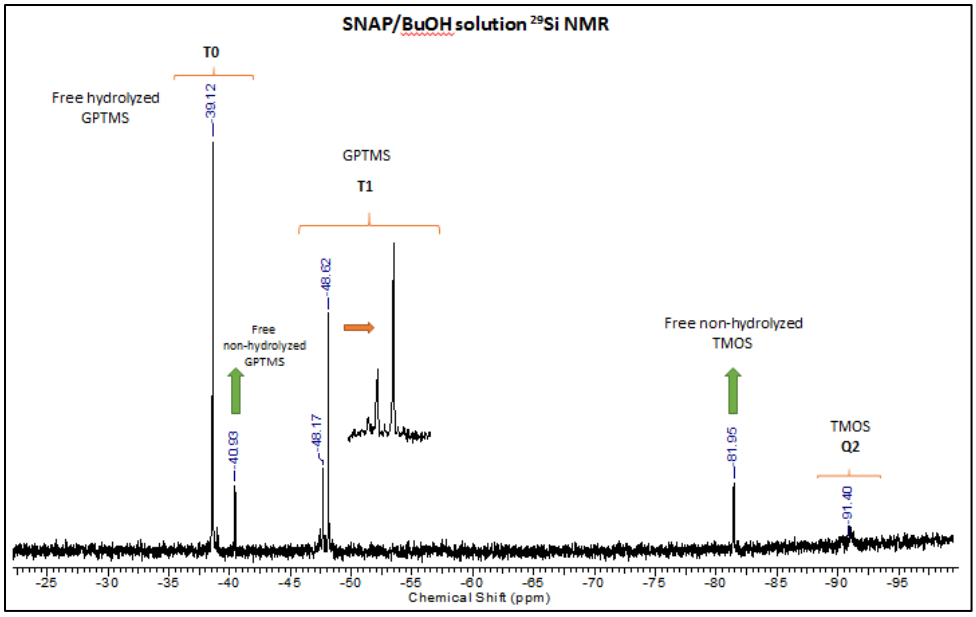

Figure 4.9: SNAP/Butanol Solution ^{29}Si NMR

The ^{1}H NMR results for GPTMS dissolved in chloroform are shown in Figure 4.10. The bonding schemes for GPTMS are indicated by the variables a, b, c, d, e, and f. The corresponding peaks on the ^{1}H NMR graph are indicated by the same variables.

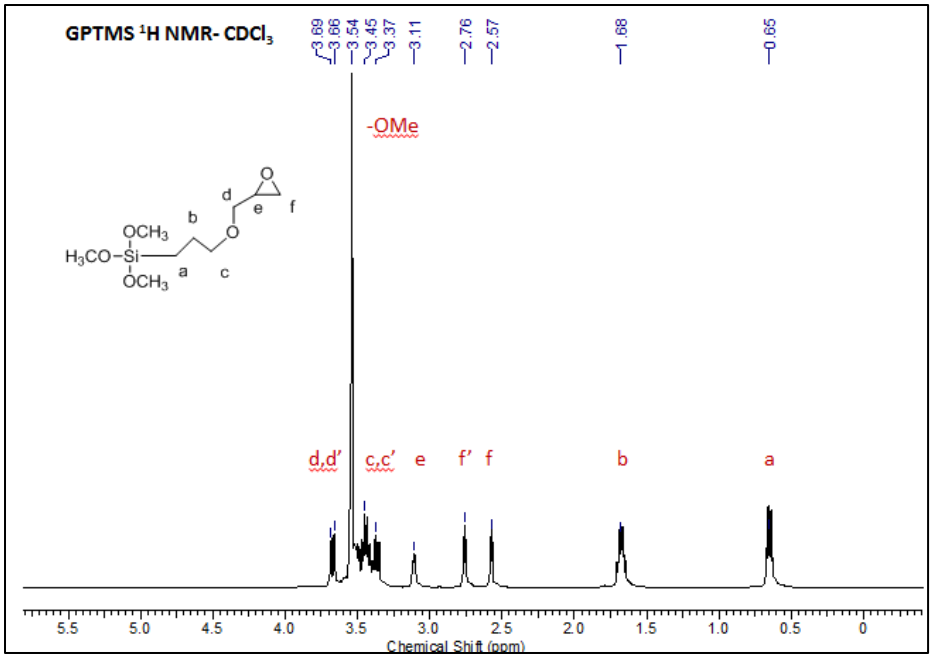

Figure 4.10: GPTMS ^{1}H NMR in Chloroform

The ^{1}H NMR results for the SNAP particles in butanol are shown in Figure 4.11. The peaks associated with n-butanol are indicated by the red cross, and the peaks associated with GPTMS are shown with the blue star. The ^{1}H NMR and ^{29}Si NMR indicate that there is difficulty in getting the GPTMS and TMOS to react in a non-aqueous medium.

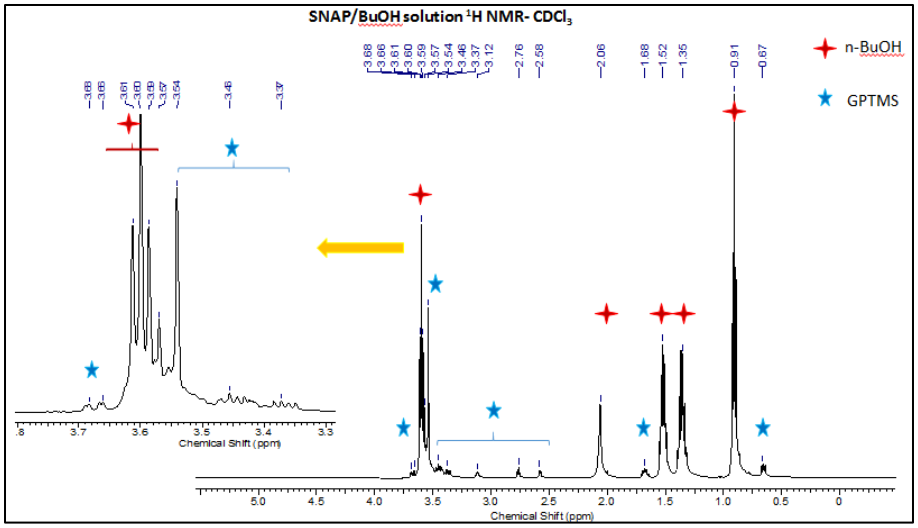

Figure 4.11: SNAP/Butanol Solution ^{1}H NMR in Chloroform

The ^{13}C NMR results for the SNAP particles in n-butanol are shown in Figure 4.12. The peaks at 73.6 and 70.97 ppm pertain to the 3 and 4 bonding positions at GPTMS, respectively. The peak at 51.07 pertains to the GPTMS bonding position 5, and the peaks at 44.28 and 44.23 pertain to the bonding position of 6. The peak at 22.61 ppm pertains to the bonding position at 2, and the peaks at 8.60 and 8.33 ppm correspond to the bonding position of 1. The peaks at 61.29, 34.17, 18.64, and 13.24 ppm correspond to n-butanol.

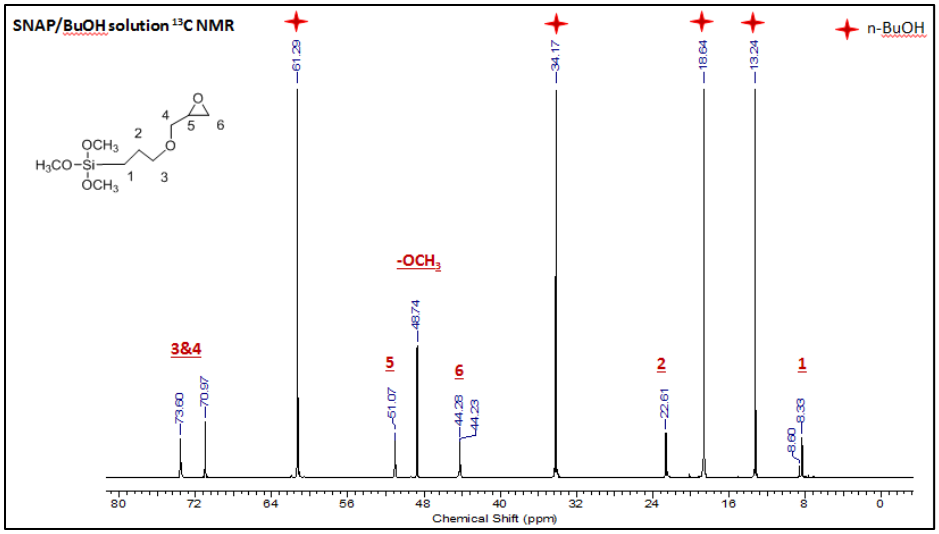

Figure 4.12: SNAP/Butanol Solution ^{13}C NMR

The ^{1}H NMR spectrum for the SNAP in H_2O is shown in Figure 4.13. The peak at -3.47 ppm corresponded to the O-Me groups, while the peaks labeled a through f corresponded to bonding on the GPTMS moiety. The star corresponds to broadening related to the presence of –OH groups, and the question mark is related to the aliphatic chain hydrogens. The peak between 4.5 and 5.0 ppm is related to the presence of water.

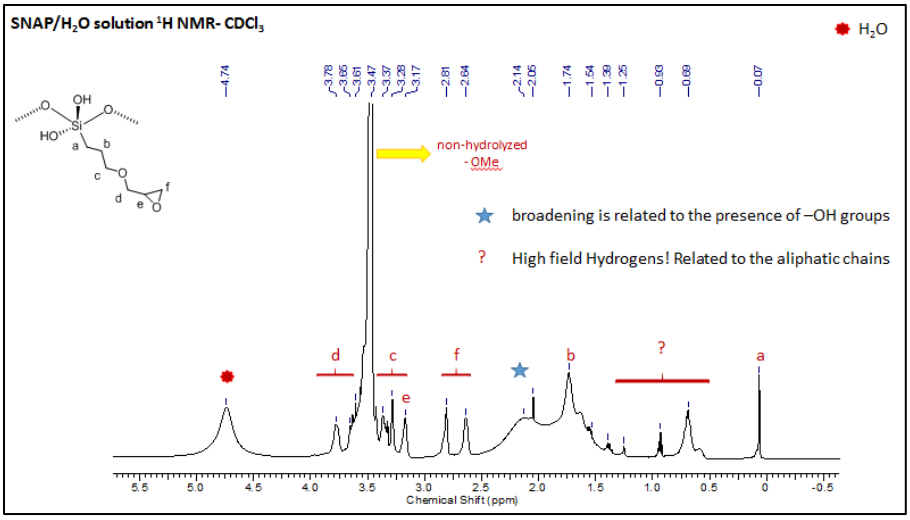

Figure 4.13: SNAP/H_2O Solution ^{1}H NMR in Chloroform

The ^{13}C NMR spectrum is shown in Figure 4.14. The peaks around 8, 22, 44, 49, and 51 ppm correspond to the GPTMS bonding groups of 1, 2, 6, O-Me, and 5, respectively. The range of peaks from 68 to 73 ppm corresponded to the GPTMS bonding groups for 3 and 4. The peaks at 58 and 63 ppm corresponded to low field carbons related to C-OH groups and miscellaneous carbon chains.

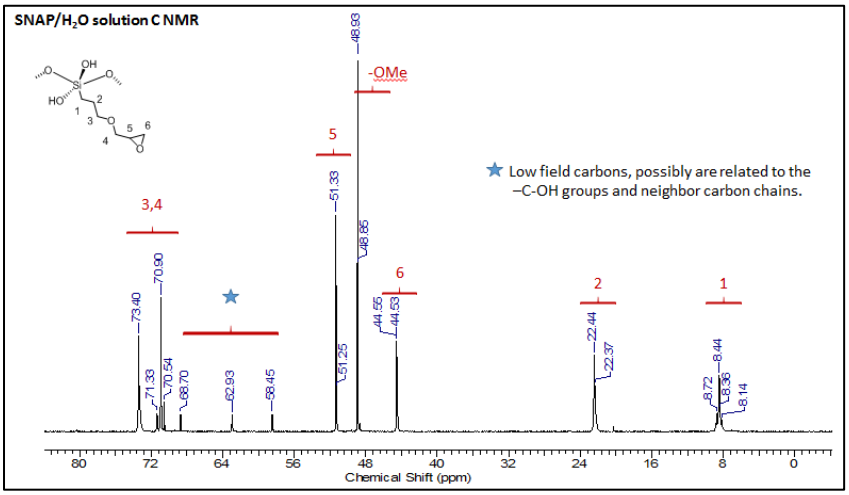

Figure 4.14: SNAP/H_2O Solution ^{13}C NMR

There were two epoxide equivalent weight measurements for neat GPTMS samples. The first measurement was 256.98, and the second measurement was 253.43. Considering the fact that GPTMS has a molecular weight of 236.11 and one oxirane group, there is close agreement between the EEW measurements and the theoretical EEW of GPTMS. The EEW measurements of SNAP particles in butanol were 230.51 and 227.09, indicating that some of the GPTMS oxirane end groups underwent ring opening reactions.

When compared to the SNAP particles synthesized in H_2O, the SNAP particles undergo less hydrolysis and condensation reactions to form sol-gel networks, although it is notable that a minority of SNAP colloids are formed in the process. It is evident that there is greater difficulty in utilizing n-butanol as a reactive solvent due to the larger size of n-butanol. This is attributed to the lower reactivity of the "carbon-oxygen bonds" in non-aqueous polar solvents.[172]

The MALDI-MS results of the 20:1 SNAP particles in n-butanol are shown in Figure 4.15. The molecular weights are larger than the molecular weights for 10:1 SNAP particles, indicating that larger solvent ratios produce larger molecular structures.

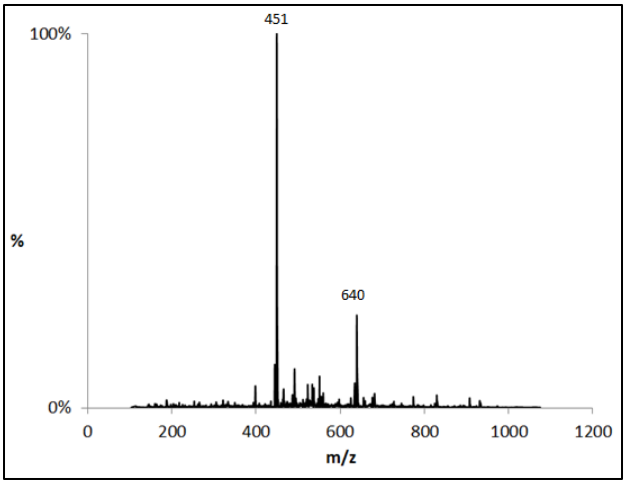

Figure 4.15: MALDI-MS Results for 20:1 SNAP Particles in n-Butanol

The ^{29}Si and ^{13}C NMR data of the 20:1 SNAP particles are shown in Figures 4.16 and 4.17.

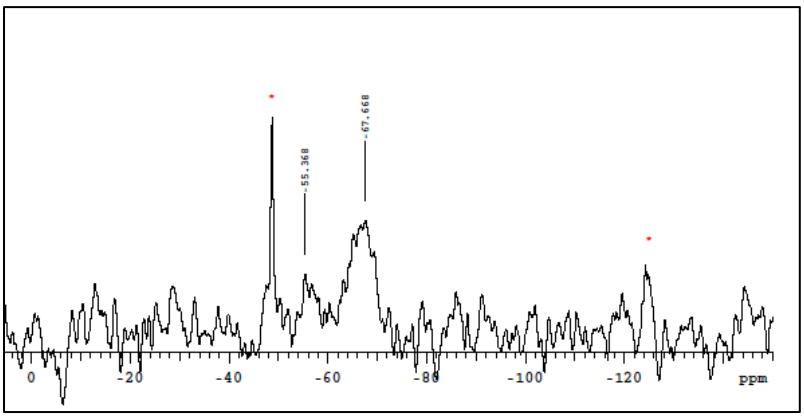

Figure 4.16: 20:1 SNAP ^{29}Si NMR Spectrum

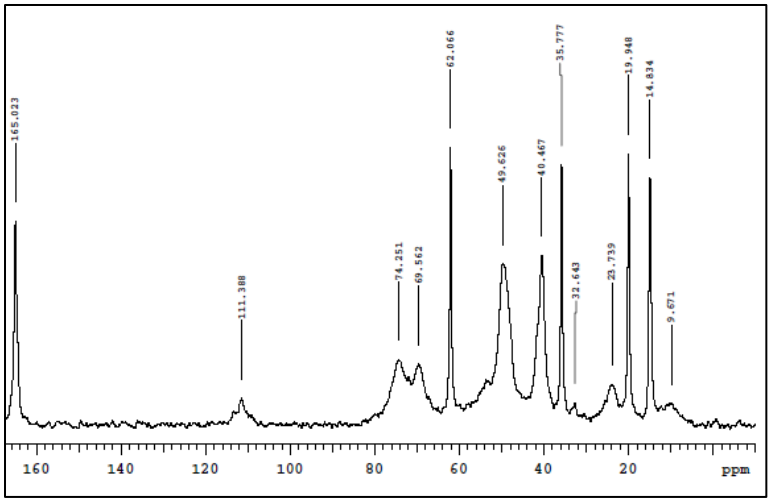

Figure 4.17: 20:1 SNAP ^{13}C NMR Spectrum

The ^{29}Si peaks at -50, -55.368, -67.668, and -120 are attributed to the T1, T2, T3, and Q4 siloxane functionalities.[162-170] The ^{13}C peaks at 9.671 and 23.739 are associated with the ≡Si-CH_2-CH_2 bonds, the peak at 14.834 is associated with the carbons in ethoxy groups, the peak at 69.562 is associated with carbon species 6 in dioxanes or diols, the peak at 49.626 is associated with carbons in residual methanol or methoxy groups, and the peak at 74.251 is associated with carbon species in 6 in PEO chains. This indicates that some of the GPTMS are reacting with one another in addition to TMOS due to the slightly acidic environment provided by the acetic acid. The peak at 32.643 is associated with some residual butanol, the peak at 40.467 is associated with the CH_2 bonding in the DETA crosslinker, and the peak at 165.023 is associated with C-N bonding.

Past literature has indicated that -68 can be attributed to cage-like T3 structures.[168] It is notable that the 10:1 SNAP particles have a higher percentage of T3 structures than the 20:1 SNAP particles. This can explain the better barrier properties of the 10:1 coating systems against corrosion as well as the higher crosslink density.

4.3.2 TEM Microscopy of SNAP Particles

TEM pictures of 10:1 and 20:1 SNAP particles are shown in Figures 4.17 and 4.18.

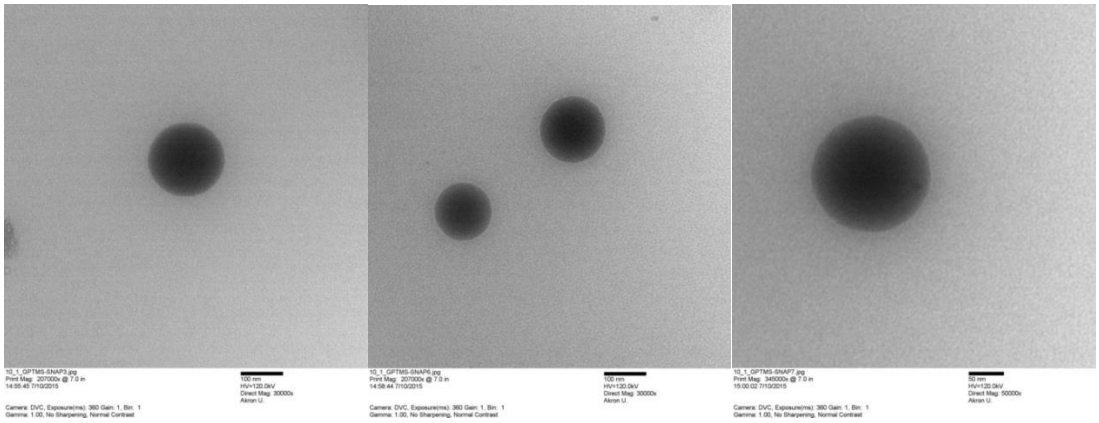

Figure 4.18: TEM Pictures of 10:1 SNAP Particles

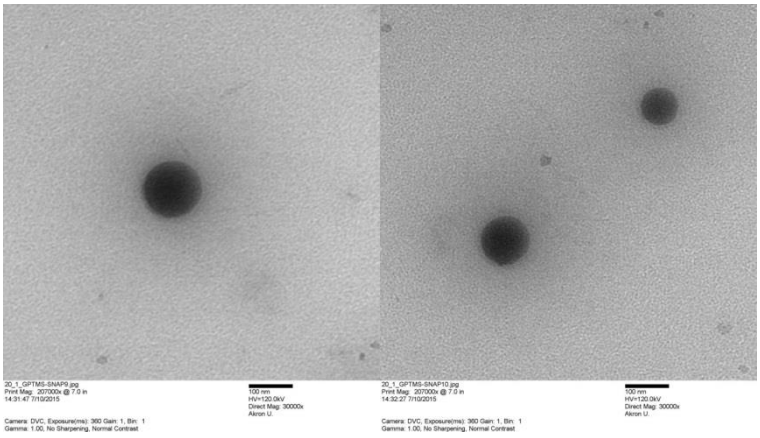

Figure 4.19: TEM Pictures of 20:1 SNAP Particles

The diameters of the 10:1 GPTMS-TMOS particles ranged from 144 to 172.5 nanometers. The 20:1 GPTMS-TMOS SNAP particles ranged in diameter from 100 to 135.5 nanometers. The TEM pictures did not indicate a difference in the size of the SNAP particles.

4.3.3 Dynamic Light Scattering: Particle Size Analysis of SNAP Particles

The issue with transmission electron microscopy is that the SNAP particles must be dried to observe their size and morphology. In order to obtain a more realistic picture of their size distribution, DLS was employed to determine the size of the particles while still in solution. In addition, evidence of sol-gel aggregation was investigated as well.

γ (a measure of frequency) is plotted versus the hydrodynamic radius (R_H) in Figure 4.20.

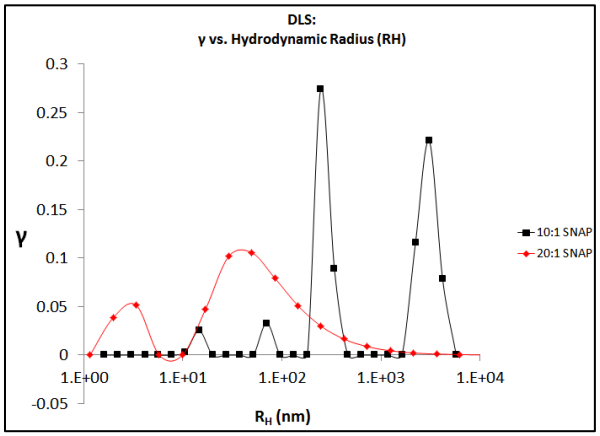

Figure 4.20: DLS Results of SNAP Particles

The 10:1 SNAP particles display several peaks (15 nm, 70 nm, 247 nm, 2,233 nm, and 4,192 nm). Although micron sized peaks were not observed during TEM, it is notable that the size distribution is much wider than the 20:1 SNAP particles. The 20:1 SNAP particles display two peaks at 3 and 85 nm. The peaks are more gradual than the 10:1 particle sizes. The average sizes of the particles are given in Table 4.3.

Table 4.3: Hydrodynamic Radii of SNAP Sol-Gel Particles

Name	Average R_H (nm)
10:1 GPTMS-TMOS SNAP Particles	68
20:1 GPTMS-TMOS SNAP Particles	44

The average R_H is 24 nm larger for the 10:1 SNAP particles. Smaller amounts of solvent are associated with larger particle sizes, which is in accordance with past literature.[173]

Based upon the sizes of the SNAP particles observed via TEM, it is assumed that some of the larger particles sizes observed in the SEM are attributed to aggregation of the particles. The lower solvent amounts might have contributed to higher particle concentrations and therefore greater aggregation. This may have played a role in the mechanical properties of the epoxide-polyamide films; greater aggregation of SNAP particles in the epoxide films led to weaker particle-binder interactions at higher loading of SNAP particles, which culminated in the mechanical properties peaking at 2.5% SNAP. 20:1 SNAP particles have smaller particle concentrations and therefore are more easily dispersed within the epoxide matrix with smaller degrees of aggregation. This ultimately created better mechanical properties.[174]

Conversely, the greater degree of aggregation of 10:1 SNAP particles in the epoxide matrix did have a positive effect; the formation of higher crosslink densities and better barrier properties as observed through EIS.

4.3.4 The Interaction of SNAP Sol-Gel Molecules with Epoxides and Polyamides

Figure 4.21 shows an idealized reaction showing a SNAP particles and epoxides crosslinking with polyamides. The hydroxyl groups on the DGEBA-epoxides as well as the siloxane groups covalently bond with the metal surface, enhancing the adhesion strength of the coating system.

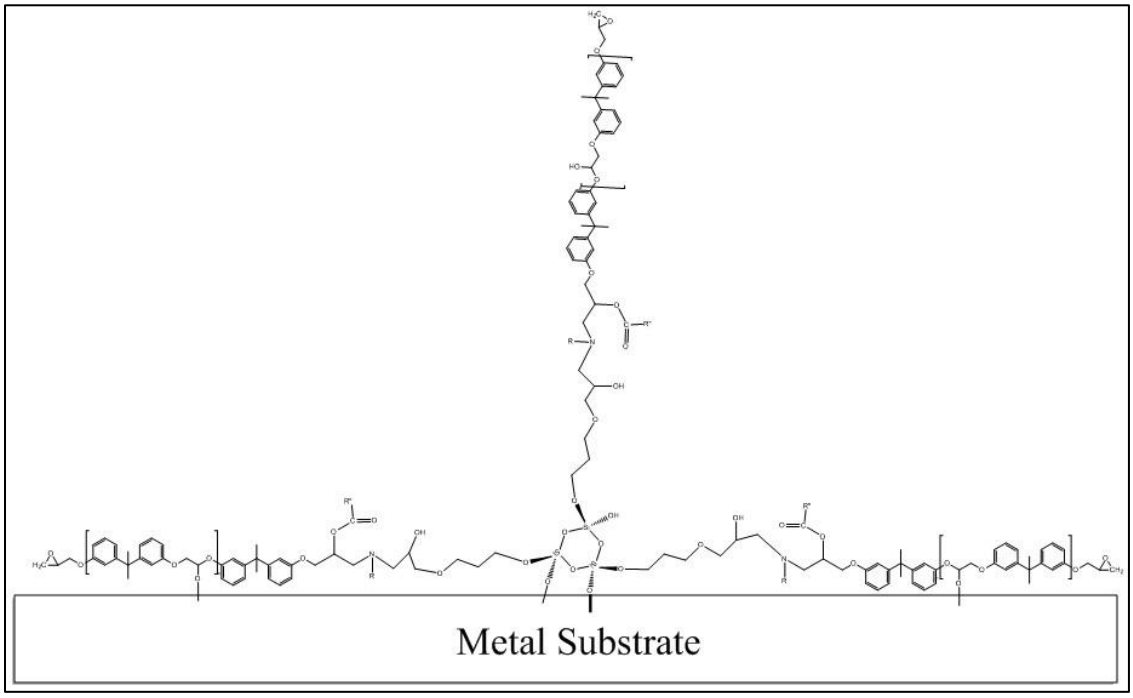

Figure 4.21: Proposed Schematic of Crosslinked SNAP-Epoxide-Polyamide Primer Coating

4.3.5 SEM Pictures of SNAP-Loaded Epoxide Films

SEM pictures of the SNAP-loaded epoxide films are shown in Figures 4.22 and 4.23. Figure 4.22 corresponds to neat epoxide epoxide films with 10:1 SNAP particles, and Figure 4.23 corresponds to epoxide films with 20:1 SNAP particles.

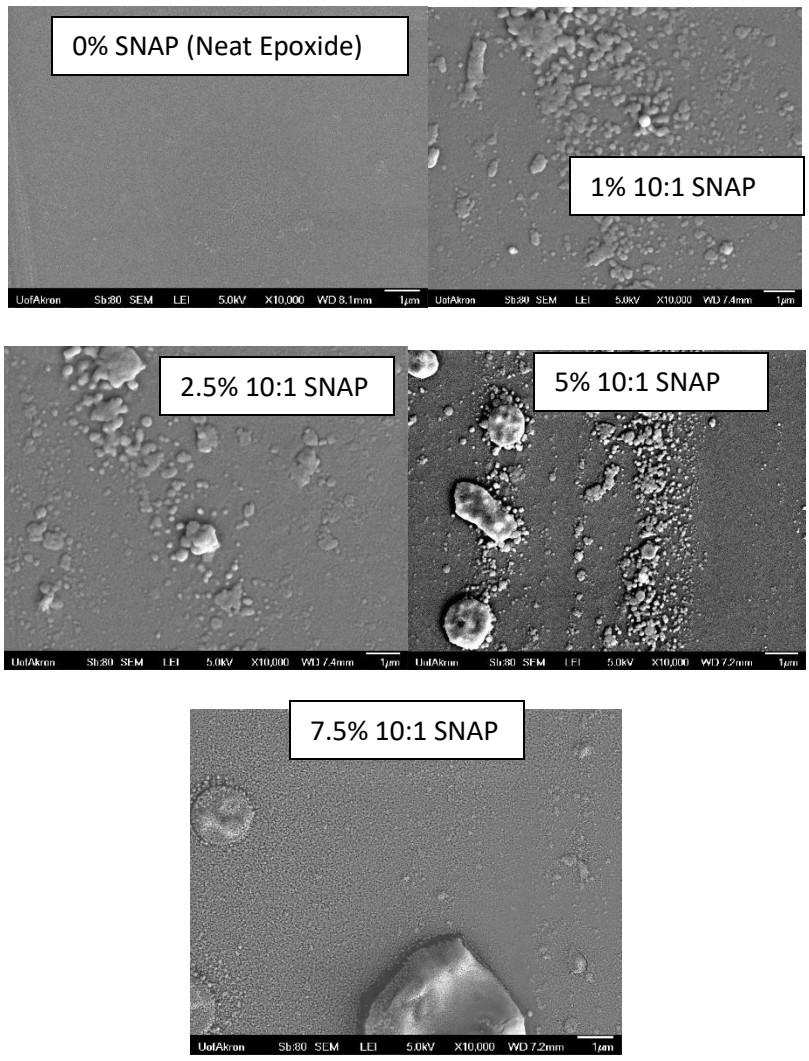

Figure 4.22: SEM Pictures of Neat Epoxide and 10:1 SNAP-Loaded Epoxide Films

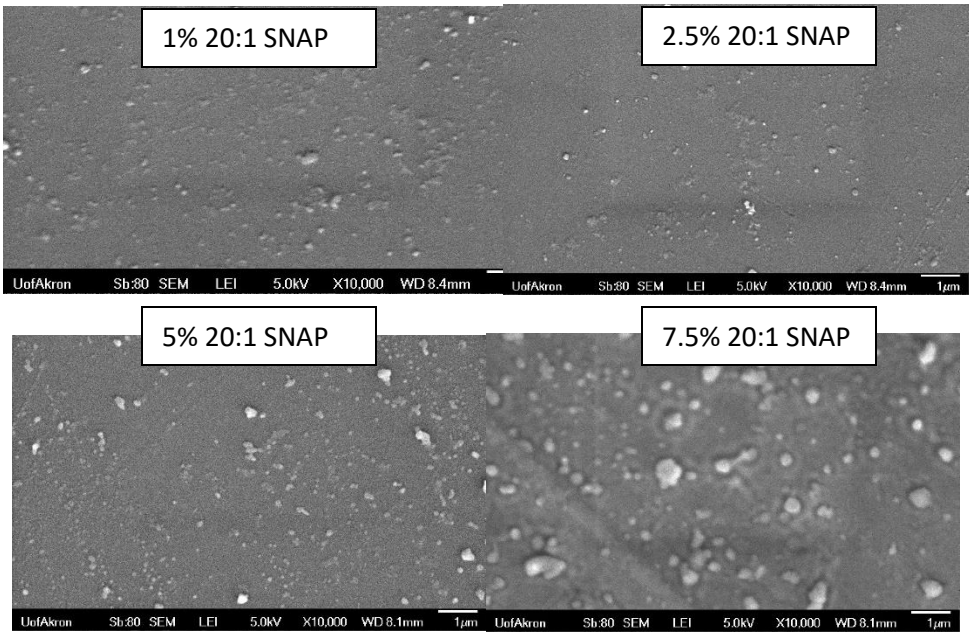

Figure 4.23: SEM Pictures of 20:1 SNAP-Loaded Epoxide Films

Neat epoxide indicates a smooth epoxide-polyamide matrix with the absence of sol-gel domains on the surface. 10:1 SNAP-loaded epoxide films indicate of aggregation of particles, producing sol-gel domains a few microns in width. Greater particle amounts occur with higher levels of SNAP content. At 7.5% 10:1 SNAP, there are innumerable sub-micron size particle sol-gel domains along with a large sol-gel particle several microns in width. The greater aggregation and larger size of the 10:1 SNAP particles may be contributing to the elevated corrosion barrier properties later observed during the EIS tests, but may also be contributing to more rigid matrices and easier fracture. 20:1 SNAP-loaded epoxide films indicates the presence of sol-gel domains on the surface of the epoxide coating, which later culminated in augmented contact angle measurements and resistances to abrasion. At 1% SNAP, the sol-gel domains range in size from less than 100 nm in diameter up to 500-1,000 nanometers in size, indicating

that some aggregation has occurred. The same phenemon is observed for 2.5% and 5% SNAP. The particle sizes are larger for 7.5% SNAP, indicating that a greater amount of aggregation has occurred. The spacing of the particles for 20:1 SNAP-loaded films is better (shows better dispersion), indicating that the greater amount of solvent led to greater dispersion of the particles while still suspended in solution prior to mixing and reaction with the epoxide-polyamide matrix. The better dispersion properties would later lead to superior physical properties of the finished films and coatings.

4.3.6 Thermal and Thermal-Mechanical Measurements of Epoxide-Polyamide Films

The DSC graphs are shown in Figures 4.24 and 4.25. The average glass transition temperature is plotted versus the SNAP weight percentage.

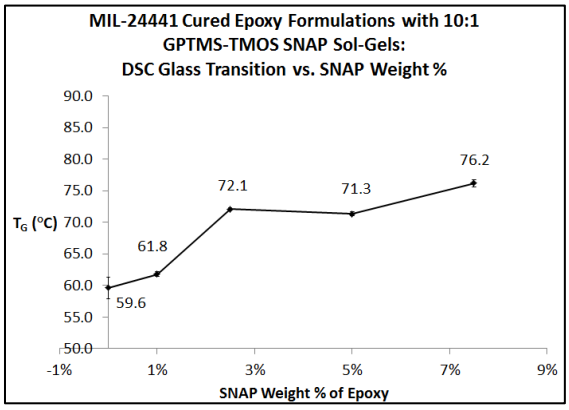

Figure 4.24: DSC T_G vs. SNAP Wt. % (10:1 SNAP Particles in n-Butanol)

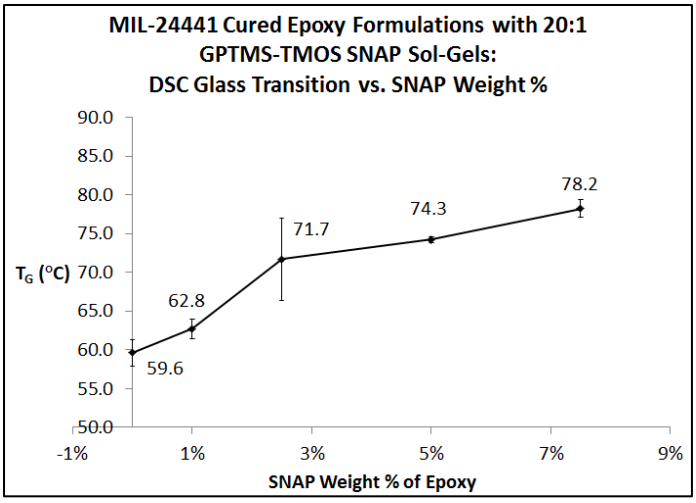

Figure 4.25: DSC T_G vs. SNAP Wt. % (20:1 SNAP Particles in n-Butanol)

The cured epoxide films loaded with SNAP particles showed a gradual increase in the glass transition temperature, which is due to the higher crosslink densities as well as the limited "chain mobility" associated with the placement of the particles.[175]

The crosslink densities of the epoxide-polyamide films (with SNAP added) are observed in Figures 4.26 and 4.27. The crosslink densities are plotted as a function of the SNAP weight %.

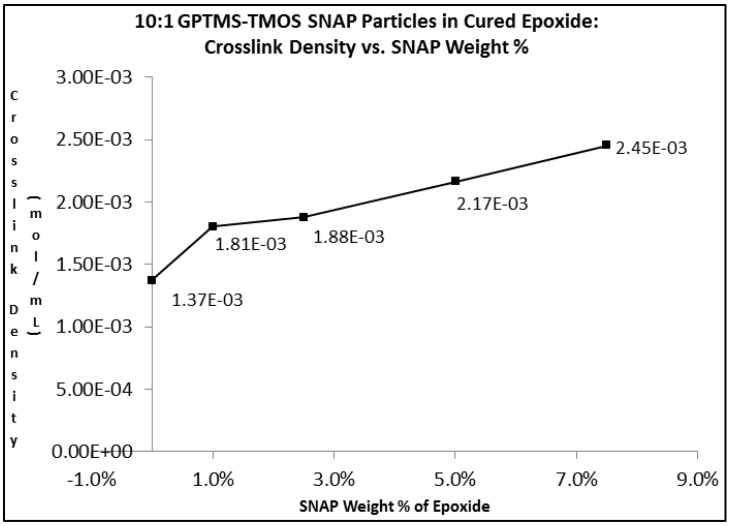

Figure 4.26: Crosslink Density (DMA) vs. SNAP Weight % (10:1 SNAP Particles in n-Butanol)

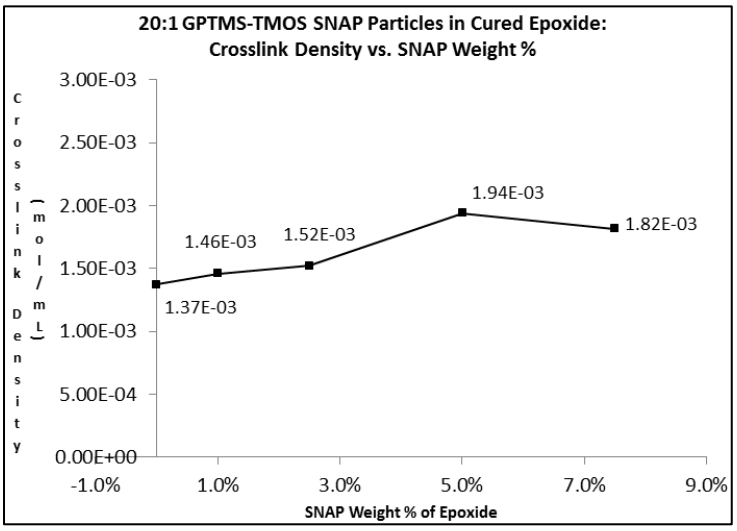

Figure 4.27: Crosslink Density (DMA) vs. SNAP Weight % (20:1 SNAP Particles in n-Butanol)

Neat films (no SNAP) had average crosslink densities of $1.46*10^{-3}$ mol/mL. Films with 10:1 SNAP particles decreased to $1.34*10^{-3}$ mol/mL at 1% SNAP content and increased to $2.45*10^{-3}$ mol/mL at 7.5% SNAP content. The average crosslink density for

epoxide-polyamide films with 20:1 SNAP particles increased to $1.94*10^{-3}$ mol/mL at 5% SNAP content and decreased to $1.82*10^{-3}$ mol/mL at 7.5% SNAP content. The crosslink density at 7.5% is 33% higher for 10:1 SNAP than for 20:1 SNAP. The higher crosslink densities are attributable to the formation of the more densely packed inorganic sol-gel networks.[147]

4.3.7 Tensile Properties of Epoxide-Polyamide Films

The tensile strengths of the epoxide-polyamide films are plotted in Figures 4.28 and 4.29 as a function of the SNAP weight percentage.

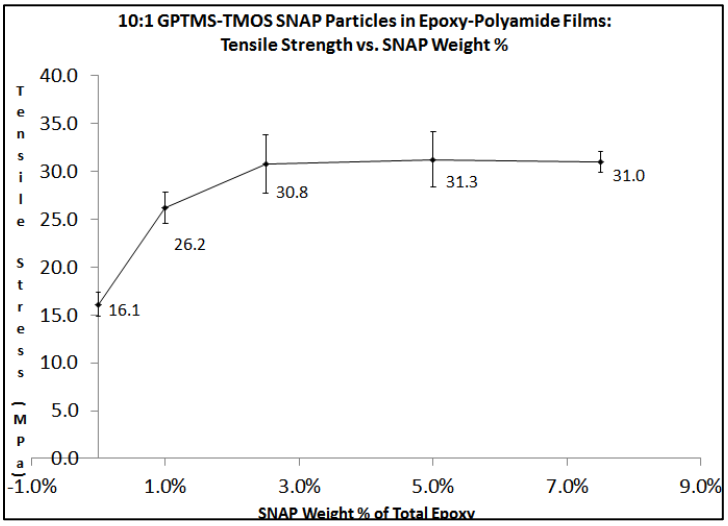

Figure 4.28: Tensile Strength vs. SNAP Weight % (10:1 SNAP Particles in Epoxide-Polyamide Films)

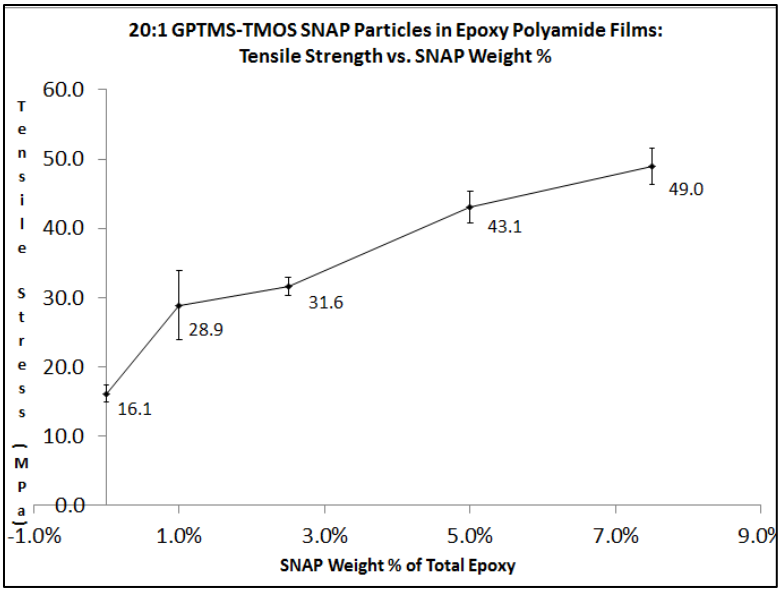

Figure 4.29: Tensile Strength vs. SNAP Weight % (20:1 SNAP Particles in Epoxide-Polyamide Films)

The average tensile strength of neat epoxide is 16.1 MPa. For epoxide polyamide films loaded with 10:1 SNAP particles, the tensile strength increases to 30.8 MPa at 2.5% and remains at this level for 5% and 7.5% SNAP. Past literature has indicated that this may be due to the formation of voids in the sample.[180] The existence of larger particles or aggregation of smaller ones as observed via DLS may be contributing to this phenomenon. The 20:1 SNAP particles continuously increase to an average tensile strength of 49.0 MPa at 7.5% SNAP. This is due to the smaller particle sizes and the larger MWs of the 20:1 colloidal molecules, which leads to greater flexibility and greater dispersion into the epoxide matrix.[176-177] The tensile strength values (20-40 MPa) and increases (generally between 30%-100% increase) are in line with past literature.[176,178] The increase in the tensile strength is due to the increased

crosslink densities, covalent bonding of the siloxane domains of the sol-gel content, and delay of fracture provided by the particle content.

The tensile strength 2-sample T tests for the 10:1 SNAP loaded films are shown in Table 4.4. All sample sets show a statistically significant difference when compared to the epoxide control set.

Table 4.4: 10:1 SNAP Loaded Film Tensile Strength 2-Sample T P-Value Results

Name	SNAP Weight %	2-Sample T P-Value from Control	Significant?
10:1 SNAP	1.0%	0.000	Yes
10:1 SNAP	2.5%	0.015	Yes
10:1 SNAP	5.0%	0.002	Yes
10:1 SNAP	7.5%	0.000	Yes

The tensile strength 2-sample T tests for the 20:1 SNAP loaded films are shown in Table 4.5. The 5% and 7.5% SNAP sample sets show a statistically significant difference when compared to the epoxide control set.

Table 4.5: 20:1 SNAP Loaded Film Tensile Strength 2-Sample T P-Value Results

Name	SNAP Weight %	2-Sample T P-Value from Control	Significant?
20:1 SNAP	1.0%	0.136	No
20:1 SNAP	2.5%	0.088	No
20:1 SNAP	5.0%	0.000	Yes
20:1 SNAP	7.5%	0.000	Yes

The elongation percentages of the epoxide polyamide films are shown in Figures 4.30 and 4.31.

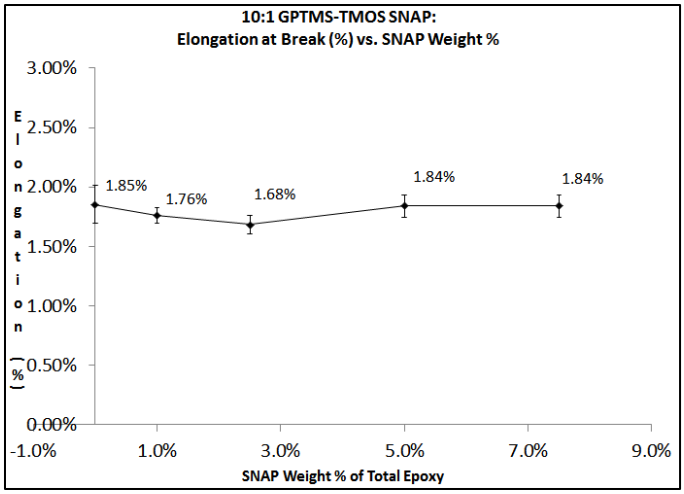

Figure 4.30: Elongation at Break (%) vs. SNAP Wt. % (10:1 SNAP Particles in Epoxide-Polyamide Films)

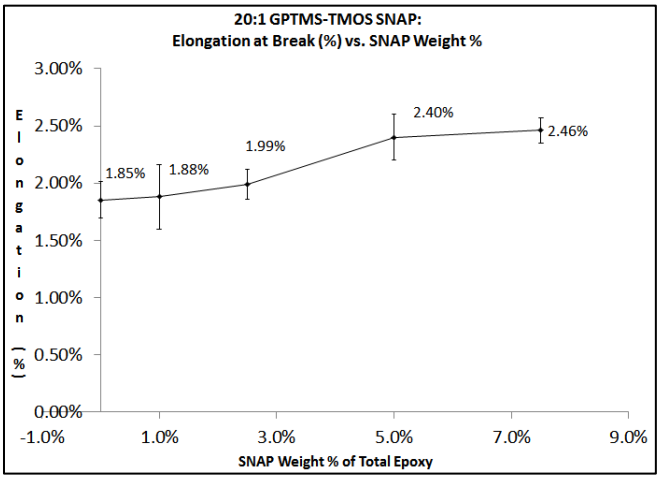

Figure 4.31: Elongation at Break (%) vs. SNAP Wt. % (20:1 SNAP Particles in Epoxide-Polyamide Films)

The elongation percentage remains approximately constant while loaded with epoxide polyamide 10:1 SNAP particles. The epoxide polyamide films loaded with 20:1 SNAP particles undergo a modest increase from 1.88% (1% SNAP) to 2.46% (7.5% SNAP).

The modest flexibility increase is due to the higher MWs associated with the 20:1 SNAP structures and better dispersion into the epoxide matrix.[179] In addition, the agglomeration of the 10:1 SNAP particles in the epoxide-polyamide films may contribute to a reduction in the elongation at break, as confirmed by Islam et al.[180] and Rubab et al.[181] The elongation at break values are within the same range as past literature investigating thermosetting epoxide materials with silica and sol-gel domains.[176]

The elongation % 2-sample T tests for the 10:1 SNAP loaded films are shown in Table 4.6. No sample set shows a statistically significant difference.

Table 4.6: 10:1 SNAP Loaded Film Elongation % 2-Sample T P-Value Results

Name	SNAP Weight %	2-Sample T P-Value from Control	Significant?
10:1 SNAP	1.0%	0.925	No
10:1 SNAP	2.5%	0.359	No
10:1 SNAP	5.0%	0.940	No
10:1 SNAP	7.5%	0.923	No

The elongation % 2-sample T tests for the 20:1 SNAP loaded films are shown in Table 4.7. The 5% and 7.5% SNAP sample sets show a statistically significant difference when compared to the epoxide control set.

Table 4.7: 20:1 SNAP Loaded Film Elongation % 2-Sample T P-Value Results

Name	SNAP Weight %	2-Sample T P-Value from Control	Significant?
20:1 SNAP	1.0%	0.934	No
20:1 SNAP	2.5%	0.520	No
20:1 SNAP	5.0%	0.047	Yes
20:1 SNAP	7.5%	0.007	Yes

The elastic moduli versus the SNAP weight percentage are plotted in Figures 4.32 and 4.33.

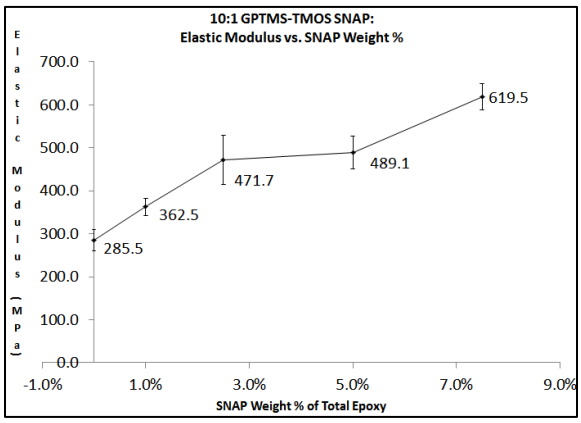

Figure 4.32: Elastic Modulus vs. SNAP Wt. % (10:1 SNAP in n-butanol)

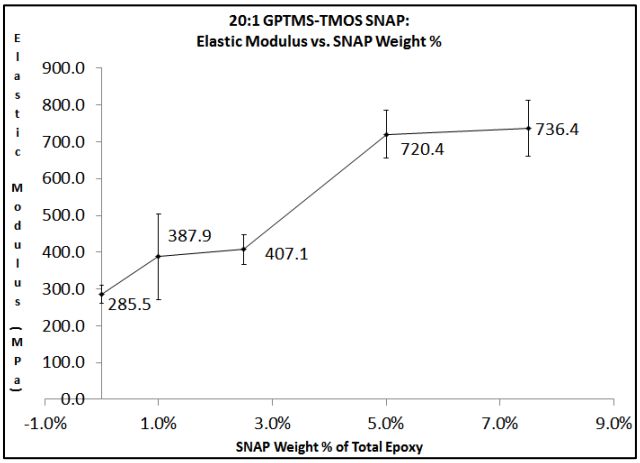

Figure 4.33: Elastic Modulus vs. SNAP Wt. % (20:1 SNAP in n-butanol)

Increases in the SNAP content correlate with increases in the elastic moduli for both the 10:1 and 20:1 SNAP-loaded films. This is like past observations in literature, which indicates that siloxane bonding and increases in the crosslink density can lead to an increase in the modulus.[41,58,147,182-183] The 20:1 SNAP particles show a slightly more substantial increase, although the difference isn't statistically significant. The slightly

higher moduli and elongation capacity of the 20:1 films explain the higher tensile strengths of the material.

The elastic modulus 2-sample T tests for the 10:1 SNAP loaded films are shown in Table 4.8. The 7.5% SNAP sample set is the only one that is significantly different.

Table 4.8: 10:1 SNAP Loaded Film Elastic Modulus 2-Sample T P-Value Results

Name	SNAP Weight %	2-Sample T P-Value from Control	Significant?
10:1 SNAP	1.0%	0.792	No
10:1 SNAP	2.5%	0.154	No
10:1 SNAP	5.0%	0.087	No
10:1 SNAP	7.5%	0.000	Yes

The elastic modulus 2-sample T results of the 20:1 SNAP filled epoxide films are shown in Figure 4.9. The 5% and 7.5% SNAP filled epoxide films are the only sample sets that are significantly different than the neat epoxide film sample set.

Table 4.9: 20:1 SNAP Loaded Film Elastic Modulus 2-Sample T P-Value Results

Name	SNAP Weight %	2-Sample T P-Value from Control	Significant?
20:1 SNAP	1.0%	0.858	No
20:1 SNAP	2.5%	0.414	No
20:1 SNAP	5.0%	0.001	Yes
20:1 SNAP	7.5%	0.001	Yes

4.3.8 Fracture Properties of Epoxide-Polyamide Films with SNAP Particles

The fracture toughness (K_{IC}) results are shown in Figure 4.34 and 4.35.

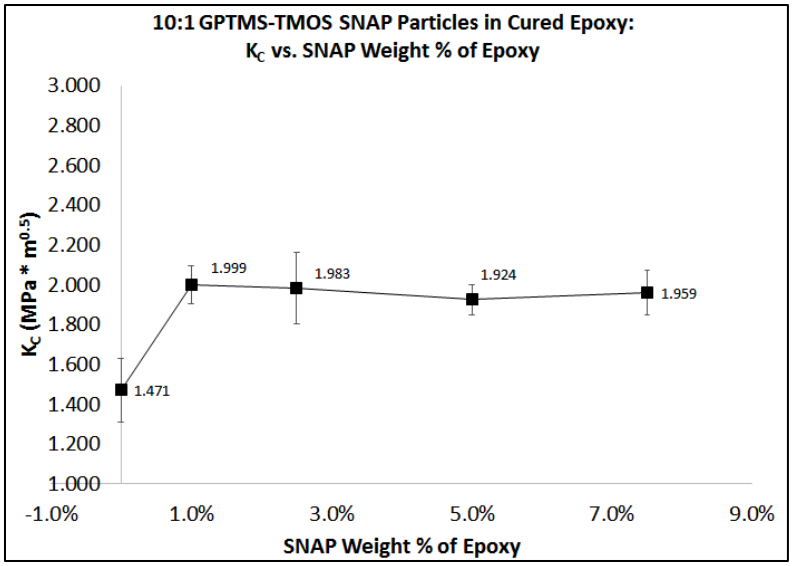

Figure 4.34: K_C at 20°C vs. SNAP Wt. % (10:1 SNAP Particles in n-Butanol)

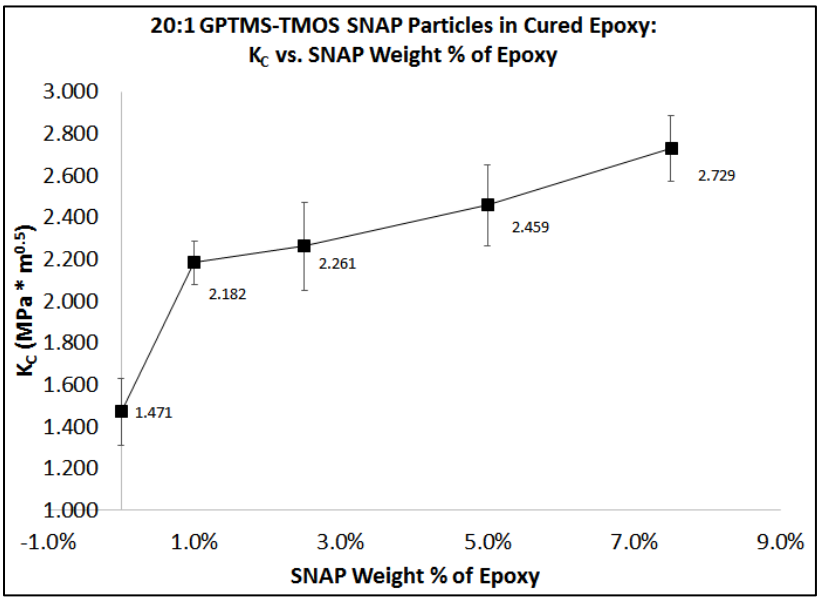

Figure 4.35: K_C at 20°C vs. SNAP Wt. % (20:1 SNAP Particles in n-Butanol)

The 10:1 epoxide-film show a 33% increase from neat epoxide (1.471 MPa*$m^{0.5}$) to 1% SNAP. The K_C values stay approximately equivalent for all other sets. The 20:1 SNAP samples sets show a continual increase up to 2.729 MPa*$m^{0.5}$, which is an 80% increase from neat epoxide. This matches the phenomena observed for the tensile

tests. Past literature has indicated that the presence of functional sol-gels can enhance the fracture toughness of a epoxide film through covalent bonding and crack deflection.[147,178] The fracture toughness values (0.5 MPa*$m^{0.5}$ to 2.8 MPa*$m^{0.5}$) match that of past literature.[176]

To determine if the differences between the sample sets, 2-sample T tests were conducted comparing the neat epoxy films to the SNAP loaded films. The points of the tests were to determine if the presence of the SNAP particles in the films led to a noticeable improvement in the fracture properties. In Table 4.10, the K_C results for the 10:1 SNAP loaded films are compared to the K_C results for the neat epoxide films. As stated before, a 2-sample T result of less than 0.05 indicates a statistically significant difference.

Table 4.10: 10:1 SNAP Loaded Film K_C 2-Sample T P-Value Results

Name	SNAP Weight %	2-Sample T P-Value from Control	Significant?
10:1 SNAP	1.0%	0.013	Yes
10:1 SNAP	2.5%	0.012	Yes
10:1 SNAP	5.0%	0.025	Yes
10:1 SNAP	7.5%	0.024	Yes

All four sample sets (1%, 2.5%, 5%, and 7.5% SNAP) show significant improvements over neat epoxide films.

The 20:1 SNAP K_C 2-sample T tests are listed in Table 4.11. All sample sets show a statistically significant difference when compared to the epoxide control set.

Table 4.11: 20:1 SNAP Loaded Film K_C 2-Sample T P-Value Results

Name	SNAP Weight %	2-Sample T P-Value from Control	Significant?
20:1 SNAP	1.0%	0.002	Yes
20:1 SNAP	2.5%	0.010	Yes
20:1 SNAP	5.0%	0.000	Yes
20:1 SNAP	7.5%	0.000	Yes

The elastic energy strain rate results (G_C) at 20°C are shown in Figures 4.36 and 4.37.

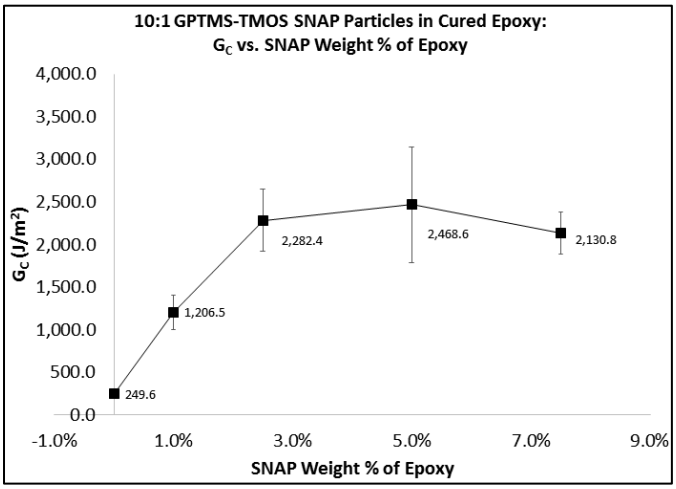

Figure 4.36: G_C at 20°C vs. SNAP Wt. % (10:1 SNAP Particles in n-Butanol)

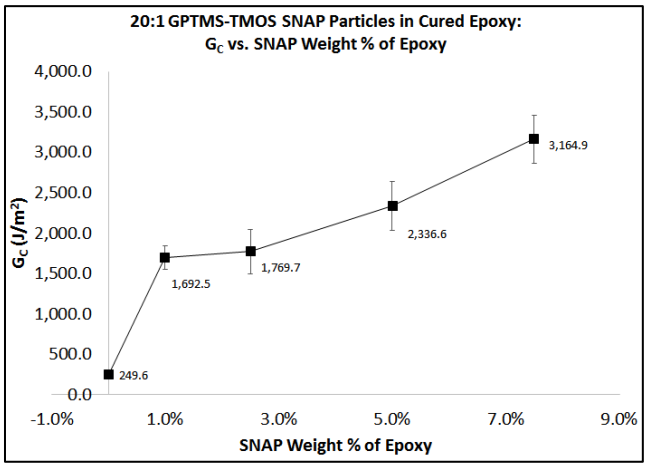

Figure 4.37: G_C at 20°C vs. SNAP Wt. % (20:1 SNAP Particles in n-Butanol)

The average G_C for neat epoxide is 249.6 J/m^2. The G_C values increase to 2,200 J/m^2 for 2.5% 10:1 SNAP and stay at approximately the same values for 5% and 7.5%. The G_C values for 20:1 SNAP particles increase to 3,164.9 J/m^2 at 7.5% SNAP content, which is greater than a 12-fold increase. The addition of SNAP particles can also increase the energy required to propagate fracture within the epoxide sample, generally by the covalent bonds of the sol-gels as well as crack deflection around the sol-gel domains. The G_C values reported in literature are within the same range (100-4700 J/m^2) as the reported results.[176]

The 10:1 SNAP G_C 2-sample T tests are listed in Table 4.12. All sample sets show a statistically significant difference when compared to the epoxide control set.

Table 4.12: 10:1 SNAP Loaded Film G_C 2-Sample T P-Value Results

Name	SNAP Weight %	2-Sample T P-Value from Control	Significant?
10:1 SNAP	1.0%	0.001	Yes
10:1 SNAP	2.5%	0.001	Yes
10:1 SNAP	5.0%	0.002	Yes
10:1 SNAP	7.5%	0.000	Yes

The 20:1 SNAP G_C 2-sample T tests are listed in Table 4.13. All sample sets show a statistically significant difference when compared to the epoxide control set.

Table 4.13: 10:1 SNAP Loaded Film G_C 2-Sample T P-Value Results

Name	SNAP Weight %	2-Sample T P-Value from Control	Significant?
20:1 SNAP	1.0%	0.000	Yes
20:1 SNAP	2.5%	0.000	Yes
20:1 SNAP	5.0%	0.000	Yes
20:1 SNAP	7.5%	0.000	Yes

The K_C values at 60°C are shown in Figures 4.38 and 4.39.

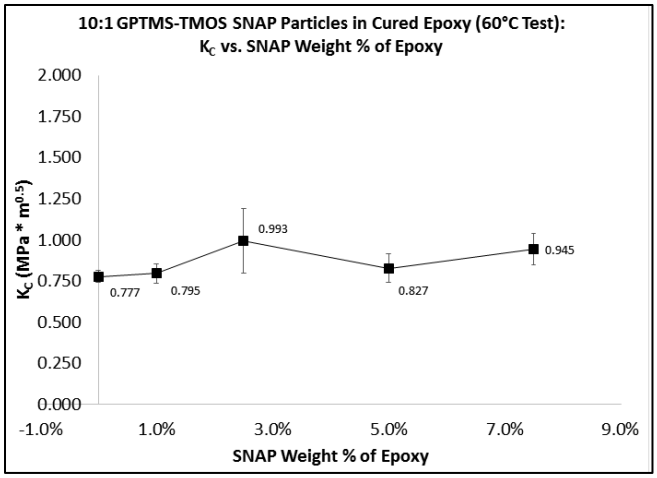

Figure 4.38: K_C at 60°C vs. SNAP Wt. % (10:1 SNAP Particles in n-Butanol)

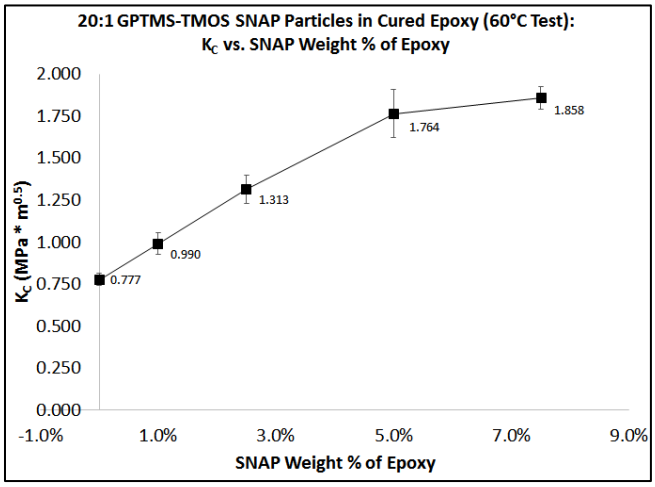

Figure 4.39: K_C at 60°C vs. SNAP Wt. % (20:1 SNAP Particles in n-Butanol)

10:1 SNAP formulations undergo a modest increase at 2.5%, but the increase is not statistically significant. The average K_C at 60°C is largely the same for all SNAP percentages. 20:1 SNAP formulations undergo a linear increase in the K_C up to 5% SNAP and then level off to 1.858 MPa*$m^{0.5}$ at 7.5% SNAP. There is a 2.5-fold increase in the K_C at 60°C. It is assumed that the larger colloidal silica MWs associated with the 20:1 SNAP content will provide greater fracture toughness values at elevated temperatures.[179]

The G_C values at 60°C are shown in Figure 4.40 and 4.41.

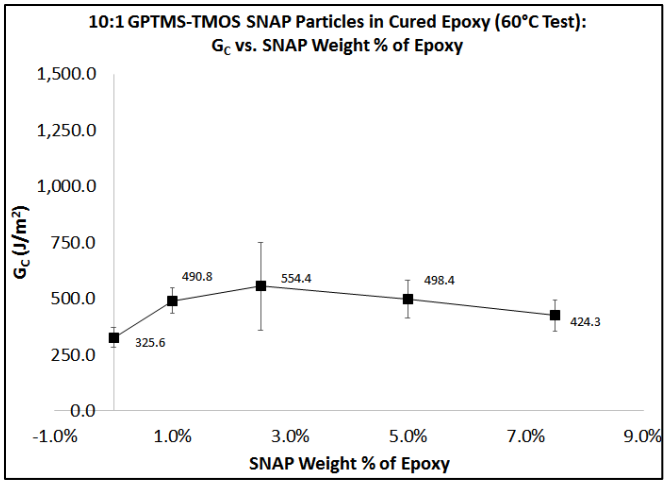

Figure 4.40: G_C at 60°C vs. SNAP Wt. % (10:1 SNAP Particles in n-Butanol)

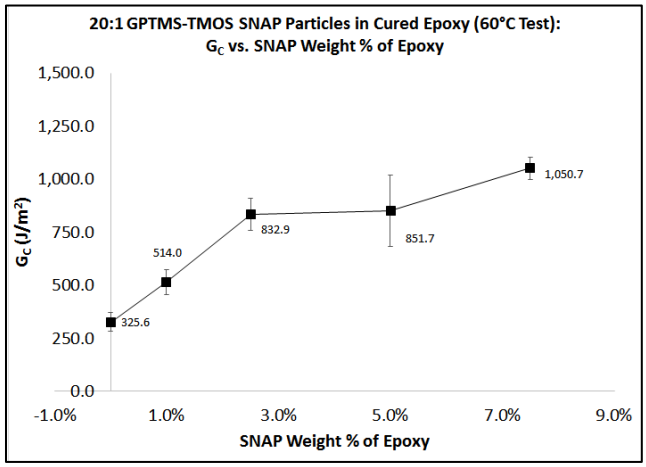

Figure 4.41: G_C at 60°C vs. SNAP Wt. % (20:1 SNAP Particles in n-Butanol)

The G_C values increase from 325.6 J/m^2 (neat epoxide) to 554.4 J/m^2 at 2.5% and modestly decrease to 424.3 J/m^2 at 7.5% 10:1 SNAP. The G_C values from 1% to 7.5% overlap, however. The 20:1 SNAP sample sets increase from 325.6 J/m^2 (neat epoxide) to 1,050.7 J/m^2 (7.5% SNAP). This is approximately a three-fold increase.

There are few phenomena associated with the increase in the fracture toughness and elastic energy strain rate. First, the dispersion of the SNAP sol-gel particles causes

the tensile force to be dissemination around the sol-gel particles, delaying the propagation of fracture (see Figure 4.42).[34]

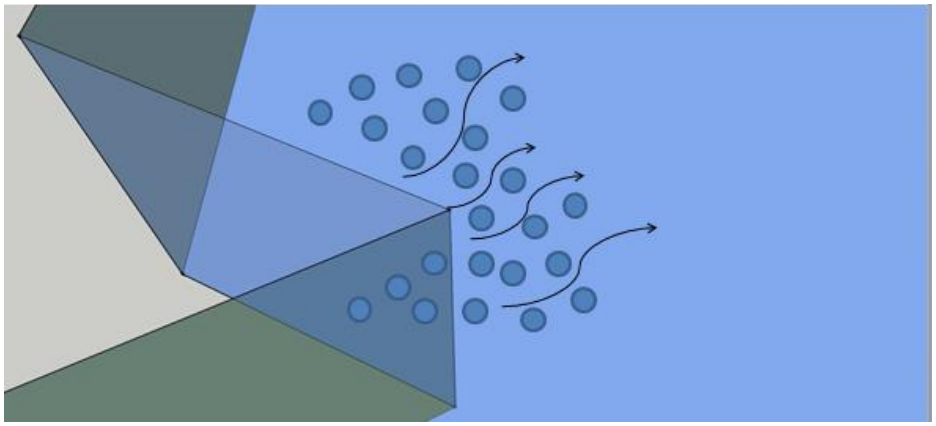

Figure 4.42 Dissemination of Tensile Force Around Sol-Gel Particles

The second phenomenon that occurs is due to the interconnected networks created by their inorganic-organic functionalities, the SNAP particles contribute to increases in the K_C and G_C at both ambient and elevated temperature conditions, and increases in the tensile strength and modulus. The larger colloidal molecules associated with the 20:1 SNAP particles lead to more enhanced tensile and fracture properties.[145,177]

The third phenomenon is the residual stresses that occur with the epoxide binder molecules around the SNAP particles. As the thermoset-sol-gel network cures, the stresses are frozen in place, strengthening the materials against crack propagation. This is depicted in Figure 4.43.[34] Judging from the isolated phases observed during through SEM, it is likely that the enhancements to the fracture toughness and elastic

energy strain rate mostly arise from the reduction of internal stresses and crack deflection around the SNAP sol-gel domains.

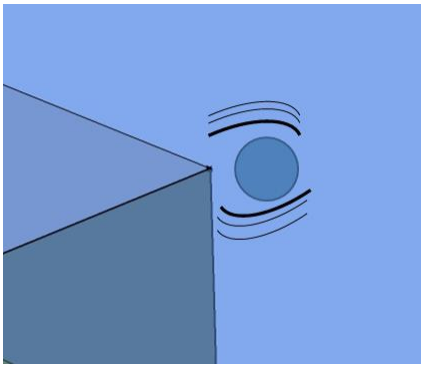

Figure 4.43: Frozen Internal Stress of Epoxides Around Sol-Gel Particles

4.3.9 Taber Abrasion Results of MIL-DTL-24441 Coatings with SNAP Particles

Coating systems loaded with 10:1 or 20:1 SNAP particles were tested for abrasion resistance via a Taber Abrader. The absolute weight losses of the coating systems versus the SNAP particle weight %s are given in Figure 4.44.

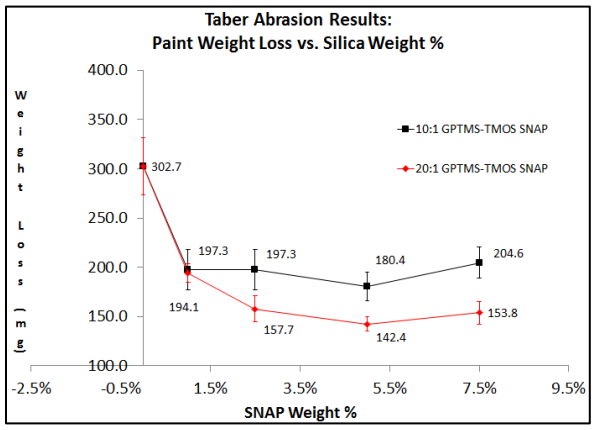

Figure 4.44: Taber Abrasion Weight Loss vs. SNAP Wt. %

The addition of 10:1 SNAP particles results in a 33% reduction in the weight loss of the paint, while the addition of 20:1 SNAP particles results in a 50% reduction in the

weight loss of the paint. In the pattern of the tensile and fracture tests, the addition of 10:1 SNAP particles lead to an immediate reduction in the weight loss but further loading of particles provides no further weight loss. The addition of 20:1 particles at 1.0 wt. % begins at approximately the same weight loss as 10:1 1.0 wt. % SNAP particles and continues to decrease until reaching a minimum at 5%. As elucidated by Palraj et al.[173], The enhanced abrasion resistance is due to the inorganic silica content from the SNAP particles, which are generally more abrasion resistant than epoxide. Since SNAP particles appear on the surface of the coatings/films, it is likely that the presence of abrasion resistant SNAP is directly responsible for the reduction of weight loss.

The Taber Abrasion 2-sample T results for the 10:1 SNAP-loaded epoxide coatings are shown in Table 4.14. All four coating sets are significantly different than the neat epoxide control coating.

Table 4.14: 10:1 SNAP Loaded Coatings Taber Abrasion 2-Sample T P-Value Results

Name	SNAP Weight %	2-Sample T P-Value from Control	Significant?
10:1 SNAP	1.0%	0.009	Yes
10:1 SNAP	2.5%	0.009	Yes
10:1 SNAP	5.0%	0.008	Yes
10:1 SNAP	7.5%	0.013	Yes

The Taber Abrasion 2-sample T results for the 20:1 SNAP-loaded epoxide coatings are shown in Table 4.15. All four coating sets are significantly different than the neat epoxide control coating.

Table 4.15: 20:1 SNAP Loaded Coatings Taber Abrasion 2-Sample T P-Value Results

Name	SNAP Weight %	2-Sample T P-Value from Control	Significant?
20:1 SNAP	1.0%	0.015	Yes
20:1 SNAP	2.5%	0.005	Yes
20:1 SNAP	5.0%	0.008	Yes
20:1 SNAP	7.5%	0.006	Yes

4.3.10 Pull-Off Adhesion Strengths of MIL-DTL-24441 Coatings with SNAP Particles

The pull-off adhesion test results are shown in Figure 4.45. The addition of 10:1 SNAP particles results in a three-fold increase to the adhesion strength from neat epoxide, but given the degree of error in the results, adding higher amounts of 10:1 SNAP particles does not increase the adhesion strength. The same behavior is exhibited in terms of the 20:1 SNAP particles, although the increase in the adhesion strength is only a 2.5-fold increase. The presence of the SNAP particles leads to alkoxysilane linkages with the substrate, which provides an increase in the adhesion strength.[147] The greater crosslink density indicated in the 10:1 SNAP particles means a greater plethora of bonding to the substrate and higher adhesion strengths.

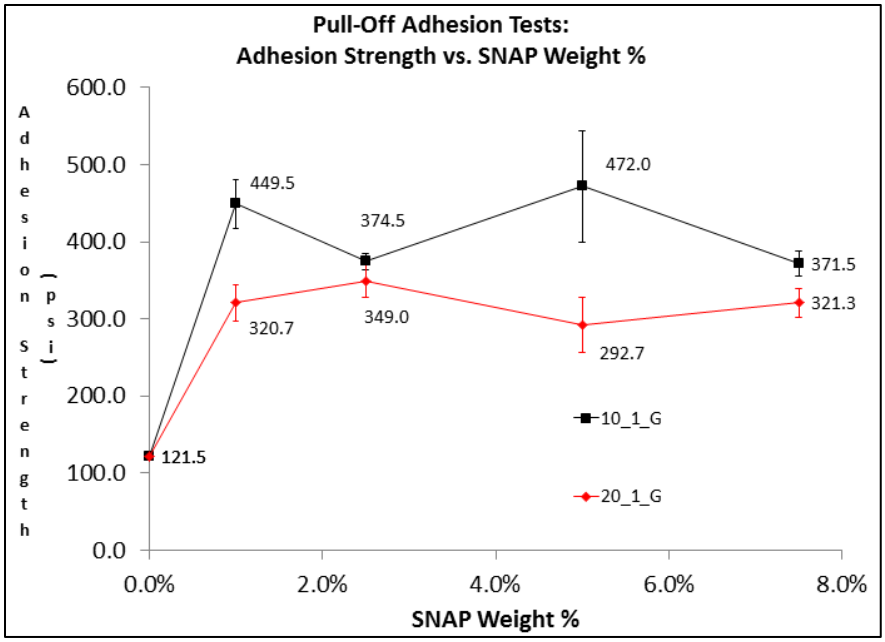

Figure 4.45: Pull-Off Adhesion Strength vs. SNAP Wt. %

The pull-off adhesion 2-sample T results for the 10:1 SNAP-loaded epoxide coatings are shown in Table 4.16. All four coating sets are significantly different than the neat epoxide control coating.

Table 4.16: 10:1 SNAP Loaded Coatings Pull-Off Adhesion 2-Sample T P-Value Results

Name	SNAP Weight %	2-Sample T P-Value from Control	Significant?
10:1 SNAP	1.0%	0.012	Yes
10:1 SNAP	2.5%	0.013	Yes
10:1 SNAP	5.0%	0.003	Yes
10:1 SNAP	7.5%	0.037	Yes

The pull-off adhesion 2-sample T results for the 20:1 SNAP-loaded epoxide coatings are shown in Table 4.17. All four coating sets are significantly different than the neat epoxide control coating.

Table 4.17: 20:1 SNAP Loaded Coatings Pull-Off Adhesion 2-Sample T P-Value Results

Name	SNAP Weight %	2-Sample T P-Value from Control	Significant?
20:1 SNAP	1.0%	0.012	Yes
20:1 SNAP	2.5%	0.007	Yes
20:1 SNAP	5.0%	0.042	Yes
20:1 SNAP	7.5%	0.008	Yes

4.3.11 EIS Results of MIL-DTL-24441 Coatings with SNAP Particles

The EIS results include the Nyquist and Bode plots at Day 30 as well as the impedance modulus at 1 Hz. versus the immersion time. A Nyquist plot with a linear, vertical plot indicates a coating with excellent corrosion resistance. Generally, a Nyquist plot with a steeper (larger) slope indicates a coating indicates superior resistance. A Nyquist plot with a dome-shaped plot indicates a coating that has undergone failure (i.e. corrosive substances such as salt water found a way to permeate through the coating and corrode the substrate underneath the coating).

A Bode plot with a linear downward slope is an indication of a coating with excellent corrosion resistance. A Bode plot with multiple horizontal regions is indicative of a coating that has undergone failure. A Bode plot with a horizontal region in the beginning and then a downward slope is indicative of a coating with low pore resistance (i.e. does not provide a substantial protective barrier against external corrosive forces) but ultimately a coating that does provide some level of resistance against corrosion. Generally, coatings with higher impedance moduli indicate elevated levels of corrosion resistance.

The Nyquist plots are shown in Figures 4.46 and 4.47.

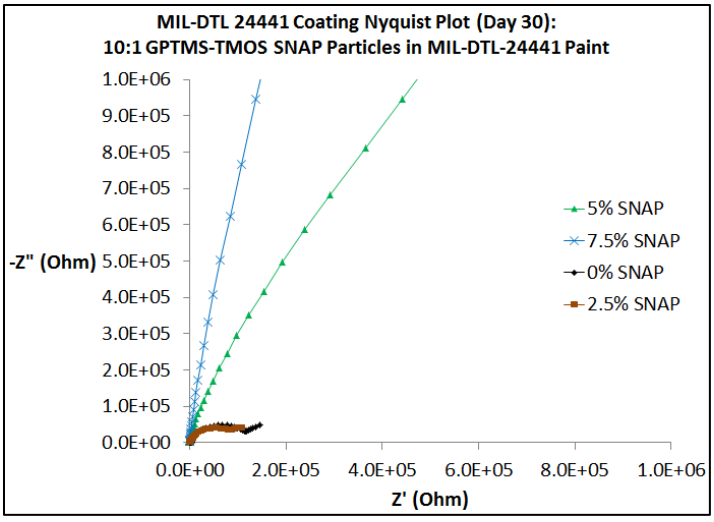

Figure 4.46: Nyquist Plots (Day 30) of Epoxide-Polyamide Coatings (10:1 SNAP Particles)

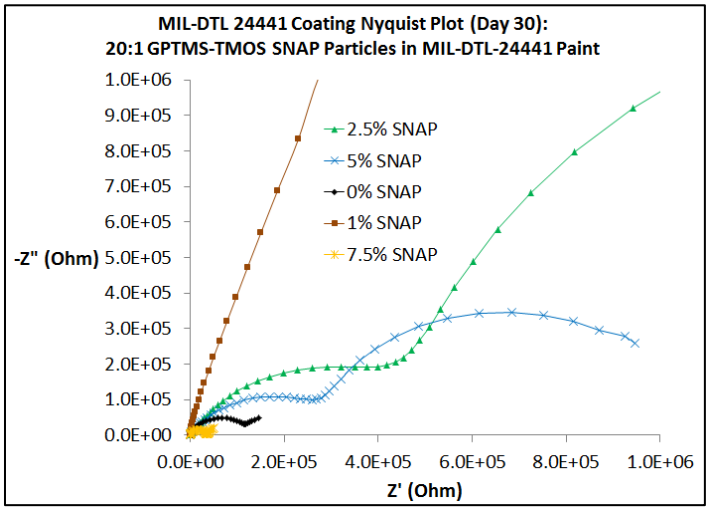

Figure 4.47: Nyquist Plots (Day 30) of Epoxide-Polyamide Coatings (20:1 SNAP Particles)

A dome shape to a Nyquist plot curve shows coating corrosion failure, and a steeper curve shows greater corrosion resistance. Neat epoxide coating systems show coating corrosion failure after 20 and 30 days of immersion, while 5% and 7.5% 10:1 GPTMS-TMOS SNAP systems show coating corrosion protection after 20 and 30 days of immersion. 7.5% 10:1 GPTMS-TMOS SNAP systems show the greatest corrosion

resistance. 2.5% 20:1 GPTMS-TMOS SNAP coating systems show robust corrosion protection after Days 20 and 30 of immersion, while the remaining systems show coating corrosion failure.

The Bode plots for the epoxide-polyamide coatings are shown in Figures 4.48 and 4.49.

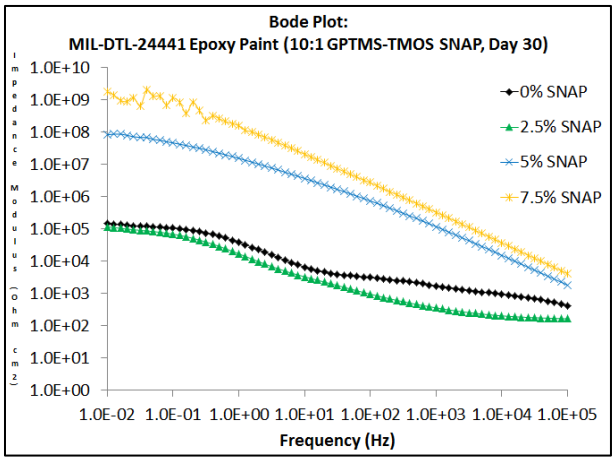

Figure 4.48: Bode Plots (Day 30) of Epoxide-Polyamide Coatings (10:1 SNAP Particles)

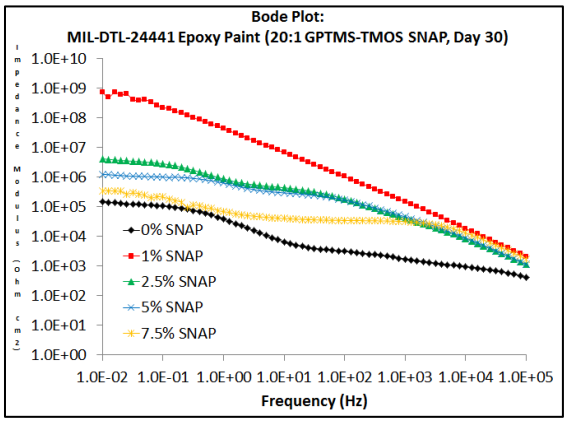

Figure 4.49: Bode Plots (Day 30) of Epoxide-Polyamide Coatings (20:1 SNAP Particles)

At Day 30 of immersion, coating systems loaded with 7.5% 10:1 GPTMS-TMOS SNAP particles show the greatest resilience to corrosion, which is followed by 5% SNAP.

The neat epoxide coating systems show a slight improvement over epoxide coatings loaded with 2.5% SNAP particles. For the epoxide coating systems loaded with 20:1 GPTMS-TMOS SNAP particles, the corrosion resistance is maximized at 1% SNAP at Days 20 and 30 of immersion. 2.5% and 5% SNAP show corrosion resistance values that are roughly similar to one another, while 7.5% is an order of magnitude worse. While all paint formulations show superiority to neat epoxide formulations, it is theorized that higher amounts of inorganic silane content have superior barrier properties to organic silane content due to the higher and smaller crosslinks that are formed. This has been related in past literature, which showed that smaller inorganic silane molecules (TMOS in comparison to TEOS[147] or TEOS in comparison to TEOS in comparison to GOTMS[183]) are superior in corrosion[147] and solvent resistance.[184] The higher crosslink densities (attributed to more tightly packed aggregated sol-gel networks) associated with the 10:1 SNAP particles leads to more enhanced barrier properties.[147] In addition, the presence of the SNAP particles leads to greater hydrophobicity and less water uptake of the coatings, which in turn prevents corrosion.

4.3.12 Water Uptake EIS Test Results

The water uptake tests as measured via EIS are shown in Figures 4.50 and 4.51. The water uptake percentages are plotted as a function of the SNAP weight percentage.

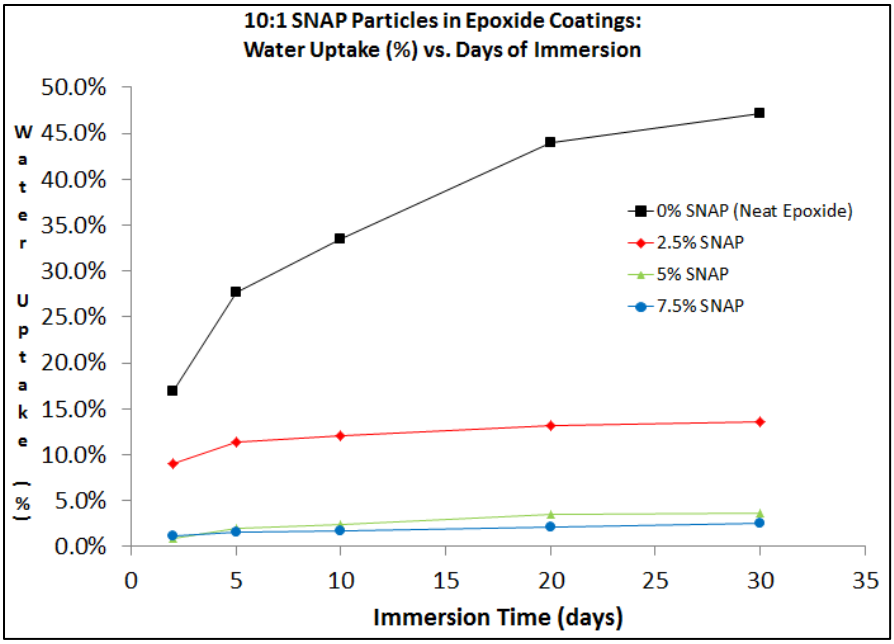

Figure 4.50: EIS Water Uptake of Epoxide Coatings Loaded with 10:1 SNAP Particles

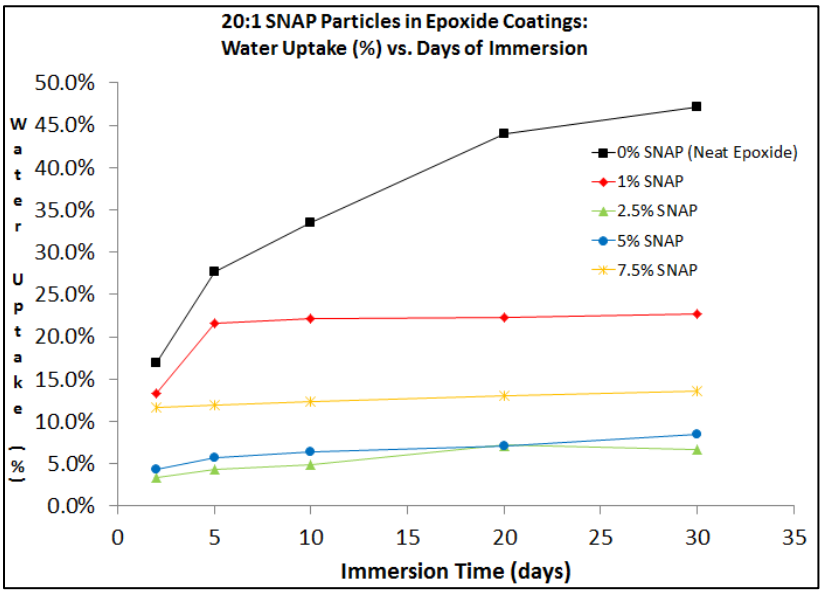

Figure 4.51: EIS Water Uptake of Epoxide Coatings Loaded with 20:1 SNAP Particles

The water uptake is plotted versus the time spent immersed in the salt water (in days). For 10:1 SNAP particle loaded coatings, there is an initial increase in the water

uptake for neat epoxide (0% SNAP) and 2.5% SNAP. 0% SNAP (neat epoxide) continually increases until the final day of testing, but 2.5% SNAP remains constant thereafter. 5% and 7.5% SNAP have lower uptake levels and remain constant from day 2 to 30 of testing. For 10:1 SNAP particles, there is an inverse relationship between water uptake and the SNAP weight percentage. For 20:1 SNAP particle loaded coatings, there is an initial increase in the water uptake from day 2 to 5 for 0% and 1% SNAP. The neat epoxide water uptake continues to increase until the last day of testing, while 1% SNAP levels out after day 5 of testing. 2.5% 5% and 7.5% SNAP have lower water uptake levels, which remain constant after day 2. 2.5% SNAP has the lowest water uptake level, and there is an increase in the water uptake from 2.5% to 5% and 7.5% SNAP. However, higher levels of SNAP coatings ensure that the water uptake of the coatings remains constant after 30 days of testing. The 10:1 and 20:1 SNAP loaded epoxide coatings show that there is a direct inverse relationship with the crosslink density. Past research indicated that the water uptake (and ultimate the barrier properties) of the SNAP loaded coatings are due to two factors: the presence of a silica barrier and the contribution of SNAP coatings to elevated crosslink densities, which also hinder the diffusion of water.[63,145] Judging from the direct inverse relationship of the crosslink density to the water uptake, it is more likely that the reduction of the water uptake is due to the increase in crosslink density provided by the SNAP functional content.

4.3.13 Contact Angles of SNAP Loaded Epoxide Coatings

The contact angles of the 10:1 and 20:1 SNAP particle loaded epoxide coatings are plotted as a function of the SNAP weight percentage in Figure 4.52.

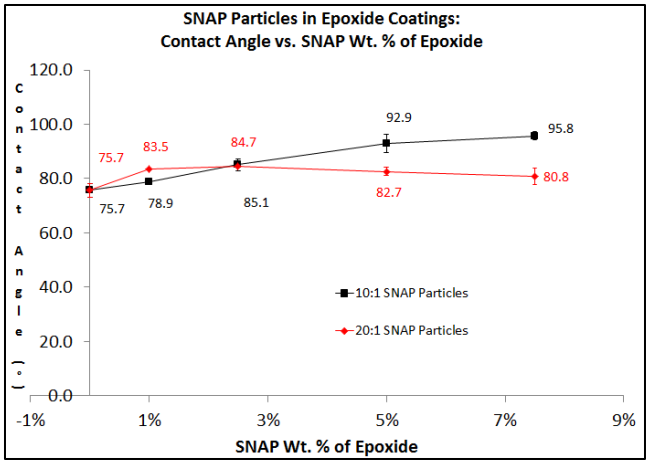

Figure 4.52: Contact Angles of SNAP Particle Loaded Epoxide Coatings

The contact angle of the unmodified epoxide is equivalent to measurements reported in past literature (73 +/- 3°).[185] There is a moderate increase in the contact angle with the SNAP weight percentage. The increase correlates with the increase in the crosslink density provided by the presence of the SNAP particles, indicating the presence of SNAP particles at the surface of the epoxide. This correlates with SNAP sol-gel domains observed via SEM. This implies that the presence of SNAP particles leads to a more hydrophobic surface than neat epoxide, which in turn contributes to increases in the barrier properties of the coating. Past literature has indicated that while the sol-gel materials are more hydrophobic (ranging from 88° for TMOS to 172° for vinyltriethoxysilane sol-gel coatings) than epoxides, the greater hydrophobicity in crosslinked epoxide coatings might have more to do with "chemical durability, extensive crosslink, and excellent adhesion to the substrate rather than via surface energy modification."[63]

The contact angle 2-sample T results of the 10:1 SNAP filled epoxide films are listed in Table 4.18. Except for 1%, all sample sets are significantly different from the neat epoxide film set.

Table 4.18: 10:1 SNAP Loaded Film Contact Angle 2-Sample T P-Value Results

Name	SNAP Weight %	2-Sample T P-Value from Control	Significant?
10:1 SNAP	1.0%	0.280	No
10:1 SNAP	2.5%	0.022	Yes
10:1 SNAP	5.0%	0.003	Yes
10:1 SNAP	7.5%	0.000	Yes

The contact angle 2-sample T results of the 20:1 SNAP filled epoxide films are listed in Table 4.19. Except for the 7.5% set, all sample sets are significantly different than the neat epoxide film set.

Table 4.19: 20:1 SNAP Loaded Film Contact Angle 2-Sample T P-Value Results

Name	SNAP Weight %	2-Sample T P-Value from Control	Significant?
20:1 SNAP	1.0%	0.034	Yes
20:1 SNAP	2.5%	0.022	Yes
20:1 SNAP	5.0%	0.049	Yes
20:1 SNAP	7.5%	0.232	No

4.4 Discussion

The intention of this body of research was to answer several questions. Inorganic-organic silica based sol-gels have proved to be an effective coating additive in terms of preventing corrosion and enhancing the coating's mechanical properties. Most academic literature on the subject has been devoted towards simplified paint formulations, so would an inorganic-organic silica based sol-gel system enhance a

military specification coating system commonly used for industrial and commercial purposes? Also, the use of SNAP particles in military specification coating systems provides an opportunity to see if SNAP particles can be utilized as a functional coating additive instead of a surface preparation for aluminum substrates. Last, it has been proven that the solvent amount can play a role in the construction of sol-gel materials. How might this affect the formation of inorganic-organic colloids in a non-aqueous polar solvent?

The results indicated that the solvent amount can play a role in the formation and aggregation of SNAP particles. As confirmed by DLS results, there is the existence of larger size particles or greater aggregation of SNAP particles. In addition, there appears to a greater amount of inorganic silane content in SNAP particles with smaller solvent ratios. This forms tighter linkages and greater crosslink densities, which is instrumental in ensuring higher adhesion strengths and greater crosslink densities. With smaller solvent ratios, there is a limit to the mechanical enhancements (i.e. fracture, tensile properties, abrasion resistance) that are provided with SNAP content. This might be due to aggregation and phase separation of the SNAP content, which leads to films that are more brittle than films with 20:1 SNAP particles. Larger solvent ratios come with larger molecules with longer chains, which partake greater flexibiliy onto epoxide polyamide films. The limiting factor of the 20:1 SNAP particles is that the SNAP particles don't work as efficiently at 10:1 SNAP particles in providing an effective barrier against corrosion. This is due to the smaller amount of crosslinks and perhaps the lower amount of aggregation on the surface of the coating.

The addition of SNAP particles has enhanced the mechanical properties of the films and coating systems, which confirms previous literature results with inorganic-organic hybrids. Past researchers have noted that added silica/sol-gel content can improve several physical aspects of the coating system, notably the tensile strength,[31,180,181,186,187] fracture toughness[138, 186,188-195], wear resistance[196-198], adhesion strength[198], and corrosion resistance. The fracture toughness and tensile behavior stem from the ability of the sol-gel content to provide chemical linkages between inorganic and organic content as well as the strength of the siloxane bonds.[198] It is also due to the presence of isolated sol-gel domains, which delay fracture of the tensile specimens through crack deflection. The abrasion resistance stems from augmented resistance of the silica content to abrasion, the adhesion strength stems from the fact that silanes can serve as a tether between the epoxide backbone and the metal surface.[198] Past studies with SNAP sol-gels show that crosslinked SNAP particles can serve well as a corrosion inhibitor due to their barrier properties.[59-72]

Islam et al. provided an excellent article on the use of silica-epoxide nanocomposites that explains some of the limits (from a mechanical standpoint) of utilizing sol-gels in an epoxide matrix.[180] In their publication, they stated that the central factors behind the macroscopic properties of silica-epoxide hybrids are interactions between the particles themselves and interactions between the particles and the epoxide matrix. The two main types of interactions are van der Waals interactions and electrostatic force. Sol-gel and silica nanoparticles tend to agglomerate, which can lead to limitation and depletion of the physical properties of a coating system. Similar

conclusions were confirmed by Rubab[181], who found that when inserting titania sol-gel particles into cured epoxide-amines consisting of diglycidyl ether of bisphenol A (DGEBA) and poly(oxypropylene) diamine (POPDA) at titania weight ratios of 2.5%, 5%, 7.5%, and 10%, the tensile strength increased by a factor of approximately 12.5% and 25% for titania weight ratios of 2.5% and 5%, respectively. Higher levels of titania loading saw no increase in the tensile strength when compared to neat epoxide-amine films (7.5%) or approximately a 25% reduction in the tensile strength. The authors attributed this to the instigation of micro-sized cracks during testing that occur because of weak interactions between the particles and epoxide base (which has a higher probability of occurring at higher loading content). Agglomeration of particles was confirmed by DLS results and might explain the mechanical behavior of the epoxide-polyamide films loaded with 10:1 SNAP particles.

The use of nano-fillers is useful to enhance the corrosion resistance and weatherability of coatings. This is useful for the coatings formulators that want to eliminate the use of multiple topcoats or create a useful uni-coat system, which saves money. Primer coatings are there to prevent corrosion of the substrate, which is relatable to good adhesion strength (indicating that the coating is firmly attached to the substrate and thereby provides a strong barrier against corrosive substances such as oxygen and water). However, coatings can be aided by the presence of alternative phases such as sol-gels that reduce the "porosity" of the coating and provide a tortuous pathway that makes it more difficult for corrosive substances to diffuse through.[199] Also, the use of nanoparticles dispersed evenly throughout a coating systems will "fill

cavities" and "defects" in the coating system, preventing dimensional changes incurred during the curing process and "acting as a bridge interconnecting more molecules."[199] Consequently, the free volume of the coating is smaller, and the crosslink density becomes larger. Furthermore, organic silanes are hydrophobic, which also aids in repelling corrosive agents such as water. The phenomenon of the particles reducing the amount of free volume contributes to larger elastic moduli and higher glass transition temperatures. The presence of agglomeration of the particles will contribute to higher crosslink densities, higher moduli, and ultimately better barrier properties. However, this comes with a limitation to other physical properties such as the fracture and tensile properties.[199]

The best indication or parameter of the physical properties of a nancomposite material or coating is the "filler-matrix interaction."[200] Having functional nanoparticles can improve the dispersion by enhancing the surface charge of the materials. Also, smaller particle sizes means a greater surface area and greater amounts of "filler-matrix interactions."[200] As evidenced in previous literature, smaller particle sizes are equivalent to greater degrees of dispersion and better mechanical properties.[200]

The unexpected results of the SNAP sol-gel particles were as follows. While it was assumed that the particles would form some isolated particle-like phases within the epoxide matrix, it was unexpected that the isolated sol-gel phases would be as numerous as they were. In addition, it was also assumed (from past literature) that the organic siloxane bonding was the reason for the enhancement of the fracture and

tensile properties of the epoxide matrices. While this is a definite possibility for the SNAP sol-gels, it is more likely that the particles are impeding and disseminating crack voids around the sol-gel phases and throughout the sample, delaying macroscale fracture. Therefore, the delay of fracture is observed at a nanoscale level instead of at a molecular level.

Much of the enhanced corrosion resistance of the samples is due to the enhanced hydrophobicity of the sol-gel regions. The enhanced moduli of the samples signify denser crosslinks of the material, signifying that the sol-gel region is more tightly packed and less porous than the epoxide phases. The combination of sol-gel phases with lower porosity and greater hydrophobicity contribute to the presence of enhanced corrosion resistance.

To determine that the presence of sol-gel phases is useful in preventing the permeation of all corrosive substances (i.e. oxygen), future work will include oxygen permeation studies with the SNAP-loaded epoxide films.

Other unexpected results include the differences between the epoxide formulations incorporating 10:1 and 20:1 SNAP particles. Based upon past literature, it was assumed that larger amounts of solvent would contribute to more comprehensive siloxane networks that in turn would contribute to denser sol-gel phases and better corrosion resistance. Conversely, it was assumed that more tightly arranged sol-gel networks might also contribute to higher moduli and greater brittleness. The results indicated the opposite phenomena. Smaller amounts of solvent led to larger aggregates

of sol-gel phases, which contributed to more enhanced coating resistance to corrosion. Conversely, the aggregation of the sol-gel phases led to limited enhancement of mechanical properties, notably the fracture and tensile properties of the materials. The larger amounts of solvent for the 20:1 SNAP particles led to greater dispersion within the epoxide matrix, culminating in better mechanical properties. The limited aggregation within the epoxide matrix, however, resulted in corrosion resistance values that were less than the 10:1 SNAP particle coating formulations. There is a trade-off associated with using SNAP particles in epoxide matrices; greater dispersion will lead to better mechanical properties although the corrosion resistance will be diminished compared to SNAP-loaded epoxide matrices with greater aggregation. Conversely, aggregated SNAP particles have limitations in terms of the mechanical property enhancements.

Ultimately, electrochemical impedance spectroscopy (EIS), fracture property, and tensile property testing all attempt to quantify how long a coating will last if placed on a substrate in an outside condition. Past literature has illustrated that coatings with enhanced tensile properties indicate coatings with greater weatherability. The coatings require a greater amount of stretching to damage, and the coatings have a greater resistance to being stretched, indicating that the coating is resistant to physical trauma. Fracture property testing is very much like tensile testing due to the fact that both tests relate to the stretching of a film. Fracture property testing determines the damage tolerance of a coating once it has already been damaged. Coatings with excellent tensile strength may also display brittleness, leading to a large-scale fracture after a

small amount of flexing. Fracture properties factor the damage tolerance from the perspective of both strength and flexibility. In addition, fracture properties are related to the process of corrosion. Corrosion can age and damage a coating over time. Fracture properties can indicate the resistance of a coating to damage, which is useful in determining the coating's resistance to further damage by corrosion. Last, electrochemical impedance spectroscopy is useful in determining the coating's resistance to forming an electrochemical circuit, indicating that a coating with a good electrochemical resistance is a solid, intact coating with no irregularities. A coating that maintains its uniformity over a period of being exposed to corrosion should also be a damage resistant coating. Therefore, all three tests ascertain in varying ways the longevity of a coating. Other tests, such as adhesion strength, determine the coating's ability to stay adhered to a substrate and is relatable to other coating properties such as flexibility.

4.5 Conclusions

In this publication, SNAP particles were formulated from epoxidesilanes (3-glycidylpropyltrimethoxysilane) and alkoxysilanes (tetramethyl orthosilicate) and later placed into epoxide-polyamide films and MIL-DTL-24441 epoxide-polyamide coating systems, where they were associated with enhancements in the abrasion resistance, pull-off adhesion strength, fracture toughness, and corrosion resistance. The reaction was acid-catalyzed and took place in an n-butanol medium. Two different sets of particles were created by adjusting the amount of solvent utilized. The particles were characterized for molecular structure via for size via transmission electron microscopy

(TEM) and dynamic light scattering (DLS), and were characterized for molecular structure and bonding via ^{29}Si NMR, ^{13}C NMR, ^{1}H NMR, and ESI-MS. Later, SNAP particles were inserted into epoxide-polyamide films and MIL-DTL-24441 epoxide-polyamide coating systems in 1%, 2.5%, 5%, and 7.5% weight ratios of the base epoxide. The films were tested for fracture toughness, tensile strength, crosslink density, and glass transition temperature, while the coating systems were tested for abrasion resistance, pull-off adhesion, and corrosion resistance (Bode/Nyquist plots). Loading of SNAP sol-gel particles correlated with an increase in the mechanical properties, the crosslink density, the glass transition temperature, and the corrosion resistance.

CHAPTER V

AMINOSILANE INORGANIC-ORGANIC SOL-GELS IN EPOXIDE-POLYAMIDE FIMS AND COATINGS: CHARACTERIZATION, THERMAL AND MECHANICAL PROPERTIES, AND CORROSION RESISTANCE

5.1 Introduction

Amine-based silane and sol-gels have been utilized in epoxide materials and coatings. In the past, it has been grafted onto substrates and epoxides generally by crosslinking. The grafted silane content has enhanced the corrosion resistance and mechanical properties of the epoxide materials and coatings. Amine-based sol-gels have also been utilized as surface preparations on metal substrates in order to protect the substrate against corrosion. One of the publications on SNAP surface preparations focused on crosslinked systems based upon the synthesis of an aminosilane (APTES) and TMOS. As elucidated in Chapter II and IV, Self-assembled NAnoPhase (SNAP) particles are aluminum surface preparations processed from the synthesis of inorganic and organic sol-gel content and were pioneered as a nontoxic replacement for chromate conversion coatings (noted for concerns over toxicity and carcinogenity).[59-72]

Chapter 4 indicated that SNAP particles can be utilized as functional additives in epoxide coating systems. The particles, by nature of the functional groups, are

covalently bonded to the existing functional groups in the coating system such as the epoxide base or amine/amide curative. A continuous phase of the sol-gel content and epoxide-curative matrix was formed by crosslinking the sol-gels, epoxide, and curatives together. This approach allowed for the enhancement of not only the corrosion resistance of the coating system but also the mechanical properties. Due to the fact that epoxide functionalities grafted to aminosilanes have improved the corrosion resistance and mechanical properties of epoxide coatings, it would follow that APTES and TMOS could be co-polymerized in solution and later added into epoxide coatings.[62,201-204] Like the GPTMS-TMOS SNAP particles, the APTES-TMOS sol-gels could form a continuous sol-gel-epoxide matrix with better mechanical properties and corrosion resistance than the neat epoxide. In addition, the use of inorganic-organic aminosilane (specifically with APTES and TMOS) sol-gels in epoxide coating systems (specifically MIL-24441 epoxide coatings systems) has not yet been attempted. The closest aspect explored in past literature was the use of APTES, TMOS, and epoxide to produce aerogels.[204]

In this chapter, sol-gel content based on the synthesis of APTES (an aminosilane) and TMOS (inorganic precursor) was added into epoxide-polyamide military specification coating systems and epoxide-polyamide films. The functional groups on the aminosilane content bond and the existing polyamide curatives react with the epoxide. The coatings were tested for corrosion resistance via electrochemical impedance spectroscopy (EIS), while the coatings and films were tested for mechanical properties such as the abrasion resistance, adhesion strength, and fracture properties.

Furthermore, the sizing of the APTES-TMOS sol-gels was determined via dynamic light scattering (DLS). Sol-gel loaded epoxide films were also tested via contact angle measurements. The experimentation, characterization, and materials testing proceeded in a comparable manner to Chapter IV.

The questions to ponder with the current chapter are:

1. When added into epoxide coatings, would ex-situ sol-gels consisting of APTES and TMOS form a continuous system that enhances the mechanical properties and corrosion resistance of an epoxide coating?
2. How do the mechanical properties and corrosion resistance of the APTES-TMOS loaded epoxide-coatings compare to the epoxide coatings loaded with SNAP particles?

5.2 Experimental

5.2.1 Materials

Aminopropyltriethoxysilane (APTES), tetramethyl orthosilicate (TMOS, 98%), 1-butanol (ACS reagent, 99.4%), and acetic acid (ACS reagent, 99.7%) were all purchased from Sigma-Aldrich. Epon 828 (diglycidyl ether of bisphenol A epoxide) was purchased from Hexion, Ancamide 507 and Ancamide 700B75 were both purchased from Air Products, Disparlon 6500 and Disparlon NS-30 were purchased from King Industries, Nicron 503 was purchased from Imerys Talc, Tipure TiO_2 was purchased from DuPont/Chemours, and Naphtha was purchased from VM&P. All materials were used as received.

5.2.2 Synthesis of Aminosilane Sol-Gel Particles

With the exception of the solvent type and amount, sol-gel particles were synthesized similarly to previous literature.[59] APTES and TMOS were combined in a 3:1 molar ratio and manually shook in a glass vial. Later, the contents were added dropwise into a 250-mL round-bottomed flask containing 0.05 M acetic acid in 1-butanol. The contents were continuously stirred via a magnetic stir bar during and silane addition. In order to completion the synthesis of SNAP particles via hydrolysis and condensation, the stirring continued for another 72 hours. The solution was then stored until further use. The amount of solvent was calculated by multiplying the cumulative molar amount of silanes (APTES and TMOS) by 15.

5.2.3 Dynamic Light Scattering (DLS) of Sol-Gel Particles

Dynamic light scattering (DLS) acted as a supplement to TEM in determining the dimensions of the APTES-based sol-gels. The tests were conducted according to the method described in Section 4.2.8.

5.2.4 Epoxide-Polyamide Film Preparation and Application

Films were created by mixing the epoxide, polyamide crosslinkers, and the SNAP functional sol-gel particles dissolved in 1-butanol. The epoxide was Epon 828, and the polyamide crosslinkers were Ancamide 700B75 and Ancamide 507. The components and amounts are taken from military specification 24441 epoxide-polyamide coating systems. For purposes of simplicity, all non-functional content (pigments, thixotropes, etc.) weren't included in the formulation.

Each set of SNAP particles (10 and 20 solvent molar ratios) were added to the mixtures in weight percentages of 1%, 2.5%, 5%, or 7.5% of the total weight of the base epoxide. In order to keep the epoxide weight content (Epon 828 + SNAP) the same for each formulation, Epon 828 was deducted by the same weight that the sol-gels were added. Crosslinked epoxide-polyamide films with no SNAP added were prepared as controls. The component and component weights for the sample sets are shown in Table 5.1.

Table 5.1: Epoxide-Polyamide Film Formations with APTES-TMOS Sol-Gel Addition

Formulation	SNAP Wt. %	Solvent to Silane Ratio	Ancamide 507 (g)	Ancamide 700B75 (g)	Epon 828 (g)	SNAP (g)	SNAP + N-Butanol (g)
No SNAP	0.0%	NA	0.68	9.64	17.21	0	0
APTES-TMOS SNAP	1.0%	15	0.67	9.45	17.21	0.17	1.1
APTES-TMOS SNAP	2.5%	15	0.65	9.18	17.21	0.42	2.71
APTES-TMOS SNAP	5.0%	15	0.62	8.74	17.21	0.82	5.28
APTES-TMOS SNAP	7.5%	15	0.59	8.33	17.21	1.2	7.74

After mixing, each formulation was cast onto PET film via a drawdown bar. PET film was used to provide a non-stick surface to ensure easy removal of crosslinked epoxide matrix films. The wet film thickness was 8 mils. After application onto PET, the cast film was left to dry and cure under ambient conditions.

5.2.5 Thermal and Thermal-Mechanical Measurements

Thermal and thermal-viscoelastic measurements (crosslink density, glass transition temperature) of the epoxide-polyamide films were conducted according to Sections 3.2.7 and 4.2.12. Both parameters were measured as a function of the sol-gel weight percentage.

5.2.6 Tensile Testing of Epoxide-Polyamide Films

Tensile tests were conducted according to the method described in Section 4.2.13. 10-15 samples were tested per sample set.

5.2.7 Fracture Toughness Testing of Epoxide-Polyamide Films

Fracture toughness tests were conducted according to the method described in Section 3.2.11. Fracture toughness tests were employed at -55°C, 20°C, and 60°C.

5.2.8 MIL-DTL-24441 Coating Preparation and Application

The SNAP particles were included with MIL-DTL-24441 Epoxide-Polyamide White[149] coating samples at percentages of 1.0%, 2.5%, 5.0%, and 7.5% weight. The weight percentage is indicated as a weight percentage of the epoxide material (Epon 828) in the coating system. The amount of Epon 828 was adjusted to keep the total weight of functional material (epoxide and SNAP) constant for each sample set. The sample sets and the amount of each component are indicated in Table 5.2.

Table 5.2: MIL-DTL 24441 Paint Formulations with APTES-TMOS Sol-Gel Addition

Formulation	Sol-Gel Wt. %	Solvent to Silane Ratio	Disparlon 6500 (g)	Nicron 503 (g)	Naphtha (g)	Disparlon NS-30 (g)	TiO2 (g)	N-Butanol to Add (g)
No S	0.0%	NA	0.49	8.60	7.18	0.49	20.42	8.77
APTES-TMOS	1.0%	15	0.49	8.60	7.18	0.49	20.42	7.67
APTES-TMOS	2.5%	15	0.49	8.60	7.18	0.49	20.42	6.06
APTES-TMOS	5.0%	15	0.49	8.60	7.18	0.49	20.42	3.49
APTES-TMOS	7.5%	15	0.49	8.60	7.18	0.49	20.42	1.03

The coating formulations were mixed together in a Thinky mixer for 5 minutes at 2,000 revolutions per minute. Afterwards, they were cast onto Al-2024 aluminum samples at wet film thicknesses of 5 mils and steel Taber Abrasion 4” x 4” panels at

thicknesses of 10 mils. The aluminum samples were utilized for pull-off adhesion and EIS tests. The steel Taber Abrasion panels were utilized for Taber Abrasion tests.

5.2.9 Taber Abrasion Testing of MIL-DTL-24441 Coatings Loaded with Sol-Gels

The Taber Abrasion tests were completed according to the method described in Section 4.2.16.

5.2.10 Pull-Off Adhesion Testing of MIL-DTL-24441 Coatings Loaded with Sol-Gels

The pull-off adhesion tests were completed according to the method described in Section 3.2.9.

5.2.11 Electrochemical Impedance Spectroscopy (EIS) Testing of MIL-DTL-24441 Coatings Loaded with Sol-Gels

Electrochemical impedance spectroscopy (EIS) tests and water uptake measurements were completed according to the method described in Section 3.2.13.

5.2.12 Contact Angle Measurements of APTES-TMOS Loaded Epoxide Films

Contact angle measurements of APTES-TMOS loaded epoxide films were measured as specified in Sections 3.2.12 and 4.3.13. The contact angle was measured as a function of the sol-gel weight percentage.

5.3 Results

The APTES-TMOS sol-gels were subjected to the same series of characterization tests as the SNAP particles discussed in Chapter 4. The sol-gels were characterized for size via DLS and TEM. Later, the APTES-TMOS sol-gels were added into epoxide-

polyamide films and coatings and characterized for thermal and thermal-mechanical properties via DSC and DMTA, respectively. The films were also tested for tensile and fracture properties. Last, the sol-gels were loaded into MIL-DTL-24441 coating systems and tested for abrasion resistance, adhesion strength, and corrosion resistance via EIS.

5.3.1 Dynamic Light Scattering of APTES-TMOS Sol-Gels

The dynamic light scattering results of the APTES-TMOS sol-gels dissolved in n-butanol solvent are shown in Figure 5.1. The γ (a measure of frequency) is plotted versus the hydrodynamic radius (R_H).

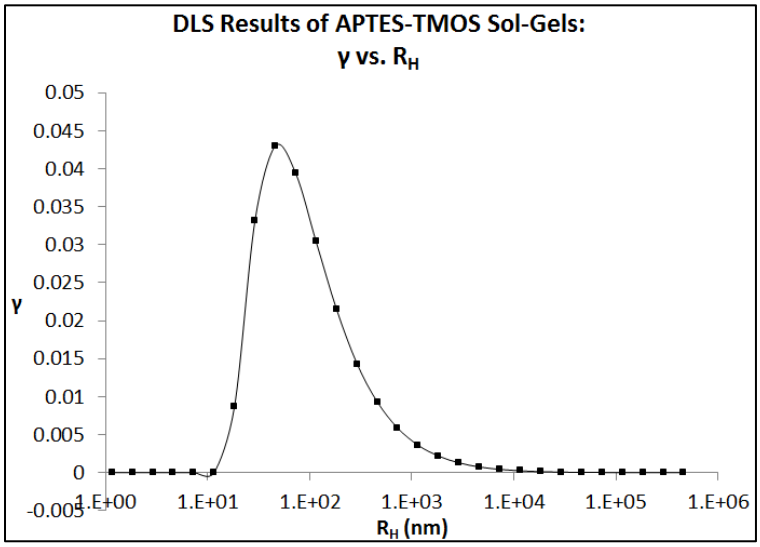

Figure 5.1 DLS Characterization of APTES-TMOS Sol-Gels via DLS

The average R_H is 60 nm. There is broad range of sol-gel sizes ranging from 10 to 1,000 nm in range. However, there are no peaks exceeding 1,000 nm in size. The size distribution is similar to the 20:1 SNAP particles, indicating that the formation of sol-gels does not undergo a great deal of agglomeration. The minimal agglomeration of the sol-

gels later contributed to continuous improvements in the mechanical properties with the addition of APTES-TMOS sol-gels.

5.3.2 DSC Results of Epoxide-Polyamide Films Loaded with APTES-TMOS Sol-Gels

The T_G results measured by DSC are plotted in Figure 5.2 as a function of the sol-gel weight %. There is a 20°C increase in the glass transition temperature with the addition of 7.5% wt. sol gels. This is similar with results observed with other researchers, which indicated an increase in the glass transition temperature with the addition of sol-gel content .[45,46,52] The elevated glass transition temperatures are due to the higher crosslink densities and the constrained movement of the epoxide-sol-gel binder. The glass transition temperatures are approximately the same as the temperatures reported for the SNAP-loaded epoxide coatings. Like the SNAP-loaded epoxide, the APTES-TMOS loaded epoxide coating have a wider temperature performance window and better weatherability.

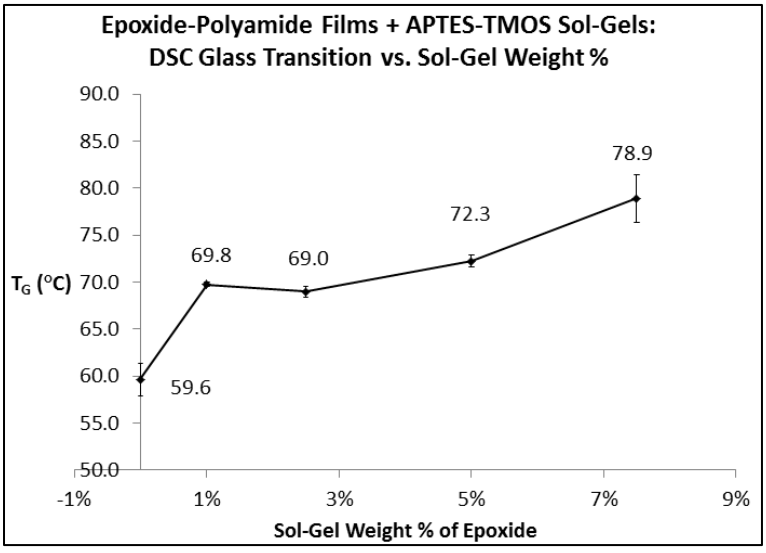

Figure 5.2: DSC T_Gs of Epoxide-Polyamide Films with APTES-TMOS Sol-Gels

5.3.3 DMA Results of Epoxide-Polyamide Films Loaded with APTES-TMOS Sol-Gel Particles

The crosslink density of the APTES-TMOS sol-gel loaded epoxide polyamide films are plotted in Figure 5.3 as a function of the sol-gel weight %. There is a moderate increase in the crosslink density from neat epoxide to 7.5% APTES-TMOS sol-gels. This indicates that the presence of the sol-gels contributes to an increase in the crosslink density. The crosslink densities reported are between the ones reported for 10:1 and 20:1 SNAP loaded epoxide coatings. The higher crosslink densities are attributable to the formation of the more densely packed inorganic sol-gel networks that bind to the epoxide matrix.[145]

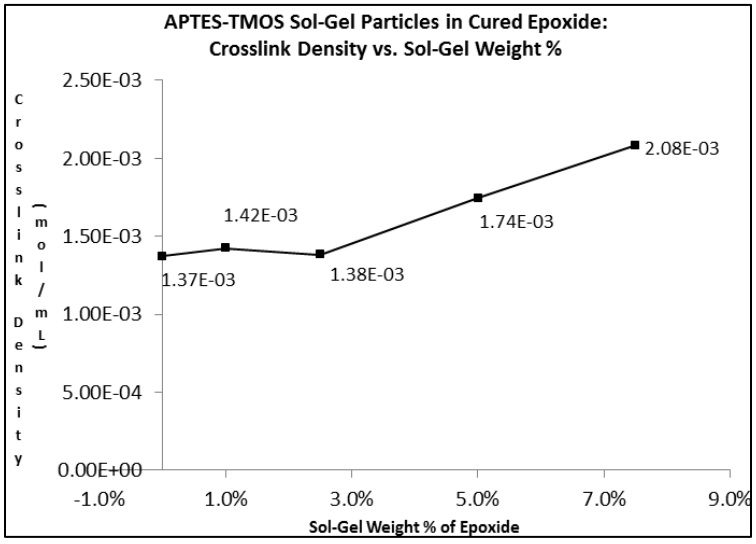

Figure 5.3: Crosslink Density vs. Sol-Gel Wt. % of Epoxide

5.3.4 Tensile Properties of Epoxide-Polyamide Films Loaded with APTES-TMOS Sol-Gels

The tensile strength of the epoxide-polyamide films loaded with APTES-TMOS sol-gels is shown in Figure 5.4. There is a continuous increase in the tensile strength

from neat epoxide to 7.5% wt. The results here are similar to reported results for SNAP sol-gels in epoxide-polyamide films. The increase in the tensile strength is due to the increased crosslink densities, covalent bonding of the siloxane domains of the sol-gel content, and delay of fracture provided by the particle content. The lack of aggregation leads to better dispersion into the epoxide matrix, which results in a continuous increase to the tensile strength.[176-177] The tensile strength values (20-40 MPa) and increases (generally between 30%-100% increase) are in line with past literature.[176-177]

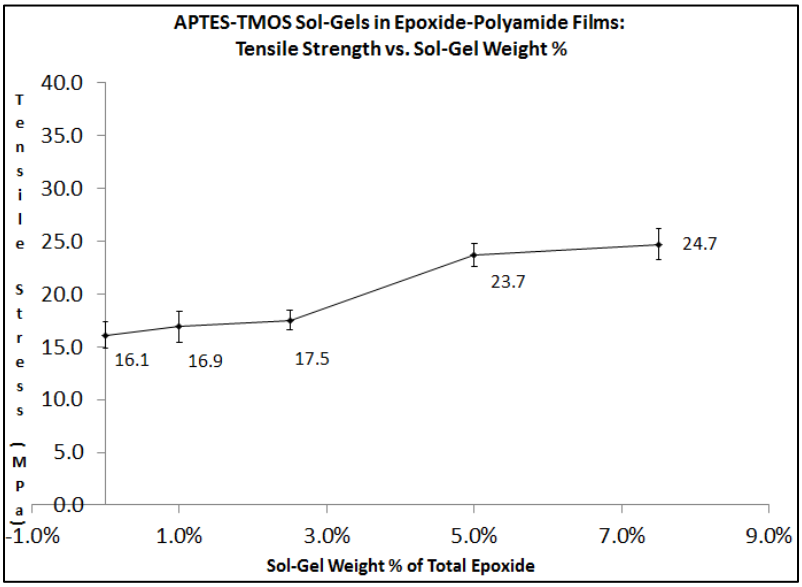

Figure 5.4: Tensile Strength vs. Sol-Gel Wt. %

The tensile strength 2-sample T results of the APTES-TMOS sol-gel filled epoxide films are listed in Table 5.3. Only the 5% and 7.5% sample sets are significantly different from the neat epoxide control set.

Table 5.3: APTES-TMOS Sol-Gel Filled Film Tensile Strength 2-Sample T P-Value Results

Name	Sol-Gel Weight %	2-Sample T P-Value from Control	Significant?
APTES-TMOS	1.0%	0.678	No
APTES-TMOS	2.5%	0.373	No
APTES-TMOS	5.0%	0.001	Yes
APTES-TMOS	7.5%	0.001	Yes

The elongation at break (%) of the epoxide-polyamide films loaded with APTES-TMOS sol-gels is shown in Figure 5.5. There is a continuous increase in the elongation at break (%) from neat epoxide to 7.5% wt. The modest flexibility increase is due to better dispersion into the epoxide matrix. The results here are similar to reported results for SNAP sol-gels in epoxide-polyamide films. The elongation-at-break values are within the same range as past literature investigating thermosetting epoxide materials with silica and sol-gel domains.[176]

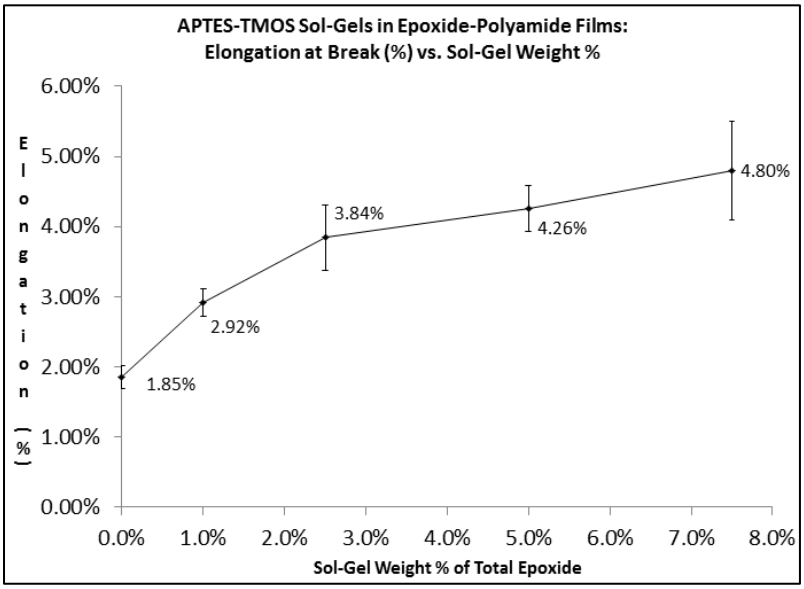

Figure 5.5: Elongation at Break (%) vs. Sol-Gel Wt. %

The elongation % 2-sample T results of the APTES-TMOS sol-gel filled epoxide films are listed in Table 5.4. The 2.5%, 5%, and 7.5% sample sets are significantly different from the neat epoxide film set.

Table 5.4: APTES-TMOS Sol-Gel Filled Film Elongation % 2-Sample T P-Value Results

Name	Sol-Gel Weight %	2-Sample T P-Value from Control	Significant?
APTES-TMOS	1.0%	0.265	No
APTES-TMOS	2.5%	0.005	Yes
APTES-TMOS	5.0%	0.000	Yes
APTES-TMOS	7.5%	0.005	Yes

The elastic modulus of the epoxide-polyamide films loaded with APTES-TMOS sol-gels is shown in Figure 5.6. There is a continuous increase in the elastic modulus from neat epoxide to 7.5% wt. The results here are similar to reported results for SNAP sol-gels in epoxide-polyamide films, although the results are slightly lower. This is similar to past observations in literature, which indicates that siloxane bonding and increases in the crosslink density can lead to an increase in the modulus.[41,58,147,182-184]

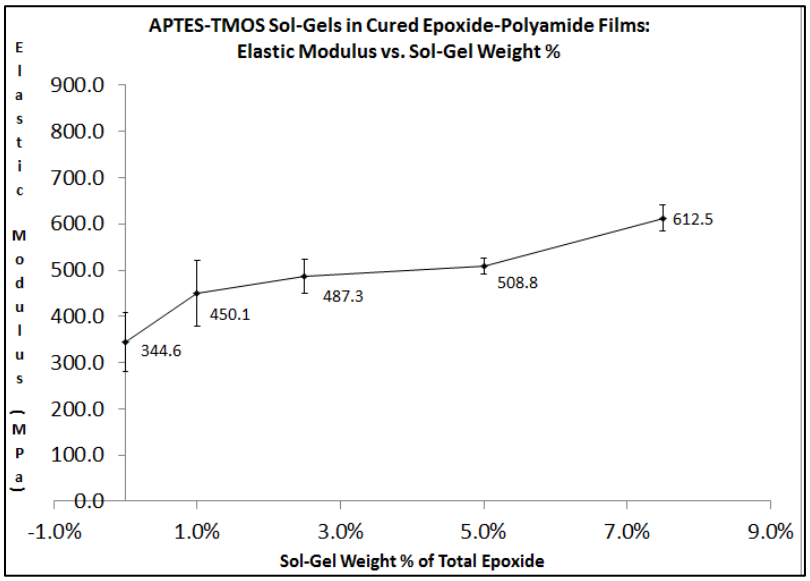

Figure 5.6: Elastic Modulus vs. Sol-Gel Wt. %

The elastic modulus 2-sample T results of the APTES-TMOS sol-gel filled epoxide films are listed in Table 5.5. All sets are significantly different from the neat epoxide film set.

Table 5.5: APTES-TMOS Sol-Gel Filled Film Elastic Modulus 2-Sample T P-Value Results

Name	Sol-Gel Weight %	2-Sample T P-Value from Control	Significant?
APTES-TMOS	1.0%	0.016	Yes
APTES-TMOS	2.5%	0.073	Yes
APTES-TMOS	5.0%	0.028	Yes
APTES-TMOS	7.5%	0.002	Yes

5.3.5 Fracture Properties of Epoxide-Polyamide Films Loaded with APTES-TMOS Sol-Gels

The fracture toughness of the films tested at a temperature of -55°C is shown in Figure 5.7. The fracture toughness values increase marginally. The limitation of the fracture toughness at lower temperatures is due to the limited crosslinked polymeric chain movement at lower temperatures.

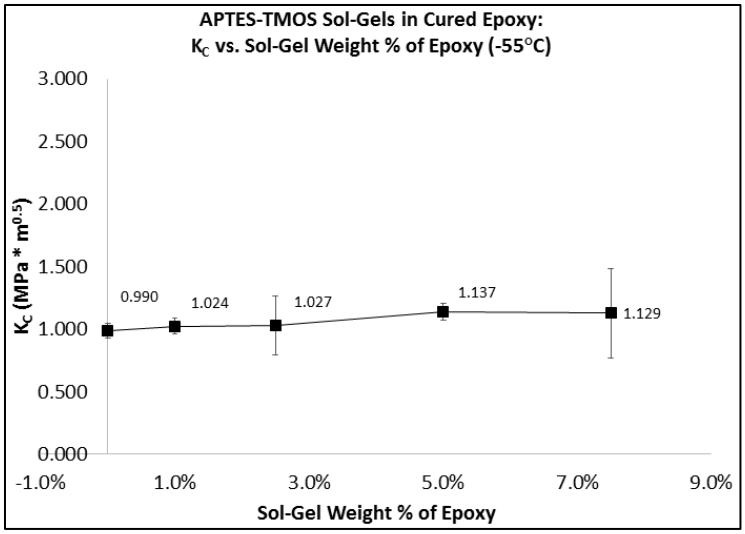

Figure 5.7: K_C vs. Sol-Gel Wt. % of Epoxide (-55°C)

The fracture toughness values of the epoxide-polyamide films at room temperature are shown in Figure 5.8. K_C is plotted as a function of the sol-gel weight percentage. There is a gradual increase in the sol-gel weight percentage with respect to the weight percentage. At 7.5% wt., the fracture toughness is 90% greater than neat epoxide. Past literature has indicated that the presence of functional sol-gels can enhance the fracture toughness of a epoxide film through covalent bonding and crack deflection.[147,178] The fracture toughness values (0.5 MPa*$m^{0.5}$ to 2.8 MPa*$m^{0.5}$) match that of past literature.[176]

The K_C results of the APTES-TMOS sol-gel filled epoxide films at -55°C are listed in Table 5.6. The 2-sample T tests, which indicate if the sample sets show a statistically significant difference between the neat epoxide control film and the sol-gel filled films, are shown for 1%, 2.5%, 5%, and 7.5% APTES-TMOS filled epoxide films. None of the sample sets show a significant difference.

Table 5.6: APTES-TMOS Sol-Gel Filled Film K_C at -55°C 2-Sample T P-Value Results

Name	Sol-Gel Weight %	2-Sample T P-Value from Control	Significant?
APTES-TMOS	1.0%	0.700	No
APTES-TMOS	2.5%	0.511	No
APTES-TMOS	5.0%	0.943	No
APTES-TMOS	7.5%	0.696	No

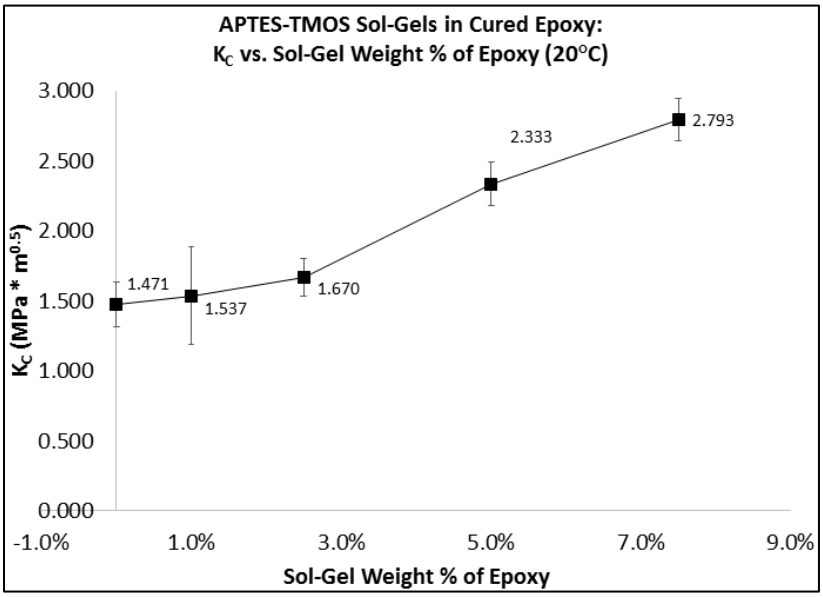

Figure 5.8: K_C vs. Sol-Gel Wt. % of Epoxide (20°C)

The K_C results of the APTES-TMOS sol-gel filled epoxide films at 20°C are listed in Table 5.7. The 2-sample T tests, which indicate if the sample sets show a statistically significant difference between the neat epoxide control film and the sol-gel filled films, are shown for 1%, 2.5%, 5%, and 7.5% APTES-TMOS filled epoxide films. The 5% and 7.5% sample sets show a significant difference.

Table 5.7: APTES-TMOS Sol-Gel Filled Film K_C at 20°C 2-Sample T P-Value Results

Name	Sol-Gel Weight %	2-Sample T P-Value from Control	Significant?
APTES-TMOS	1.0%	0.709	No
APTES-TMOS	2.5%	0.206	No
APTES-TMOS	5.0%	0.001	Yes
APTES-TMOS	7.5%	0.000	Yes

The fracture toughness values of the epoxide polyamide films at 60°C are shown in Figure 5.9. There is an increase from 0.777 to approximately 1.310 MPa*$m^{0.5}$ and then a decrease to 0.454 MPa*$m^{0.5}$ at 7.5% APTES-TMOS sol-gel content.

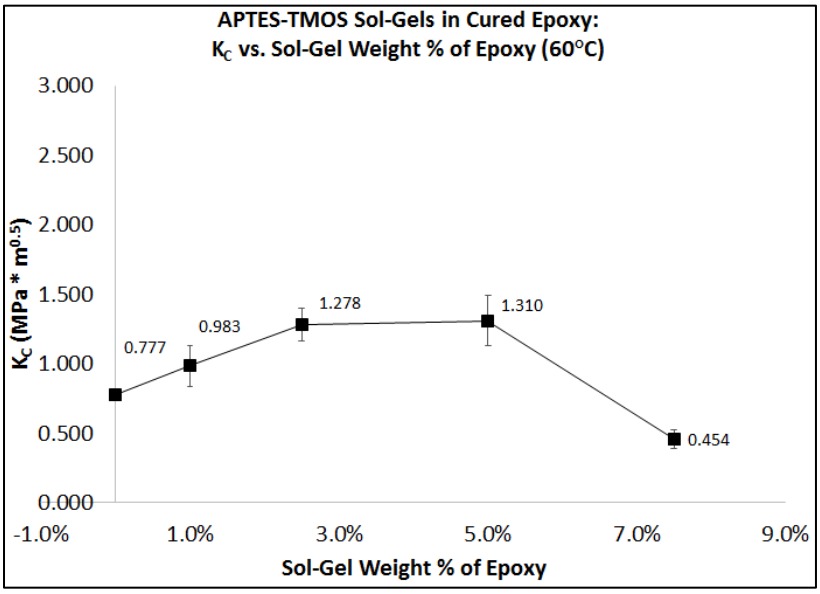

Figure 5.9: K_C vs. Sol-Gel Wt. % of Epoxide (60°C)

The K_C values of the various epoxide-polyamide films are plotted versus the temperature in Figure 5.10. All films show an increase in the fracture toughness from -55°C to 20°C and a decrease in the fracture toughness from 20°C to 60°C.

The K_C results of the APTES-TMOS sol-gel filled epoxide films at 60°C are listed in Table 5.8. The 2-sample T tests, which indicate if the sample sets show a statistically significant difference between the neat epoxide control film and the sol-gel filled films, are shown for 1%, 2.5%, 5%, and 7.5% APTES-TMOS filled epoxide films. The 2.5%, 5%, and 7.5% sample sets show a significant difference.

Table 5.8: APTES-TMOS Sol-Gel Filled Film K_C at 60°C 2-Sample T P-Value Results

Name	Sol-Gel Weight %	2-Sample T P-Value from Control	Significant?
APTES-TMOS	1.0%	0.267	No
APTES-TMOS	2.5%	0.010	Yes
APTES-TMOS	5.0%	0.042	Yes
APTES-TMOS	7.5%	0.002	Yes

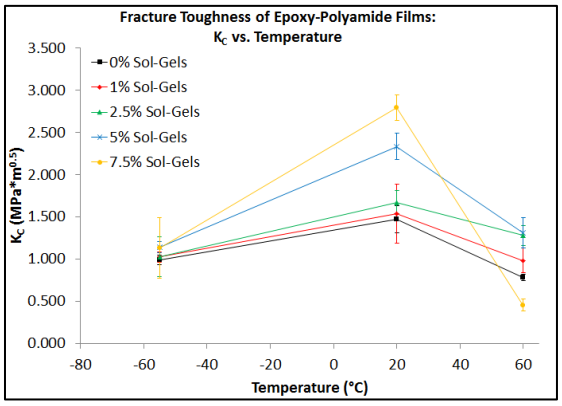

Figure 5.10: K_C vs. Temperature

The strain energy release rate (G_C) at -55°C is plotted in Figure 5.11 as a function of the sol-gel weight percentage. The strain energy release rate results are similar to the fracture toughness results: a marginal increase that isn't statistically significant.

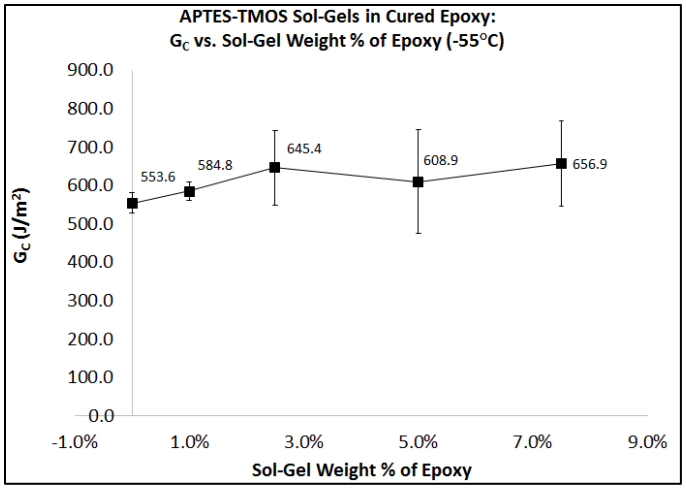

Figure 5.11: G_C vs. Sol-Gel Wt. % of Epoxide (-55°C)

The G_C results of the APTES-TMOS sol-gel filled epoxide films at -55°C are listed in Table 5.9. The 2-sample T tests, which indicate if the sample sets show a statistically significant difference between the neat epoxide control film and the sol-gel filled films, are shown for 1%, 2.5%, 5%, and 7.5% APTES-TMOS filled epoxide films. The 5% and 7.5% sample sets show a significant difference.

Table 5.9: APTES-TMOS Sol-Gel Filled Film G_C at -55°C 2-Sample T P-Value Results

Name	Sol-Gel Weight %	2-Sample T P-Value from Control	Significant?
APTES-TMOS	1.0%	0.441	No
APTES-TMOS	2.5%	0.511	No
APTES-TMOS	5.0%	0.036	Yes
APTES-TMOS	7.5%	0.049	Yes

The strain energy release rate (G_C) at 20°C is plotted in Figure 5.12 as a function of the sol-gel weight percentage. The strain energy release rate for neat epoxies is 249 J/m^2, and the values increase in a relatively linear fashion up to a maximum of 2,031.5 J/m^2 at a sol-gel weight percentage of 7.5%. This is an 8-fold increase in the strain

energy release rate over neat epoxide. The addition of the sol-gel particles augment the energy required to propagate fracture within the epoxide sample because of the siloxane covalent bonds of the sol-gels and crack deflection around the sol-gel domains.

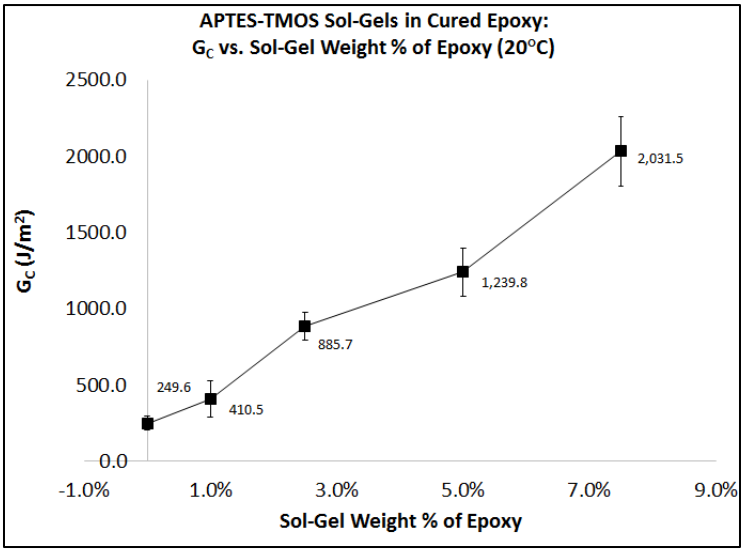

Figure 5.12: G_C vs. Sol-Gel Wt. % of Epoxide (20°C)

The G_C results of the APTES-TMOS sol-gel filled epoxide films at 20°C are listed in Table 5.10. The 2-sample T tests, which indicate if the sample sets show a statistically significant difference between the neat epoxide control film and the sol-gel filled films, are shown for 1%, 2.5%, 5%, and 7.5% APTES-TMOS filled epoxide films. The 2.5%, 5%, and 7.5% sample sets show a significant difference.

Table 5.10: APTES-TMOS Sol-Gel Filled Film G_C at 20°C 2-Sample T P-Value Results

Name	Sol-Gel Weight %	2-Sample T P-Value from Control	Significant?
APTES-TMOS	1.0%	0.273	No
APTES-TMOS	2.5%	0.001	Yes
APTES-TMOS	5.0%	0.001	Yes
APTES-TMOS	7.5%	0.000	Yes

The strain energy release rate (G_C) at 60°C is plotted in Figure 5.13 as a function of the sol-gel weight percentage. There is a 2-fold increase in the strain energy release from neat epoxide to 2.5%-5% APTES-TMOS content. The strain energy release rate then decreases for 7.5% sol-gel content, which is theorized to be an extension of the decreased fracture toughness at 7.5%.

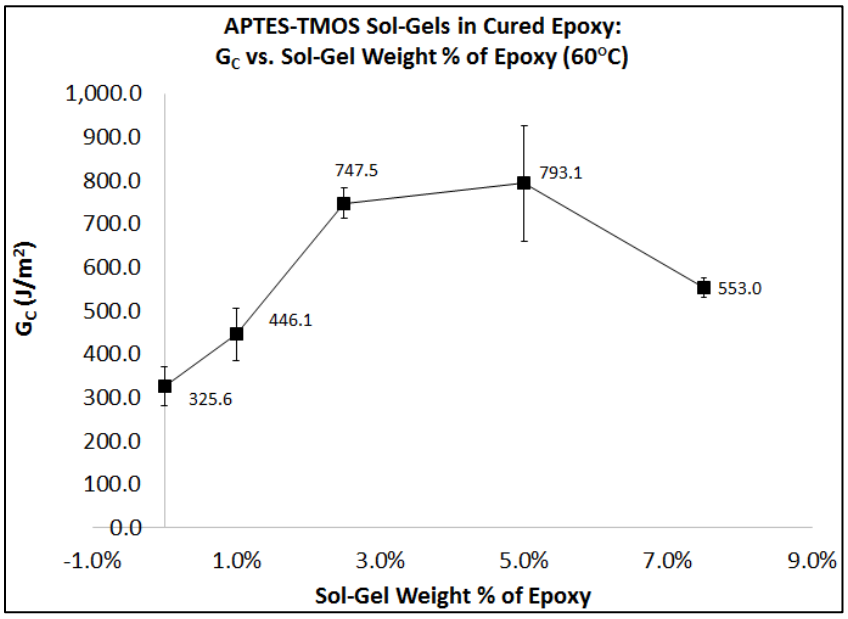

Figure 5.13: G_C vs. Sol-Gel Wt. % of Epoxide (60°C)

The G_C results of the APTES-TMOS sol-gel filled epoxide films at 60°C are listed in Table 5.11. The 2-sample T tests, which indicate if the sample sets show a statistically significant difference between the neat epoxide control film and the sol-gel filled films, are shown for 1%, 2.5%, 5%, and 7.5% APTES-TMOS filled epoxide films. The 5% and 7.5% sample sets show a significant difference.

Table 5.11: APTES-TMOS Sol-Gel Filled Film G_C at 60°C 2-Sample T P-Value Results

Name	Sol-Gel Weight %	2-Sample T P-Value from Control	Significant?
APTES-TMOS	1.0%	0.179	No
APTES-TMOS	2.5%	0.001	Yes
APTES-TMOS	5.0%	0.003	Yes
APTES-TMOS	7.5%	0.002	Yes

The strain energy release rate (G_C) as a function of the temperature is plotted in Figure 5.14. What is notable about the plots are that for neat epoxide and 1% APTES-TMOS, there is a reduction in the strain energy release rate from -55°C to 20°C and 60°C. At higher levels of sol-gel content, there is an increase in the strain energy release rate from -55°C to 20°C and then a reduction from 20°C to 60°C.

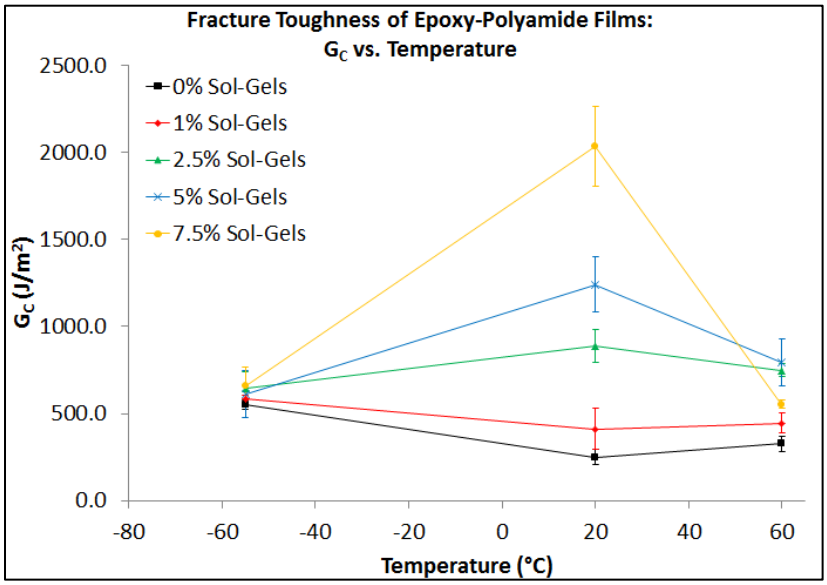

Figure 5.14: G_C vs. Temperature

5.3.6 Taber Abrasion Results of MIL-DTL-24441 Coatings Loaded with APTES-TMOS Sol-Gels

The Taber abrasion results are shown in Figure 5.15. There is a 66% reduction in the weight loss with a 7.5 wt. % addition of the sol-gel particles. There is a 50% decrease in the weight loss with the addition of 1 wt. % sol-gel content and a gradual reduction in the weight loss to 7.5 wt. %. As explained by Palraj et al.[174], the enhanced abrasion resistance is due to the inorganic silica content from the SNAP particles, which are generally more abrasion resistant than epoxide.

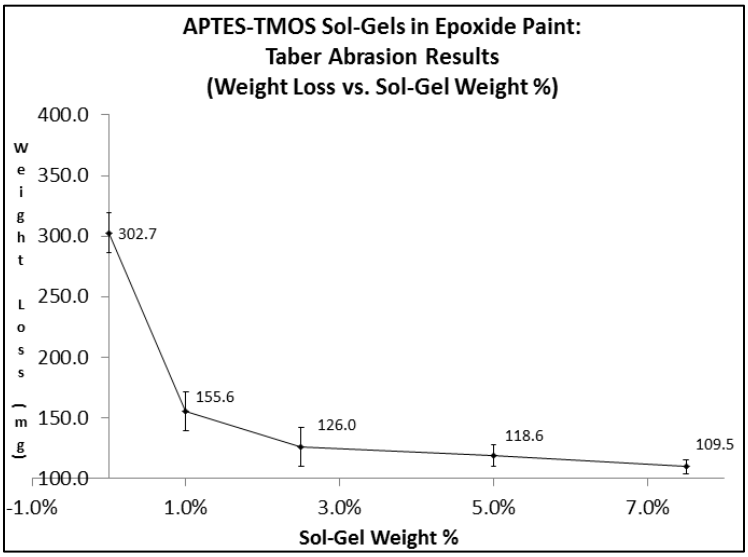

Figure 5.15: Abrasion Results of MIL-DTL-24441 Coatings Loaded with APTES-TMOS Sol-Gels

The Taber abrasion results of the APTES-TMOS sol-gel filled epoxide coatings are listed in Table 5.12. The 2-sample T tests, which indicate if the sample sets show a statistically significant difference between the neat epoxide control coatings and the sol-

gel filled coatings, are shown for 1%, 2.5%, 5%, and 7.5% APTES-TMOS filled epoxide coatings. All four sample sets show a significant difference.

Table 5.12: APTES-TMOS Sol-Gel Filled Coatings Taber Abrasion 2-Sample T P-Value Results

Name	Sol-Gel Weight %	2-Sample T P-Value from Control	Significant?
APTES-TMOS Sol-Gels	1.0%	0.003	Yes
APTES-TMOS Sol-Gels	2.5%	0.002	Yes
APTES-TMOS Sol-Gels	5.0%	0.002	Yes
APTES-TMOS Sol-Gels	7.5%	0.004	Yes

5.3.7 Adhesion Strengths of MIL-DTL-24441 Coatings Loaded with APTES-TMOS Sol-Gels

The adhesion strength versus the sol-gel weight % is shown in Figure 5.16. There is a 75% increase in the adhesion strength from neat epoxide to 1% APTES-TMOS sol-gel, a 98% increase with 2.5% sol-gel content, a 113% increase with 5% sol-gel content, and a 95% increase with 7.5% sol-gel content. The presence of the sol-gel particles leads to alkoxysilane linkages with the substrate, which provides an increase in the adhesion strength.[147] The range of error suggests that the adhesion strength remains relatively constant for 2.5%, 5%, and 7.5% sol-gel content.

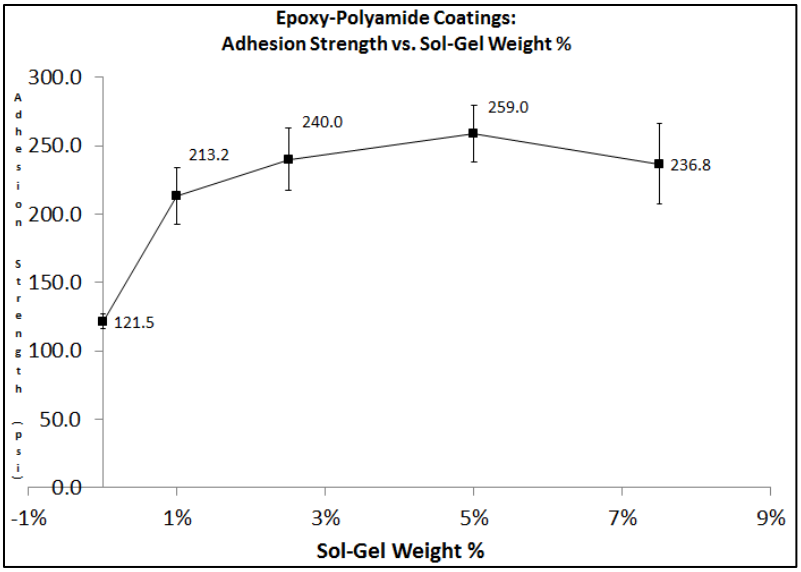

Figure 5.16: Adhesion Strength vs. APTES-TMOS Sol-Gel Wt. %

The pull-off adhesion 2-sample T results for the APTES-TMOS sol-gel filled epoxide coatings are shown in Table 5.13. All four sample sets are significantly different than the neat epoxide control coating.

Table 5.13: APTES-TMOS Sol-Gel Filled Coating Pull-Off Adhesion 2-Sample T P-Value Results

Name	Sol-Gel Weight %	2-Sample T P-Value from Control	Significant?
APTES-TMOS Sol-Gels	1.0%	0.010	Yes
APTES-TMOS Sol-Gels	2.5%	0.006	Yes
APTES-TMOS Sol-Gels	5.0%	0.002	Yes
APTES-TMOS Sol-Gels	7.5%	0.017	Yes

5.3.8 EIS Results of MIL-DTL-24441 Coatings Loaded with APTES-TMOS Sol-Gels

The Nyquist plots of the coatings systems at Day 30 are shown in Figure 5.17. Neat epoxide indicates some level of coating failure, while 1% APTES-TMOS is the beginning stages of coating failure. 2.5%, 5%, and 7.5% all show some levels of coating

resistance to corrosion. 7.5% shows the greatest coating resistance. This proves that greater levels of APTES-TMOS, by nature of the hydrophobicity, barrier properties, and increased crosslink density, enhance the corrosion resistance.

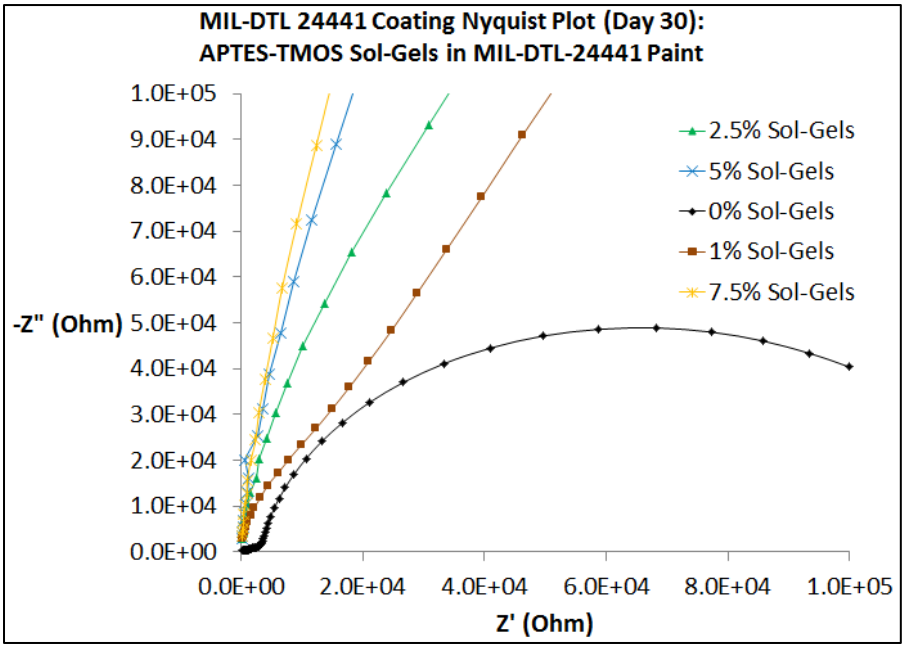

Figure 5.17: Nyquist Plots of MIL-DTL-24441 Coatings with APTES-TMOS Sol-Gels

The Bode plots for the coatings systems at Day 30 are in Figure 5.18. All coatings systems loaded with APTES-TMOS have impedance moduli two orders of magnitude higher than the neat epoxide systems. The impedance moduli as well as the shape of the curves indicate that coatings systems with 5% or 7.5% sol-gel content show the greatest resistance to corrosion. Neat epoxide, 1%, and 2.5% sol-gel content systems show metal corrosion, while 5% and 7.5% sol-gel content systems show that coatings are still acting as an effective barrier against corrosion.

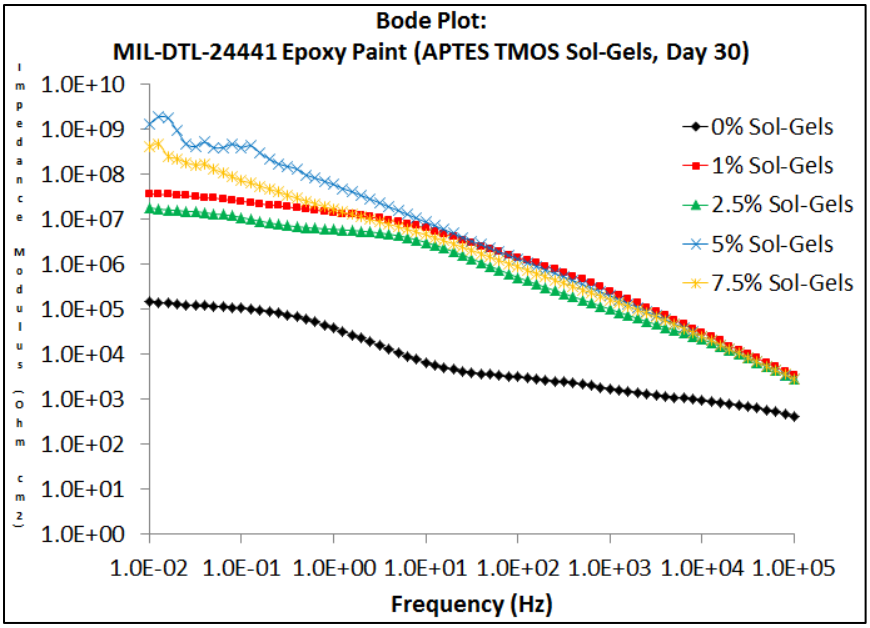

Figure 5.18: Bode Plots of MIL-DTL-24441 Coatings with APTES-TMOS Sol-Gels

The impedance moduli at 1 Hz. on Day 30 of immersion are shown in Figure 5.19.

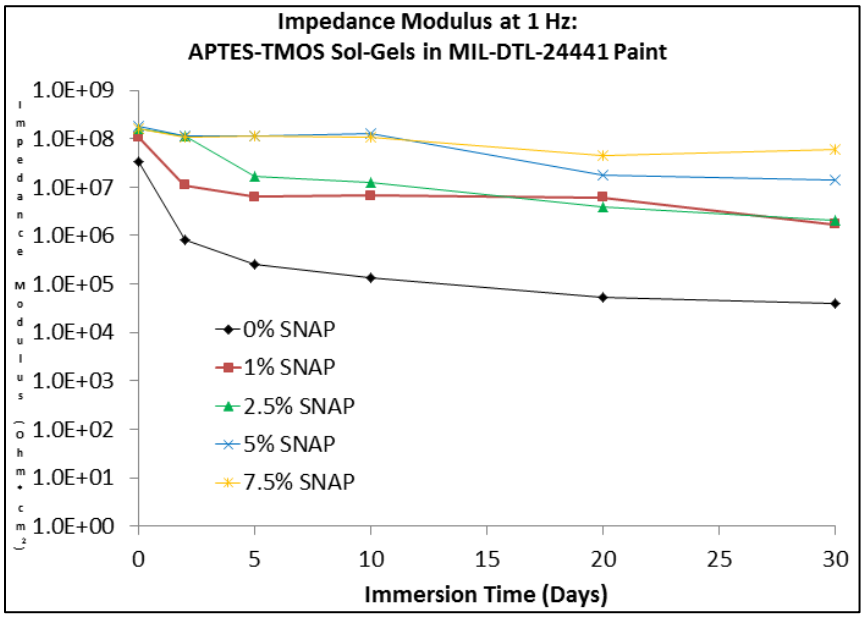

Figure 5.19: Impedance Moduli (@1Hz) of MIL-DTL-24441 Coatings with APTES-TMOS Sol-Gels

All coating systems with APTES-TMOS sol-gels have impedance moduli that are two orders of magnitude higher than neat epoxide coating systems. 1% and 2.5% APTES-TMOS coating systems have approximately the same impedance moduli. With the exception of 7.5% APTES-TMOS, all coating systems decrease in the impedance modulus from Day 0 of immersion to Day 30 of immersion, which indicates a gradual weakening of the coating system over time. This confirms that greater amounts of APTES-TMOS sol-gel content contribute to an enhancement in the barrier properties and corrosion resistance of the coating system.

5.3.9 EIS Water Uptake of APTES-TMOS Loaded Epoxide Coatings

The water uptake (%) as measured by EIS is shown in Figure 5.20. The water uptake (%) is plotted as a function of the sol-gel weight percentage.

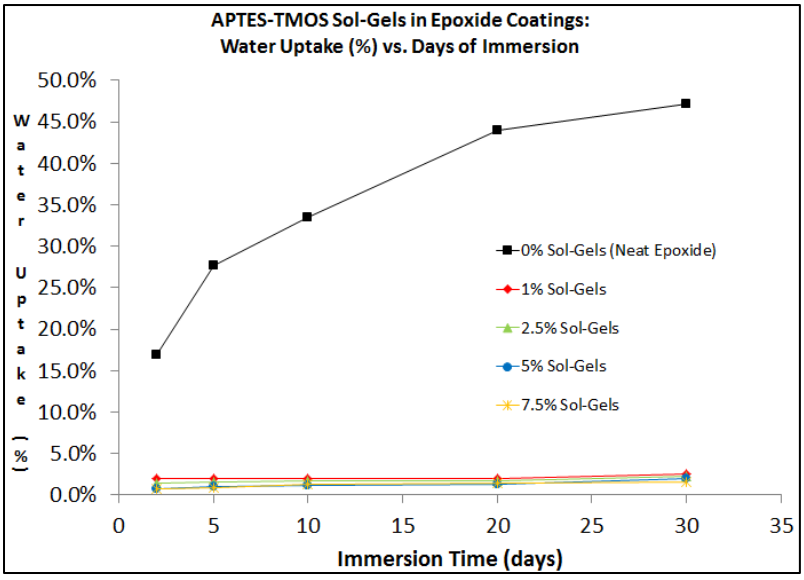

Figure 5.20: EIS Water Uptake of APTES-TMOS Loaded Epoxide Coatings

The APTES-TMOS sol-gels contribute to very low water uptake percentages (none of the sol-gel loaded epoxide coatings exceeded 3% even after 30 days of

immersion in sea water). Past research indicated that the water uptake (and ultimate the barrier properties) of the SNAP loaded coatings are due to two factors: the presence of a silica barrier and the contribution of SNAP coatings to elevated crosslink densities, which also hinder the diffusion of water.[63,147]

5.3.10 Contact Angle Measurements of Sol-Gel Loaded Epoxide Films

The contact angle of APTES-TMOS sol-gel loaded epoxide films were tested for contact angle measurements. Figure 5.21 shows the contact angle measurements versus the sol-gel weight percentage.

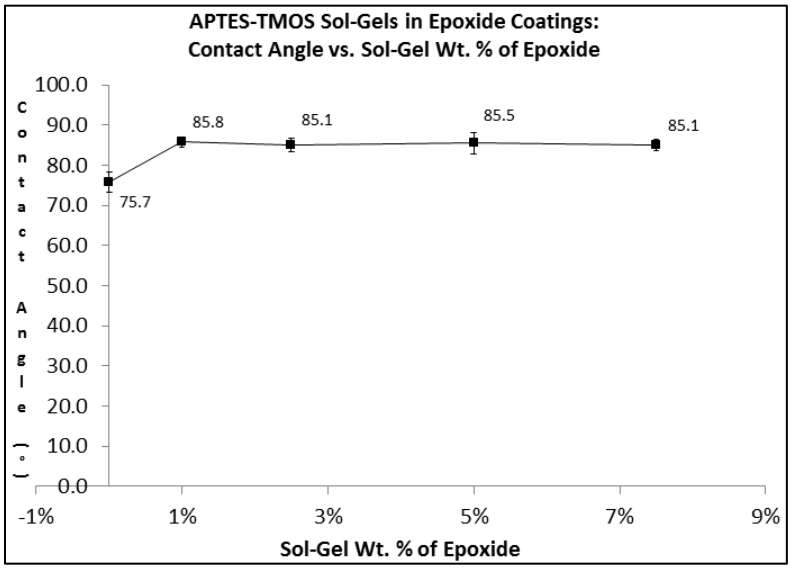

Figure 5.21: Contact Angle Measurements of APTES-TMOS Loaded Epoxide Coatings

There is a moderate increase in the contact angle from neat epoxide to APTES-TMOS loaded epoxide coatings. The contact angle of the unmodified epoxide is equivalent to measurements reported in past literature (73 +/- 3°).[183] The increase in the contact angle implies that the presence of APTES-TMSO sol-gels leads to a more hydrophobic surface than neat epoxide, which in turn contributes to increases in the

barrier properties of the coating. Past literature has indicated that while the sol-gel materials are more hydrophobic (ranging from 88° for TMOS to 172° for vinyltriethoxysilane sol-gel coatings) than epoxides, the greater hydrophobicity in crosslinked epoxide coatings might have more to do with "chemical durability, extensive crosslink, and excellent adhesion to the substrate rather than via surface energy modification."[63]

The contact angle 2-sample T results of the APTES-TMOS sol-gel filled epoxide films are listed in Table 5.14. All sample sets are significantly different from the neat epoxide film set.

Table 5.14: APTES-TMOS Sol-Gel Loaded Film Contact Angle 2-Sample T P-Value Results

Name	Sol-Gel Weight %	2-Sample T P-Value from Control	Significant?
APTES-TMOS	1.0%	0.011	Yes
APTES-TMOS	2.5%	0.019	Yes
APTES-TMOS	5.0%	0.028	Yes
APTES-TMOS	7.5%	0.015	Yes

5.4 Discussion

As demonstrated in Chapter 4, inorganic-organic sol-gels with oxirane end groups can be dispersed into and react with epoxide-polyamide matrices to form continuous films and coatings systems. The films and coatings systems are enhanced in terms of the mechanical properties and corrosion resistance. The following approach represents an improvement over simply using SNAP inorganic-organic sol-gels as a

crosslinked surface preparation in the fact that the latter can only provide a barrier against corrosion.

Aminosilane-based inorganic-organic sol-gels can be also be used as a functional additive within films and coating systems. By nature of the molecular content as well as the ability to form a continuous phase with the epoxide-polyamide matrix via crosslinking, the sol-gels are dispersed. The inorganic and organic phases within the sol-gel contribute to an enhancement in the mechanical properties. Also, the sol-gels create a better barrier against corrosion through the intrinsic nature of the sol-gels and the creation of more crosslinks. This phenomenon is in agreement with other studies on sol-gel coatings used in preventing corrosion.

Other studies have confirmed that the addition of sol-gel or silica content can improve various properties of a coating, composite, or film, such as the fracture properties[132, 165,169-176], tensile properties[31,165-168], adhesion strength[178], and the abrasion resistance.[177-179] The enhanced fracture and tensile properties of the composites come from the strength of the siloxane linkages as well as the chemical linkages between the inorganic and organic moieties. The abrasion resistance arises from the enhanced hardness of the inorganic content, and the adhesion strength arises from the siloxane covalent linkages that are formed between the coating and the substrate.

The fracture toughness and tensile strength values are roughly equivalent to what was previously reported for SNAP particles. The modulus is smaller for APTES-TMOS sol-gel loaded epoxide films, while the elongation-at-break is greater. The

abrasion resistance is better for APTES-TMOS loaded epoxide coatings, while the adhesion strength is smaller. The water uptake is lower for APTES-TMOS sol-gels than for SNAP loaded epoxide coatings. The continuous increase in the mechanical properties and corrosion resistance with the addition of APTES-TMOS sol-gels indicates a good degree of dispersion into the epoxide matrix. This is confirmed by the smaller particle sizes observed by DLS.

The results are notable in the fact that amine-based sol-gels, like the SNAP sol-gels discussed in Chapter 4, can be used to enhance the damage resistance, corrosion resistance, and longevity of epoxide coatings. In terms of coatings enhancement, there isn't a great difference in terms of the end groups that are used (be it amines or oxiranes). The properties stem from the sol-gels creating a barrier to corrosion, their ability to bond to the substrate and coating binders, and their ability to resist damage through intrinsic properties and by delaying fracture. Essentially, it may not be a matter of the end group that is used (be it an amine or oxirane), but mostly the ability to form a stable crosslink with one or more of the binder materials (be it a base epoxide or a set of amide crosslinkers) and a covalent tether to the substrate. Related future work could include exploring the concept of using inorganic (i.e. TEOS instead of TMOS) and/or organic silane molecules with longer silane backbone to determine if there is causation between silane backbone length and macroscopic coating properties. This work would include characterizing related topics such as particle size and determining its relationship to macroscopic coating properties. Other future work would include utilizing silane materials with multiple amine/oxirane functional groups to determine

the relationship between functionality (determined through NMR and epoxy/amine equivalent weight measurements) and the final macroscopic coating properties.

5.5 Conclusions

The use of APTES-TMOS sol-gel content in epoxide composite films and coating systems led to enhancements in the mechanical properties and the corrosion resistance. The sol-gels were characterized for size via dynamic light scattering. Later, the sol-gels were loaded in epoxide-polyamide films and coatings and tested for tensile properties, fracture properties, crosslink density, T_G, abrasion resistance, adhesion strength, and corrosion resistance. The addition of aminosilane sol-gel content led to the thermal and mechanical properties as well as the corrosion resistance. This is similar to the results found in Chapter 4.

CHAPTER VI

EFFECT CARBON NANOTUBE AND MAGNESIUM CONTENT ON EPOXIDE-POLYAMIDE FILMS AND COATING SYSTEMS

6.1 Introduction

Magnesium-rich primer coatings systems were pioneered by Bierwagen et. al. in 2004[10] and arose from the need to find a suitable, non-toxic replacement for chromate based coating systems. Magnesium rich primers for aluminum substrates function in the same manner as zinc-rich primers for steel substrates.[10] Primer coatings are loaded with metals that are more active than the substrate they are placed upon. In order to protect the substrate from corrosion, the metals in the coating, when confronted with an oxidizing/corrosive substance such as oxygen or water, will react to form an oxide instead of the substrate. The resulting oxide that is formed can provide a passivating layer that creates a barrier against permeating corrosive agents. In order to protect the metal substrate, the metal pigment volume concentration (PVC) must exceed the critical pigment volume concentration (CPVC) in order to provide adequate corrosion protection of the substrate.[10]

A weakness of coating systems loaded with sacrificial metals is that loading of the metals above the CPVC will weaken the mechanical properties of the coating system due to the voids that are created as a result of metal loading.[205] The coating does not last as long and requires multiple layers of topcoats to provide a proper barrier against corrosion. Loading above the CPVC, however, is necessary in order to provide proper corrosion protection because it ensures that the sacrificial metals are in physical contact with one another as well as the substrate. In order to improve the mechanical properties of the coating system and remove the added cost of adding multiple topcoats, there is a need to remove some of the metal content while maintaining the corrosion prevention properties of a metal-rich system.

The addition of carbon nanotubes into coating systems can improve the corrosion resistance by cathodic protection and providing barrier properties.[116-120] It can function as a linkage between sacrificial metals, which leads to corrosion protection.[11] Also, the addition of carbon nanotubes can improve the mechanical properties of epoxide materials/coatings (tensile strength, fracture properties, adhesion strength, etc.).[89-111] In this way, the addition of carbon nanotubes and sacrificial metals can be loaded into a coating without having to load the coating system with metals beyond the CPVC.

Castenada et al.[11] utilized various amounts of carbon nanotubes and zinc particles for coatings on steel substrates and found that the addition of the carbon nanotubes aided in corrosion protection. Also, companies such as Tesla NanoCoatings have employed CNT-loaded coating systems as part of their business strategy.[206]

What has not yet been demonstrated in literature is if CNTs will work in preventing corrosion when added into magnesium-loaded coating systems. Also, will carbon nanotubes aid in the mechanical properties of coating systems and nanocomposites that are also loaded with magnesium? If there is ample evidence to prove that the tandem use of the magnesium and carbon nanotubes can improve the corrosion resistance and mechanical properties of an epoxide coating, it could represent an improvement over existing magnesium-rich formulations and one step further in discovering a permanent replacement for chromate loaded epoxides for aluminum substrates.

The focus of this chapter is to determine how the synergy of carbon nanotubes and magnesium in epoxide primers can affect the physical properties and corrosion resistance of epoxide-polyamide films and coating systems. Varying amounts (0%, 0.25%, 0.5%, and 1%) of non-functional carbon nanotubes were added into epoxide-polyamide films or military specification MIL-DTL-24441 BLACK[207] epoxide-polyamide coating systems with varying amounts of magnesium (0%, 10%, 20%, and 40%). The films were tested for tensile and fracture properties, and the coatings were tested for corrosion resistance via electrochemical impedance spectroscopy (EIS).

6.2 Experimental Section

6.2.1 Materials

Epon 828 (diglycidyl ether of bisphenol A epoxide) was purchased from Hexion, Ancamide 507 and Ancamide 700B75 were both purchased from Air Products, naphtha

and mineral spirits were purchased from Klean-Strip, butanol and silica was purchased from Sigma Aldrich, Black Iron Oxide 318M was purchased from Bayferrox, Disparlon NS-30 and Disparlon 6500 were purchased from King Industries, magnesium was purchased from Tesla NanoCoatings, and XW22099 multi-walled carbon nanotubes were purchased from CCNI. All materials were used as supplied.

6.2.2 Formulation of Epoxide-Polyamide Coatings Loaded with CNTs and Mg

Epoxide-polyamide coatings were formulated and cast onto aluminum substrates. There were a total of 14 formulations made for the study. Carbon nanotubes were added into the epoxide-polyamide formulations in weight percentages of 0%, 0.25%, 0.5%, and 1% of the total formulation. Magnesium was added into the epoxide-polyamide formulations in weight percentages of 0%, 10%, 20%, and 40% of the total formulation. Disparlon NS-30 and Disparlon 6500 are thixotropic agents, Ancamide 507 and Ancamide 700B75 are polyamide curing agents, mineral spirits, naphtha, and butyl alcohol are solvents, Epon 828 is the base epoxide (diglycidyl ether of bisphenol A or DGEBA), and Bayferrox Black Iron Oxide 318 M is a black pigment.

Due to the difficulty of dispersing carbon nanotubes into coating formulations loaded with 40 wt. % magnesium, there were only two coatings formulations (instead of 4) that were loaded with 40 wt. % magnesium. The formulations can be viewed in Tables 6.1 and 6.2. Table 6.1 shows the amount of carbon nanotubes and magnesium in each formulation. Table 6.2 shows the rest of the components that constitute each coating formulation.

The coating formulations were mixed together in a Thinky mixer for 10 minutes at 2,000 revolutions per minute. Afterwards, they were cast onto Al-2024 aluminum samples at wet film thicknesses of 5 mils. The aluminum substrates were later utilized for EIS testing.

Table 6.1: Amounts of CNT and Mg in Epoxide-Polyamide Coating Formulations

Name	Mg Wt. %	CNT %	Mg (g)	CNT (g)
1	0%	0%	0.0	0.0
2	10%	0%	6.1	0.0
3	20%	0%	13.7	0.0
4	40%	0%	36.5	0.0
5	0%	0.25%	0.0	0.1
6	10%	0.25%	6.1	0.2
7	20%	0.25%	13.8	0.2
8	40%	0.25%	36.7	0.2
9	0%	0.5%	0.0	0.3
10	10%	0.5%	6.1	0.3
11	20%	0.5%	13.8	0.3
12	0%	1%	0.0	0.6
13	10%	1%	6.2	0.6
14	20%	1%	13.9	0.7

Table 6.2: Component Amounts in Epoxide-Polyamide Coating Formulations

Name	Disparlon NS-30 (g)	Ancamide 507 (g)	Ancamide 700B75 (g)	Quso WR-55 (g)	Mineral spirits (g)	Butyl alcohol (g)	Disparlon 6500 (g)	Epon 828 (g)	Bayferrox Black Iron Oxide 318M (g)	Naphtha (g)
1	0.3	0.9	13.4	4.6	3.1	2.9	0.3	20.1	3.6	5.9
2	0.3	0.9	13.4	4.6	3.1	2.9	0.3	20.1	3.6	5.9
3	0.3	0.9	13.4	4.6	3.1	2.9	0.3	20.1	3.6	5.9
4	0.3	0.9	13.4	4.6	3.1	2.9	0.3	20.1	3.6	5.9
5	0.3	0.9	13.4	4.6	3.1	2.9	0.3	20.1	3.6	5.9
6	0.3	0.9	13.4	4.6	3.1	2.9	0.3	20.1	3.6	5.9
7	0.3	0.9	13.4	4.6	3.1	2.9	0.3	20.1	3.6	5.9
8	0.3	0.9	13.4	4.6	3.1	2.9	0.3	20.1	3.6	5.9
9	0.3	0.9	13.4	4.6	3.1	2.9	0.3	20.1	3.6	5.9
10	0.3	0.9	13.4	4.6	3.1	2.9	0.3	20.1	3.6	5.9
11	0.3	0.9	13.4	4.6	3.1	2.9	0.3	20.1	3.6	5.9
12	0.3	0.9	13.4	4.6	3.1	2.9	0.3	20.1	3.6	5.9
13	0.3	0.9	13.4	4.6	3.1	2.9	0.3	20.1	3.6	5.9
14	0.3	0.9	13.4	4.6	3.1	2.9	0.3	20.1	3.6	5.9

6.2.3 Epoxide-Polyamide Film Formulations

Composite films were created and tested for fracture and tensile properties. There were a total of 16 formulations made for the study. The formulations utilized the same components and weights as the coating formulations, but took out all components except for the epoxide, curing agents, solvent, magnesium, and carbon nanotubes. The film formulations were cast onto PET substrates, cured to completion, and removed from the PET substrates for testing. The wet film thickness was 8 mils. The CNT and Mg amounts in the formulations can be viewed in Table 6.3.

Table 6.3: CNT and Mg Amounts in Epoxide-Polyamide Film Formulations

Name	Magnesium (g)	CNT (g)
1	0.0	0.0
2	6.1	0.0
3	13.7	0.0
4	36.5	0.0
5	0.0	0.1
6	6.1	0.2
7	13.8	0.2
8	36.7	0.2
9	0.0	0.3
10	6.1	0.3
11	13.8	0.3
12	36.9	0.5
13	0.0	0.6
14	6.2	0.6
15	13.9	0.7
16	37.2	0.9

6.2.4 Fracture Property Testing of Epoxide-Polyamide Films

Fracture property testing was conducted as described in Section 3.2.11. 10-15 samples were conducted per sample set. The elongation, tensile strength, and elastic modulus were measured as a function of the carbon nanotube and/or magnesium weight percentage.

6.2.5 Tensile Properties Testing of Epoxide-Polyamide Films

Tensile tests were conducted as described in Section 3.2.8. 10-15 samples were conducted per sample set. K_{IC} and G_{IC} were measured as a function of the carbon nanotube and/or magnesium weight percentage.

6.2.6 Electrochemical Impedance Spectroscopy (EIS) Tests

Electrochemical impedance spectroscopy (EIS) tests were conducted as described in Section 3.2.12. The coatings were tested at Day 0 (2 hours immersion), 2, 5, 10, 20, 30, 40, and 80 days of immersion. Bode and Nyquist plots were reported at Day 80.

6.3 Results

The fracture and tensile properties (fracture toughness and elastic energy release rate) are measured as functions of both the magnesium and carbon nanotube weight percentages. Also, EIS measurements (Bode and Nyquist plots) are measured as functions of the magnesium and carbon nanotube weight percentages.

6.3.1 Fracture Properties of CNT and Mg-Loaded Epoxide-Polyamide Films

The fracture toughness (K_C) in units of $MPa*m^{0.5}$ was plotted as a function of the magnesium weight percentage. The results are shown in Figure 6.1.

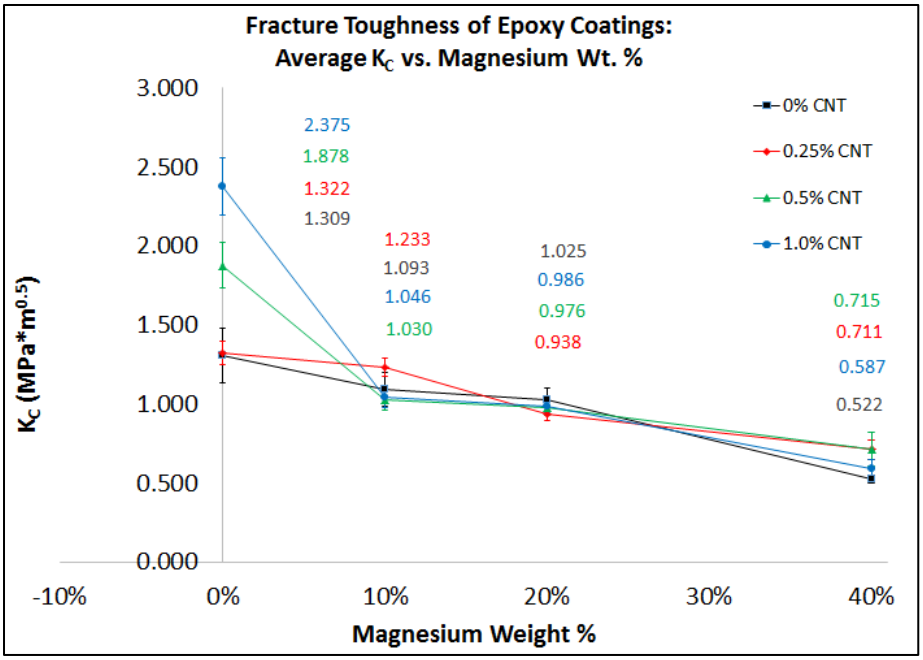

Figure 6.1: K_C vs. Magnesium Wt. %

The carbon nanotube content is associated with higher levels of fracture toughness, although the effect is minimized with moderate to high levels of magnesium. At 0% magnesium, the addition of 1% CNT is associated with an 80% increase in the fracture toughness when compared to neat epoxide without magnesium or carbon nanotube content. The addition of CNTs greater than 0.5% wt. results in significant increases to the fracture toughness. Increases in the fracture toughness with the carbon nanotube content in epoxide composites are in accordance with past literature, indicating that the enhancement to the fracture properties are most likely due to the delay of fracture by debonding and other phenomena.[110] The addition of magnesium to epoxide composites results in a reduction of the fracture toughness. Films with carbon nanotube content added to magnesium content do not lead to a significant difference in the fracture toughness. This is due to the magnesium content not forming a continuous

phase with the epoxide matrix and not having physical geometries conducive to the improvement of the fracture toughness. Also, the addition of both carbon nanotubes and magnesium to the coating formulation may result in an increase of the pigment volume concentration (PVC) to a point beyond the critical pigment volume concentration (CPVC), resulting in a reduction in the physical properties of a coating system.[1]

The K_C 2-sample T results for the films with 0% CNT are shown in Table 6.4. The only significantly different sample set is the one with 40% Mg (a reduction in K_C). The control set is the sample set with 0% Mg and 0% CNT (Formulation #1).

Table 6.4: 0% CNT Formulations K_C 2-Sample T P-Value Results

Formulation	Mg %	2-Sample T P-Value from Control	Significant?
13	10%	0.301	No
2	20%	0.149	No
3	40%	0.001	Yes

The K_C 2-sample T results for the films with 0.25% CNT are shown in Table 6.5. The 20% and 40% Mg sets are statistically different from the control set with 0.25% CNT and 0% Mg (Formulation #4).

Table 6.5: 0.25% CNT Formulations K_C 2-Sample T P-Value Results

Formulation	Mg %	2-Sample T P-Value from Control	Significant?
14	10%	0.394	No
5	20%	0.002	Yes
6	40%	0.000	Yes

The K_C 2-sample T results for the films with 0.5% CNT are shown in Table 6.6. All sample sets are significantly different from the control formulation, Formulation #7, which has 0.5% CNT and 0% Mg.

Table 6.6: 0.5% CNT Formulations K_C 2-Sample T P-Value Results

Formulation	Mg %	2-Sample T P-Value from Control	Significant?
15	10%	0.000	Yes
8	20%	0.000	Yes
9	40%	0.000	Yes

The K_C 2-sample T results for the films with 1% CNT are shown in Table 6.7. All sample sets are significantly different from the control formulation, Formulation #10, which has 1% CNT and 0% Mg.

Table 6.7: 1% CNT Formulations K_C 2-Sample T P-Value Results

Name	Mg %	2-Sample T P-Value from Control	Significant?
16	10%	0.000	Yes
11	20%	0.000	Yes
12	40%	0.000	Yes

The elastic energy strain rate (G_C) in units of J/m^2 is plotted as a function of the magnesium weight percentage in Figure 6.2.

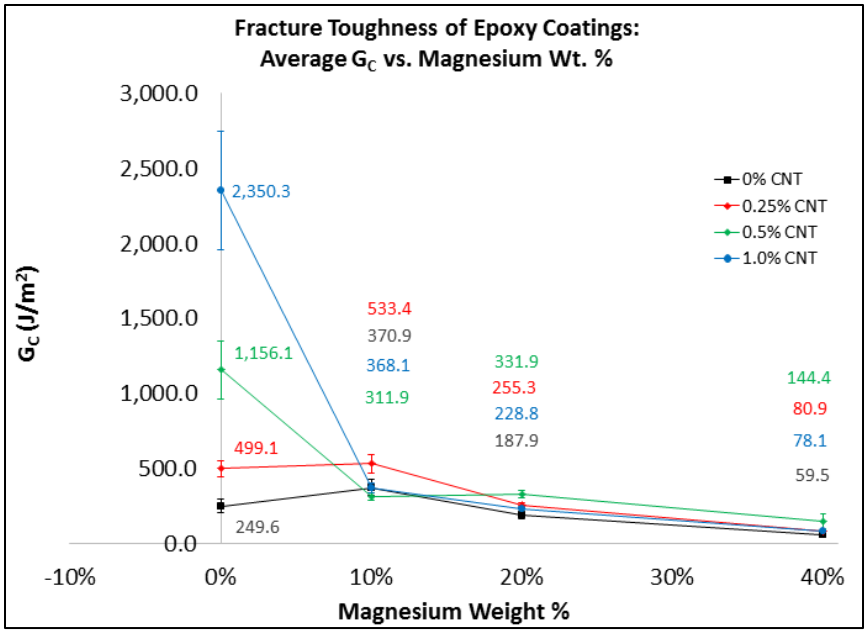

Figure 6.2: G_C vs. Magnesium Wt. %

The addition of CNT content improves the elastic energy strain rate. There is a 1-fold increase at 0.25% CNT, a 3.6-fold increase at 0.5% CNT, and the addition of 1% CNT to neat epoxide results in an 8.5-fold increase to the elastic energy strain rate required to propagate the crack. The increase is limited or nonexistent with the addition of magnesium. The same CNT content with 10 wt. % magnesium results only in a 25%-114% increase. At 20 wt. % magnesium, there is no significant change, and at 40 wt. % magnesium, there is a reduction in the elastic energy strain rate. The addition of carbon nanotubes is associated with a delay in the fracture of the epoxide by debonding and the absorption of energy.[110]

The G_C 2-sample T results for the films with 0% CNT are shown in Table 6.8. The only formulation that significantly differs from the control formulation (#1) is 40% Mg (Formulation #3), which is 0% CNT and 0% Mg.

Table 6.8: 0% CNT Formulations G_C 2-Sample T P-Value Results

Formulation	Mg %	2-Sample T P-Value from Control	Significant?
13	10%	0.101	No
2	20%	0.230	No
3	40%	0.003	Yes

The G_C 2-sample T results for the films with 0.25% CNT are shown in Table 6.9. The 20% and 40% formulations significantly differ from the control formulation (#4), which is 0.25% CNT and 0% Mg.

Table 6.9: 0.25% CNT Formulations G_C 2-Sample T P-Value Results

Formulation	Mg %	2-Sample T P-Value from Control	Significant?
14	10%	0.684	No
5	20%	0.001	Yes
6	40%	0.000	Yes

The G_C 2-sample T results for the films with 0.5% CNT are shown in Table 6.10. All three formulations significantly differ from the control formulation (#7), which is 0.5% CNT and 0% Mg.

Table 6.10: 0.5% CNT Formulations G_C 2-Sample T P-Value Results

Formulation	Mg %	2-Sample T P-Value from Control	Significant?
15	10%	0.001	Yes
8	20%	0.001	Yes
9	40%	0.000	Yes

The G_C 2-sample T results for the films with 1% CNT are shown in Table 6.11. All three formulations significantly differ from the control formulation (#10), which is 1% CNT and 0% Mg.

Table 6.11: 1% CNT Formulations G_C 2-Sample T P-Value Results

Formulation	Mg %	2-Sample T P-Value from Control	Significant?
16	10%	0.001	Yes
11	20%	0.001	Yes
12	40%	0.000	Yes

The same parameters (K_C and G_C) were also plotted as a function of the carbon nanotube weight content. The parameter K_C is plotted in Figure 6.3.

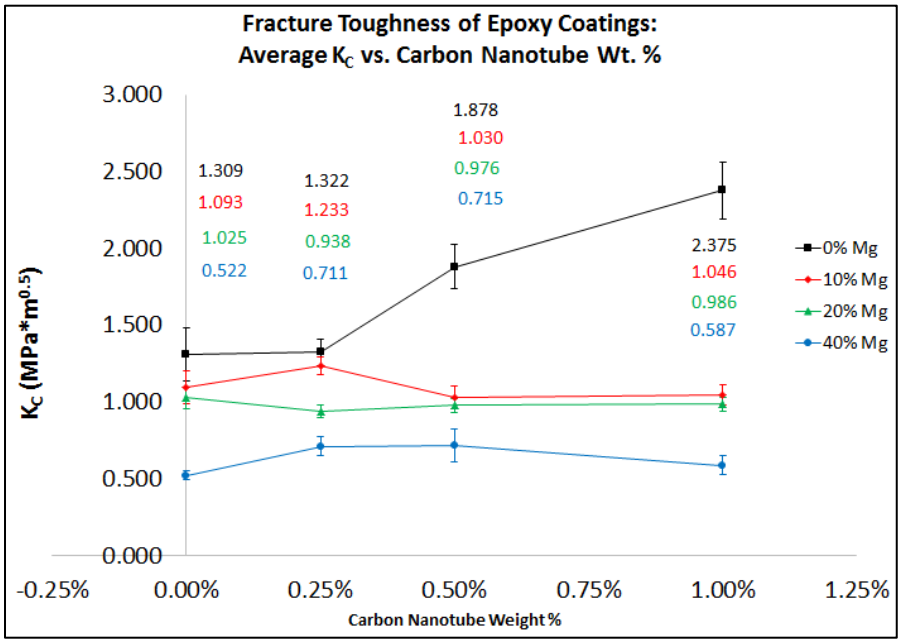

Figure 6.3: K_C vs. Carbon Nanotube Wt. %

Adding in magnesium results in a reduction in the fracture toughness. In the case of 0% CNT, the addition of 10% magnesium results in a 17% reduction in the fracture toughness. There is a 22% reduction for 20% magnesium and a 60% reduction for 40% magnesium. In the case of 0.25% CNT, 0% magnesium content results in an average fracture toughness of 1.322 MPa*m$^{0.5}$. The addition of 10% magnesium results in a 7% reduction, the addition of 20% magnesium results in a 29% reduction, and the addition of 40% magnesium results in a 46% reduction in the fracture toughness. The

average fracture toughness of 0.5% CNT and 0% magnesium is 1.878 MPa*$m^{0.5}$. The addition of 10% magnesium results in a 45% reduction of the fracture toughness, the addition of 20% magnesium results in a 48% reduction in the fracture toughness, and the addition of 40% magnesium results in a 62% reduction in the fracture toughness. The average fracture toughness for 1% CNT and 0% magnesium is 2.375 MPa*$m^{0.5}$. The addition of 10% magnesium results in a 56% reduction in the fracture toughness, the addition of 20% magnesium results in a 58% reduction, and the addition of 40% magnesium results in a 75% reduction in the fracture toughness. The addition of CNTs aid in the enhancement of the fracture toughness, but the effect is mitigated or nonexistent with the addition of magnesium and carbon nanotubes.

The K_C 2-sample T results for the films with 0% Mg are shown in Table 6.12. The 0.5% and 1% CNT sample sets are significantly different from the control formulation (Formulation #1), which is 0% Mg and 0% CNT.

Table 6.12: 0% Mg Formulations K_C 2-Sample T P-Value Results

Name	CNT %	2-Sample T P-Value from Control	Significant?
4	0.25%	0.946	No
7	0.50%	0.019	Yes
10	1.00%	0.000	Yes

The K_C 2-sample T results for the films with 10% Mg are shown in Table 6.13. No sample sets are significantly different from the control formulation (Formulation #13), which is 0% CNT and 10% Mg.

Table 6.13: 10% Mg Formulations K_C 2-Sample T P-Value Results

Name	CNT %	2-Sample T P-Value from Control	Significant?
14	0.25%	0.268	No
15	0.50%	0.635	No
16	1.00%	0.720	No

The K_C 2-sample T results for the films with 20% Mg are shown in Table 6.14. No sample sets are significantly different from the control formulation (Formulation #2), which is 0% CNT and 20% Mg.

Table 6.14: 20% Mg Formulations K_C 2-Sample T P-Value Results

Formulation	CNT %	2-Sample T P-Value from Control	Significant?
5	0.25%	0.422	No
8	0.50%	0.576	No
11	1.00%	0.756	No

The K_C 2-sample T results for the films with 40% Mg are shown in Table 6.15. No sample sets are significantly different from the control formulation (Formulation #3), which is 0% CNT and 40% Mg.

Table 6.15: 40% Mg Formulations K_C 2-Sample T P-Value Results

Formulation	CNT %	2-Sample T P-Value from Control	Significant?
6	0.25%	0.022	Yes
9	0.50%	0.108	No
12	1.00%	0.360	No

The elastic energy strain rates plotted as a function of the carbon nanotube content are shown in Figure 6.4.

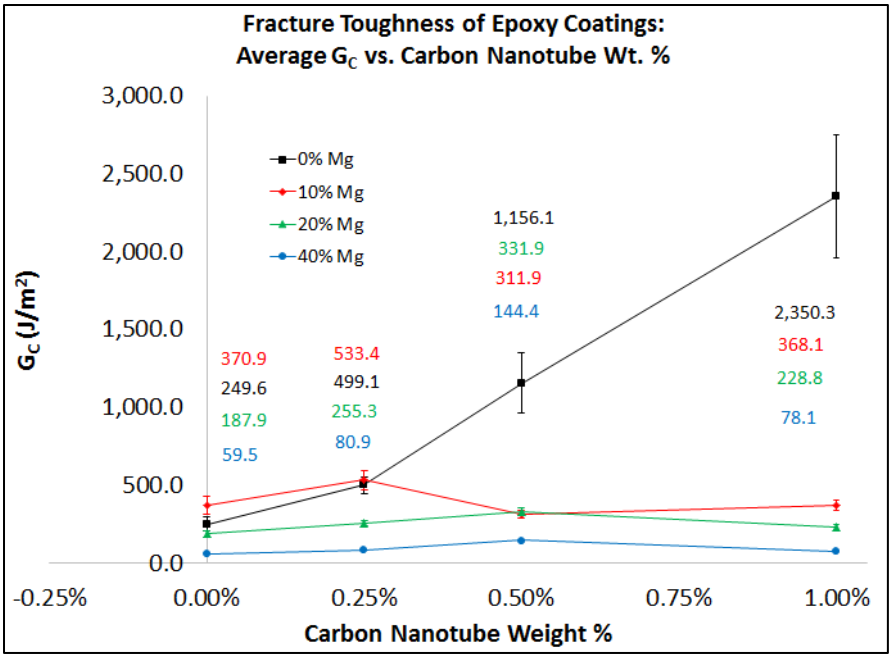

Figure 6.4: G_C vs. Carbon Nanotube Wt. %

The G_C 2-sample T results for the films with 0% Mg are shown in Table 6.16. All three formulations significantly differ from the control formulation (#1), which is 0% CNT and 0% Mg.

Table 6.16: 0% Mg Formulations G_C 2-Sample T P-Value Results

Formulation	CNT %	2-Sample T P-Value from Control	Significant?
4	0.25%	0.002	Yes
7	0.50%	0.001	Yes
10	1.00%	0.001	Yes

The G_C 2-sample T results for the films with 10% Mg are shown in Table 6.17. Formulation #14 (0.25% CNT and 10% Mg) is the only formulation that significantly differs from the control formulation (#13), which is 0% CNT and 10% Mg.

Table 6.17: 10% Mg Formulations G_C 2-Sample T P-Value Results

Formulation	CNT %	2-Sample T P-Value from Control	Significant?
14	0.25%	0.066	No
15	0.50%	0.337	No
16	1.00%	0.965	No

The G_C 2-sample T results for the films with 20% Mg are shown in Table 6.18. The 0.25% and 0.5% CNT sample sets significantly differ from the control formulation (#2), which is 0% CNT and 20% Mg.

Table 6.18: 20% Mg Formulations G_C 2-Sample T P-Value Results

Formulation	CNT %	2-Sample T P-Value from Control	Significant?
5	0.25%	0.023	Yes
8	0.50%	0.000	Yes
11	1.00%	0.178	No

The G_C 2-sample T results for the films with 40% Mg are shown in Table 6.19. No sample formulations differ significantly from the control formulation (#3), which is 0% CNT and 40% Mg.

Table 6.19: 40% Mg Formulations G_C 2-Sample T P-Value Results

Formulation	CNT %	2-Sample T P-Value from Control	Significant?
6	0.25%	0.109	No
9	0.50%	0.140	No
12	1.00%	0.241	No

There is a reduction in the elastic energy strain rate with the addition of magnesium and an expansion in the elastic energy strain rate with the addition of carbon nanotubes.

The average elastic energy strain rate of neat epoxide is 370.9 J/m^2. For 0% CNT, the addition of 10% magnesium results in a 49% increase in the elastic energy strain

rate, the addition of 20% magnesium results in a 25% reduction in the elastic energy strain rate, and the addition of 40% magnesium results in a 76% reduction in the elastic energy strain rate. The average elastic energy strain rate at epoxies loaded with 0.25% CNT and 0% magnesium is 499.1 J/m^2. There is a 7% increase in the elastic energy strain rate with the addition of 10% magnesium, a 49% reduction with the addition of 20% magnesium, and an 84% reduction with the addition of 40% magnesium. The average elastic energy strain rate of epoxide films loaded with 0.5% CNT and 0% magnesium is 1,156.1 J/m^2. There is a 73% reduction in the elastic strain rate with the addition of 10% magnesium, a 71% reduction in the elastic energy strain rate with the addition of 20% magnesium, and an 88% reduction in the elastic energy strain rate with the addition of 40% magnesium. The average elastic energy strain rate of films loaded with 1% CNT and 0% magnesium is 2,350.3 J/m^2. There is an 84% reduction in the elastic energy strain rate with the addition of 10% magnesium, a 90% reduction with the addition of 20% magnesium, and a 97% reduction with the addition of 40% magnesium.

6.3.2 Tensile Properties of CNT and Mg-Loaded Epoxide-Polyamide Films

The tensile strength as a function of the magnesium weight percentage is plotted in Figure 6.5.

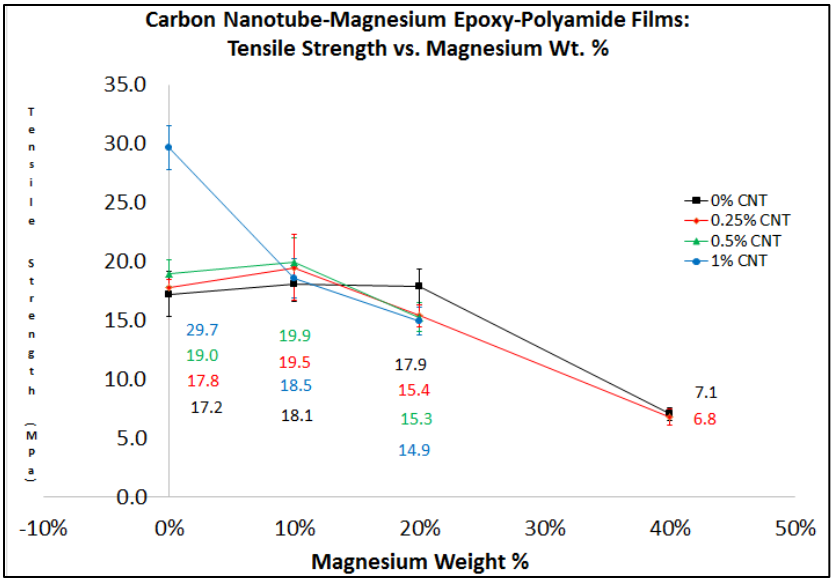

Figure 6.5: Tensile Strength vs. Magnesium Wt. %

The tensile strength decreases with the addition of magnesium. The maximum tensile strength of 29.7 MPa is found at 1% CNT and 0% magnesium. At 0% magnesium, the addition of CNTs results in a modest increase in the tensile strength until 1% CNT. The benefit of CNTs in epoxies are mitigated or erased when magnesium is added. The tensile strengths of the formulations mostly remain between 15 and 20 MPa until 40% magnesium, where it is reduced to approximately 7 MPa. The increase in the tensile strength with the addition of carbon nanotubes is in accordance with past literature and is due to the dispersion, alignment, and robust mechanical properties of the nanotubes.[105] The reduction of the tensile strength with magnesium is in alignment with the fracture property results, indicating that the tandem use of carbon nanotubes and magnesium increases the PVC beyond the CPVC. Even at low levels, the magnesium does not enhance the tensile strength, indicating that magnesium does not have the

intrinsic mechanical properties and the geometries to improve the tensile strength of epoxide materials.[1]

The tensile strength as a function of the CNT weight % is plotted in Figure 6.6.

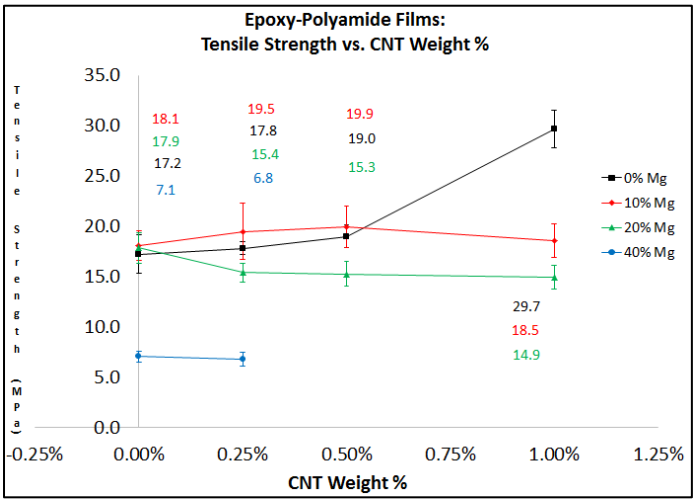

Figure 6.6: Tensile Strength vs. Carbon Nanotube Wt. %

The addition of CNTs at 0% Mg results in a modest increase in the tensile strength until 1% CNT, where the tensile strength increases by 10 MPa. At 10% magnesium, there is no significant change in the tensile strength with the addition of CNTs. At 20% magnesium, there is a slight reduction in the tensile strength when CNTs are added but upon further addition of CNTs the tensile strengths remain constant. At 40% magnesium, the tensile strengths remain constant with the addition of CNTs, but they are significantly lower than zero or smaller magnesium loading.

The tensile strength 2-sample T results for the films with 0% CNT are shown in Table 6.20. The only formulation that shows a significant difference from the control formulation (#1, 0% Mg and 0% CNT) is the formulation with 40% Mg.

Table 6.20: 0% CNT Formulations Tensile Strength 2-Sample T P-Value Results

Name	Mg %	2-Sample T P-Value from Control	Significant?
13	10%	0.735	No
2	20%	0.804	No
3	40%	0.002	Yes

The tensile strength 2-sample T results for the films with 0.25% CNT are shown in Table 6.21. The only formulation that shows a significant difference from the control formulation (#4, 0.25% CNT and 0% Mg) is the formulation with 40% Mg.

Table 6.21: 0.25% CNT Formulations Tensile Strength 2 Sample T P-Value Results

Formulation	Mg %	2-Sample T P-Value from Control	Significant?
14	10%	0.588	No
5	20%	0.057	No
6	40%	0.000	Yes

The tensile strength 2-sample T results for the films with 0.5% CNT are shown in Table 6.22. The control formulation is #7, which is 0% Mg and 0.5% CNT. The only formulation that shows a significant difference from the control formulation is Formulation #8, which is 0.5% CNT and 20% Mg.

Table 6.22: 0.5% CNT Formulations Tensile Strength 2 Sample T P-Value Results

Formulation	Mg %	2-Sample T P-Value from Control	Significant?
15	10%	0.699	No
8	20%	0.046	Yes

The tensile strength 2-sample T results for the films with 1% CNT are shown in Table 6.23. The control formulation is #10, which is 1% CNT and 0% Mg. Both sample formulations significantly differ from the control formulation.

Table 6.23: 1% CNT Formulations Tensile Strength 2 Sample T P-Value Results

Formulation	Mg %	2-Sample T P-Value from Control	Significant?
16	10%	0.001	Yes
11	20%	0.000	Yes

The elongation % as a function of the magnesium content is plotted in Figure 6.7.

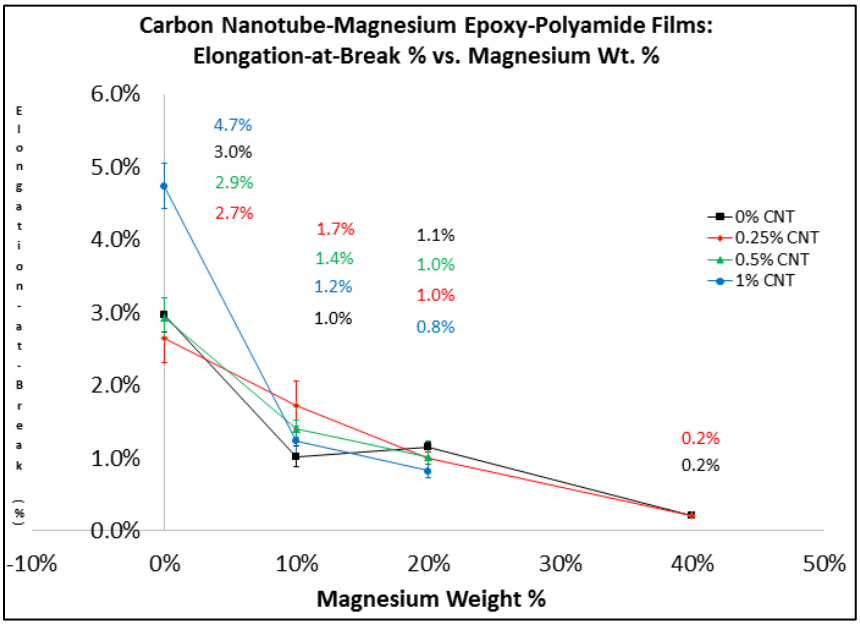

Figure 6.7: Elongation-at-Break % vs. Magnesium Wt. %

The addition of magnesium results in a reduction in the elongation-at-break %. The greatest elongation-at-break is observed at 1% CNT and 0% Mg. At 0% Mg, the addition of CNTs results in a modest increase in the elongation-at-break until 1% CNT, where the elongation-at-break increases from 3% to 4.7%. With the addition of

magnesium, the presence of CNT content does not provide any benefit in terms of extending the elongation-at-break.

The elongation-at-break as a function of CNT content is shown in Figure 6.8.

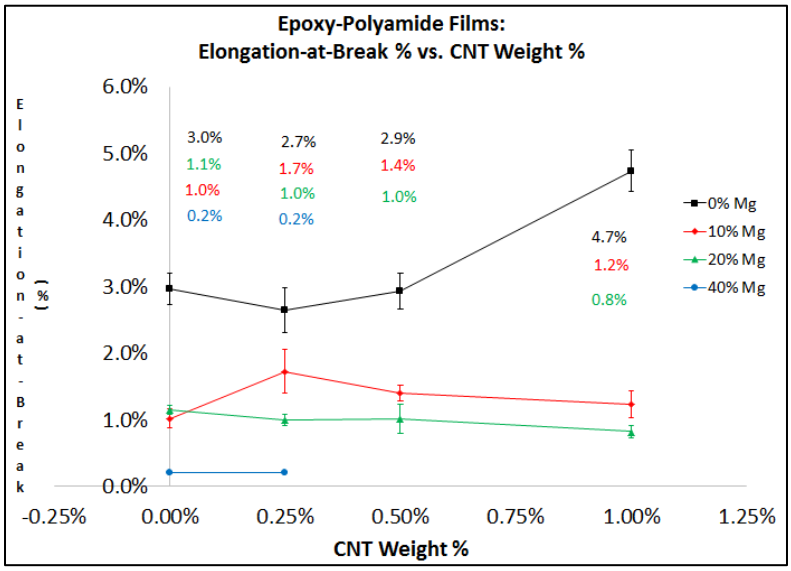

Figure 6.8: Elongation-at-Break % vs. Carbon Nanotube Wt. %

At 0% Mg content, the addition of CNTs provides no enhancement to the elongation-at-break until 1% CNT. At 10% Mg content, there is a slight increase in the elongation-at-break, but further addition of CNTs does not provide any further enhancement in the elongation-at-break. The same phenomenon is exhibited at 20% and 40% Mg content. The addition of magnesium results in a reduction in the elongation-at-break due to geometries that reduce the elongation capabilities of the epoxide matrix.

The elongation at break 2-sample T results for the films with 0% CNT are shown in Table 6.24. The control formulation is #1, which is 0% CNT and 0% Mg. All three formulations are significantly different from the control formulation.

Table 6.24: 0% CNT Formulations Elongation at Break 2 Sample T P-Value Results

Name	Mg %	2-Sample T P-Value from Control	Significant?
13	10%	0.000	Yes
2	20%	0.000	Yes
3	40%	0.000	Yes

The elongation at break 2-sample T results for the films with 0.25% CNT are shown in Table 6.25. The control formulation is #4, which is 0.25% CNT and 0% Mg. The 20% and 40% Mg formulations are significantly different from the control formulation.

Table 6.25: 0.25% CNT Formulations Elongation at Break 2 Sample T P-Value Results

Formulation	Mg %	2-Sample T P-Value from Control	Significant?
14	10%	0.078	No
5	20%	0.006	Yes
6	40%	0.002	Yes

The elongation at break 2-sample T results for the films with 0.5% CNT are shown in Table 6.26. The control formulation is #7, which is 0.5% CNT and 0% Mg. Both sample formulations differ significantly from the control formulation.

Table 6.26: 0.5% CNT Formulations Elongation at Break 2 Sample T P-Value Results

Formulation	Mg %	2-Sample T P-Value from Control	Significant?
15	10%	0.003	Yes
8	20%	0.000	Yes

The elongation at break 2-sample T results for the films with 1% CNT are shown in Table 6.27. The control formulation is #10, which is 1% CNT and 0% Mg. Both sample formulations differ significantly from the control formulation.

Table 6.27: 1% CNT Formulations Elongation at Break 2 Sample T P-Value Results

Formulation	Mg %	2-Sample T P-Value from Control	Significant?
16	10%	0.000	Yes
11	20%	0.000	Yes

6.3.3 EIS Results: Nyquist Plots

Various Nyquist plots were made based upon the results from EIS. One sample from each formulation was tested, and the results at Day 40 are shown in the following section.

The Nyquist plots for the formulations with 0% Mg are shown in Figure 6.9. –Z" is plotted versus Z'. All formulations show sufficient barrier properties against corrosion.[204] There is no significant distinction between the carbon nanotube loading and the corrosion resistance.

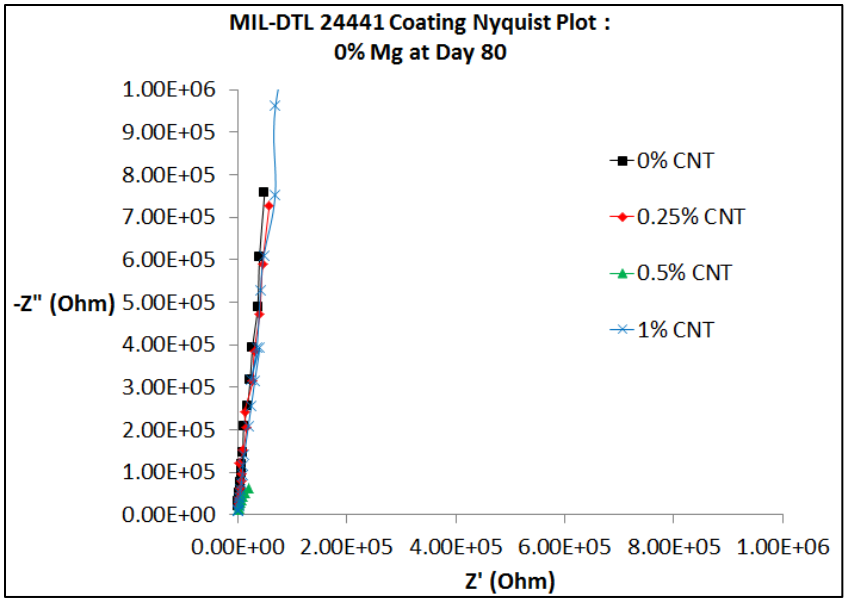

Figure 6.9: Nyquist Plots, 0% Mg, Day 80 of Immersion

The Nyquist plots for the formulations with 10% Mg are shown in Figure 6.10. There is a slight reduction in the corrosion resistance, most likely due to porosity issues created by adding additive content. All formulations, however, show sufficient coating protection at Day 40. The addition of greater amounts of CNTs (0.5% and 1%) show more enhanced properties against corrosion.[208]

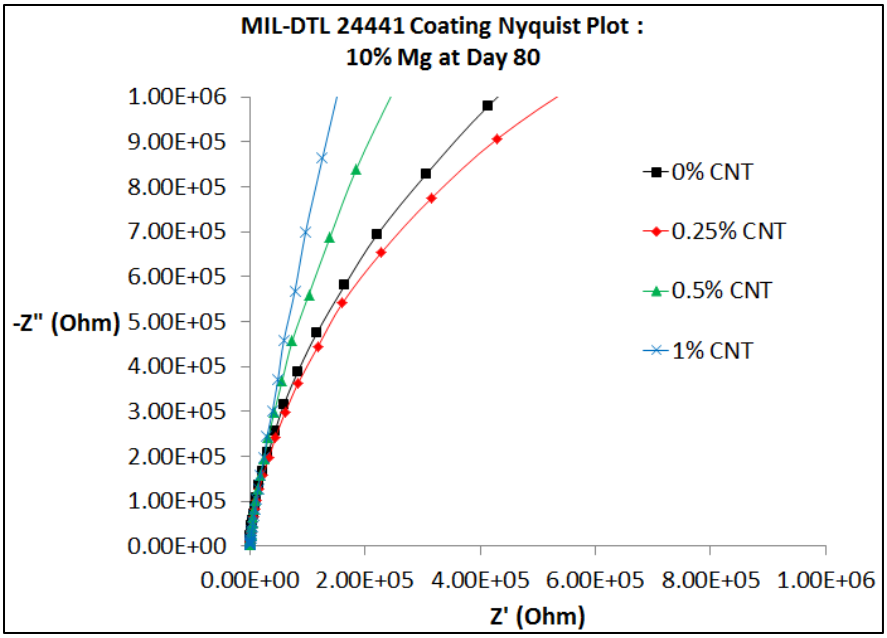

Figure 6.10: Nyquist Plots, 10% Mg, Day 80 of Immersion

The Nyquist plots for coatings systems with 20% magnesium content at Day 80 of immersion are shown in Figure 6.11. All four formulations show proper corrosion protection at Day 80. The formulations with 0% and 0.25 wt. % CNT showed approximately the same corrosion resistance, while 0.5 wt. % CNT showed an elevated corrosion resistance. The carbon nanotubes contribute to enhanced barrier properties against corrosion. 0.55 wt. % CNT shows the greatest corrosion resistance, while 1 wt. % CNT shows a reduction from 0.5 wt. % CNT. This might be due to added porosity from the pigment volume concentration exceeding the CPVC.[1]

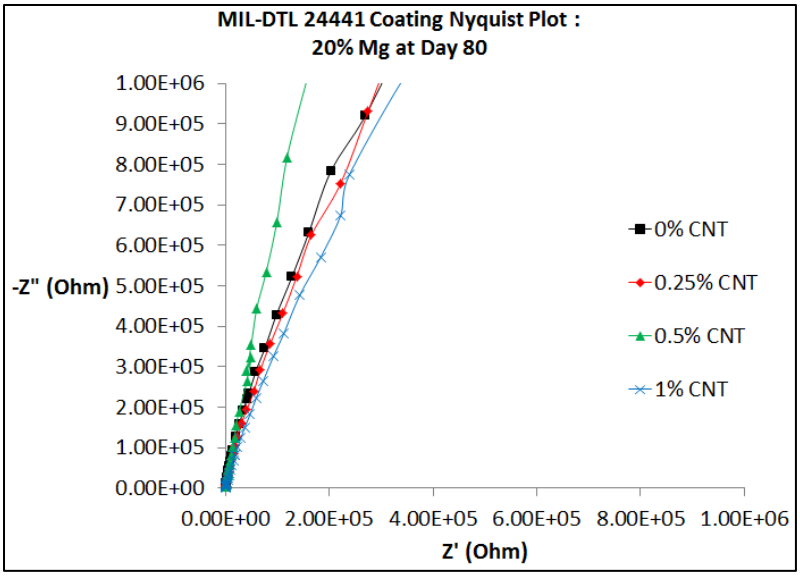

Figure 6.11: Nyquist Plots, 20% Mg, Day 80 of Immersion

The Nyquist plots of coating systems with 40% magnesium content at Day 80 are shown in Figure 6.12. Both stages appear to be undergoing coating failure.[208] This might be due to the fact that 40% magnesium is above the CPVC of the coating system.[1]

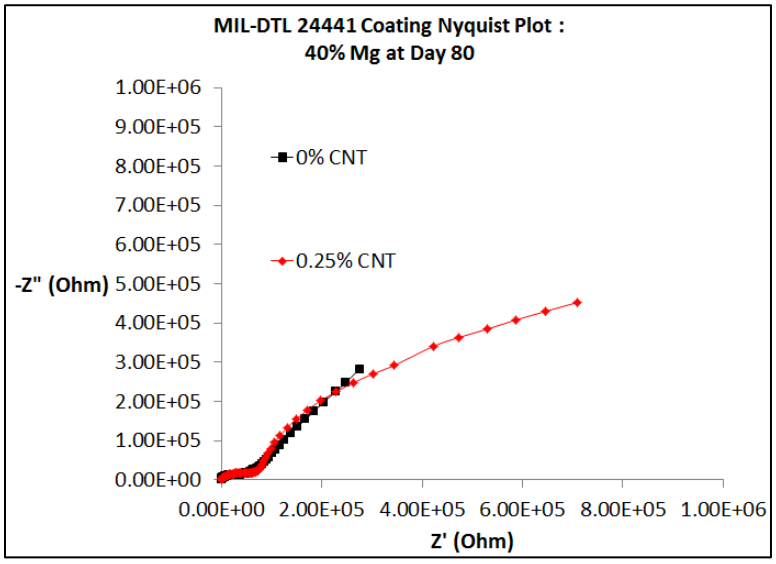

Figure 6.12: Nyquist Plots, 40% Mg, Day 80 of Immersion

The primer coating systems were also viewed in terms of the barrier properties as a function of the magnesium content. The Nyquist plots for coating systems loaded with 0% CNT content and immersed for 80 days are shown in Figure 6.13. The porosity created by the magnesium content shows diminished barrier properties with the addition of magnesium although all coating systems (with the exception of 40% Mg) shows sufficient barrier properties after immersion for 80 days.[208] This may be due to the fact that the addition of magnesium may lead to an excess of the pigment volume concentration beyond the CPVC. 40% magnesium loading indicates coating failure (dome shape).[208]

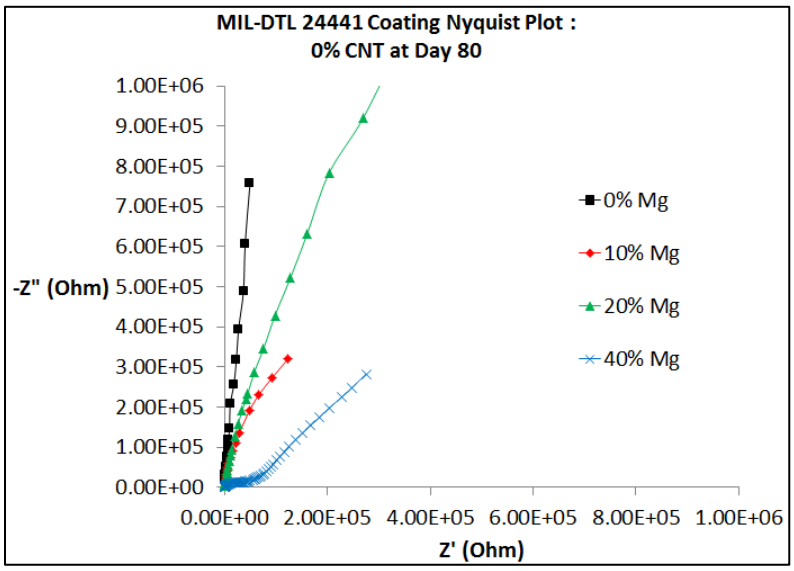

Figure 6.13: Nyquist Plots, 0% CNT, Day 80 of Immersion

The Nyquist plots for coating systems loaded with 0.25% CNT content and immersed for 80 days are shown in Figure 6.14. The indication is that the addition of 10 wt. % led to porosity issues possibly due to exceeding the critical pigment volume concentration, which is why higher levels of magnesium content are associated with

weaker levels of barrier protection. 0-20% magnesium content indicates a coating that can provide sufficient corrosion protection, which 40 wt. % magnesium shows coating failure.[208]

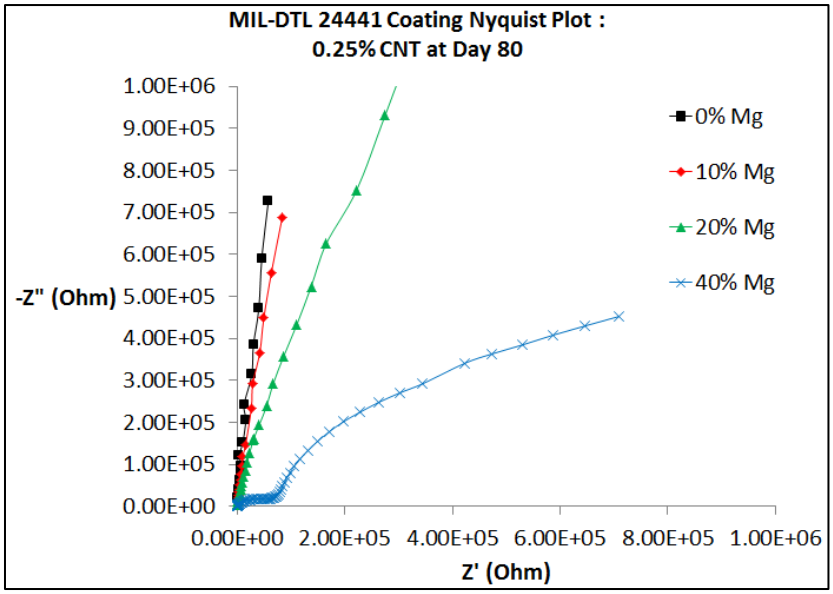

Figure 6.14: Nyquist Plots, 0.25% CNT, Day 80 of Immersion

The Nyquist plots for coating systems loaded with 0.5% CNT content and immersed for 80 days are shown in Figure 6.15. All three coatings show proper resistance to corrosion after 80 days of immersion.[208]

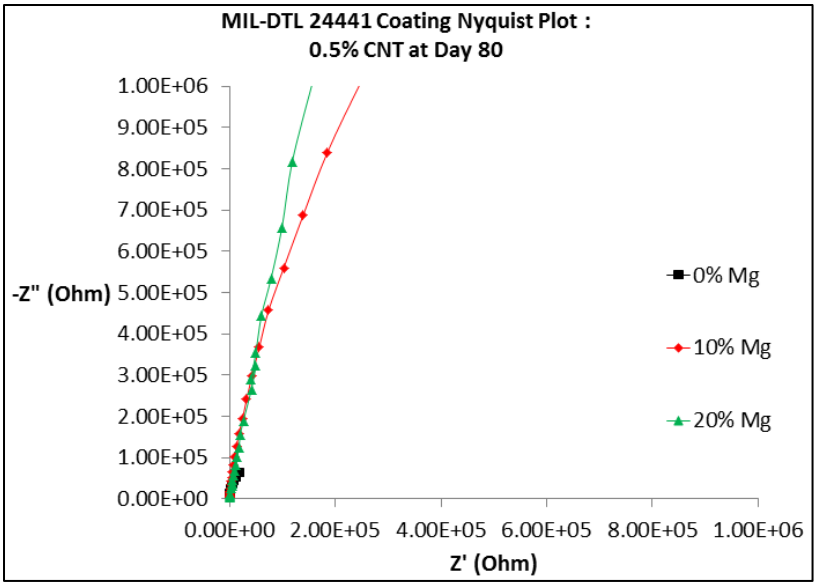

Figure 6.15: Nyquist Plots, 0.5% CNT, Day 80 of Immersion

The Nyquist plots for coating systems loaded with 1.0% CNT content and immersed for 80 days are shown in Figure 6.16. All three formulations show proper resistance to corrosion after 80 days of immersion. The 20% magnesium shows the least resistance, most likely due to the higher porosity of the coatings.

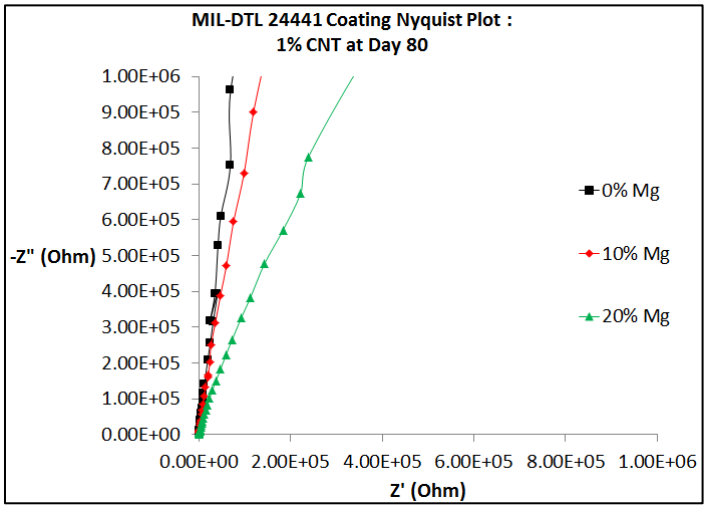

Figure 6.16: Nyquist Plots, 1% CNT, Day 80 of Immersion

The addition of carbon nanotubes creates higher levels of corrosion resistance, either from cathodic protection or providing barrier properties in terms of creating a tortuous pathway that are difficult for the salt water to breach. Much of the diminished corrosion resistance from the presence of magnesium may be due to porosity issues from exceeding the critical pigment volume concentration (CPVC).

6.3.4 Bode Plots of CNT-Mg Loaded Coating Systems

Bode plots were constructed while testing the same conditions as the Nyquist plots. The Bode plots of coating formulations with 0% Mg and at Day 80 of immersion are plotted in Figure 6.17.

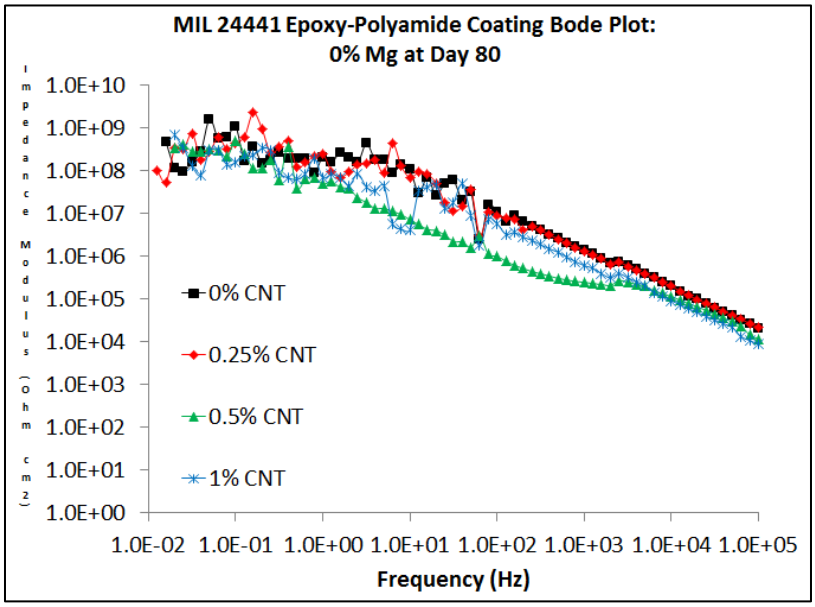

Figure 6.17: Bode Plots, 0% Mg, Day 80 of Immersion

0%, 0.25% and 1% CNT are showing corrosion resistance, while 0.5% CNT indicates some level of corrosion. It is not known why 0.5% wt. CNT is an anomaly.

The Bode plots of coating formulations with 10% Mg and at Day 80 of immersion are plotted in Figure 6.18. 0%, 0.25%, and 0.5% wt. CNT, although indicating low levels of pore resistance (non-linear between impedance modulus and electrical frequency), show higher levels of corrosion resistance than 0% CNT, which shows evidence of a corroding substrate.[208]

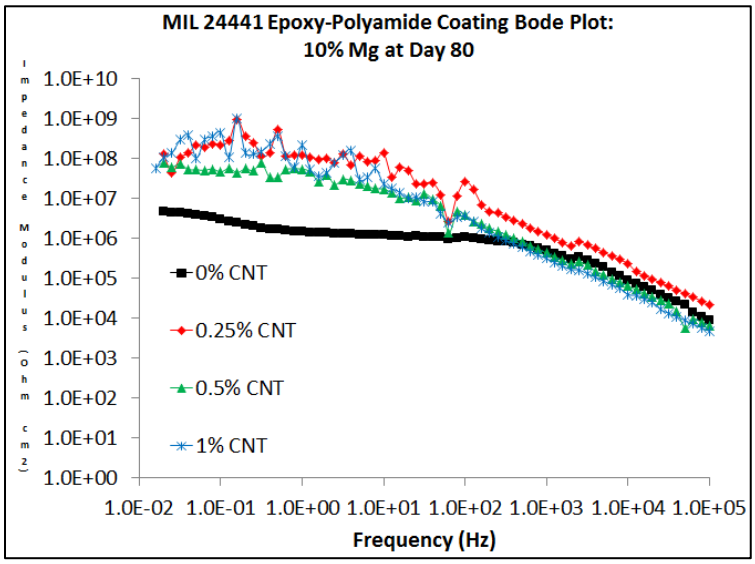

Figure 6.18: Bode Plots, 10% Mg, Day 80 of Immersion

The Bode plots of coating formulations with 20% Mg and at Day 80 of immersion are plotted in Figure 6.19. The plots for 0% CNT and 0.25% CNT indicate a corroding metal substrate, while 0.5% CNT shows a low pore resistance. 1% CNT has the highest corrosion resistance as indicated by the relatively linear shape of the curve versus the frequency.[204]

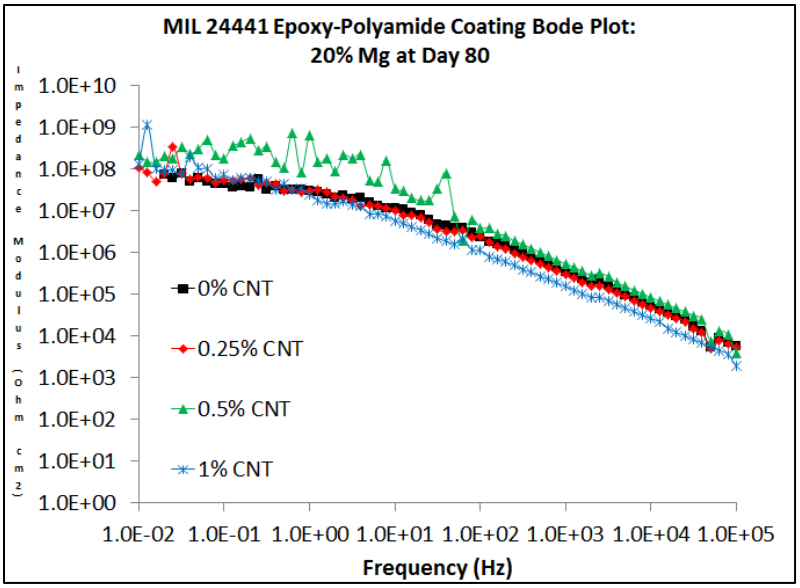

Figure 6.19: Bode Plots, 20% Mg, Day 80 of Immersion

The Bode plots of coating formulations with 40% Mg and at Day 80 of immersion are plotted in Figure 6.20. Both curves show evidence of a corroding metal substrate, which has been produced as a result of the porosity of the coating system.

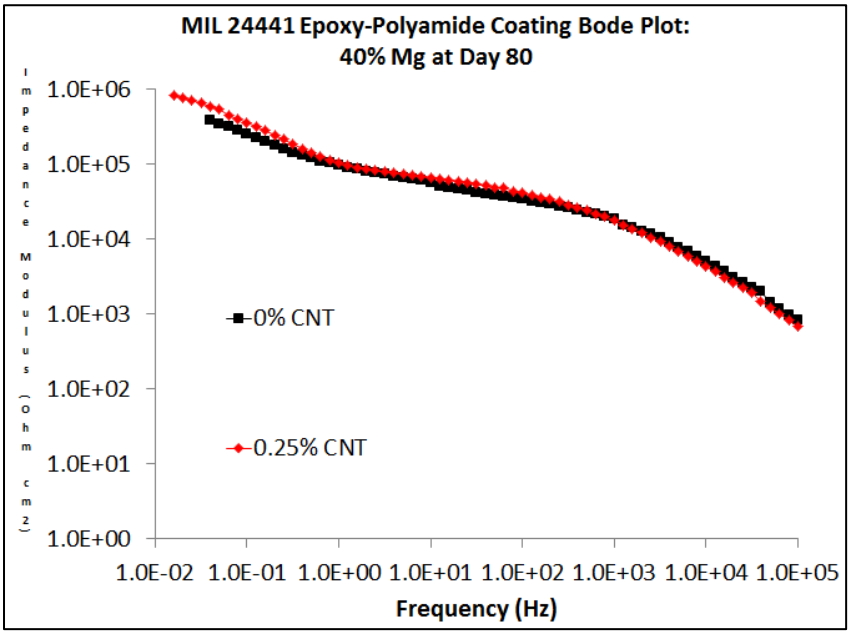

Figure 6.20: Bode Plots, 40% Mg, Day 80 of Immersion

To correlate the corrosion resistance or barrier properties of the CNT-Mg coating systems, the Bode plots also compared differing amounts of magnesium. The Bode plots of coating formulations with 0% CNT and at Day 80 of immersion are plotted in Figure 6.21.

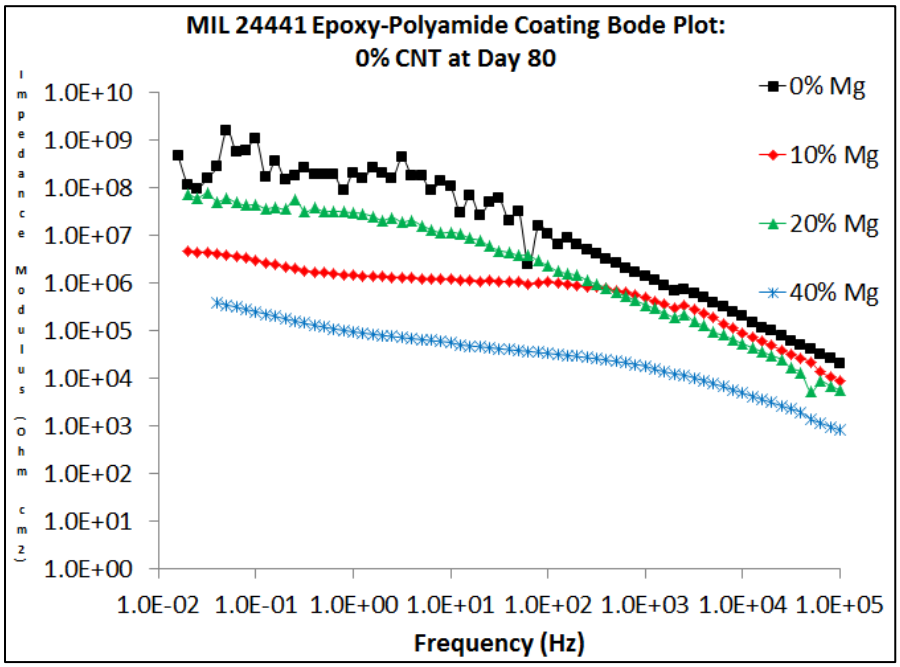

Figure 6.21: Bode Plots, 0% CNT, Day 30 of Immersion

The 20% and 40% magnesium plots show evidence of metal corrosion, while the 0% and 10% Mg plots shows low pore resistance, although no evidence of metal corrosion is noted.[208] 0% display better barrier properties due to lower levels of porosity.

The Bode plots of coating formulations with 0.25% CNT and at Day 40 of immersion are plotted in Figure 6.22. 40% magnesium shows metal corrosion, while 0%, 10%, and 20% magnesium indicates some resistance to the corrosion. The increased

barrier properties provided by the presence of CNTs as well as the cathodic protection of the higher levels of magnesium are contributing to the corrosion resistance.[11] 0% and lower levels of magnesium contribute to better corrosion protection.

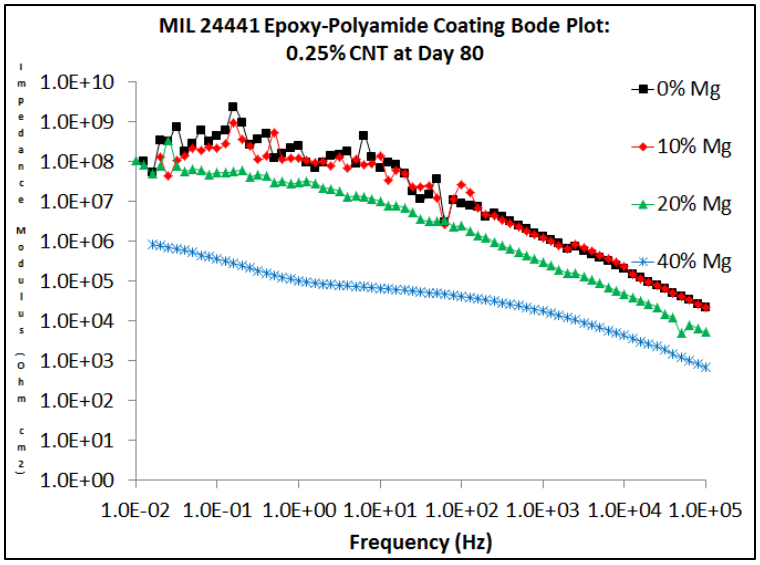

Figure 6.22: Bode Plots, 0.25% CNT, Day 80 of Immersion

The Bode plots of coating formulations with 0.5% CNT and at Day 80 of immersion are plotted in Figure 6.23. All formulations show evidence of metal corrosion.[204]

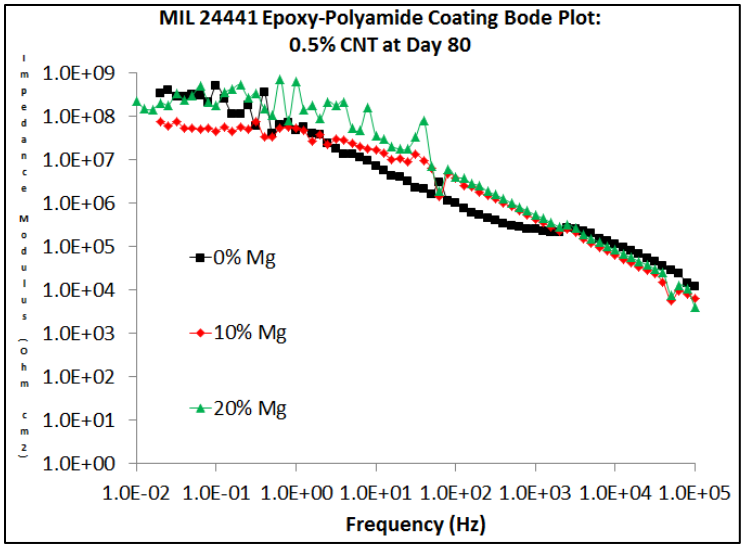

Figure 6.23: Bode Plots, 0.5% CNT, Day 80 of Immersion

The Bode plots of coating formulations with 1% CNT and at Day 40 of immersion are plotted in Figure 6.24. 0%, 10% and 20% Mg show corrosion resistance albeit with low pore resistance.[208]

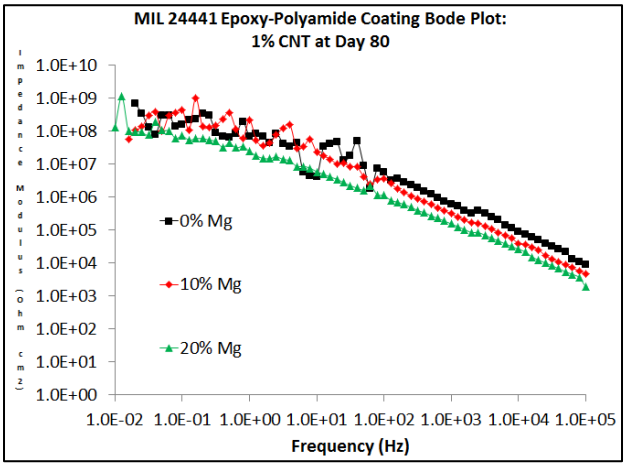

Figure 6.24: Bode Plots, 1% CNT, Day 40 of Immersion

6.4 Discussion

The addition of CNTs have aided in the mechanical and corrosion properties of MIL-DTL-24441 coating systems. Carbon nanotubes have a more positive effect against corrosion in the presence of magnesium. This is due to the cathodic protection that helps to provide as well as its enhancement to the barrier properties of the coating system.[11] Additions of 20% or 40% magnesium led to a reduction in the corrosion resistance, which was due to the increased porosity of the coating system due to the addition of magnesium. A potential limitation of this study was the fact that CNTs and Mg were added to existing military specification formulations instead of constructing coating systems with only CNT and Mg content as additives. The limited corrosion resistance associated with the augmented amounts of Mg (greater than or equal to 20%) is due to porosity created by overloading the coating system, also known as exceeding the critical pigment volume concentration (CPVC). Future work will include re-formulating the coatings with respect to measuring the CPVC.[1]

The shortcoming of the experiment with the carbon nanotubes and magnesium loading into epoxide coatings was the formulation setup. Military specification coating systems have been specifically formulated at levels close to the critical pigment volume concentration to maximize coating properties. The loading of the carbon nanotubes and magnesium into a military specification coatings increases the pigment volume concentration beyond the critical pigment volume concentration. The issue that arises is that the mechanical properties decrease and porosity increases when a coating is loaded beyond the critical pigment volume concentration. Future work on the subject

should involve formulating a coating system with only the base epoxy, curing agents, the carbon nanotubes and magnesium only, and a sufficient amount of solvent to properly disperse the pigments. In other words, the same formulations that were used to measure the fracture and tensile properties should also be used for corrosion resistance measurements. The fracture and tensile property results are notable in that they show a collective increase with the amount of carbon nanotubes added, indicating that the mechanical robustness of the carbon nanotubes will enhance the mechanical properties of the epoxide composite/coating. This also indicates that the loading of the carbon nanotubes is below the critical pigment volume concentration of the coating/composite, meaning that the porosity of the coating is not adversely affected by the presence of the carbon nanotubes. Conversely, the reduction or minimal change in the mechanical properties with the presence of both magnesium and carbon nanotubes may be occurring for two reasons: magnesium is a pigment that either diminishes the mechanical properties or provides no property enhancements. In addition, it may be due to the presence of both carbon nanotubes and magnesium in neat epoxide systems, which results in the pigment volume concentration exceeding the critical pigment volume concentration. The missing link in these results are microscopy pictures that provide a pictorial measure of the porosity of the coatings systems.

The addition of carbon nanotubes also aided the epoxide polyamide films due to their robust mechanical properties and their relative degree of compatibility with the epoxide matrix. The addition of magnesium, however, due to its lack of compatibility with the epoxide matrix as well as lack of flexibility and limiting geometries, result in a

reduction in the mechanical properties in the absence of carbon nanotubes and limit the enhancement in the mechanical properties that carbon nanotubes provide. In the absence of magnesium, the best mechanical properties (fracture parameters, tensile strength, and elongation-at-break) are achieved at 1% CNT. At this point improvement in the mechanical properties with both magnesium and carbon nanotubes is not possible, at least with non-functionalized carbon nanotubes.

6.5 Conclusions

Carbon nanotubes and magnesium content were added into MIL-DTL-24441 epoxide-polyamide coating formulations and epoxide-polyamide films in weight percentages of 0%, 0.25%, 0.5%, and 1% for carbon nanotubes and 0%, 10%, 20%, and 40% for magnesium. In the absence of magnesium content, the addition of carbon nanotubes led to enhancements in the mechanical and fracture properties of the epoxide-polyamide films due to their robust mechanical properties. These enhancements were marginalized when magnesium was added. The addition of carbon nanotubes to coating systems also led to enhancements in the corrosion resistance of the coatings system due to the cathodic protection provided as well as enhancements to the barrier properties. The corrosion resistance was mitigated with the addition of magnesium content. This was due to the added porosity created with the addition of the magnesium content.

CHAPTER VII

CONCLUSIONS AND FUTURE WORK

The subject of this dissertation pertained to the enhancement of epoxide materials and coatings through the addition of polysulfides, functional silica-based materials, carbon nanotubes, and magnesium. Chapter III pertained to the bonding of two different polysulfide oligomers to DGEBA to create epoxide-polysulfide resins, Chapters IV and V pertained to the use of functional sol-gels in epoxide-polyamide films and coatings, and Chapter 6 pertained to the use of magnesium and carbon nanotubes as anti-corrosion additives in epoxide-polyamide coatings.

Epoxide-polysulfides are useful sealant resins that arise from the flexibility of the materials. While epoxide-polysulfides have been thoroughly researched in literature, an overarching study investigating the coating and fracture properties at different temperatures has not been attempted. Investigating the fracture toughness (i.e. damage tolerance) properties at various temperatures would be relevant given the use of epoxide-polysulfide as outdoor sealant materials on metal substrates. The resins were crosslinked with a polyamide to form solid films and coatings. The addition of 5-10% wt. polysulfide resulted in a tougher, more flexible film/coating with greater elastic and storage moduli, glass transition temperatures, tensile properties, fracture properties at low and ambient temperatures, adhesive properties, and corrosion

resistance. This was attributed to longer aliphatic chains occurring without a concurrent reduction in the crosslink density. This produced the unusual effect of a more flexible and tougher coating/film. Higher additions (15-20% wt.) of polysulfide resulted in a more malleable film with reduced toughness due to the reduction in crosslink density and the presence of larger isolated polysulfide domains within the epoxide-polysulfide matrix. The results indicated that the addition of 5-10% wt. polysulfide resulted in a resin with greater damage tolerance and enhanced coating properties, making it ideal as an outdoor sealant on metal substrates, particularly substrates with uneven geometries.

Chapter IV pertained to the use of Self-Assembled Nanophase (SNAP) sol-gel particles in epoxide-polyamide films and coatings. While SNAP sol-gel particles have been investigated as surface preparations for aluminum substrates, these sol-gels have not been investigated as functional additives within epoxide films and coatings. The use of SNAP particles to enhance the mechanical properties and corrosion resistance is a novel use of such materials and an improvement over earlier researchers (who strictly sought to use it as an environmentally benign surface preparation to prevent corrosion). SNAP particles were formulated in non-aqueous and aqueous solutions and characterized via NMR and ESI-MS. SNAP particles formulated in non-aqueous solutions indicated the difficulty of grafting organo silanes and inorganic precursors in non-aqueous mediums. The particles were analyzed for size via DLS and TEM, indicating that the particles were approximately 100 nm in diameter. Evidence of SNAP particles on the surface of SNAP-loaded epoxide films was ascertained through the use of SEM. Later, the particles were added into epoxide-polyamide coatings and films and found to

enhance the crosslink density, T_G, tensile properties, fracture properties, adhesion strength, abrasion resistance and corrosion resistance via EIS, indicating that SNAP-loaded epoxide coatings have greater damage and barrier properties than neat epoxide systems. The enhancements to the mechanical properties and corrosion resistance were attributed to the enhanced crosslink densities, siloxane bonding, and good dispersion provided by the SNAP particles. The fact that SNAP can form continuous systems with MIL-DTL-24441 epoxide coatings indicates that there are potential industrial uses for such applications. A separate study (Chapter V) showed that loading the same film and coating formulations with APTES-TMOS sol-gels can also enhance the physical properties and corrosion resistance.

While magnesium and carbon nanotubes have been explored as anti-corrosive additives in epoxide coating systems, the tandem use of magnesium and carbon nanotube has not been investigated. Epoxide-polyamide films and coatings were investigated for tensile and fracture properties as well as the corrosion resistance. Without magnesium, the addition of carbon nanotubes led to improvements in the tensile and fracture properties of the epoxide-polyamide films. These enhancements were minimalized when magnesium was added. The addition of carbon nanotubes to coating systems also led to improvements in the corrosion resistance of the coatings system due to the cathodic protection provided as well as improvements to the barrier properties. The corrosion resistance was mitigated with the addition of magnesium content. This was due to the added porosity created with the addition of the

magnesium content, indicating that the tandem use of the two pigments exceeded the CPVC of the epoxide coating.

This dissertation also allows for the opportunity for future projects and work opportunities. Future work on polysulfides will include the same testing of epoxide-polysulfides with different type of crosslinkers. Future work on SNAP sol-gels and amine-functional sol-gels will include the synthesis of the sol-gels in water and incorporation into waterborne epoxide coating systems and testing for the physical properties and corrosion resistance. Future work on carbon nanotubes and magnesium in epoxide coating systems will include reformulating the coatings at points below and at the CPVC.

REFERENCES

1. Wicks, Z., Jr., Jones, R., Pappas, S., and Wicks, D. *Organic Coatings Science and Technology: Third Edition*. John Wiley and Sons, Inc., Hoboken, New Jersey, 2007.
2. Zhang, H., Zhang, Z., Friedrich, K., and Eger, C. Property Improvements of In Situ Epoxide Nanocomposites with Reduced Interparticle Distance at High Nanosilica Content. *Acta Materialia* **2006**, 54, 1833-1842.
3. Nikolic, G., Zlatkovic, S., Cakic, M., Lacnjevac, C., and Rajic, Z. Fast Fourier Transform IR Characterization of Epoxide GY Systems Crosslinked with Aliphatic and Cycloaliphatic EH Polyamine Adducts. *Sensors* **2010**, 10, 684-696.
4. Spicer, M. Flexible Primer Problem Statement.
5. Arundati, Singhal, R., and Nagpal, A. Effect of Polysulfide Modifier on Mechanical and Morphological Properties of Epoxide/Phthalic Anhydride System. *Int J Plast Technol* **2010**, 13, 193-204.
6. Farajpour, T., Bayat, Y., Keshavarz, M., and Zanjirian, E. Viscoelastic and Thermal Properties of Polysulfide Modified Epoxide Resin: the Effect of Modifier Molecular Weight. *Materialwissenschaft und Werkstofftechnik* **2013**, 44, 991-996.

7. Olsson, R., Hedenqvist, M., Strom, V., Deng, J., Savage, S., and Gedde, U. Core-Shell Structure Ferrite-Silsesquioxane-Epoxide Nanocomposites: Composite Homogeneity and Mechanical and Magnetic Properties. *Polymer Engineering and Science* **2011**, 862-874.
8. Vreugdenhil, A., Balbyshev, V., and Donley, M. Nanostructured Silicon Sol-Gel Surface Treatments for Al 2024-T3 Protection. *Journal of Coatings Technology* **2001**, 73, 35-43.
9. Verbiest, P. Using Zinc Dust Primers for Corrosion Protection. *JPCL* **2013**, 34-43.
10. Nanna, M. and Bierwagen, G. Mg-Rich Coatings: A New Paradigm for Cr-Free Corrosion Protection of Al Aerospace Alloys. *JCT Research* **2004**, 1, 69-80.
11. Cubides, Y. and Castaneda, H. Corrosion Protection Mechanisms of Carbon Nanotube and Zinc-Rich Epoxide Primers on Carbon Steel in Simulated Concrete Pore Solutions in the Presence of Chloride Ions. *Corrosion Science* **2016**, 109, 145-161.
12. Ya, M. and Pyrz., R. Reinforcement Role of Carbon Nanotubes, Part I: High-Performance Epoxide Resin. *Polymer Composites* **2015**, 2212-2219.
13. Shen, W., Feng, L., Liu, X., Luo, H., Liu, Z., Tong, P., and Zhang, W. Multiwall Carbon Nanotube-Reinforced Epoxide Hybrid Coatings with High Electrical Conductivity and Corrosion Resistance Prepared via Electrostatic Spraying. *Progress in Organic Coatings* **2016**, 90, 139-146.

14. Ellis, B. Introduction to the Chemistry, Synthesis, Manufacture, and Characterization of Epoxide Resins. In *Chemistry and Technology of Epoxide Resins*. Ellis, B., Ed. Springer Science, Dordrecht, the Netherlands, 1993.
15. Petrie, E. Epoxide Resin Chemistry. In *Epoxide Adhesive Formulations*. Petrie, E., Ed. McGraw Hill Professional, 2005.
16. Tess, R. Epoxide Resin Coatings. In *Epoxide Resins: Chemistry and Technology, Second Edition*. May, C., Ed. Marcel Dekker, Inc., New York, NY, 1988.
17. Hentges, S. About BPA: Epoxide Resins. American Chemistry Council, April 2013.
18. Evaluation of Alternatives for Compounds under Risk Assessment in the EU, Bisphenol A. Environmental Project 901, 2004. Accessed 18 Sep 2016. http://www2.mst.dk.
19. Hara, O. Curing Agents for Epoxide Resin. Three Bond Technical News, 20 Dec 1990. Tokyo, Japan.
20. Pascault, J. and Williams, R. General Concepts about Epoxide Polymers. In *Epoxide Polymers: New Materials and Innovations*. Pascault, J. and Williams, J., Eds. Wiley-VCH, Weinheim, Germany, 2010.
21. Polysulfides. *Encyclopedia of Polymer Science and Technology: 3rd Edition*. John Wiley and Sons, 2004.
22. Fettes, E. and Jorczak, J. Polysulfide Polymers. *Industrial and Engineering Chemistry* **1950**, 2217-2223.
23. Lowe, G. The Cure Chemistry of Polysulfides. *International Journal of Adhesion and Adhesives* **1997**, 17, 345-348.

24. Wilford, A., Lee, T., and Kemp, T. Phase Separation of Polysulphide Polymers in Epoxide Adhesives. *International Journal of Adhesion and Adhesives* **1992**, 12, 171-177.

25. Cranker, K. and Breslau, A. Epoxide Casting Resins Modified with Polysulfide Liquid Polymer. *Industrial and Engineering Chemistry* **1956**, 48, 98-103.

26. Abdouss, M. The Effect of Epoxide-Polysulfide Copolymer Curing Methods on Mechanical-Dynamical and Morphological Properties. *Iran. J. Chem. Chem. Eng.* **2011**, 30, 37-44.

27. Abdouss, M., Farajpour, T., and Derakhshani, M. Investigating of Polysulfide and Epoxide-Polysulfide Copolymer Curing. *Mat.-wiss. u. Werkstofftech.* **2010**, 41, 884-888.

28. Zhang, G., Fan, K., Quan, Y., and Chen, Q. The Preparation and Physical Properties of Polysulfide-Based Elastomers Through One-Pot Thiol-Ene Click Reaction. *eXPRESS Polymer Letters* **2013**, 7, 577-584.

29. Kemp, T., Wilford, A., and Howarth, O. Structural and Materials Properties of a Polysulphide-Modified Epoxide Resin. *Polymer* **1992**, 33, 1860-1871.

30. Wilford, A., Lee, T., and Kemp, T. Phase Separation of Polysulphide Polymers in Epoxide Adhesives. *International Journal of Adhesion and Adhesives* **1992**, 12, 171-177.

31. Wu, K., Cheng, K., Yang, C., Wang, C., and Liu, C. Thermal and Optical Properties of Epoxide/Siloxane Hybrimer Based on Sol-Gel-Derived Phenyl-Siloxane. *Open Journal of Composite Materials* **2015**, 5, 49-59.

32. Penn, L. and Chiao, T. Epoxide Resins. In *Handbook of Composites*. Lubin, G., Ed. Van Nostrand Reinhold Company, Inc., New York, NY, 1982.
33. Phonthammachai, N., Chia, H., and He, C. One-Step Synthesis of Oval Shaped Silica/Epoxide Nanocomposite: Process, Formation Mechanism, and Properties. *The Delivery of Nanoparticles*. Hashim, A., Ed. InTech.
34. Wetzel, B., Rosso, P., Haupert, F., and Friedrich, K. Epoxide Nanocomposites – Fracture and Toughening Mechanisms. *Engineering Fracture Mechanics* **2006**, 73, 2375-2398.
35. Chen, C., Justice, R., Schaefer, D., and Baur, J. Highly Dispersed Nanosilica-Epoxide Resins with Enhanced Mechanical Properties. *Polymer* **2008**, 49, 3805-3815.
36. Zhang, H., Tang, L., Zhang, Z., Friedrich, K., and Sprenger, S. Fracture Behaviors of In Situ Nanoparticle-Filled Epoxide at Different Temperatures. *Polymer* **2008**, 49, 3816-3825.
37. Johnsen, B., Kinloch, A., Mohammed, R., Taylor, A., and Sprenger, S. Toughening Mechanisms of Nanoparticle-Modified Epoxide Polymers. *Polymer* **2007**, 48, 530-541.
38. Bray, D., Dittanet, P., Guild, F., Kinloch, A., Masania, K., Pearson, R., and Taylor, A. The Modelling of the Toughening of Epoxide Polymers via Silica Nanoparticles: The Effects of Volume Fraction and Particle Size. *Polymer* **2013**, 54, 7022-7032.

39. Rosso, P., Ye, L., Friedrich, K., and Sprenger, S. A Toughened Epoxide Resin by Silica Nanoparticle Reinforcement. *Journal of Applied Polymer Science* **2006**, 100, 1849-1855.

40. Ma., J., Mo, M., Du, X., Rosso, P., Friedrich, K., and Kuan, H. Effect of Inorganic Nanoparticles on Mechanical Property, Fracture Toughness, and Toughening Mechanism of Two Epoxide Systems. *Polymer* **2008**, 3510-3523.

41. Zhang, H., Zhang, Z., Friedrich, K., and Eger, C. Property Improvements of In Situ Epoxide Nanocomposites with Reduced Interparticle Distance at High Nanosilica Content. *Acta Materialia* **2006**, 54, 1833-1842.

42. Preghenella, M., Pegoretti, A., and Migliaresi, C. Thermo-Mechanical Characterization of Fumed Silica-Epoxide Nanocomposites. *Polymer* **2005**, 46, 12065-12072.

43. Cantwell, W., Smith, J., Kausch, H., and Kaiser, T. Examination of the Processes of Deformation and Fracture in a Silica-Filled Epoxide Resin. *Journal of Materials Science* **1990**, 25, 633-648.

44. Spanoudakis, J. and Young, R. Crack Propagation in a Glass Particle-Filled Epoxide Resin Part 1: Effect of Particle Volume Fraction and Size. *Journal of Materials Science* **1984**, 19, 473-486.

45. Kang, S., Hung, S., Choe, C., Park, M., Rim, S., and Kim, J. Preparation and Characterization of Epoxide Composites Filled with Functionalized Nanosilica Particles Obtained Via Sol-Gel Process. *Polymer* **2001**, 42, 879-887.

46. Wang, W., Chen, H., Tsai, S., and Wu, J. Thermal Property of Epoxide/SiO_2 Hybrid Material Synthesized by the Sol-Gel Process. *Journal of Applied Polymer Science* **2004**, 91, 532-537.

47. Macan, J., Ivankovic, H., Ivankovic, M., and Mencer, H. Preparation of Epoxide-Based Organic-Inorganic Hybrids by Sol-Gel Process.

48. Perchacz, M., Benes, H., Zhigunov, A., Serkis, M., and Pavlova, E. Differently-Catalyzed Silica-Based Precursors as Functional Additives for the Epoxide-Based Hybrid Materials. *Polymer* **2016**, 99, 434-446.

49. Oh, S., Chae, W., and Choi, S. Optimal Mixing Ratios of Silica and Hybrid Resin with Epoxide Resin for Concrete Floor Surface Covering. *J. Mater. Civ. Eng.* **2015**, 27, 1-10.

50. Saliba, P., Mansur, A., Santos, D., and Mansur, H. Fusion-Bonded Epoxide Composite Coatings on Chemically Functionalized API Steel Surfaces for Potential Deep-Water Petroleum Exploration. *Applied Adhesion Science* **2015**, 3, 1-22.

51. Cakir, M., Kartal, I., Demirer, H., and Samur, R. Effect of Water Absorption on the Wear Behavior of Sol-Gel Processed Epoxide/Silica Hybrids. *Scientific Research and Essays* **2012**, 7, 805-812.

52. Nikje, M., Khanmohammadi, M., Garmarudi, A., and Hagshenas, M. Nanosilica Reinforced Epoxide Floor Coating Composites: Preparation and Thermophysical Characterization. *Current Chemistry Letters 1* **2012**, 13-20.

53. Bakhshandeh, E., Jannesari, A., Ranjbar, Z., Sobhani, S., and Saeb, M. Anti-Corrosion Hybrid Coatings Based on Epoxide-Silica Nano-Composites: Towards

Relationship Between the Morphology and EIS Data. *Progress in Organic Coatings* **2014**, 77, 1169-1183.

54. Lamaka, S., Montemor, M., Galio, A., Zheludkevich, M., Trindade, C., Dick, L, and Ferreira, M. Novel Hybrid Sol-Gel Coatings for Corrosion Protection of AZ31B Magnesium Alloy. *Electrochimica Acta* **2008**, 53, 4773-4783.
55. Zandi-Zand, R., Ershad-Langroundi, A., and Rahimi, A. Organic-Inorganic Hybrid Coatings for Corrosion Protection of 1050 Aluminum Alloy. *Journal of Non-Crystalline Solids* **2005**, 351, 1307-1311.
56. Tavandashti, N., Sanjabi, S., and Shahrabi, T. Preparation and Characterization of Silica/Epoxide Hybrid Nanocomposite Coatings Containing Boehmite Nanoparticles for Corrosion Protection. *Corrosion Engineering, Science, and Technology* **2011**, 46, 661-666.
57. Tavandashti, N., Sanjabi, S., and Shahrabi, T. Corrosion Protection Evaluation of Silica/Epoxide Hybrid Nanocomposite Coatings to AA2024. *Progress in Organic Coatings* **2009**, 65, 182-186.
58. Chen, Q., Tan, J., Shen, S., Liu, Y., Ng, W., and Zeng, X. Effect of Boehmite Nanorods on the Properties of Glycidoxypropyltrimethoxysilane (GPTS) Hybrid Coatings. *Journal of Sol-Gel Science and Technology* **2007**, 44, 125-131.
59. Voevodin, N., Balbyshev, V., Khobaib, M., and Donley, M. Nanostructured Coatings Approach for Corrosion Protection. *Progress in Organic Coatings* **2003**, 47, 416-423.

60. Khramov, A., Voevodin, N., Balbyshev, V., and Donley, M. Hybrid Organo-Ceramic Corrosion Protection Coatings with Encapsulated Organic Corrosion Inhibitors. *Thin Solid Films* **2004**, 447-448, 549-557.
61. Khramov, A., Voevodin, N., Balbyshev, V. and Mantz, R. Sol-gel-Derived Corrosion-Protective Coatings with Controllable Release of Incorporated Organic Corrosion Inhibitors. *Thin Solid Films* **2005**, 483, 191-196.
62. Voevodin, N., Kurdziel, J., and Mantz., R. Corrosion Protection for Aerospace Aluminum Alloys by Modified Self-Assembled NAnophase Particle (MSNAP) Sol-Gel. *Surface and Coatings Technology* **2006**, 201, 1080-1084.
63. Vreugdenhil, A., Gelling, V., Woods, M., Schmelz, J., and Enderson, B. The Role of Crosslinkers in Epoxide-Amine Crosslinked Silicon Sol-Gel Barrier Protection Coatings. *Thin Solid Films* **2008**, 517, 538-543.
64. Croes, K., Vreugdenhil, A., Yan, M., Singleton, T., Boraas, S., and Gelling, V. An Electrochemical Study of Corrosion Protection by *In Situ* Oxidative Polymerization in Phenylenediamine Crosslinked Sol-Gel Hybrid Coatings. *Electrochimica Acta* **2011**, 56, 7796-7804.
65. Donley, M., Balbyshev, V., and Voevodin, N. Self-Assembled NAnophase Particle (SNAP) Surface Treatments for Corrosion Protection of AA2024-T3. *Progress in Organic Coatings* **2005**, 52, 34-38.
66. Vreugdenhil, A. and Woods, M. Triggered Release of Molecular Additives from Epoxide-Amine Sol-Gel Coatings. *Progress in Organic Coatings* **2005**, 53, 119-125.

67. Zheludkevich, M., Serra, R., Montemor, M., Yasakau, K., Salvado, I., and Ferreira, M. Nanostructured Sol-Gel Coatings Doped with Cerium Nitrate as Pre-Treatments for AA2024-T3 Corrosion Protection Performance. *Electrochemica Acta* **2005**, 51, 208-217.

68. Makote, R., Khobaib, M., Chen, C., and Cussler, E. Synthesis of Self-Assembled Nanophase Particles from Alkoxysilane Solutions.

69. Fu, J., Chen, T., Wang, M., Yang, N., Li, S., Wang, Y., and Liu, X. Acid and Alkaline Dual Stimuli-Responsive Mechanized Hollow Mesoporous Silica Nanoparticles as Smart Nanocontainers for Intelligent Anticorrosion Coatings. *ACS Nano* **2013**, 7, 11397-11408.

70. Scully, A., Mao, Q., and Fell, C. High-Performance Oxygen Barrier Inorganic-Organic Coating for Polymeric Substrates. *Surface and Coatings Technology* **2014**, 239, 222-226.

71. Mao, Q., Fell, C., and Scully, A. Self-Assembled Nano-Phase Particles for Enhanced Oxygen Barrier Coatings on Polymeric Materials. *Progress in Organic Coatings* **2013**, 76, 51-59.

72. Guo, X., An, M., Yang, P., Su, C., and Zhou, Y. Property Characterization and Formation Mechanism of Anticorrosion Film Coated on AZ31B Mg Alloy by SNAP Technology. *J Sol-Gel Sci Technol* **2009**, 52, 335-347.

73. Nanna, M. and Bierwagen, G. Mg-Rich Coatings: A New Paradigm for Cr-Free Corrosion Protection of Al Aerospace Alloys. *JCT Research* **2004**, 1, 69-80.

74. Bierwagen, G., Brown, R., Battocchi, D., and Hayes, S. Observations on the Testing of Mg-Rich Primers for Totally Chromate-Free Corrosion Protection of Aerospace Alloys. 2009 Department of Defense Corrosion Conference.

75. Bierwagen, G., Nanna, M., and Stamness, A. Examining Mg-Rich Primers for Al 2024 T-3: Recent Results and Application of Coating System Test Protocol. AMPTIAC Tri-Service Corrosion Conference. AMPTIAC Document Number AM025722. 17 Nov 2003.

76. Chisholm, B., Schulz, D., McCarthy, G., Battocchi, D., and Bierwagen, G. Durable Hybrid Coatings Annual Performance Report (2007). October, 2007. AFRL-RX-WP-TR-2008-4170.

77. Balbyshev, V., Chisholm, B., Schulz, D., McCarthy, G., Pederson, L., Battocchi, D., Allahar, K., and Bierwagen, G. Durable Hybrid Coatings Annual Performance Report (2009). October, 2009. AFRL-RX-WP-TR-2010-4028.

78. Balbyshev, V. Pederson, L., Battocchi, D., and Bierwagen, G. Durable Hybrid Coatings Annual Performance Report (2010). January, 2010. AFRL-RX-WP-TR-2011-4046.

79. Bierwagen, G., Mabutt, S., and He, L. Aircraft Coatings Testing, Corrosion Sensors in Coatings, and Mg-Rich Coatings as Cr-Free Primers for Al 2024 T-3. AMPTIAC Tri-Service Corrosion Conference. AMPTIAC Document Number AM025863. 14 Jan 2002.

80. Price, C., Naumann, R., and Shell, E. ESTCP Final Report: Joint DoD Demonstration and Validation of Magnesium-Rich Primer Coating Technology. ESTCP Project WP-0731. January, 2012.

81. Bierwagen, G., Brown, R., Battocchi, D., and Hayes, S. Active Metal-Based Corrosion Protective Coating Systems for Aircraft Requiring No-Chromate Pretreatment. *Progress in Organic Coatings* **2010**, 67, 195-208.

82. Pathak, S., Mendon, S., Blanton, M., and Rawlins, J. Review: Magnesium-Based Sacrificial Anode Cathodic Protection Coatings (Mg-Rich Primers) for Aluminum Alloys. *Metals* **2012**, 2, 353-376.

83. Hare, C. Corrosion Control of Steel by Organic Coatings. In *Uhlig's Corrosion Handbook*, 2nd Edition, Review, R.W. (Ed.), Ch. 55, John Wiley and Sons, New York, 1023-1038, 2000.

84. Felix, S., Barajas, R., Bastidas, J., Morcillo, M., and Feliu, S. Study of Protections Mechanism of Zinc-Rich Paints by Electrochemical Impedance Spectroscopy. In *Electrochemical Impedance Spectroscopy*, ASTM STP 1188, Scully, J., Silverman, D., and Kendig, M. (eds.). American Society of Testing and Materials (ASTM), Philadelphia, PA, 438-449, 1993.

85. Battocchi, D., Simoes, A., Tallman, D., and Bierwagen, G. Electrochemical Behavior of a Mg-Rich Primer in the Protection of Al Alloys. *Corrosion Science* **2006**, 48, 1292-1306.

86. Pathak, S., Blanton, M., Mendon, S., and Rawlins, J. Carbonation of Mg Powder to Enhance the Corrosion Resistance of Mg-Rich Primers. *Corrosion Science* **2010**, 52, 3782-3792.

87. Pathak, S., Blanton, M., Mendon, S., and Rawlins, J. Investigation on Dual Corrosion Performance of Magnesium-Rich Primer for Aluminum Alloys Under Salt Spray Test (ASTM B117) and Natural Exposure. *Corrosion Science* **2010**, 1453-1463.

88. Xu, H., Battocchi, D., Tallman, D., and Bierwagen, G. Use of Magnesium Alloys as Pigments in Magnesium-Rich Primers for Protecting Aluminum Alloys. *Corrosion* **2009**, 65, 318-325.

89. Jakubinek, M., Ashrafi, B., Zhang, Y., Martinez-Rubi, Y., Kingston, C., Johnston, A., and Simard, B. Single-Walled Carbon Nanotube-Epoxide Composites for Structural and Conductive Aerospace Adhesives. *Composites: Part B* **2015**, 87-93.

90. Nam, T., Goto, K., Nakayama, H., Oshima, K., Premalal, V., Shimamura, Y., Inoue, Y., Naito, K., and Kobayashi, S. Effect of Stretching on Mechanical Properties of Aligned Multi-Walled Carbon Nanotube/Epoxide Composites. *Composites: Part A* **2014**, 64, 194-202.

91. Bie, B., Han, J., Lu, L., Zhou, X., Qi, M., Zhang, Z., and Luo, S. Dynamic Fracture of Carbon Nanotube/Epoxide Composites under High Strain-Rate Loading. *Composites: Part A* **2015**, 68, 282-288.

92. Shimamura, Y., Oshima, K., Tohgo, K., Fujii, T., Shirasu, K., Yamamoto, G., Hashida, T., Goto, K., Ogasawara, T., Naito, K., Nakano, T., and Inoue, Y. Tensile Mechanical Properties of Carbon Nanotube/Epoxide Composite Fabricated by Pultrusion of Carbon Nanotube Spun Yarn Preform. *Composites: Part A* **2014**, 62, 32-38.

93. Bal, S. and Saha, S. Comparison and Analysis of Physical Properties of Carbon Nanomaterial-Doped Polymer Composites. *High Performance Polymers* **2014**, 26, 953-960.

94. Sun, T., Fan, H., Zhuo, Q., Liu, X., and Wu, Z. Covalent Incorporation of Aminated Carbon Nanotubes into Epoxide Resin Network. *High Performance Polymers* **2014**, 26, 892-899.

95. Konnola, R., Nair, C., and Joseph, K. High Strength Toughened Epoxide Nanocomposite based on Poly(Ether Sulfone)-Grafted Multi-Walled Carbon Nanotube. *Polymers Advanced Technologies* **2016**, 27, 82-89.

96. Liu, L., Shen, L., and Zhou Y. Improving the Interlaminar Fracture Toughness of Carbon/Epoxide Laminates by Directly Incorporating with Porous Carbon Nanotube Buckypaper. *Journal of Reinforced Plastics and Composites* **2016**, 35, 165-176.

97. Alamry, A., Prusty, B., Mada, M., and Bandyopadhyay, S. Improved Crack Resistance and Fracture Toughness using MWCNT Modified Epoxide for Delaminated Composite Structures. *Procedia Materials Science* **2014**, 3, 805-810.

98. Ashrafi, B., Martinez-Rubi, Y., Khoun, L, Yourdkhani, M., Kingston, C., Hubert, P., Simard, B., and Johnston, A. Influence of the Reaction Stoichiometry on the Mechanical and Thermal Properties of SWCNT-Modified Epoxide Composites. *Nanotechnology* **2013**, 24, 1-9.
99. Zwang, Z., Tan, Y., Wang, X., in, Y., and Wang, L. Synergetic Effects on the Mechanical and Fracture Properties of Epoxide Composites with Multiscale Reinforcements: Carbon Nanotubes and Short Carbon Fibers. *Journal of Applied Polymer Science* **2016**.
100. Praharaj, A., Behera, D., Bastia, T., and Rout, A. Functionalized Multiwalled Carbon Nanotubes – Reinforced Vinylester/Epoxide Blend based Nanocomposites: Enhanced Mechanical, Thermal, and Electrical Properties. *Journal of Nanotechnology* **2015**.
101. Ganesan, Y., Salahshoor, H., Peng, C., Khabashesku, V., Zhang, J., Cate, A., Rahbar, N., and Lou, J. Fracture Toughness of the Sidewall Fluorinated Carbon Nanotube-Epoxide Interface. *Journal of Applied Physics* **2014**, 115, 224305.
102. Yoonessi, M., Lebron-Colon, M., Schieman, D., and Meador, M. Carbon Nanotube Epoxide Nanocomposites: the Effects of Interfacial Modifications on the Dynamic Mechanical Properties of the Nanocomposites. *ACSA Appl. Mater. Interfaces* **2014**, 6, 16621-16630.
103. Brancato, V., Visco, A., Pistone, A., Piperno, A., and Iannazzo, D. Effect of Functional Groups of Multi-Walled Carbon Nanotubes on the Mechanical,

Thermal, and Electrical Performance of Epoxide Resin Based Nanocomposites. *Journal of Composite Materials* **2012**, 47, 3091-3103.

104. Ya, M. and Pyrz., R. Reinforcement Role of Carbon Nanotubes, Part I: High-Performance Epoxide Resin. *Polymer Composites* **2015**, 2212-2219.
105. Tsuda, T., Ogasawara, T., Moon, S., Nakamoto, K., Takeda, N., Shimamura, Y., and Inoue, Y. Three Dimension Orientation Angle Distribution Counting and Calculation for the Mechanical Properties of Aligned Carbon Nanotube/Epoxide Composites. *Composites: Part A* **2014**, 65, 1-9.
106. Li, M., Wang, Z., Liu, Q., Wang, S., Gu, Y., Li, Y., and Zhang, Z. Carbon Nanotube Film/Epoxide Composites with High Strength and Toughness. *Polymer Composites* **2015**, 1-9.
107. Opelt, C., Becker, D., Lepienski, C., and Coelho, L. Reinforcement and Toughening Mechanisms in Polymer Nanocomposites – Carbon Nanotubes and Aluminum Oxide. *Composites Part B* **2015**, 75, 119-126.
108. Ma, C., Liu, H., Du, X., Mach, L., Xu, F., and Mai, Y. Fracture Resistance, Thermal and Electrical Properties of Epoxide Composites Containing Aligned Carbon Nanotubes by Low Magnetic Field. *Composites Science and Technology* **2015**, 114, 126-135.
109. Sul, J., Prusty, B., and Crosky, A. Effect of the Addition of Multi-Walled Carbon Nanotubes on the Thermomechanical Properties of Epoxide Resin. *Polymer Composites* **2015**.

110. Hsieh, T., Kinloch, A., Taylor, A., and Kinloch, I. The Effect of Carbon Nanotubes on the Fracture Toughness and Fatigue Performance of a Thermosetting Epoxide Polymer. *Material Science* **2011**, 46, 7525-7535.

111. Park, S., Heo, G., and Jin, F. Rheological Properties and Fracture Toughness of Epoxide Resin/Multi-Walled Carbon Nanotube Composites. *Polymer Engineering and Science* **2015**, 2676-2682.

112. Khun, N., Troconis, R., and Frankel, G. Effects of Carbon Nanotube Content on Adhesion Strength and Wear and Corrosion Resistance of Epoxide Composite Coatings on AA2024-T3. *Progress in Organic Coatings* **2014**, 77, 72-80.

113. Jeon, H., Park, J., and Shon, M. Corrosion Protection by Epoxide Coating Containing Multi-Walled Carbon Nanotubes. *Journal of Industrial and Engineering Chemistry* **2013**, 19, 849-853.

114. Shen, W., Feng, L., Liu, X., Luo, H., Liu, Z., Tong, P., and Zhang, W. Multiwall Carbon Nanotube-Reinforced Epoxide Hybrid Coatings with High Electrical Conductivity and Corrosion Resistance Prepared via Electrostatic Spraying. *Progress in Organic Coatings* **2016**, 90, 139-146.

115. Gkikas, G., Lekatou, A., Sioulas, D., and Paipetis, A. Effect of Carbon Nanotube Enhanced Adhesives on Degradation of Bonded Corrosive Environments. *Plastics, Rubber, and Composites* **2014**, 43, 322-330.

116. Cubides, Y. and Castaneda, H. Corrosion Protection Mechanisms of Carbon Nanotube and Zinc-Rich Epoxide Primers on Carbon Steel in Simulated Concrete

Pore Solutions in the Presence of Chloride Ions. *Corrosion Science* **2016**, 109, 145-161.

117. Park, S. and Shon, M. Effects of Multi-Walled Carbon Nano Tubes on Corrosion Protection of Zinc Rich Epoxide Resin Coating. *Journal of Industrial and Engineering Chemistry* **2015**, 21, 1258-1264.
118. Gergely, A., Paszti, Z., Bertoti, I., Torok, T., Mihaly, J., and Kalman, E. Novel Zinc-Rich Epoxide Paint Coatings with Hydrated Alumina and Carbon Nanotubes Supported Polypyrrole for Corrosion Protection of Low Carbon Steel. Part II: Corrosion Prevention Behavior of the Hybrid Paint Coatings. *Materials and Corrosion* **2013**, 64, 1091-1103.
119. Gergely, A., Paszti, Z., Bertoti, I., Torok, T., Pfeifer, E., and Kalman, E. Novel Zinc-Rich Epoxide Paint Coatings with Hydrated Alumina and Carbon Nanotubes Supported Polypyrrole for Corrosion Protection of Low Carbon Steel. Part I: Inhibitor Particles and their Dispersions. *Materials and Corrosion* **2013**, 64, 1082-1090.
120. Yi, H., Chen, C., Zhong, F., and Xu, Z. Preparation of Aluminum Oxide-Coated Carbon Nanotubes and the Properties of Composite Epoxide Coatings Research. *High Performance Polymers* **2014**, 26, 255-264.
121. Kinloch, A., Lee, S., and Taylor, A. Improving the Fracture toughness and Cyclic-Fatigue Resistance of Epoxy-Polymer Blends. *Polymer* **2014**, 55, 6325-6334.
122. Ress, T., Thompson, N., and Wilford, A. The Modern Approach to Modifying Epoxide Resins Using Liquid Polysulfides. *J.O.C.C.A.* **1988**.

123. Krishnan, K. and Ninan, K. Thermal and Mechanical Studies on the Cure Time Optimisation of Polysulphide Resin. *Journal of Thermal Analysis* **1989**, 35, 1223-1228.

124. Donaldson, J., Grimes, S., Houlson, A., and Behn, S. Curing of a Polysulfide Sealant with Sodium Birnessite. *Journal of Applied Polymer Science* **2008**, 77,1177-1181.

125. Dong, W., Quan, Y., Zhang, J., and Chen, Q. The Structure and Mechanical Properties of Polysulfide-Based Polyurea. *Polymer International* **2003**, 52, 1925-1929.

126. Quan, Y., He, P., Zhou, B., and Chen, Q. Modification of Polysulfide Sealant with Polysulfide Polythio-Urethane-Urea. *Journal of Applied Polymer Science* **2007**, 106, 2599-2604.

127. Committee on Evaluation of Long-Term Aging of Materials and Structures Using Accelerated Test Methods, National Research Council. *Accelerated Aging of Materials and Structures: the Effects of Long-Term Elevated-Temperature Exposure*. National Academy Press, Washington, D.C., 1996.

128. Woodfield, A. and Haynes, P. *Measurement of Air Temperature on an Aircraft Travelling at High Subsonic and Supersonic Speeds*. Her Majesty's Stationery Office, London, England, 1965.

129. Performance Specification: Coating System, Advanced Performance, for Aerospace Applications. MIL-PRF-32239. 3 May 2007.

130. Thioplast G4 Data Sheet. AkzoNobel, January 2009.

131. Thioplast G112 Data Sheet. AkzoNobel, January 2009.

132. Sales, R. and Brunelli, D. Luminescence Spectroscopy Applied to a Study of the Curing Process of Diglycidyl-Ether of Bisphenol-A (DGEBA). *Mat. Res.* **2005**, 8, 3.

133. TxDOT TEX-815-B. Determining the Epoxide Equivalent and Amine Value of Resins. October 2014.

134. ASTM D1652: Standard Test Method for Epoxide Content of Epoxide Resins. ASTM International, West Conshohocken, PA.

135. ASTM D2074: Standard Test Methods for Total, Primary, Secondary, and Tertiary Amine Values of Fatty Amines by Alternative Indicator Method. ASTM International, West Conshohocken, PA.

136. ASTM D7234: Standard Test Method for Pull-Off Adhesion Strength of Coatings on Concrete Using Portable Pull-Off Adhesion Testers. ASTM International, West Conshohocken, PA.

137. Williams, J. *Fracture Mechanics of Polymers*. John Wiley and Sons, New York, NY, 1987.

138. Ballard, R., Sailer, R., Larson, B., and Soucek, M. Fracture Toughness of Inorganic-Organic Hybrid Coatings. *Journal of Coatings Technology* **2001**, 73.

139. He, Z. Organic/Inorganic Hybrid Coatings for Anticorrosion. Ph.D. Dissertation, the University of Akron, Akron, OH, 2015.

140. Olivier, M. and Poelman, M. Use of Electrochemical Impedance Spectroscopy (EIS) for the Evaluation of Electrocoatings Performances. In *Recent Researches in Corrosion Evaluation and Protection*. Razavi, R., Ed. InTech, 2002.

141. Arundati, Singhal, R., and Nagpal, A. Thermal and Chemical Resistance Behavior of Cured Epoxy Based on Diglycidyl Ether of Bisphenol-A and Thiol Treated Liquid Polysulfide Blends. *Adv. Mat. Let.* **2010**, 1, 238-245.

142. Guchhait, P., Bhandari, S., Singh, S., and Rahaman, M. Study on the Effect of Nanosilica Particles on Morphology, Thermo-Mechanical, and Electrical Properties of Liquid Polysulfide Modified Epoxy Hybrid Nanocomposites. *Indian Journal of Plastics* Technology **2011**.

143. Kochergin, Y., Grigorenko, T., Grigorenko, M., and Lazareva, L. Properties of Materials Effect of Thiokol on Properties of Epoxy Polymers. *Polymer Science* **2011**, 4, 295-300.

144. Chapter 6: Dynamic Mechanical Analysis (DMA). 236-252.

145. David, R., Raja, V., and Singh, S. High Performance Anti-Corrosive Epoxy Based Coating System for Marine Applications. *Corcon East Asia and Pacific Area Corrosion Conference and Expo* **2011**, 1-8.

146. Scherrer, M., Vietti, D., and Fiorillo. Polysulfides. In *Concise Polymeric Materials Encyclopedia*. Salamone, J., Ed. CRC Press, Boca Raton, Florida, 1999.

147. Serra, A., Ramis, X., and Fernandez-Francos, X. Review: Epoxide Sol-Gel Hybrid Thermosets. *Coatings* **2016**, 6, 8.

148. Innocenzi, P., Brusatin, G., Guglielmi, M., and Babonneau, F. Structural Characterization of Hybrid Organic-Inorganic Materials. *Handbook of Sol-Gel Science and Technology: Processing, Characterization, and Applications. Volume II: Characterization and Properties of Sol-Gel Materials and Products.* Sakka, S.

and Almeida, R., Eds. Kluwer Academic Publishers, Norwell, Massachusetts, 2005.

149. Guo, Q., Ghadiri, R., Weigel, T., Aumann, A., Gurevich, E., Esen, C., Medenbach, O., Cheng, W., Chichkov, B., and Ostendorf, A. Comparison of *in Situ* and *ex Situ* Methods for Synthesis of Two-Photon Polymerization Polymer Nanocomposites. *Polymers* **2014**, 6, 2037-2050.

150. Agunsoye, J., Talabi, S., Hassan, S., Awe, I., Bello, S., and Aziakpono, E. The Development and Characterization of Aluminum Dross-Epoxide Resin Composite Materials. *Journal of Materials Science Research* **2014**, 3, 23-37.

151. Liu, Y., Lin, Y., Chen, C., and Jeng, R. Preparation of Epoxide Resin/Silica Hybrid Composites for Epoxide Molding Compounds. *Journal of Applied Polymer Science* **2003**, 90, 4047-4053.

152. Bondoli, F., Cannillo, V., Fabbri, E., and Messori, M. Preparation and Characterization of Epoxide Resin Filled with Submicron Spherical Zirconia Particles. *Polimery* **2006**, 51, 794-798.

153. Lee, J. and Yee, A. Inorganic Particle Toughening I: Micro-Mechanical Deformations in the Fracture of Glass Bead Filled Epoxies. *Polymer* **2001**, 42, 577-588.

154. Rosso, P., Ye, L., Friedrich, K., and Sprenger, S. A Toughened Epoxide Resin by Silica Nanoparticle Reinforcement. *Journal of Applied Polymer Science* **2006**, 100, 1849-1855.

155. Soucek, M. and He, J. UV-Curable Vinyl Functionalized Siloxane Colloids. *Radtech Report* **2007**, 10-16.

156. Dworak, D. and Soucek, M. Effect of Mixed Sol-Gel Precursors on the Metal-Oxo Phase Within a UV-Curable Silicone Hybrid Material. *Macromolecular Chemistry and Physics* **2006**, 207, 1220-1232.

157. Zand, R., Langroudi, A., and Rahimi, A. Synthesis and Characterization of Nanocomposite Hybrid Coatings Based on 3-Glycidoxypropyl-trimethoxysilane and Bisphenol A. *Iranian Polymer Journal* **2005**, 14, 371-377.

158. Donley, M., Mantz, R., Khramov, A., Balbyshev, V., Kasten, L., and Gaspar, D. The Self-Assembled Nanophase Particle (SNAP) Process: a Nanoscience Approach to Coatings. *Progress in Organic Coatings* **2003**, 47, 401-415.

159. Haso, F. The Effect of Specific Non-Covalent Interactions on the Assembly Behavior of Macroions in Solution. Ph.D. Dissertation, the University of Akron, Akron, OH, 2015.

160. ASTM D2730: Standard Test Method for Tensile Properties of Organic Coatings. ASTM International, West Conshohocken, PA, 2010.

161. MIL-DTL-24441 Paint, Epoxide, White, Formula 152, Type III. http://quicksearch.dla.mil/. April, 2015.

162. ASTM D4060: Standard Test Method for Abrasion Resistance of Organic Coatings by the Taber Abraser. ASTM International, West Conshohocken, PA.

163. Chiang, C. and Ma, C. Synthesis, Characterization, and Thermal Properties of Novel Epoxide Containing Silicon and Phosphorus Nanocomposites by Sol-Gel Method. *European Polymer Journal* **2002**, 38, 2219-2224.

164. Hoebbel, D., Nacken, M., and Schmidt, H. On the Existence and Hydrolytic Stability of Titanosiloxane Bonds in the System: Glycidoxypropyltrimethoxysilane-Water-Titaniumtetraethoxide. *Journal of Sol-Gel Science and Technology* **1998**, 13, 37-43.

165. Da, Z., Zhang, Q., Wu, D., Yang, D., and Qiu, F. Synthesis, Characterization, and Thermal Properties of Inorganic-Organic Hybrid. *eXPRESS Polymer Letters* **2007**, 1, 698-703.

166. Preparation of Sol-Gel Hybrid Materials from γ-Methacryloxypropyltrimethoxysilane and Tetramethyl Orthosilicate: Study of the Hydrolysis and Condensation Reactions. *Colloid Polymer Science* **2011**, 289, 1875-1883.

167. Innocenzi, P., Figus, C., Kidchob, T., Valentini, M., Alonso, B., and Takahasi, M. Sol-Gel Reactions of 3-Glycidoxypropyltrimethoxysilane in a Highly Basis Aqueous Solution. *Dalton Transactions* **2009**, 9146-9152.

168. Innocenzi, P., Figus, C., Kidchob, T., and Takahashi, M. Crystallization in Hybrid Organic-Inorganic Materials through Self-Organization from 3-Glycidoxypropyltrimethoxysilane. *Journal of the Ceramic Society of Japan* **2011**, 119, 387-392.

169. Alonso, B., Massiot, D., Babonneau, F., Brusatin, G., Giustina, G., Kidchob, T., and Innocenzi, P. Structural Control in Germania Hybrid Organic-Inorganic Materials. *Chem. Mater.* **2005**, 17, 3172-3180.

170. Hartono, A., da Silva, E., Grasdalen, H., and Svendsen, H. Qualitative Determination of Species in DETA-H_2O-CO_2 System Using ^{13}C NMR Spectra. *Ind. Eng. Chem. Res.* **2007**, 46-249-254.

171. Li, C., Glass, T., and Wilkes, G. NMR Studies of Sol-Gel Derived Hybrid Materials Based on Triethoxysilylated Diethylenetriamine and Tetramethoxysilane. *Journal of Inorganic and Organometallic Polymers* **1999**, 9, 79-106.

172. Niederberg, M. Aqueous and Nonaqueous Sol-Gel Chemistry. In *Metal Oxide Nanoparticles in Organic Solvents*. Springer London, 2009.

173. Sumathi, R. and Thenmozhi, R. Synthesis and Characterization of Spherical Silica Nanoparticles by Sol-Gel Method. *ISCCCCET* **2015**, 204-208.

174. Palraj, S., Selvaraj, M., Maruthan, K., and Rajagopal, G. Corrosion and Wear Resistance Behavior of Nano-Silica Epoxy Composite Coatings. *Prog. Org. Coat.* **2015**, 81, 132–139.

175. Sitthiracha, M., Kilmartin, P., and Edmonds, N. Novel Organic-Inorganic Hybrid Materials Based on Epoxy-Funtionalized Silanes. *Journal of Sol-Gel Science and Technology* **2015**, 76, 542-551.

176. Domun, N., Hadavinia, H., Zhang, T., Sainsbury, T., Liaghat, G., and Vahid, S. Improving the Fracture toughness and the Strength of Epoxy Using

Nanomaterials - a Review of the Current Status. *Nanoscale* **2015**, 7, 10294-10329.

177. Wen, J. and Wilkes, G. Organic/Inorganic Hybrid Network Materials by the Sol-Gel Approach. *Chem. Mater.* **1996**, 8, 1667-1681.
178. Nazir, T., Afzal, A., Siddiqi, H., Saeed, S., and Dumon, M. The Influence of Temperature and Interface Strength on the Microstructure and Performance of Sol-Gel Silica-Epoxy Nanocomposites. *Polym. Bull.* **2011**, 67, 1539-1551.
179. Shi, F., Wang, X., Guo, R., Zhong, M., and Xie, X. Highly Stretchable and Super Tough Nanocomposite Physical Hydrogels Facilitated by the Coupling of Intermolecular Hydrogen Bonds and Analogous Chemical Crosslinking of Nanoparticles. *J. Mater. Chem. B* **2015**, 3, 1187-1192.
180. Islam, M., Masoodi, R., and Rostami, H. The Effect of Nanoparticles Percentage on Mechanical Behavior of Silica-Epoxide Nanocomposites. *Journal of Nanoscience* **2013**, 2013, 1-10.
181. Rubab, Z., Afzal, A., Siddiqi, H., and Saeed, S. Preparation, Characterization, and Enhanced Thermal and Mechanical Properties of Epoxide-Titania Composites. *The Scientific World Journal* **2014**, 2014, 1-7.
182. Piscitelli, F., Buonocore, G., Lavorgna, M., Verdolotti, L., Pricl, S., Gentile, G., and Mascia, L. Peculiarities in the Structure-Properties Relationship of Epoxy-Silica Hybrids with Highly Organic Siloxane Domains. *Polymer* **2015**, 63, 222–229.

183. Allauddin, S., Chandran, M.K.A., Jena, K.K., Narayan, R., and Raju, K. Synthesis and Characterization of APTMS/Melamine cured Hyperbranched Polyester-Epoxy Hybrid Coatings. Prog. Org. Coat. **2013**, 76, 1402–1412.

184. Prezzi, L. and Mascia, L. Network Density Control in Epoxy-Silica Hybrids by Selective Silane Functionalization of Precursors. *Advances in Polymer Technology* **2005**, 24, 91-102.

185. Spori, D. Structural Influences on Self-Cleaning Surfaces. PhD Dissertation, ETH Zurich, Zurich, Switzerland, 1979.

186. Liu, H., Wang, G., Mai, Y., and Zeng, Y. On Fracture Toughness of Nano-Particle Modified Epoxide. *Composites B* **2011**, 42, 2170-2175.

187. Mahrolz, T., Stangle, J., and Sinapius, M. Quantitation of the Reinforcement Effect of Silica Nanoparticles in Epoxide Resins used in Liquid Composite Molding Processes. *Composites A* **2009**, 40, 235-243.

188. Tuman, S. and Soucek, M. Novel Inorganic/Organic Hybrid Materials Based on Drying Oils with Sol-Gel Precursors. *Polymer Preprints* **1995**, 36.

189. Ballard, R., Tuman, S., Fouquette, D., Stegmiller, W., and Soucek, M. Effects of an Acid Catalyst on the Inorganic Domain of Inorganic-Organic Hybrid Materials. *Chem. Mater.* **1999**, 11.

190. Ballard, R., Tuman, S., Fouquette, D., Stegmiller, W., and Soucek, M. Inorganic-Organic Hybrid Coatings with Mixed Metal-Oxides. *European Polymer Journal* **2001**, 37.

191. Zou, K. and Soucek, M. UV-Curable Organic-Inorganic Hybrid Film Coatings Based on Epoxidized Cyclohexene Derivatized Linseed Oil. *Macro. Chem. Phys.* **2004**, 204.

192. Liang, Y. and Pearson, R. The Toughening Mechanism in Hybrid Epoxide-Silica-Rubber Nanocomposites (HESRNs). *Polymer* **2010**, 51, 4880-4890.

193. Kinloch, A. and Taylor, A. The Mechanical Properties and Fracture Behavior of Epoxide-Inorganic Micro- and Nanocomposites. *Journal of Materials Science* 2006, 41, 3271-3297.

194. Liu, J., Chaudhury, M., Berry, D., Seebergh, J., Osborne, J., and Blohowiak, K. Fracture Behavior of an Epoxide/Aluminum Interface Reinforced by Sol-Gel Coatings. *J. Adhesion Sci. Technol.* **2006**, 20, 277-305.

195. Kinloch, A., Mohammed, R., Taylor, A., Eger, C., Sprenger, S., and Egan, D. The Effect of Silica Nano Particles and Rubber Particles on the Toughness of Multiphase Thermosetting Epoxide Polymers. *Journal of Materials Science* **2005**, 40, 5083-5086.

196. Li, C. and Wilkes, G. Silicone/Amine Resin Hybrid Materials as Abrasion Resistant Coatings. *Chem. Mater.* **2001**, 13, 3663-3668.

197. Materne, T. and Buyl, F. Organosilane Technology in Coating Applications: Review and Perspectives. Dow Corning Corporation, Midland, MI.

198. Gupta, N., Sinha, T., and Varma, I. Development of an Abrasion Resistant Coating from Organic-Inorganic Polymeric Network by Sol-Gel Process. *Indian Journal of Chemical Technology* **1997**, 4, 130-134.

199. Saravanan, P., Jayamoorthy, K., and Kumar, S. Design and Characterization of Non-Toxic Nano-Hybrid Coatings for Corrosion and Fouling Resistance. *Journal of Science: Advanced Materials and Devices* **2016**, 1, 367-378.

200. Rahman, I. and Padavettan, V. Synthesis of Silica Nanoparticles by Sol-Gel: Size-Dependent Properties, Surface Modification, and Applications in Silica-Polymer Nanocomposites – A Review. *Journal of Nanomaterials* **2012**, 1-15.

201. Ahmad, Z. and Al-Sagheer, F. *J. Sol-Gel Sci. Technol.* **2014**, 72, 334-343.

202. Piscitelli, F. Epoxy-Based Organic-Inorganic Hybrid Materials by Sol-Gel Method: Chemical Tailoring and Multi-Scale Characterization. PhD Dissertation, Universita Degli Studi Di Napoli "Federico II," 2010.

203. Yao, H., Hang, J., Sun, X., Jin, L., and Shi, L. Preparation and Anticorrosive Behavior of Epoxy-Polysiloxane Hybrid Coatings Modified by Polyetheramines. *Journal of Adhesion Science and Technology* **2014**, 12, 1103-1116.

204. Meador, M., Fabrizio, E., Ilhan, F., Dass, A., Zhang, G., Vassilaras, P., Johnston, C., and Leventis, N. Cross-Linking Amine-Modified Silica Aerogels with Epoxies: Mechanically Strong Lightweight Porous Materials. *Chem. Mater.* **2005**, 17, 1085-1098.

205. Baczoni, A. and Molnar, F. Advanced Examination of Zinc Rich Primers with Thermodielectric Spectroscopy. *Acta. Polytechnica Hungarica* **2011**, 8, 43-51.

206. Tesla NanoCoatings. 25 Aug 2016. http://www.teslanano.com/

207. MIL-DTL-24441 Paint, Epoxide, Black, Formula 152.

208. Loveday, D., Peterson, P., and Rodgers, B. Evaluation of Organic Coatings with Electrochemical Impedance Spectroscopy. *JCT Coatings Tech* **2004**, 84-93.